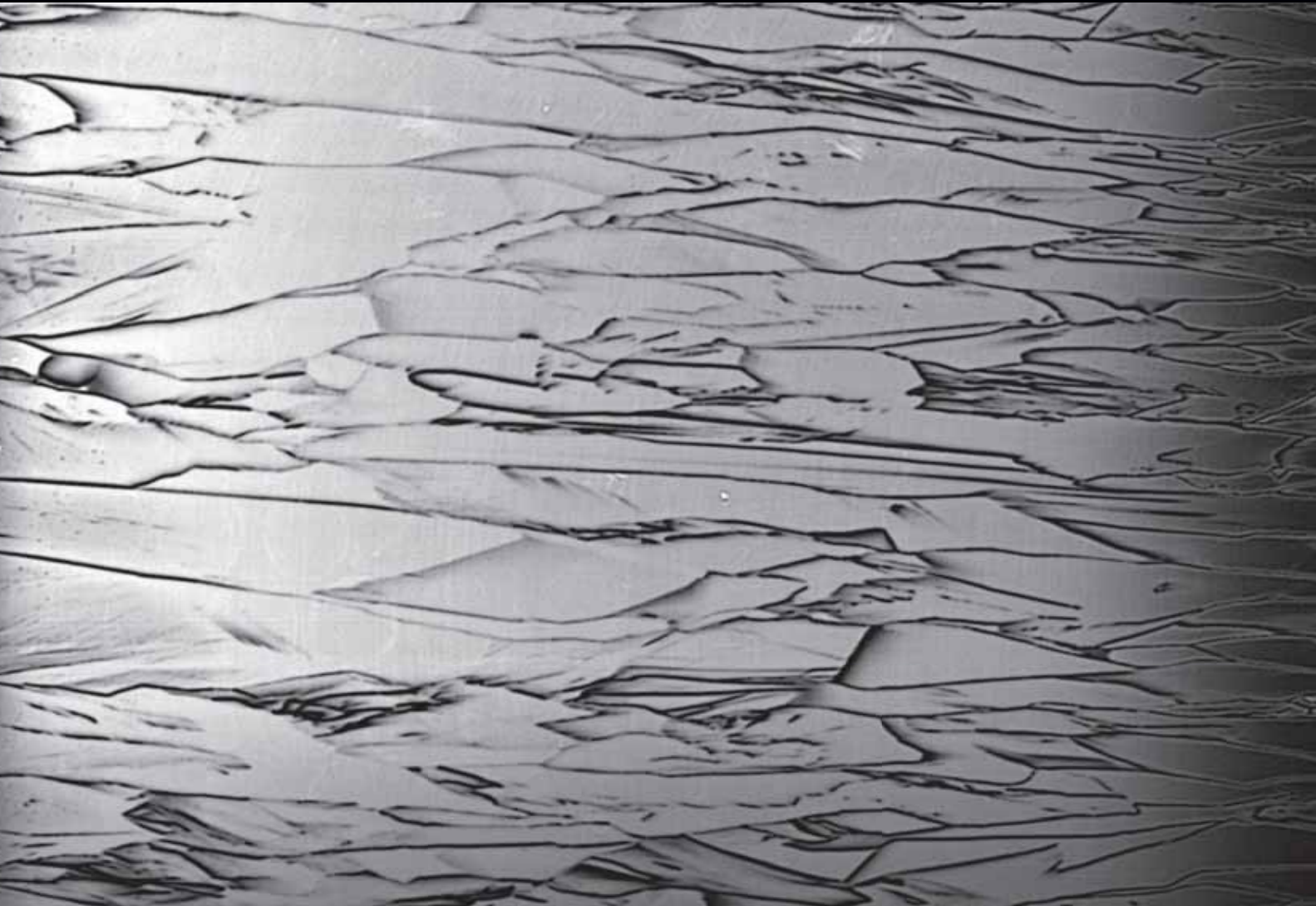


Thirty Third Edition

# Photovoltaics

International

THE TECHNOLOGY RESOURCE FOR PV PROFESSIONALS

- 
- University of New South Wales** Metrology at the ingot level: Addressing the growing importance of bulk material quality
  - ISFH** BiCoRE: Combining a PERC-type cell process with n-type wafers
  - ECN** Positive cell-to-module change: Getting more power out of back-contact modules
  - Solar Intelligence** Cell technology trends impacting module supply in 2017
  - CEA Tech-INES & AET Technologies** Oxygen-defect characterization for improving R&D relevance and Cz-Si solar cell efficiency
  - University of New South Wales** Techniques for mitigating light-induced degradation (LID) in commercial silicon solar cells

**JA SOLAR**

[www.jasolar.com](http://www.jasolar.com)



# Harvest the Sunshine

Premium Cells, Premium Modules

**JA Solar Holdings Co., Ltd.**

Building No.8, Nuode Center, Automobile Museum East Road, Fengtai District, Beijing

Tel: +86 (10) 63611888 Fax: +86 (10) 63611999 Email: [sales@jasolar.com](mailto:sales@jasolar.com); [market@jasolar.com](mailto:market@jasolar.com)

Photovoltaics International's primary focus is on assessing existing and new technologies for "real-world" supply chain solutions. The aim is to help engineers, managers and investors to understand the potential of equipment, materials, processes and services that can help the PV industry achieve grid parity. The Photovoltaics International advisory board has been selected to help guide the editorial direction of the technical journal so that it remains relevant to manufacturers and utility-grade installers of photovoltaic technology. The advisory board is made up of leading personnel currently working first-hand in the PV industry.



## Editorial Advisory Board

Our editorial advisory board is made up of senior engineers from PV manufacturers worldwide. Meet some of our board members below:



*Prof Armin Aberle, CEO, Solar Energy Research Institute of Singapore (SERIS), National University of Singapore (NUS)*

Prof Aberle's research focus is on photovoltaic materials, devices and modules. In the 1990s he established the Silicon Photovoltaics Department at the Institute for Solar Energy Research (ISFH) in Hamelin, Germany. He then worked for 10 years in Sydney, Australia as a professor of photovoltaics at the University of New South Wales (UNSW). In 2008 he joined NUS to establish SERIS (as Deputy CEO), with particular responsibility for the creation of a Silicon PV Department.



*Dr. Markus Fischer, Director R&D Processes, Hanwha Q Cells*

Dr. Fischer has more than 15 years' experience in the semiconductor and crystalline silicon photovoltaic industry. He joined Q Cells in 2007 after working in different engineering and management positions with Siemens, Infineon, Philips, and NXP. As Director R&D Processes he is responsible for the process and production equipment development of current and future c-Si solar cell concepts. Dr. Fischer received his Ph.D. in Electrical Engineering in 1997 from the University of Stuttgart. Since 2010 he has been a co-chairman of the SEMI International Technology Roadmap for Photovoltaic.



*Dr. Thorsten Dullweber, R&D Group Leader at the Institute for Solar Energy Research Hamelin (ISFH)*

Dr. Dullweber's research focuses on high efficiency industrial-type PERC silicon solar cells and ultra-fine-line screen-printed Ag front contacts. His group has contributed many journal and conference publications as well as industry-wide recognized research results. Before joining ISFH in 2009, Dr. Dullweber worked for nine years in the microelectronics industry at Siemens AG and later Infineon Technologies AG. He received his Ph. D. in 2002 for research on Cu(In,Ga)Se<sub>2</sub> thin-film solar cells.



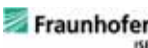
*Dr. Wei Shan, Chief Scientist, JA Solar*

Dr. Wei Shan has been with JA Solar since 2008 and is currently the Chief Scientist and head of R&D. With more than 30 years' experience in R&D in a wider variety of semiconductor material systems and devices, he has published over 150 peer-reviewed journal articles and prestigious conference papers, as well as six book chapters.



*Jim Zhu, Chief Scientist, Wuxi Suntech*

Jim Zhu has bachelor and master's degrees from Fundan University and a Ph.D. from the Shanghai Institute of Technical Physics of the Chinese Academy of Sciences. In 2007 he joined Suntech as group VP with responsibility for customer service, quality management and R&D. He has been the company's Chief Scientist since 2013.



*Florian Clement, Head of Group, MWT solar cells/printing technology, Fraunhofer ISE*

Dr. Clement received his Ph.D in 2009 from the University of Freiburg. He studied physics at the Ludwigs-Maximilian-University of Munich and the University of Freiburg and obtained his diploma degree in 2005. His research is focused on the development, analysis and characterization of highly efficient, industrially feasible MWT solar cells with rear side passivation, so called HIP-MWT devices, and on new printing technologies for silicon solar cell processing.



*Sam Hong, Chief Executive, Neo Solar Power*

Dr. Hong has more than 30 years' experience in solar photovoltaic energy. He has served as the Research Division Director of Photovoltaic Solar Energy Division at the Industry Technology Research Institute (ITRI), and Vice President and Plant Director of Sinonar Amorphous Silicon Solar Cell Co., the first amorphous silicon manufacturer in Taiwan. Dr. Hong has published three books and 38 journal and international conference papers, and is a holder of seven patents. In 2011 he took office as Chairman of Taiwan Photovoltaic Industry Association.



*Matt Campbell, Senior Director, Power Plant Products, SunPower*

Matt Campbell has held a variety of business development and product management roles since joining the SunPower, including the development of the 1.5MW AC Oasis power plant platform, organized SunPower's power plant LCOE reduction programmes, and the acquisition of three power plant technology companies. Campbell helped form a joint venture in Inner Mongolia, China for power plant project development and manufacturing. He holds an MBA from the University of California at Berkeley and a BBA in Marketing, Finance, and Real Estate from the University of Wisconsin at Madison.



*Ru Zhong Hou, Director of Product Center, ReneSola*

Ru Zhong Hou joined ReneSola as R&D Senior Manager in 2010 before being appointed Director of R&D in 2012. Before joining ReneSola he was a researcher for Microvast Power Systems, a battery manufacturer. His work has been published in numerous scientific journals. He has a Ph.D. from the Institute of Materials Physics & Microstructures, Zhejiang University, China.



No matter where you are,  
together we **MASTER** the future.



The Future of Solar is Us.  
Run with Us!

*Suntech - Be unlimited!*  
*Learn more at: [www.suntech-power.com](http://www.suntech-power.com)*

 **SUNTECH**  
BE UNLIMITED

# Contents

## 08 Product Reviews

## 13 Section 6 Market Watch

+ NEWS

Page 15

### Cell technology trends impacting module supply in 2017

**Finlay Colville**, Head of Market Research, Solar Media



13

## 20 Section 1 Fab & Facilities

+ NEWS

Page 22

### PV manufacturing capacity expansion announcement plans and analysis for 1H 2016

**Mark Osborne**, Senior News Editor, Photovoltaics International



20

## 31 Section 2 Materials

+ NEWS

Page 34

### Metrology at the ingot level: Addressing the growing importance of bulk material quality

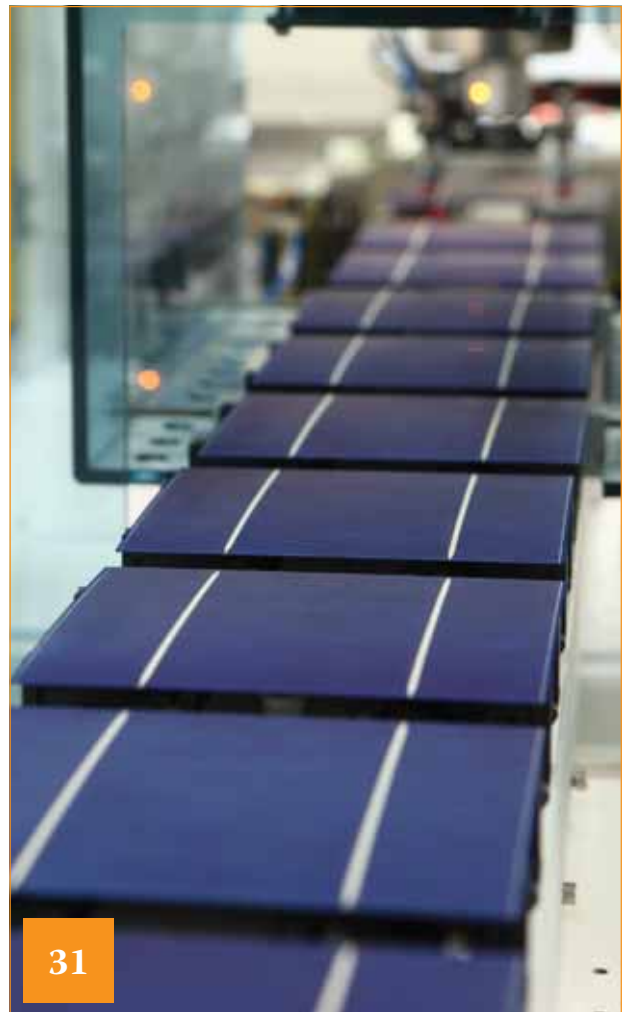
**Bernhard Mitchell<sup>1</sup>**, **Daniel Chung<sup>1</sup>**, **Jürgen Weber<sup>2</sup>** & **Thorsten Trupke<sup>1,2</sup>**

<sup>1</sup>University of New South Wales (UNSW), Sydney; <sup>2</sup>BT Imaging Pty Ltd, Sydney, Australia

Page 41

### Oxygen-defect characterization for improving R&D relevance and Cz-Si solar cell efficiency

**Jordi Veirman**, **Benoît Martel**, **Nicolas Enjalbert** & **Sébastien Dubois**, CEA Tech-INES, Le Bourget du Lac, & **Catherine Picoulet** & **Pierre Bonnard**, AET Technologies, Meylan, France



31

# MONO IS THE FUTURE



## About LERRI Solar

**A world leading mono-crystalline solar module manufacturer for achieving best LCOE (levelized cost of electricity) solutions.**

LERRI Solar is a world leading manufacturer of high-efficiency mono-crystalline solar cells and modules. The company was founded in 2007 and later on acquired by Longi Group in 2014. Longi Group (SH601012) is the largest supplier of mono-crystalline silicon wafers in the world, with total assets above \$1.7 billion. (2016)

Armed and powered by the advanced technology and long standing experience of Longi Group in the field of mono-crystalline silicon, LERRI Solar has shipped over 1GW products in 2015 and is estimated to double the revenue by the end of 2016.

With strong focus on R&D, production and sales & marketing of mono-crystalline silicon products, LERRI Solar is committed to providing the best LCOE solutions as well as promoting the worldwide adoption of mono-crystalline technology.

[www.lerrisolar.com](http://www.lerrisolar.com)



### Visit us at Solar Energy UK

**Date:** Oct 4 – Oct 6

**Booth:** NO. A20

**Venue:** The National Exhibition Centre (NEC),  
Hall 3, Birmingham, UK

# Contents

## 50 Section 3 Cell Processing

+ NEWS

Page 53

### Techniques for mitigating light-induced degradation (LID) in commercial silicon solar cells

**Brett Hallam<sup>1</sup>, Catherine Chan<sup>1</sup>, David Payne<sup>1</sup>, Dominik Lausch<sup>2</sup>, Marcus Gläser<sup>2</sup>, Malcolm Abbott<sup>1</sup> & Stuart Wenham<sup>1</sup>**

<sup>1</sup>University of New South Wales (UNSW), Sydney, Australia; <sup>2</sup>Fraunhofer Center for Silicon Photovoltaics (CSP), Halle (Saale), Germany

Page 64

### BiCoRE: Combining a PERC-type cell process with n-type wafers

**Thorsten Dullweber, Nadine Wehmeier, Anja Nowack, Till Brendemühl, S. Kajari-Schröder & R. Brendel**, Institute for Solar Energy Research Hamelin (ISFH), Emmerthal, Germany

Page 72

### Stencil printing and metal squeegees for improved solar cell printing results

**Andrew Zhou, Rado Yang, Tom Falcon & Jessen Cunnusamy**, ASM Alternative Energy & **Thorsten Dullweber & Helge Hannebauer**, Institute for Solar Energy Research Hamelin (ISFH)



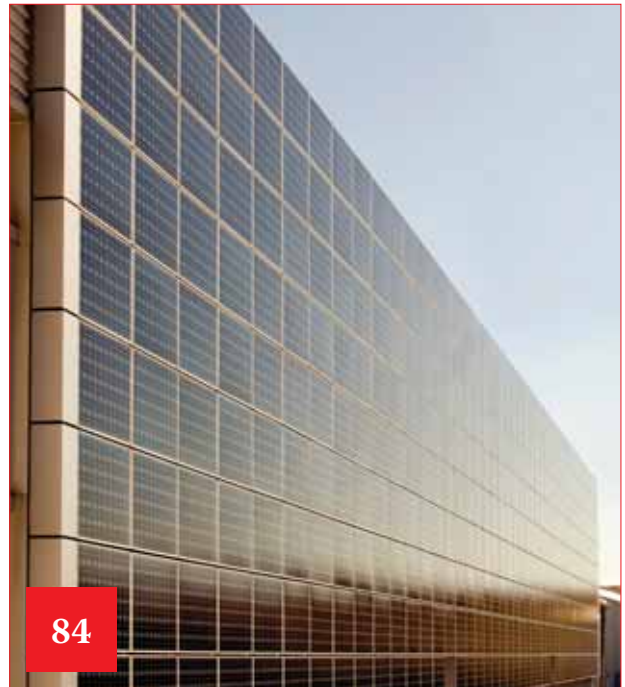
## 78 Section 4 Thin Film

+ NEWS

Page 82

### Significant progress in CIGS thin-film solar cell technology reported at IWCIGSTech7

**Rutger Schlatmann & Hans Werner Schock**, Helmholtz-Zentrum Berlin für Materialien und Energie, **Michael Powalla**, Centre for Solar Energy and Hydrogen Research Baden-Württemberg (ZSW)



## 84 Section 5 PV Modules

+ NEWS

Page 88

### Reducing the electrical and optical losses of PV modules incorporating PERC solar cells

**Henning Schulte-Huxel, Robert Witteck, Malte Ruben Vogt, Hendrik Holst, Susanne Blankemeyer, David Hinken, Till Brendemühl, Thorsten Dullweber, Karsten Bothe, Marc Köntges & Rolf Brendel**, Institute for Solar Energy Research Hamelin (ISFH), Emmerthal, Germany

Page 97

### Positive cell-to-module change: Getting more power out of back-contact modules

**Bas B. van Aken & Lenneke H. Slooff-Hoek**, ECN – Solar Energy, Petten, The Netherlands

Page 106

### Electroluminescence (EL) studies of multicrystalline PV modules

**Sreenivasa Murty Dasari, Chandra Mauli Kumar, Amresh Mahajan & Nagesh C**, Tata Power Solar, Bengaluru, India

111 Subscription / Advertisers Index

112 The PV-Tech Blog



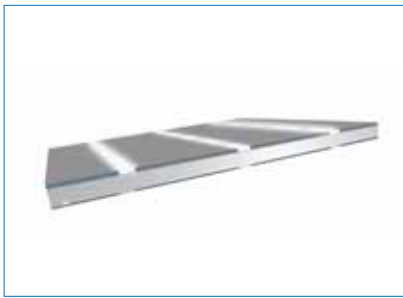
Intersolar South America | São Paulo | August 23–25, 2016  
Intersolar Middle East | Dubai | September 19–21, 2016  
Intersolar India | Mumbai | October 19–21, 2016  
Intersolar Europe | Munich | May 31–June 2, 2017  
Intersolar North America | San Francisco | July 11–13, 2017  
Intersolar Summit Iran | Tehran | November 15, 2016  
Intersolar Summit USA East | New York | Spring 2017





# Product Reviews

## Heraeus



### Heraeus' 'SOL9631' front-side paste offers new glass chemistry for PERC cells

**Product Outline:** Heraeus Photovoltaics has launched a new PERC metallization paste, tailored for ultra-fine line printability and low-temperature firing.

**Problem:** The increased migration to PERC solar cells to boost conversion efficiencies has highlighted that lower process (firing) temperatures are required, while providing excellent adhesion. PERC cells also need to have limited impact from light-induced degradation (LID).

**Solution:** The SOL9631 Series has been developed based on new glass chemistry, combined with the latest organic vehicle system for ultra-fine-line printing. As confirmed by customers SOL9631 Series has improved LID performance and improved reliability for both cells and modules, according to Heraeus. SOL9631B has a wide firing window and can be fired at low temperatures, which makes the paste specifically suitable for PERC cells. At the same time, the paste shows excellent performance at regular firing temperatures. The paste is specifically strong in the feature of adhesion. The SOL9631 supports a finger geometry that can print defect-free through a less than 30µm screen opening in high-throughput mass production, resulting in an efficiency gain through reduced optical shading and less contact area.

**Applications:** Ultra-fine line printability for screen printing of PERC solar cells and BSF cells.

**Platform:** The SOL9631's glass chemistry enables low firing temperatures. After low-temperature firing the microstructure of the fired finger shows a much more densified structure including the Ag-Silicon interface, enhancing adhesion, grid resistivity and solderability.

**Availability:** May 2016 onwards.

## HORIBA



### HORIBA provides advanced POCl3 delivery system for high-volume solar cell processing

**Product Outline:** HORIBA has developed a Phosphorus Oxychloride (POCl<sub>3</sub>) delivery systems that is being implemented for atmospheric and low pressure diffusion furnaces in Europe and Asia.

**Problem:** POCl<sub>3</sub> is delivered in 1-litre quartz vessels that typically require more than 200 exchanges in a 200MW line each year. Most quartz bubbler exchanges are performed at a height where there is always a risk to the health of operators and to the process itself. There is also a two-hour downtime to consider for each exchange. Each quartz bubbler vessel typically can be used down to 10% of POCl<sub>3</sub> remaining before the process becomes less stable. This 'waste' POCl<sub>3</sub> cannot be used and needs to be disposed of.

**Solution:** POCl<sub>3</sub> is delivered in 20-litre canisters reducing tank exchanges from 200 to just 10 per year. Tank exchange is safer as the canister is constructed from ETFE lined stainless steel and performed at ground level. Furnace downtime is eliminated as production continues even when the bulk POCl<sub>3</sub> tank is being exchanged. Financial and environmental benefits are also delivered as POCl<sub>3</sub> waste is reduced from 10% to less than 2%.

**Applications:** Atmospheric and low pressure diffusion furnaces for the delivery of POCl<sub>3</sub> or BBr<sub>3</sub> to produce n-type and p-type solar cells.

**Platform:** HORIBA has designed a robust refill system featuring fully automatic purge and safety check with integrated gas and liquid leak detection and full containment. The refill system is connected via dual containment tubing to up to 20 HORIBA advanced bubblers. The fixed bubblers are fully integrated and interlocked with the furnace.

**Availability:** Currently available.

## JRT Photovoltaics



### JRT Photovoltaics enables 'highest throughput' single-track cell tester and sorter

**Product Outline:** JRT Photovoltaics, a subsidiary of the Jonas & Redmann Group, has optimized the testing and sorting of solar cells, claiming to significantly reducing the total cost of ownership with its 'CTS 3600' single-track cell tester and sorter

**Problem:** PV manufacturers require high cell processing throughput with reliable, quality of results and lower cost per tested cell to increase both the efficiency of production systems and planning certainty. A short return on investment time is also required.

**Solution:** During the fully automated quality assessment and sorting of solar cells with the CTS 3600, the fully processed solar cells are tested and then sorted on a single track.

Up to 3,600 solar cells per hour with a guaranteed yield of over 99.5% and a guaranteed availability in practice of 98% makes the CTS 3600 most efficient and reliable single-track cell tester and sorter, according to the company.

**Applications:** Testing and sorting all types of high-efficiency solar cells.

**Platform:** The central transport system of the test unit is based on circulating vacuum conveyor belts and gentle cell handling. Once the cells have been positioned flat and fixed securely they pass through the specified measuring stations. Critical transfer or handling processes are kept to a minimum. Quality measurements are performed by non-contact systems and with gentle contact using minimal force ensuring optimum measurement results. The result is a claimed above-average yield and the lowest breakage rates. The CTS 3600 can quickly be converted to different cell layouts and handles very thin busbars.

**Availability:** Currently available.

# Product Reviews

## Meco



**Meco's 'Cell Plating Line' enables lower cost high-efficiency solar cells**

**Product Outline:** Meco Equipment Engineers provides its Cell Plating Line (CPL) for a wide variety of next-generation solar cell architectures migrating from silver to copper contacts.

**Problem:** Typically screen-printed contact fingers are printed 90-100 microns wide to obtain sufficient electrical conductance. To further increase the cell efficiency the contact finger width can be reduced as the active area of the cell increases. However, cell efficiency improvement is limited as the poor aspect ratio of screen-printed contact fingers leads to an increase of the contact finger resistance value at the same time.

**Solution:** The process starts on a narrow and thin seed layer of Ag paste where the electrical conductance of the contact finger is further enhanced by electroplating either Ag or Ni-Cu-Sn on to it, giving a narrow contact finger and improving the resistance value. With the CPL, an overall absolute cell efficiency improvement of 0.3-0.5% can be obtained and expensive Ag paste can be saved. Therefore with the CPL a return on investment of < 1 year can be achieved.

**Applications:** Copper plating of Heterojunction cells, IBC cells, bifacial cells, PERC and MWT cells as well as the capability to plate on both sides of the cell at the same time.

**Platform:** The total CPL throughput is 1,500 to 3,000 cells/hour in the high volume manufacturing line configuration. The Meco CPL is based on vertical wafer transportation providing minimum drag-out of chemicals and waste discharge and has seamless integration with cassette transfer systems. Metal options include Ag, Ni-Cu-Sn, Cu-Sn (for IBC) cells.

**Availability:** Currently available.

## 3D-Micromac



**3D-Micromac's 'microCELL' TLS solar cell cutting tool uses thermal laser separation**

**Product Outline:** 3D-Micromac's 'microCELL' TLS is a highly productive laser system for separation of standard silicon solar cells into half cells. The microCELL TLS meets cell manufacturers' demands for retaining the mechanical strength of the cut cells.

**Problem:** Current solutions for the growing industry demand for half-cell solutions are conventional laser based scribe and break processes. Ablation is done through half of the cell's thickness with subsequent mechanical cleaving. Such a process is comparably slow, and creates crystal dislocation and micro-cracks that lower the electrical and mechanical performance of the cells.

**Solution:** 3D-Micromac's microCELL TLS enables an ablation-free process that is designed to provide the edge quality needed in volume manufacturing. Laser processing on-the-fly and an innovative handling concept enable maximum throughput and yield for crystalline half cells. Simply by a laser-induced temperature gradient, a crack is guided at up to 300mm/s through the cell. Without the usual ablation, no dust or crystal defects by re-molten silicon occur. The results are higher efficiency, higher mechanical strength and better performance at highly increased throughput.

**Applications:** High-volume solar-cell cutting.

**Platform:** microCELL TLS can be installed as an in-line or stand-alone solution. The tool design allows easy access for operation and service at minimum footprint. A one-pass contactless dicing process enables high throughput of >3,800 wph on a single lane system. Options include a wafer buffer system, MES system and loading and unloading handling to customer specifications.

**Availability:** Currently available.

## SCHMID



**SCHMID optimizes PERC cell production by reducing the consumption of chemicals**

**Product Outline:** SCHMID Group is offering its 'Inline System' for alkaline texturing that provides a lower cost option for PERC cell architectures and is claimed to reduce the consumption of chemicals.

**Problem:** PERC technology improves the efficiency of solar cells by giving photons a 'second chance to generate power. However, PV manufacturers fabricating PERC cells require the smoothest possible back surface field to minimize recombination on the back of the solar cell. The surface on the front, however, should still be textured. The problem is that since both sides are textured in a batch process, the texture on the back must be removed again in a separate step. This always consumes large quantities of chemistry.

**Solution:** The SCHMID Inline System for alkaline texture provides the ability for wafers to be irrigated with potassium hydroxide and additives from the top side and textured. At the same time the process ensures a smoother back, which is followed by a polish step for a high quality surface. Instead of hydrofluoric and nitric acids that are difficult to handle SCHMID now uses an alkaline solution. The effect is lower process costs, since no polluting nitrogen oxide is produced, which is expensive to dispose of. SCHMID claims its PERC system improves efficiencies by 0.3-0.4%, based on production results by customers.

**Applications:** PERC solar cells.

**Platform:** The SCHMID Inline System for alkaline texturing contains separate chemical baths including a variety of selected chemicals for individual processing steps.

**Availability:** Currently available.

# Product Reviews

## Sentech



**Sentech provides quality control for PERC back side processing in production**

**Product Outline:** SENTECH Instruments has designed the SENperc PV for the measurement of Al<sub>2</sub>O<sub>3</sub>/Si<sub>x</sub>N<sub>x</sub> layer stacks and single films for the passivation of PERC (passivated emitter rear cell) solar cells.

**Problem:** Due to the backside of PERC cells being poorly reflective, standard ellipsometry techniques cannot be applied to characterize the Al<sub>2</sub>O<sub>3</sub>/Si<sub>x</sub>N<sub>x</sub> layers for deposition quality control. The special measurement set-up needs a highly sensitive detection unit with a special correction for the depolarization of light scattering effects, and easy-to-operate hard- and software suited for QC in the production line.

**Solution:** To make the quality control for PERC cells easier and more efficient, the SENperc system comes with recipe-based push-button operation and industrial user interface. The PERC solar cell is placed with the deposited backside on the sample table. The wafer's ID is entered and the measurement begins. No sample alignment is required. Thickness and refractive index are measured and saved to the SQL database. Statistical process control is applied to evaluate the deposition process of the PERC solar cells. Preset ranges are applied for yield analysis. Direct and long-term feedback is provided to the operator for immediate intervention.

**Applications:** Measuring thickness and refractive index of Al<sub>2</sub>O<sub>3</sub> and Si<sub>x</sub>N<sub>x</sub> films on backside of PERC solar cells.

**Platform:** The compact design of the SENperc PV combined with push-button operation and data access via LAN make the system an ideal solution for quality control of deposition processes of PERC cell manufacturing.

**Availability:** Currently available.

## 1366 Technologies



**1366 Technologies develops thin wafers with thick border to limit breakage**

**Product Outline:** 1366 Technologies has unveiled the first of a series of R&D achievements using its proprietary 'Direct Wafer' process to grow a three-dimensional wafer or a thin wafer with a thick border.

**Problem:** To decrease the amount of silicon used in PV wafers, manufacturers have long pursued methods to reduce wafer thickness. While wire sawing can be used to produce wafers thinner than the standard 180-200 micron thickness, these thin wafers can break during cell fabrication, electrical interconnection and encapsulation in modules. As such, standard industry wafer thickness has remained between 180-200 microns.

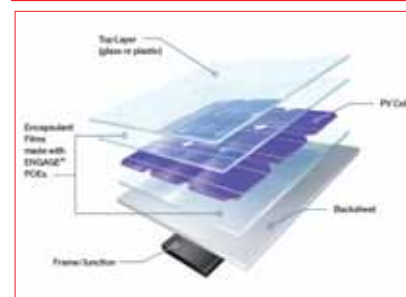
**Solution:** 1366's Direct Wafer process has the ability to locally control wafer thickness and provide standard 180-200 micron thickness in stress-critical areas such as wafer perimeter or ribs where busbar soldering will occur, while reducing thickness to 100-120 microns for the remainder of the wafer. This cuts silicon consumption to ~1.5g/W and creates a strong, thin wafer able to withstand typical manufacturing stresses. It also allows the dominant crystalline silicon PV supply chain to lower costs while leveraging its existing infrastructure.

**Applications:** Direct Wafer production of thin wafers with thick border.

**Platform:** 1366's Direct Wafer technology is a transformative manufacturing process claimed to offer significant advantages over traditional ingot-based wafer production technologies. The process makes wafers in a single step, pulling them directly from molten silicon instead of today's multi-step, energy- and capital-intensive approach, resulting in significant wafer production cost savings.

**Availability:** Under development.

## Dow Chemical



**Dow Chemical's polyolefin elastomer encapsulants improve performance and reliability**

**Product Outline:** Dow Chemical's polyolefin elastomer (POE) technology used for PV module encapsulation under its 'ENGAGE' POE brand is designed to meet the needs of PV manufacturers' demand for modules with longer energy production life and better durability.

**Problem:** PV modules have typically been encapsulated with a wide-range of ethylene-vinyl acetate (EVA)-based materials that have lower upfront costs than other forms of encapsulant. However, numerous technical studies have shown limitations of EVA in mechanical and thermal properties, water ingress and the production of acetic acid that can lead to premature module failure. More recently, studies have shown the use of EVA-based encapsulants has been linked to potential-induced degradation (PID) due to moisture ingress and other factors permeating the EVA.

**Solution:** Extensive laboratory and field testing has shown that PV modules manufactured using ENGAGE POE-based encapsulant film can achieve improved performance results in terms of increased power generation, module longevity and durability. The encapsulant film offers greater moisture resistance eliminating corrosion problems, while limiting PID issues associated with the use of EVA encapsulants. Better long-term weathering performance enables better durability and power output for the life of the module.

**Applications:** PV modules, including n-type cells, glass/glass, high power and bifacial.

**Platform:** ENGAGE polyolefin elastomers are used commercially in PV top and back encapsulants, providing improvements in PID performance, cure time, adhesion/delamination and optical transmission.

**Availability:** Currently available.

# Product Reviews

## Ecoprogetti



**Ecoprogetti's Ecosun Plus LED-based sun simulator is A+A+A+ Class certified**

**Product Outline:** Ecosun Plus is the latest innovative sun simulator with LED technology in A+A+A+ Class certified and verified by TÜV from Ecoprogetti.

**Problem:** Performing the measurement of the power and I-V curve of PV modules is important to warrant to the final customer the quality of the modules. The Ecosun Plus technology is claimed to offer reliable testing results and to guarantee to the customers a high quality power measurement.

**Solution:** LED technology has several advantages over other sun simulators, such as xenon-lamps. The LED light source offers a 40 million-pulse lifetime with no spare part costs. A calibrated pyranometer provides for accurate irradiance measurements with non-uniformity constant at less than 1% with an LED light source. The system can be provided in manual and automatic motorized versions.

**Applications:** Precise and reliable I-V curve tests of both standard PV modules and mainly for testing all new high-efficiency cell technologies, such as solar cells PERC, HIT, MWT, bifacial, back-contact and hybrid-silicon solar cells. The system can also handle CIGS solar modules, with the possibility to perform light soaking for thin-film modules.

**Platform:** Ecoprogetti's Ecosun Plus is provided with own-developed software with advanced data management features. Thanks to the traceability of every measurement and to the SQL database data storage embedded in the machine's PC or directly in customer's server, it is easily possible to store each measurement and to generate reports. The included bar code reader simplifies the testing process and data reading.

**Availability:** Currently available.

## HIUV



**HIUV develops high reflective encapsulant improving the power of a PV module**

**Product Outline:** HIUV New Materials Co has developed a high reflection rate encapsulant, 'S201W', for conventional c-Si PV modules. By adding high quality TiO<sub>2</sub> (Titanium Dioxide) and using pre-crosslinking technology, S201W is porcelain white with above 90% high light reflection rate.

**Problem:** In general the correlation between the average reflectance from a module encapsulant material and the short circuit current (Jsc) is almost linear. As a result, encapsulants with higher reflectance are necessary to improve the power of a PV module.

**Solution:** The pre-crosslinking technology in the S201W encapsulant is a similar technology used in the HIUV white encapsulant G401W for double-glass modules. By using the high reflection rate encapsulant for the bottom layer, higher conversion efficiencies are possible, compared with conventional encapsulant as more visible light can be harvested due to its high reflectivity properties. The company claims that by using S201W, a standard 60-cell module can achieve around 1.5-2.5 watts more power.

**Applications:** Crystalline silicon modules.

**Platform:** Because of the pre-crosslinking technology, there is no white colour overflow on the cell edge and ribbon in the lamination process. Lamination conditions are the same as making standard modules. In the laminator the white encapsulant faces the laminator's rubber cover. Because of pre-crosslink of S201W, the lamination time can be slightly shortened in order to improve module production throughput, according to the company.

**Availability:** Currently available.

## MBJ Solutions



**MBJ Solutions 'backend' module testing solution operates 'sunny side down' position**

**Product Outline:** MBJ Solutions has introduced a new integrated 'backend' module testing system to provide greater production line operability for PV manufacturers.

**Problem:** Micro-cracks can progress over time and lead to a significant loss in module power. Providing PV manufacturers with a high-volume, accurate testing solution in a small footprint is required to meet quality control requirements and the possibility of line integration to increase throughput and reduce the cost per watt.

**Solution:** The new backend solution combines the TÜV-certified flasher technology with a hipot and grounding test with proven electroluminescence technology from MBJ. The electroluminescence technology allows the visualization and detection of defects otherwise not visible to the human eye. Flash pulse duration of up to 200ms, long-term stability and the long lifetime of the LED light source are the main arguments in favour of the new LED sun simulator technology, compared to XENON technology. In addition to low maintenance costs, the compact layout and the 'sunny side' down transport are further benefits of the system.

**Applications:** All the traditional micro-crack module inspection steps are performed 'sunny side down' to make integration into production lines easier.

**Platform:** The fully automated inspection system includes all mandatory test procedures for the qualification of solar modules at the end of the production line. A LED A+A+A+ sun simulator, hipot and grounding test as well as a high resolution electroluminescence inspection system are combined to the MBJ Backend Solution.

**Availability:** Currently available.

# Market Watch

---

Page 13  
News

---

Page 15  
Cell technology trends  
impacting module supply in  
2017

Finlay Colville, Head of Market  
Research, Solar Media

---

13



15



## Solar yieldco model ‘flawed from the beginning’, says US bank executive

The solar yieldco business model was “flawed from the beginning” according to Santosh Raikar, managing director of renewable energy investments at State Street Bank.

Raikar cites unsustainable promises of large dividends and prolonged growth as reasons why the financing mechanism was doomed from the start – irrespective of troubles later encountered when sponsor SunEdison was unable to provide projects to its yieldcos, rendering the model tainted in the eyes of many. “The yieldco sector is fairly aligned in the sense that it has become a difficult proposition for them to raise capital in the market,” said Raikar.

In the solar industry, there is only a finite number of operating projects – and herein lies the problem, added SunLight General CEO Stacey Hughes: “If you isolate [yieldcos] where they are only making investments in solar or even only in wind, there are not enough new projects to fill the yieldcos supply that they need in order to deliver the economies of scale.

“To the extent it is limited to solar I think it is probably an unrealistic approach and I don’t think the yields that they are delivering were sufficient for either the risk they were taking or the capital they were putting up and nor were the yields reflective of the fact that these are ultimately deteriorating assets. I think the yield target was wrong for solar.”

Hughes also said that large-scale solar yieldcos would be difficult to sustain. But the structure and cost of a yieldco necessitates a high and growing volume of projects, and therefore makes it a hard-sell for solar.



Credit: SunEdison

The solar yieldco model was ‘flawed’ from the start, according to finance experts.

## Australian anti-dumping commissioner seeks to terminate investigation again

Australia’s Anti-Dumping Commission proposes to terminate its investigation into the alleged dumping of certain crystalline silicon PV modules exported from China into Australia.

The commission decided to end the original investigation in October 2015 on the grounds that the effects of dumping had been “negligible”, however, the Anti-Dumping Review Panel decided to revoke this decision and the investigation was reopened in late December 2015.

Nevertheless, once again the inquiry into dumping of Chinese modules between July 2012 and December 2013 has found that, despite uncovering evidence of dumping, the impacts were negligible.

In a public notice dated 2 September 2016, the commissioner has proposed to end the investigation and is seeking comments from interested parties. The ADRP still has the power to revoke the proposal.

Australian PV manufacturer Tindo Manufacturing lodged the original complaint in February 2014 claiming that Chinese imports had caused material injury to the Australia’s domestic solar manufacturing industry.

## Southern states to continue dominating Indian solar for two years

Around 75% of all India’s solar capacity additions in the last 12 months have been

in southern states, according to the latest industry update from consultancy firm Bridge to India.

India recently surpassed the 8GW solar deployment milestone and now stands at 8.1GW. Capacity grew by 80% over the latest 12 month period, with 2.7GW out of 3.6GW added in the south. Meanwhile, the southern state of Tamil Nadu became the country’s largest solar state by adding more than 1.2GW. Bridge to India said this was partly down to developers taking advantage of a generous feed-in tariff of INR7.01/kWh (US\$0.104/kWh).

The report finds that solar deployment is highly concentrated in just six states – Tamil Nadu, Andhra Pradesh, Telangana,

Rajasthan, Gujarat and Madhya Pradesh – which account for 80% of capacity, but only 38% of India’s overall power capacity.

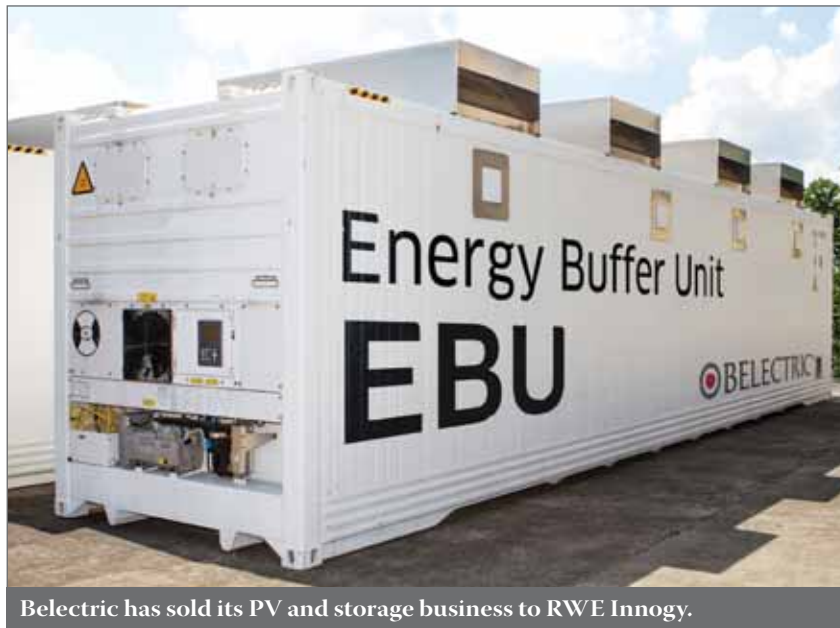
As more than half of the current 14GW solar pipeline will come up in the south, Bridge to India expects demand to weaken in these areas, although these regions will dominate additions for another two years.

Where future demand for solar will come from is now a concern for the industry with oversupply in some regions – Tamil Nadu and Rajasthan are already facing curtailments – combined with worries over grid balancing and management as the sector grows.



Credit: Welspun

Six states in India account for more than 80% of the country’s total solar capacity.



Credit: Belectric

Belectric has sold its PV and storage business to RWE Innogy.

## Americas

### Lazard erroneously undervalued SolarCity by US\$400 million in Tesla deal

Lazard, the financial advisory that advised SolarCity on its US\$2.6 billion all-stock sale to Tesla, made an error in its analysis resulting in the solar installer being undervalued by US\$400 million, according to a regulatory filing with the Securities and Exchange Commission (SEC) on Wednesday.

Lazard's analysis calculated SolarCity equity value between US\$14.75 and US\$34.00 per share, which was incorrect due to double-counting some of the company's projected indebtedness, the filing reveals.

Two weeks after the transaction was complete, Lazard realised the equity value should have been between US\$18.75 and US\$37.75 per share, with the actual purchase price Tesla paid equating to US\$25.37 per share.

The filing confirms however that both Tesla and SolarCity do not change their view of the deal regardless.

### Florida voters go big for solar in overwhelming approval of tax break

In August, 73% of Florida voters approved Amendment 4, a ballot measure that now makes solar and renewable energy equipment on commercial buildings exempt from property taxes for 20 years, beginning in 2018.

The victory, passed by a wide margin, is a big win for solar in the Sunshine State and will help propel Florida forward as a leading state in the industry. According to the Solar Energy Industries Association

(SEIA), Florida has the third-highest solar potential in the nation, but is only 14th in actual installed capacity. Until now, it has been hampered by utility-friendly solar policies and a lack of a renewable portfolio standard (RPS).

Once enacted by the state legislature, the constitutional amendment will be a big driver in lowering energy costs by reducing the tax burden that currently exists for solar equipment, according to the Amendment 4 website. Better economics for solar in Florida is set to pave the way for better solar development and a more sustainable energy future in the state.

## Europe

### RWE Innogy to acquire Belectric's solar and storage business

Innogy SE, the renewable energy subsidiary of German utility RWE, has signed a share purchase agreement to take over the solar and energy storage business of Belectric at a share price agreement in the "high double-digit million euro range".

In addition, the takeover of Belectric's utility-scale PV plants and batteries is "an important contribution to the expansion of the decentralised, renewable energy system of the future" according to RWE, who will be called innogy SE from September 2016 onwards. As well as agreeing with Belectric Holding to buy the entire PV and battery business, all related companies will now be brought into Belectric Solar and Battery Holding in order to structure the transaction, a RWE innogy spokesperson said. Further, RWE is buying out the brand Belectric, while Belectric Holding will be renamed and

will keep its real estate, OPV, automotive suppliers and electric mobility capabilities.

The acquisition means significant growth for RWE, as Belectric has built more than 280 utility-scale PV plants and rooftop solar systems with a total installed capacity of more than 1.5GWp.

### France launches 3GW solar tender

France's Ministry of Environment, Energy and Sea is launching 3GW of solar PV tenders over a three-year period.

Energy minister Ségolène Royal plans to increase the country's current installed solar capacity from 6.7GW to 10.2GW by the end of 2018, and up to 20.2GW by 2023.

The capacity up for grabs will be divided into six sections of 500MW each, with six months between each tender, meaning projects will be commissioned between the years 2017 and 2020, deliberately spread out to ensure the availability of manufacturers, installers and developers.

Bidders will be selected based on their competitiveness, carbon impacts and the environmental impacts of their proposed site location.

Successful developers will receive subsidy support in the form of "additional remuneration," as per announcements made in May this year.

French tender announcements in July also led to France being tipped to potentially become the biggest end-demand solar market in Europe.

## Middle East and Africa

### Nigeria signs first ever solar PPA

Federal government-owned public liability, the Nigerian Bulk Electricity Trading (NBET), has signed the country's first ever solar power purchase agreement (PPA) with more than 10 project developers, totalling 975MW of utility-scale solar.

As other countries across the continent make solar waves with successful auctions and feed-in tariff programmes, Nigeria had, until now, stayed relatively quiet in its solar energy ventures.

The first official project to be implemented under the 20-year PPA is a 75MW solar plant in Katsina state, to be developed by European/Nigerian utility-scale investor and developer Pan Africa Solar, in collaboration with JCM Capital, an Ontario-based developer.

The commissioning of the Katsina project represents a giant step forward for Nigeria's solar progress, constituting the largest plant of its kind in Sub-Saharan Africa, excluding South Africa.

# Cell technology trends impacting module supply in 2017

Finlay Colville, Head of Market Research, Solar Media

Market Watch

Fab & Facilities

Materials

Cell Processing

Thin Film

PV Modules

## ABSTRACT

The rebound in solar cell capital expenditures during 2015 and 2016 has resulted in strong capacity additions and upgrade spending that is set to redefine the technology landscape in 2017 and beyond. Within this however is a broad range of drivers, impacting the mix of n-type and p-type cells produced, in addition to the various strategies employed to increase cell efficiencies while reducing overall blended manufacturing costs. Coupled with the various module types being selected within the key global end markets, and the balance between effective capacity and market demand, 2017 is forecast to see a range of approaches adopted by cell producers, with technology differentiation becoming increasingly important across the entire industry.

Historically, when the solar industry has gone through previous overcapacity cycles, the outcome has been characterized by surviving cell manufacturers prioritizing cost reduction as the key metric to focus on, in order to restore manufacturing gross margins to acceptable mid-teen percentage levels. At the same time, process optimization and yield enhancements have also been targeted, often being the driving force behind efficiency improvements.

This was seen last in the solar industry back in 2011-2012, while at the same time some of the more speculative challenging technology approaches (largely coming from thin-film variants) were removed from the manufacturing landscape going forward.

During this previous overcapacity phase in the industry, few companies (with the exception of SunPower and First Solar) elected to perform process flow changes that would see stepwise cell improvements.

As we move into the final quarter of 2016, once again we are confronted by a cell and module overcapacity situation. However, in contrast to 2011-2012, the industry is already in the midst of process flow changes to both p-type mono and multi technologies. This is creating new benchmarks for cell producers to reach in order to stay competitive and will ensure that 2017 sees continued investments into process flow changes, despite any significant levels of new cell capacity being required to be brought online.

This article reviews the main cell technologies that are likely to become industry-standard by the end of 2017, highlighting the leading companies that are pivotal to the competing upgrade paths coming to fruition during the year. In addition, a short-term roadmap is presented that reflects the dominant mainstream supply of p-type mono and multi cells to the market.

The basis of the forecasts comes

directly from a three-month research phase that overlapped with a series of interviews with the technical advisory board for the forthcoming PV CellTech conference in Penang, Malaysia on 14-15 March 2017. The findings are supplemented here by data and graphics derived from the October 2016 release of the PV Technology & Manufacturing Quarterly report from Solar Media, publisher of *Photovoltaics International*.

## The interplay between effective capacity, capex and market demand

Underpinning the need for new cell capacity is primarily the balance between effective cell capacity and end-market demand. Adding to this are the various aspirations of component manufacturers to increase market share, and the impact of trade-barrier restrictions (mainly into the US market) on manufacturing cells and modules in China and Taiwan.

The overcapacity phase of the industry

during 2011-2012 was largely corrected during 2013 and 2014, with limited capex being allocated by cell manufacturers. This saw the effective-capacity/market-demand balance restored by the end of 2015, with the growth in demand being the main driver for this change. In 2015, effective cell capacity was approximately 15% above end-market demand, representing a relatively healthy situation.

However, during 2015 and 2016, there has been a significant uptick in cell capex that has caused the overcapacity factor to rebound and will approach 25% during 2017. This dynamic is largely behind the current cell overcapacity situation that is impacting the industry today and is likely to continue to at least the end of 2017. This is illustrated clearly in Figure 1.

## Competition within mainstream p-type cell manufacturing

In contrast to other solar technology roadmaps that are offered to forecast



Wafer cost reduction looks set to become an increasingly important driver for manufacturers going into 2017.

Credit: SolarWorld



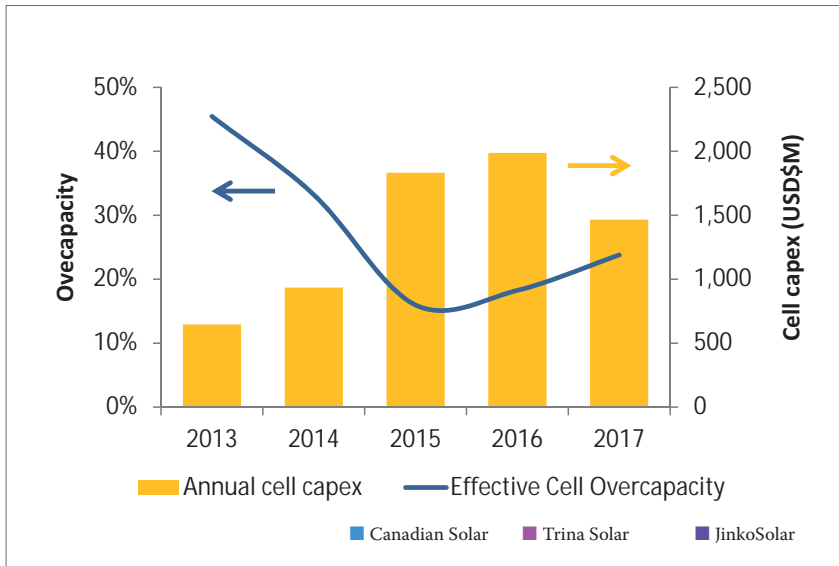


Figure 1. Effective cell overcapacity declined from over 40% in 2013 to a more acceptable level of approximately 15% in 2015, but will rebound to 25% in 2017 following the cell capex uptick in 2015 and 2016 that was above end-market growth requirements. Source: Solar Intelligence, Solar Media.

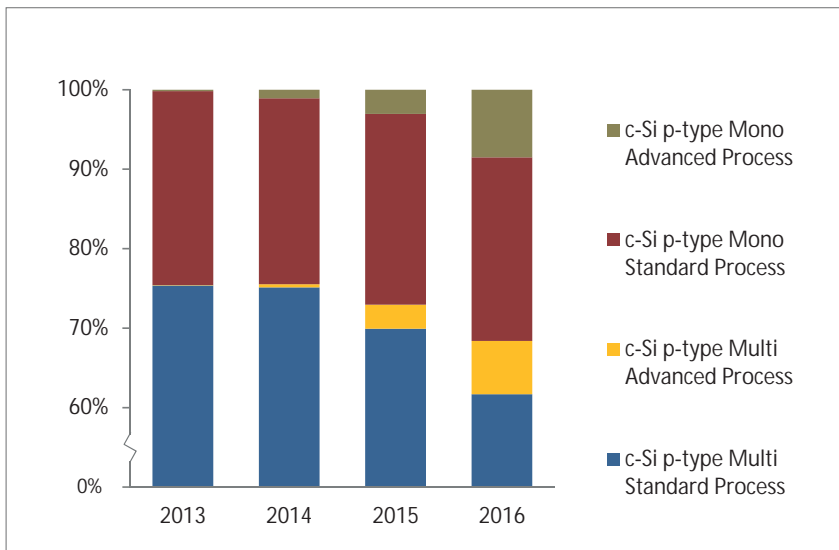


Figure 2. During 2015 and 2016, p-type mono has seen modest market-share gains, compared to p-type multi that was contributing about 75% of p-type market demand in 2013. Each of p-type mono and multi have seen process flow changes to advanced process flow options, with PERC the leading candidate until now. Source: Solar Intelligence, Solar Media.

trends in manufacturing, we use a different means of isolating the key drivers today. This is done by effectively removing all thin-film approaches, in addition to n-type cell manufacturing.

While thin-film and n-type manufacturing are, of course, fundamentally different in nature, the strategies adopted by the various companies producing these type of modules can be grouped together, and isolated from the dominant (90%-plus) market share that p-type cell production commands in the industry.

The companies in question, comprising thin-film and n-type production, are mainly First Solar, Solar Frontier,

SunPower, Panasonic and LG Electronics. Today, these companies have very different strategies to all other module suppliers that are focused on p-type silicon.

Therefore, we can largely focus on the legacy mono versus multi share trends for p-type and how each of these variants is undergoing productivity enhancements to increase cell efficiency levels. Figure 2 shows the market share trends of mono and multi cell production, specific to p-type supply during 2013 to 2016.

During 2016, we can see several drivers behind the mono versus multi changes for p-type cell production. Before looking at the advanced cell gains, the overall shift

to mono can largely be traced back to the aggressive upstream ingot/wafer capacity expansion plans from LONGi Silicon.

Focused specifically on mono wafer supply, and now incorporating its subsidiary LERRI Solar for cell and module production, LONGi has driven the supply of mono wafers more than any other mono wafer supplier to the industry until now. Benefiting also from low-cost manufacturing, LONGi has now evolved into the leading supplier of mono wafers to the solar industry, growing its share of p-type mono wafers from approximately 10% in 2013 to more than 30% during 2016, with upside to reach almost 40% during 2017 if expansions continue next year as planned. This is shown in Figure 3.

The timing of LONGi's expansion plans is also significant. Currently, the leading end market for solar demand is China, and this country has established a dedicated demand portion (under the banner of Front Runner) that demands high-efficiency module supply. This has created an uptick in mono module supply, in contrast to p-type multi modules that were dominant in the country during its early growth phase.

Another factor for LONGi's success can be seen with the convergence of mono and multi wafer pricing recently, caused in part by the production excess created by LONGi's ramp, but also reflecting an inevitable pricing equivalence that allows cell makers to decide upon wafer supply (mono versus multi) based largely on pricing alone.

The final driver for increased mono adoption has been coming from the relative ease with which Asian p-type cell manufacturers have been able to upgrade mono cell lines to incorporate passivated emitter rear contact (PERC) based technologies. Coupled with the challenges in upgrading p-type multi lines to PERC, this has ensured that mono has not only caught up with multi this year, but is challenging to gain more market share next year.

### What next for p-type multi?

In looking at p-type multi cell production, again we cannot decouple wafer supply from cell production. In fact, the link between ingot-to-cell stages for p-type multi is more important than for p-type mono, based on the requirement of multi wafer quality to be aligned to cell process flow changes.

When viewing the development of p-type multi in this way, it is important to highlight the role of GCL Poly as analogous to that of LONGi for mono wafer supply. GCL Poly was largely responsible for multi retaining market-share levels of 75% back in 2013, and if multi is to see a resurgence it is hard to



MEYER BURGER

# Meyer Burger congratulates Solar Impulse

Clean technology pioneers Bertrand Piccard and André Borschberg have successfully completed the first ever round-the-world solar flight in Solar Impulse. Meyer Burger warmly congratulates them and the entire Solar Impulse crew on their ground-breaking achievement.

Meyer Burger is very proud to have provided the cutting edge premium cell connection technology to connect the over 17,000 high-efficiency solar cells to the 269.5 m<sup>2</sup> wing panel of the Solar Impulse airplane, enabling the collection of up to 340 kWh of solar energy per day.

Meyer Burger's innovative strength is enabling tomorrow's energy solutions.

[www.meyerburger.com](http://www.meyerburger.com)

---

“The sun and cutting-edge technology can indeed achieve what some consider impossible”

Bertrand Piccard & André Borschberg, co-founders of Solar Impulse



**SOLARIMPULSE**

[www.solarimpulse.com](http://www.solarimpulse.com)

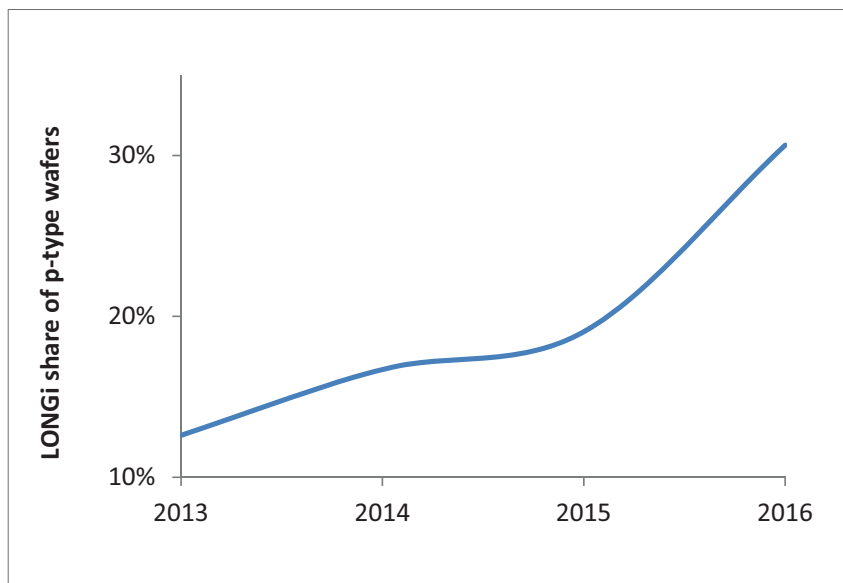


Figure 3. LONGi Silicon has increased its share of p-type mono wafers to more than 30% in 2016, with 2017 likely to grow to almost 40%, following an aggressive and highly-focused strategy to become the leading supplier of mono products to the solar industry. Source: Solar Intelligence, Solar Media.

see how GCL Poly's wafer strategy can be decoupled.

While LONGi has a clear strategy to focus on mono, GCL Poly (and also that of its affiliate GCL Systems Integration for cell and module manufacturing) has been somewhat dabbling in other solar technologies, all the way from polysilicon supply (by virtue of its attempts to move into FBR production) through to cell manufacturing (plans for n-type bifacial, n-type heterojunction, p-type mono PERC, and p-type multi black silicon).

Indeed, at the ingot/wafering stage, GCL Poly had for some time been presenting an internal roadmap that suggested increased cast-mono and mono pulling adoption, to complement its core strengths in p-type casting and multi wafer supply to the industry. However, in recent weeks, the company appears to have reprioritized p-type multi wafering, with suggestions that large-scale deployment of diamond wire sawing could be implemented.

While such a move by GCL Poly would be significant for p-type wafer supply – and subsequent developments in 2017 at p-type cell production generally – it does still contradict the midstream strategy of GCL Systems Integration. Nonetheless, the drivers here are highly significant, in terms of introducing diamond wire sawing (previously confined to mono wafer slicing) for p-type multi wafering.

The background to this claim can be framed as follows. With PERC being the industry's chosen candidate for p-type efficiency enhancements, and set against a backdrop of Hanwha Q-CELLS and REC Solar having effectively solved the multi-PERC manufacturing challenge, many cell producers in Taiwan and China went

through a phase of thinking that multi-PERC would simply follow mono-PERC as the upgrade path for p-type multi cell production.

This roadmap did not come to fruition for p-type multi PERC in Taiwan and China, leaving p-type multi without a clear upgrade path in 2017, and at risk of being left behind in an environment where LONGi was increasing supply of p-type mono wafers at near multi-wafer price equivalence. So what was left for multi cell producers?

The answer to this question may well reside in a dual approach by multi ingot/wafer suppliers and multi cell producers, whereby the cost reductions that are characteristic of moving to diamond wire sawing are implemented for the multi segment. However, this now requires that both wafer suppliers and cell producers are fully aligned in solving the upgrade path, previously held back by the requirement to change front-side texturing of multi cells.

This is where the so-called black silicon cell processing emerges today. Previously, black silicon was a term given to highly complex, largely lab-based, texturing methods that created a black absorber surface on the cells, thereby enabling passivation layer deposition to be optimized in isolation from its current dual role in depositing an anti-reflection coating onto the solar cells.

Now, black silicon is being used as the term that describes an etching process (either dry or reactive ion etching, or metal-assisted chemical etching) that provides the correct front-end step needed when using p-type wafers, sliced using diamond wire saws.

This route would appear to be

emerging as the next upgrade path for p-type multi wafering and cell production, with wafer cost reduction being the dominant driver, as opposed to the incremental efficiency changes seen in resulting cell production. However, by focusing on this approach, it also buys p-type multi cell producers time to work out how properly to implement multi-PERC upgrades.

Therefore, in looking at a simplified p-type multi cell roadmap going forward, we may see the remainder of 2016 and the whole of 2017 as a period where diamond wire sawing becomes standard for p-type multi wafers, and cell lines are upgraded at the front-end texturing stage. Then, in 2018, multi-PERC could be reintroduced as the next upgrade step for multi. Combined, these two improvements would help multi to see both strong cost reductions and efficiency gains that now appear to be essential to stop mono supply seeing more market-share gains.

## Topics to dominate PV CellTech in March 2017

By the time we get to March 2017, and the second PV CellTech conference in Penang, Malaysia, it will be much clearer what has been achieved by multi wafer/cell production, and also how this is reflected in wafer ASPs and average cell efficiencies using the new front-end texturing tools. Whether the industry manages however to be aligned on multi wafer and cell roadmaps does remain to be seen, with the track record here not particularly impressive.

If multi does rebound in this way, it will largely be done as a result of LONGi's threat in terms of changing the status quo within p-type wafer supply. Either way, LONGi is almost certain to go from strength to strength, becoming a more dominant factor in mono versus multi in the market today than the cell manufacturers that have traditionally been regarded as the key instrument of change when compiling technology roadmaps for future market share trends.

### About the Author



**Finlay Colville** joined Solar Media in June 2015 as head of the new Solar Intelligence activities. Until October 2014, he was vice president and head of solar at NPD Solarbuzz. Widely recognised as a leading authority on the solar PV industry, he has presented at almost every solar conference and event worldwide, and has authored hundreds of technical blogs and articles in the past few years. He holds a BSc in Physics and a PhD in nonlinear photonics.

# Fab & Facilities

---



20

Page 20  
News

---

Page 22  
PV manufacturing capacity  
expansion announcement  
plans and analysis for 1H  
2016

Mark Osborne, Senior News Editor,  
Photovoltaics International

---



22

## Canadian Solar revises capacity expansion plans for third time in 2016

Canadian Solar has made a third major revision to its planned manufacturing capacity expansion plans for 2016, while reiterating previously guided PV module shipments and revenue for the year.

Canadian Solar said in reporting second quarter financial results and subsequent earnings call that it was revising its cell manufacturing nameplate capacity expectations for the end of the year, primarily due to the impact of tornado damage at its JV solar cell factory in Funing County, Jiangsu Province, in June 2016.

The Funing facility will be out of action until the first quarter of 2017, with volume production back on line in the second quarter. The Funing plant would have added a further 500MW of capacity by July 2016 to reach a nameplate capacity of 1GW.

As a result, Canadian Solar expects in-house cell capacity to reach around 3.05GW by the end of 2016, compared to the last revision expectation of 3.9GW.

Canadian Solar also noted that it would be curtailing PV module capacity expansions due to the threat of overcapacity, increased ASP declines and an overall industry downturn. Management noted that keeping strong control of module inventory would be a key strategy during this period. Canadian Solar said that it expected in-house module capacity to reach 5.8GW by the end of year, instead of previous guidance of 6.43GW.

In contrast to the curtailment of capacity expansions in solar cell and module assembly segments, Canadian Solar highlighted that its multicrystalline wafer manufacturing capacity was expected to reach 1.3GW by the end of 2016, up from previous guidance of reaching 1GW by year end.



Credit: Canadian Solar

Canadian Solar has revised its capacity expansion plans for the third time this year.

### Capacity expansions

## Global PV manufacturing capacity expansion announcements in April close to 9GW

Analysis of global PV manufacturing capacity expansion announcements in April 2016 by *Photovoltaics International* sister website, PV Tech, revealed nearly 9GW of planned future expansions of thin-film modules, solar cells and module assembly production, up from over 7.3GW in the previous month and the third consecutive monthly increase.

Total planned expansions reached 8,935MW in April, which included thin-film modules, dedicated crystalline silicon solar cells and dedicated module assembly, but no integrated solar cell and module assembly.

In contrast to the previous month, when several manufacturers announced further capacity expansions to meet expected global demand in 2016, April was characterised by new entrants and small-scale module manufacturers.

Dedicated solar cell capacity expansions announcements reached 3.75GW in April, compared to 3.1GW in March. The increase was primarily driven by new entrant, Mundra Solar PV Ltd, a new subsidiary of India-based Adani Enterprises.

Overall, April has followed the previous months of 2016 with a relatively balanced number of solar cell and module assembly expansions, while total MW capacity announcements have remained at higher intensities than in 2015, excluding the months of May and November in 2015.

## PV manufacturing capacity expansion announcements fall significantly in May

Global PV manufacturing capacity expansion announcements in May 2016 fell significantly for the first time this year.

May revealed just over 4GW of planned future expansions of thin-film module, solar cell and module assembly production, as well as fully integrated (wafer/cell/module) new capacity, compared to nearly 9GW of planned future expansions in the previous month.

The decline ends a strong consecutive monthly increase since February, 2016, which was around 50% higher than in the same period in 2015.

A total of seven companies announced expansion plans in May, compared to 13 in April.

There was an absence of any silicon-based capacity expansions being announced in China, although Canadian Solar and Hareon Solar were responsible for small capacity expansion plans in Southeast Asia and Morocco, respectively.

### Emerging markets

## ABB India doubles inverter manufacturing capacity with new facility

Inverter manufacturer ABB India, a subsidiary of global technology firm ABB, has opened a solar inverter manufacturing facility in the southern city of Bangalore, Karnataka, which doubles the firm's capacity in the country.

The new factory manufactures ABB's PVS800 central inverter series, which the company claims has proven popular in India due to ease of commissioning and reliable performance in some harsh environments.

ABB began manufacturing solar inverters in India with its Bangalore factory in 2012, with inverters ranging from 2kW to 2MW. ABB said these inverters manufactured at Nelamanagala already help to deliver 40% of the energy from utility-scale PV plants in the country. Of India's more than 8GW installed PV capacity, 6.5GW use ABB inverters.

## Canadian Solar and Flextronics partner on 360MW module factory in Brazil

Chinese solar firm Canadian Solar and OEM giant Flextronics are working together on an US\$80 million module

manufacturing facility in Sao Paulo, according to the Brazilian Solar PV Association, Absolar.

The plant, to be located in Sorocaba in the state of São Paulo, will create 400 direct jobs and is expected to start producing modules this year.

This is Canadian Solar's first factory in Brazil. In May the firm reported that its utility-scale solar PV project pipeline in Brazil stood at 384MW, having won capacity in the various Brazilian solar auctions over the last two years.

In May, NEXTracker, which is now owned by Flextronics, received certification for compliance with Brazilian domestic content rules for its manufacturing operations.

### Solar in JV to build 160MW cell and module plant in Morocco

Hareon Solar has recently signed an MOU with partners to build and operate a 160MW cell and module plant in Morocco with a total investment of around US\$114 million.

Moroccan general contractor Jet Contractors, which issued a statement on the JV signing in May, will build the facilities and will hold a 40% stake in the new business, alongside a 40% stake held by Hareon Solar. Investment and management firm, System Industry Electronic Holding AG (SIE) will hold a 20% stake.

Included in the agreement as a first phase of the plan is the establishment of a 30MW module assembly line and obtaining international certifications for the modules. The plant is expected to ship modules to projects in the region and overseas.

#### New ventures

### Linde opens R&D facility in Taiwan on South East Asia solar manufacturing growth

Electronic gases specialist, Linde, has established a new R&D facility in Taiwan to better serve the growth in solar cell manufacturing capacity expansions in Southeast Asia.

Operated by Linde Electronics the new facility is located Taichung, Taiwan and was officially opened on 1 September 2016 and is designed to provide advanced analytical processes and quality control systems for a wide range of materials required in the electronics and PV sectors.

In 2016, Linde has secured a number of key gas and chemical supply wins from leading solar cell manufacturers in Southeast Asia.

Linde also noted that it would be



Credit: Solar Frontier

Solar Frontier has begun production at its new 150MW CIS plant at Tohoku, Japan.

entering into a collaboration agreement with the Industrial Technology Research Institute (ITRI) in Taiwan.

### JA Solar plans major capacity expansion in Vietnam

According to Vietnam news reports, JA Solar is planning to invest between US\$300 million and US\$1 billion of building a PV manufacturing hub in Song Khe-Noi Hoang Industrial Park, Bac Giang Province, Vietnam. OEM module manufacturer Boviet Solar is also based at the same industrial park.

### Seraphim obtains CSA certification for US module assembly plant, weighs new manufacturing locations

Seraphim Solar Manufacturing has said its US assembly plant had received the "Witness Laboratory Accreditation Certificate" (WMTC) authorized by CSA Group, which meant the facility in Mississippi had officially become a CSA-accredited witness laboratory. Seraphim currently has a global capacity of 1.9GW (1.6GW in Changzhou, China) and 300MW entering production in the US.

In addition, Justin Xi, executive general manager at Seraphim Solar, revealed at Intersolar Europe that the company was looking at another production plant outside of China, while Mexico had multiple benefits. Chief among these are the cost advantages paired with the ease of access to both the North and South American markets.

The company praised Mexico as both an end market and a potential production centre.

### Solar Frontier starts production at 'advanced' 150MW facility

Solar Frontier has begun commercial production at its new 150MW plant in Tohoku.

The facility will cut one third off the cost of its modules, on track with the company's stated goal for the plant when it was announced in 2014. According to Solar Frontier, the "advanced" manufacturing plant can produce its CIS modules for two-thirds of the cost, with two-thirds of the manpower and in one third of the time, when compared to its flagship 900MW Kunitomi plant.

It is looking to push the output of modules from the plant past 180W. The first products from the new facility will go on sale in Japan this summer.

### Daqo's polysilicon Phase 3a expansion said to be on track

China-based polysilicon and multicrystalline ingot/wafer producer Daqo New Energy was said to be on track to complete its Phase 3a polysilicon plant expansion and full ramp-up by mid-2017, according to ROTH Capital analyst, Philip Shen.

Shen said in an investor note that a recent visit to Daqo's facilities, confirmed the 6,000MT polysilicon production expansion was 'well underway' and would be fully financed via bank loans, with capital expenditure requirements of around US\$90 million to US\$100 million.

Upon completion and ramp-up, Daqo would have a polysilicon nameplate capacity of around 18,000MT. Shen also noted that Daqo had the lowest polysilicon production costs across the sector with a GAAP cost structure of US\$9.65/kg and cash cost of US\$7.62/kg in the first quarter of 2016.

# PV manufacturing capacity expansion announcement plans and analysis for 1H 2016

Mark Osborne, Senior News Editor, Photovoltaics International

## ABSTRACT

In this quarterly report of global PV manufacturing capacity expansion announcements in the first half of 2016, key analysis is given on the continued high level of activity through the second quarter of the year. This report also includes a new bottom-up analysis of 'effective' capacity expansions since the beginning of 2014 to provide a better and more accurate assessment of the current manufacturing environment.

## April 2016

The scale and intensity of global PV manufacturing capacity expansion announcements since November 2015 led to numerous enquiries and subsequent updates to previous preliminary monthly reports, first posted on Photovoltaics International's sister website, PV-Tech.org.

Unlike past checks, whereby only small updates to monthly and subsequent quarterly and half-yearly analysis were required, preliminary

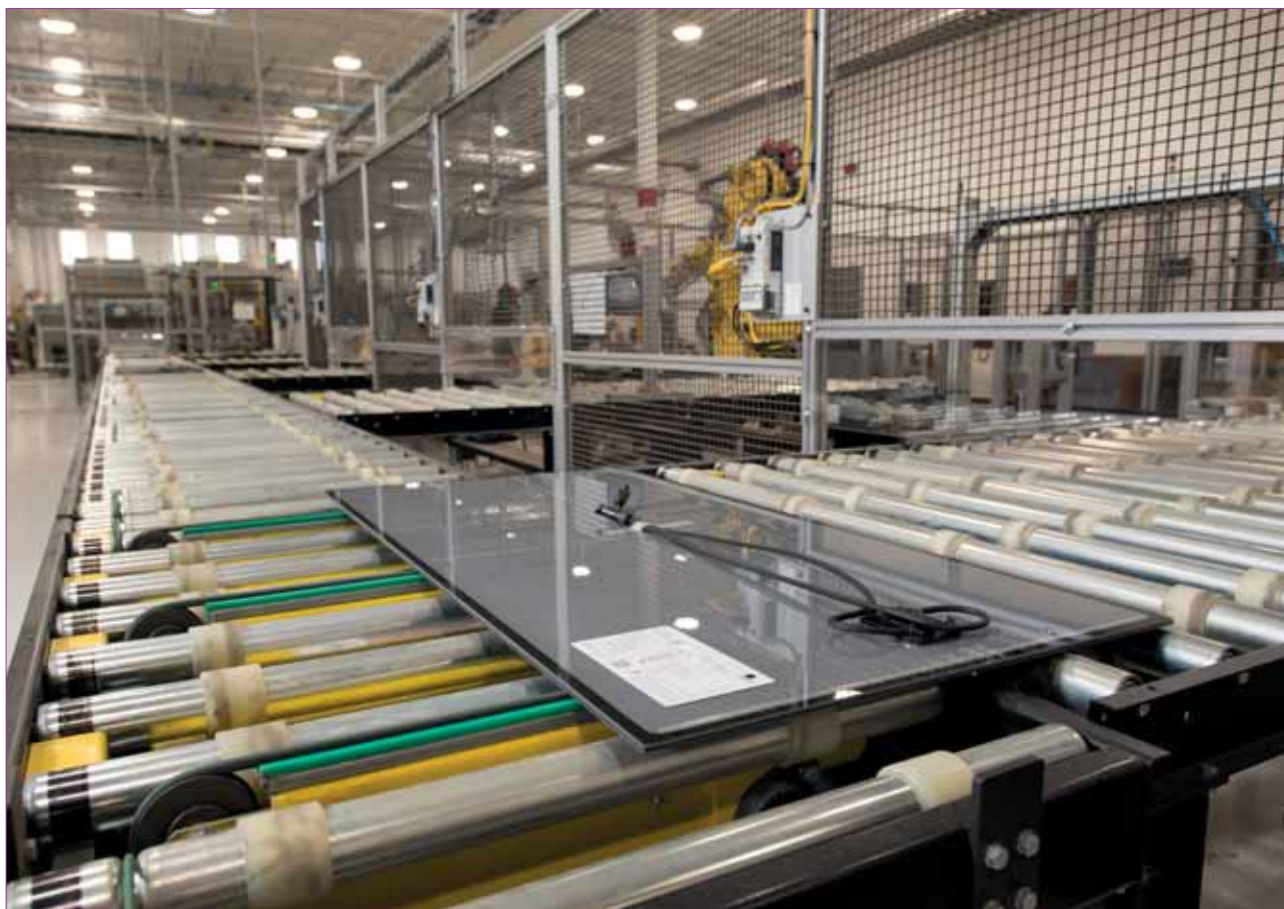
monthly reports since February 2016 have undergone major revisions.

PV Tech's preliminary analysis of expansion announcements for April 2016 indicated nearly 9GW of planned future expansions of thin-film modules, solar cells and module assembly production, up from over 7.3GW in the previous month and the third consecutive monthly increase. Preliminary, total planned expansions reached 8,935MW. However, revised figures show that a further 1GW

of announcements were made in April, bringing the combined total to 9,935MW.

Revised dedicated solar cell capacity expansions announcements reached 4.25GW in April, up from 3.75GW in preliminary findings. This was down compared to revised March figures, which reached 6.55GW, up significantly from preliminary figures of 3.1GW in March 2016.

The increase in March figures was primarily due to updated information



Plans for new thin-film manufacturing capacity have featured in the most recent round of capacity expansion announcements

Credit: First Solar



# BiN Solar Cells

- BiN solar cells utilise long lifetime n type materials with a bifacial structure to achieve high efficiency
- Glass-glass modules with BiN solar cells can generate more electrical power by using both sides
- Glass-glass modules have better reliability, more stability and a longer life cycle
- Excellent LID-free and PID-free features
- Superior appearance, perfect for BIPV and other applications



# Hipro Solar Cells

- Advantage of rear side passivation technology, significantly improving solar cell efficiency
- 240MW production capacity with average solar cell efficiency greater than 20.8%
- Higher power output modules, satisfying the demands of high-end markets all over the world

中利腾晖官方微信



扫一扫 与我们互动

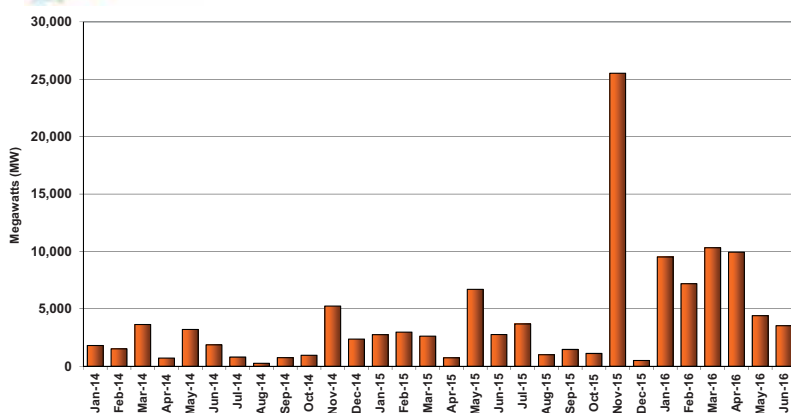
Zhongli Talesun Solar Co., Ltd.

**E:** sales@talesun.com | **W:** www.tailesun.com | **T:** +86 512 8235 5888 | **F:** +86 512 8235 5588





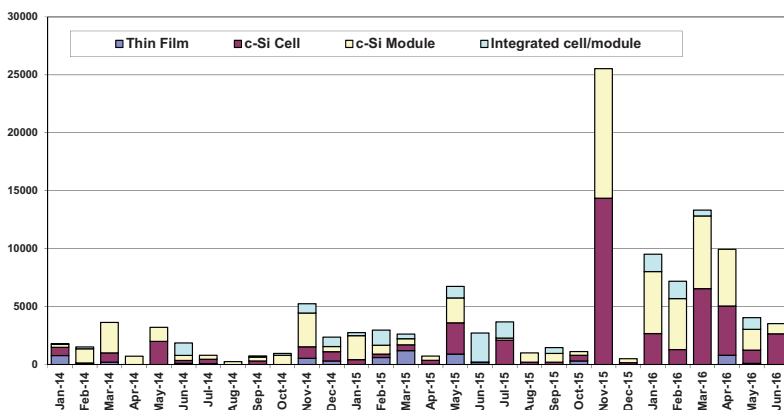
Combined Total (c-Si Cell, Module & Thin Film)  
Expansion Announcements by Month (MW)



Combined total expansion announcements (c-Si cell, module & thin film) by month (MW)



Capacity Expansion Announcements by Product Type Monthly (MW)



Capacity expansion announcements by product type, monthly (MW)

on expansions plans by provided by Risen Energy and Vina Solar in Vietnam. The increase in April's figures, meanwhile, was primarily driven by confirmations to PV Tech by new entrant, Mundra Solar PV Ltd, a new subsidiary of India-based Adani Enterprises.

Having initially sought manufacturing partnerships, including an integrated multi-gigawatt operation with SunEdison that included polysilicon, modules and downstream PV power plant development, Adani is currently establishing its own operations.

First-phase plans include 1.2GW of multicrystalline and monocrystalline solar cell and module assembly,

including 900MW multi-c-Si cell, 200MW of mono-c-Si PERC production and 100MW of bifacial production. Mundra Solar plans to start initial production in October 2016. Plans also include a further 1.8GW of cell and module production at facilities being built in Mundra, Gujarat, India.

Revised dedicated module assembly capacity expansions announced in April reached 4.85GW, up from preliminary figures of 4.38GW. However, revised March figures of 4.88GW, up from preliminary figures of 3.7GW, again indicated the intensity of planned expansions but were actually lower month on month.

Aside from Mundra Solar's

ambitious plans, April generated announcements from module manufacturers in Taiwan, China and India. However, the second largest module assembly announcement in April was by German distributor CS Wismar, which revealed plans to restart module assembly operations at the former Sonnenstromfabrik facility in Wismar, Germany. This was previously owned by Centrosolar, whose bankruptcy in 2014 rival module manufacturer, Solar-Fabrik acquiring the facility in July, 2014. However, Solar-Fabrik itself went bankrupt in February 2015.

CS Wismar said the manufacturing facility had a capacity of around 525MWp and would primarily offer OEM services for companies focused on the fast-growing US market.

Breaking a sixth consecutive month of zero thin-film module production expansions, laser systems specialist LPKF Laser & Electronics said it had secured a major systems order from an unnamed customer within the PV thin-film manufacturing sector. With limited thin-film activity, only two customers are likely, First Solar and Avancis. However, the size of the LPKF order indicates it relates to First Solar and the upgrade of 800MW of mothballed capacity from the closure of its two production plants in Germany a few years ago.

### Geographical split

With the absence of 'Silicon Module Super League' members and the confirmed plans of Mundra Solar, India accounted for 6.1GW of total new capacity expansion announcements in April.

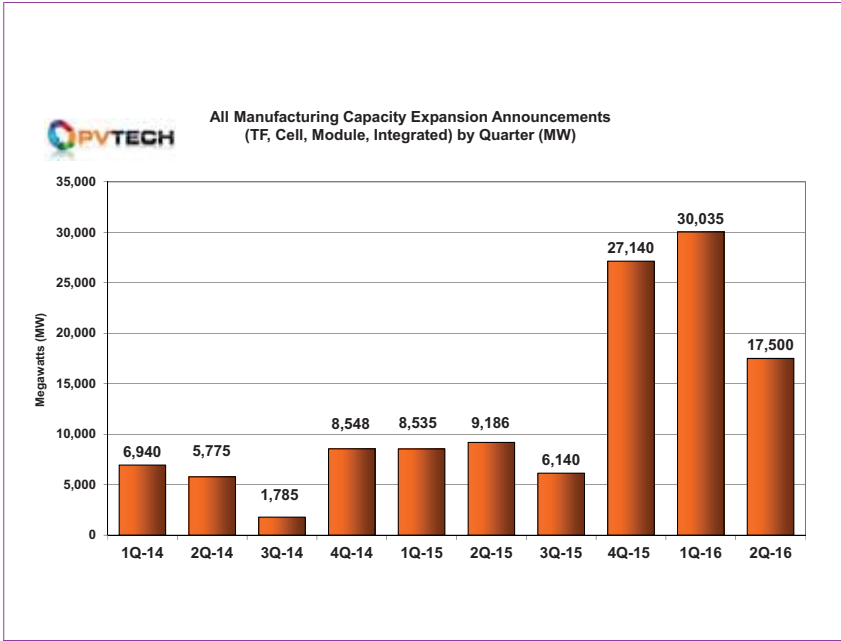
Purely from a capacity expansion announcement perspective, India became the second largest to China in 2015 with over 7.8GW of manufacturing plans, and with the Mundra Solar plans India remains a key potential emerging manufacturing market.

With a planned 200MW of solar cell expansions at TS Solartech, Malaysia accounted for 1GW of the total announced in April, should the First Solar equipment mothballed in Germany, head for Malaysia.

In the last two years to April 2016, Malaysia saw over 3.6GW of new capacity announcements and Thailand 2.3GW, confirming Southeast Asia's growing importance as a PV manufacturing hub.

A lull in China announcements led to only two companies planning capacity expansions, which totalled only 600MW.

Overall, April followed the



All manufacturing capacity expansion announcements (thin-film, cell, module, integrated) by quarter (MW)

new plans and a significant slowdown of over 58%, compared to the previous month.

The absence of major expansions from the SML members and some China-based manufacturers cautiously extending their footprints outside China kept overall planned capacity expansions low, relative to the previous months of 2016.

This also resulted in the absence of any silicon-based capacity expansions being announced in China, although Canadian Solar and Hareon Solar were responsible for small capacity expansion plans in Southeast Asia and Morocco, respectively.

Several speculative announcements were also made in May, including big ambitions in Iran and India, though initial expansion phases were small and did not carry timelines to execution. Discounting these plans, announcements slumped by around a further 2GW in May.

Dedicated solar cell capacity expansions totalled 1.14GW in May, which included a 160MW expansion of monocrystalline capacity in South Korea by Shinsung Solar Energy. Dedicated PV module capacity expansion announcements reached 1.8GW.

The most meaningful capacity

previous months of 2016 with a relatively balanced number of solar cell and module assembly expansions, while total MW capacity announcements have remained at higher intensities than in 2015, excluding the month of November in 2015.

**May 2016**

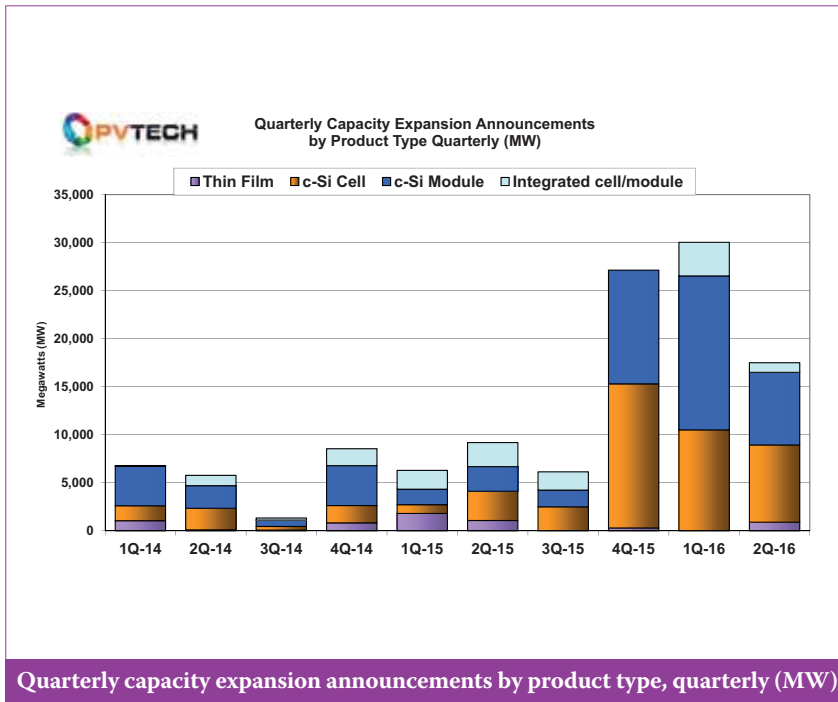
The month of May 2016 was a key point in time for global PV manufacturing capacity expansion announcements as not only were revisions very small, but the month also revealed only 4.04GW of total

**KUKA**

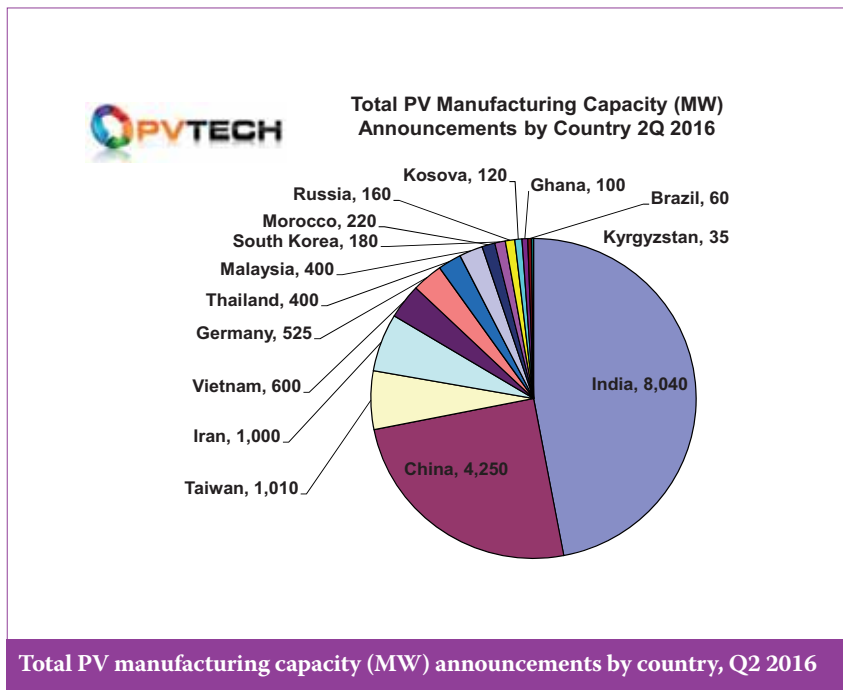


**Innovation**  
Made by KUKA Industries

- Planning and Engineering
- Laser and Arc Welding Solutions
- Magnetarc and Friction Welding Systems
- Casting Technologies
- Automated Production Solutions
- Customer Services



Quarterly capacity expansion announcements by product type, quarterly (MW)



Total PV manufacturing capacity (MW) announcements by country, Q2 2016

announcement made in May was that of Taiwan-based PV manufacturer Neo Solar Power (NSP), which announced the closure of an existing 60MW assembly plant in Taiwan but a 500-600MW new expansion in Vietnam.

Vietnam has rapidly emerged to become an alternative destination for module assembly by China and Taiwan-based PV manufacturers with meaningful solar cell production expected to follow in due course.

The fully integrated (200MW to 1GW) planned new build in Iran was announced by the Industrial Development & Renovation Organization of Iran (IDRO) and turnkey equipment supplier, SCHMID Group.

An announcement made at SNEC 2016 marked the second consecutive month of CdTe thin-film expansions (100MW), led by a consortium of China-based firms and Western equipment suppliers. This was the only announcement of capacity expansions in China in May.

#### Geographical split

With China only contributing one 100MW expansion plan in May, the majority of announcements were centred on Southeast Asia. Three companies planned expansions in the region totalling almost 1,200MW.

This was followed by India and one company planning an initial 120MW

of module capacity plans over the next five years to add 500MW of wafer production, 600MW of solar cell and reach 840MW of module assembly by 2021.

However, the Middle East and North Africa region emerged from a long lull in planned expansions, with Morocco and Iran contributing a total of nearly 1,200MW. Europe, North America and Latin America were not represented with new expansions planned in May.

#### June 2016

The month of June confirmed a second consecutive month of announcement declines. The month had a total of 3.52GW of planned capacity expansions, compared to 4.04GW in May, around a 12% decline, following a 58% decline in May.

Unlike the previous month, when a speculative announcement in May was made for 1GW of integrated c-Si capacity in Iran, June proved to better represent the slowdown underway.

Preliminary dedicated solar cell capacity expansions in June totalled only 960MW. However, updated information primarily from GCL Systems pushed the figure much higher to 2.65GW. Other notable solar cell expansions in June were made by Taiwan producers, Gintech and Motech, following announcements from several other cell producers in Taiwan in both May (Solartech & NSP) and April (TSEC).

Dedicated PV module capacity expansion announcements in June were significantly below dedicated solar cell plans at 875MW, compared to 1.8GW in May. There were no thin-film or integrated PV manufacturing capacity expansion announcements made in the month.

#### Geographical split

Without the 1.85GW of solar cell expansions by GCL Systems, which included a planned 250MW n-type monocrystalline heterojunction solar cell line, China-based expansions would have been negligible.

Once again, Southeast Asia (Taiwan, Thailand and Malaysia) attracted more plans: a combined total 800MW of planned expansions, compared to 1.2GW in May 2016. The small balance was made up from Russia, Kosovo, Brazil and Kyrgyzstan.

#### Q2 2016 analysis

With revised figures included for both the first quarter and second quarter of 2016, it is clear that total capacity expansions since the fourth quarter

of 2015 have been significantly higher than at any period since the first quarter of 2014.

Total combined expansions in this nine-month period have exceeded 74.5GW. In comparison, total expansions from the first quarter of 2014 through the third quarter of 2015 (21 months) only reached around 47GW.

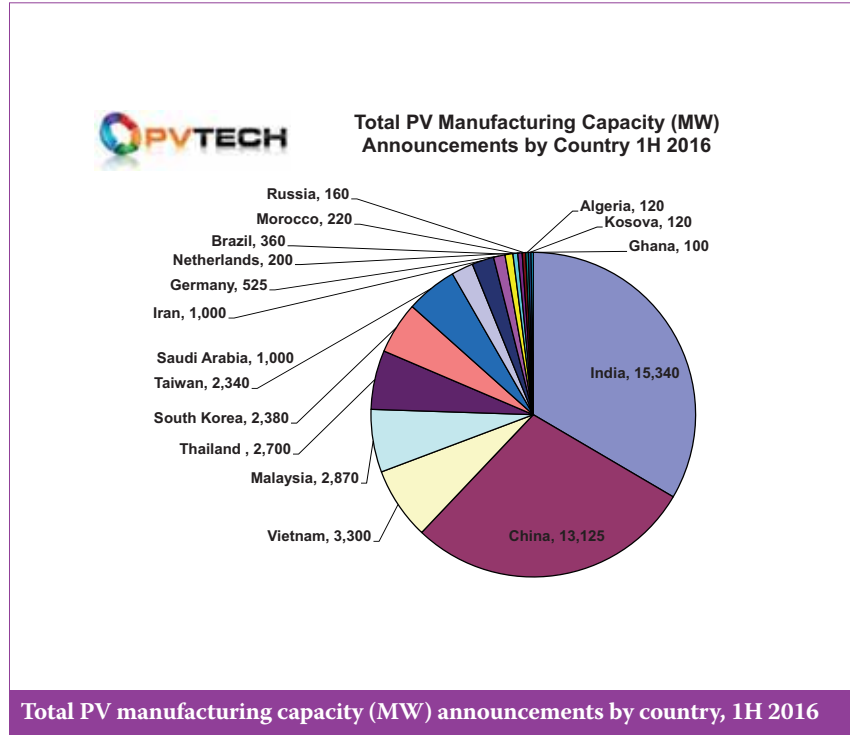
The first quarter of 2016 has proved to be a new record high in total announcements, just topping 30GW, compared to just over 27GW in the fourth quarter of 2015.

The slowdown from these elevated heights is clearly seen in the total number of announcements made in the second quarter of 2016, which represented around a 40% decline quarter on quarter at 17.5GW.

The second quarter of 2016 included 900MW of thin-film planned expansions, 8.04GW of dedicated solar cell and 7.56GW of dedicated module assembly plans. Integrated PV manufacturing plans totalled 1GW in the quarter.

### Geographical split Q2 2016

In the first quarter of 2016, in which revised figures highlight that China



continued to lead new capacity announcements with a total of 8.87GW, in contrast the second quarter was led by India with 8.04GW of plans, while China attracted less than half the amount from the first quarter at 4.25GW.

Indeed, India was the destination for a total of 7.3GW of announcements in the first quarter of 2016, second only to China and totalling almost the same amount (7.85GW) announced for the whole of 2015.

# VON ARDENNE

PIA|nova®

SCALA

GC60V

XEA|nova®

XENIA

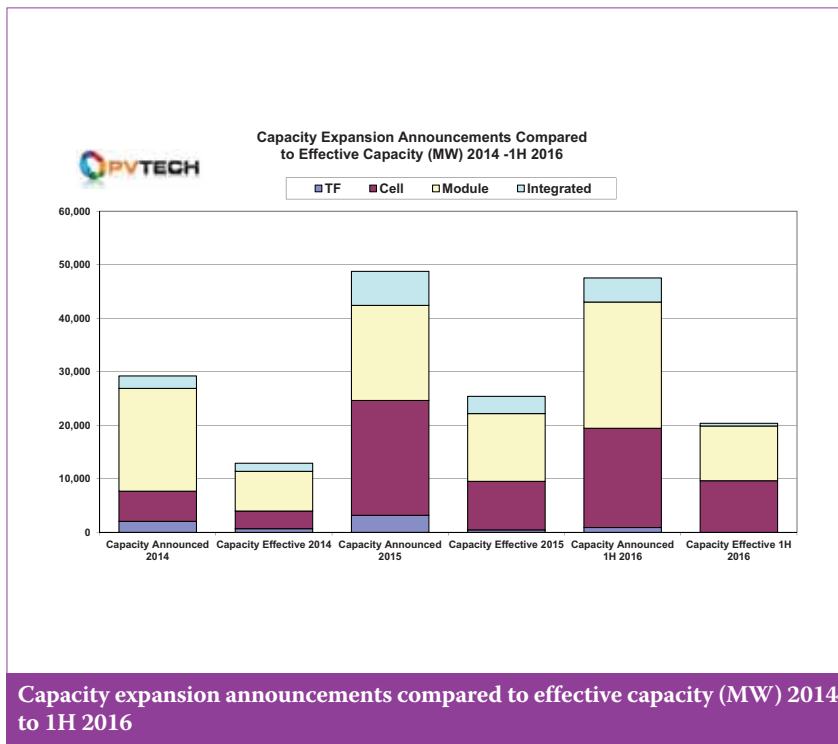
## ADVANCED COATING EQUIPMENT FOR HIGH-PERFORMANCE PHOTOVOLTAICS

If you are looking for coating equipment with low cost of ownership for thin-film photovoltaics or crystalline solar cells, VON ARDENNE is your partner of choice.

Our **PIA|nova**® and **GC60V** coating systems deposit functional layers on glass for thin-film solar modules. The **XEA|nova**® is designed for the deposition of high-performance contact layers on silicon wafers. The coating systems **SCALA** and **XENIA** are suited for both applications.

Learn more at the **PV Taiwan 2016**, booth K0814.

[www.vonardenne.biz](http://www.vonardenne.biz)



Capacity expansion announcements compared to effective capacity (MW) 2014 to 1H 2016

As already highlighted on a monthly basis, Southeast Asia proved to be a continued strong focal point for expansions, while specifically Taiwan was the third largest single destination (1.01GW) in the quarter, though down from 1.34GW in the previous quarter.

### 1H 2016 analysis

Total global PV manufacturing capacity expansion announcements in the first half of 2016 exceeded 47.53GW, almost as much as the total for 2015 of 48.76GW.

This included 18.55GW of dedicated solar cell expansion plans and 23.58GW of module assembly expansion plans. A total of 4.5GW of integrated cell and module expansion plans were announced in the period, while 900MW of thin-film expansions were also planned.

### Geographical split 1H 2016

Perhaps the most surprising aspect of this period was that India surpassed China for announcements. India had 15.34GW of announcements in the first half of 2016, while China had a total of 13.12GW.

However, the period also reveals the attraction of Vietnam, primarily for China-based PV manufacturers in establishing OEM operations via two companies, Boviet Solar and Vina Solar.

Combined with Malaysia and Thailand, these three countries attracted 8.87GW of new capacity expansion plans in the first half of 2016.

### Capacity expansion announcements versus effective capacity analysis, 2014-2016

The hardest and most controversial aspect of analysing capacity expansion announcements is converting them to actual or 'effective' new nameplate capacity.

In an ideal world the tracked announcements should all convert to effective nameplate capacity over a given period of time, providing a clear understanding of the global PV manufacturing landscape.

In the period 2014 through to mid-2016, total capacity expansion announcements have reached over 120GW, which includes over 6GW of thin-film, almost 48GW of dedicated solar cell and over 52GW of module assembly expansions. Integrated manufacturing plans almost reached 14GW.

A new bottom-up analysis was undertaken line by line to establish which of these announcements actually went ahead and whether the nameplate capacity could be categorised as effective capacity by the end of 2016.

Extensive checks were made on all listed announcements in our database from January 2015 to December 2015 to establish if the plans were actioned, completed and ramped. In regards to announcements in the first half of 2016, checks along the same lines were made, although these comprise a higher degree of theoretical production ramp modelling due to being more recently announced.

Therefore a higher degree of certainty was given to major PV manufacturers than for example small or start-up phase producers, based on historical evidence of significantly longer lead-times required to migrate to effective capacity status.

### 2014

In 2014 a total of 26.8GW of capacity expansion announcements were made. By the end of 2016 the effective capacity from these announcements is expected to have reached 12.9GW. This equates to a total conversion rate of about 52%.

In 2014 a total of just over 2GW of thin-film expansion announcements were made, however only 678MW was converted to effective capacity. This equates to a conversion rate of only around 33%.

Dedicated solar cell announcements in 2014 reached 5.6GW, while effective capacity at the end of 2016 is expected to have reached 3.3GW, a conversion rate of nearly 59%.

Total module assembly announcements reached 19.2GW in 2014, while the effective capacity from these plans topped 7.4GW. This equates to a conversion rate of around 38%.

In 2014 a total of just over 2.3GW of integrated cell and module plans were announced, of which 1.5GW has turned into effective capacity by the end of 2016. This equates to a conversion rate of around 65%.

### 2015

In 2015 a total of over 48.7GW of capacity expansion announcements were made. By the end of 2016 the effective capacity from these announcements is expected to have reached 25.3GW. This equates to a total conversion rate of around 48%.

Thin-film announced expansions in 2015 reached nearly 3.2GW but effective capacity by the end of 2016 is expected to have only reached less than 470MW. This would equate to a total conversion rate of only around 14%.

Dedicated solar cell expansions plans reached over 21.4GW in 2015. Effective capacity from these announcements is expected to reach just over 9GW by the end of 2016. This would equate to a total conversion rate of around 42%.

In 2015 a total of over 17.7GW of module assembly expansion plans were announced, while effective capacity of around 12.6GW would have been achieved by the end of 2016. This would equate to a total conversion rate of around 71%.

Integrated capacity plans reached over 6.3GW in 2015. A total of over 3.2GW is expected to have been converted to effective capacity by the end of 2016, a conversion rate of nearly 51%.

## 2016

As previously noted, capacity expansion announcements in the first half of 2016 reached around 47.53GW. Not surprisingly, a lower conversion rate to effective capacity would be expected by the end of the year, compared to the previous two years, due to capacity expansion start dates and ramp rates.

However, we expect around 20GW of these announcements to convert to effective capacity by the end of the 2016, giving a conversion rate of around 43%.

None of the 900MW of thin-film expansions announced in the first half of 2016 are expected to convert to effective capacity by the end of the year. These plans are 2017 and beyond.

Dedicated solar cell expansion plans expected to convert to effective nameplate capacity could reach 9.6GW by year-end, nearly a 52% conversion rate from the 18.5GW of announcements.

The module assembly conversion rate is expected to reach around 42%, from over 23.4GW of announcements, providing an effective module capacity figure of around 10.2GW by the end of 2016.

As a result of this analysis, effective capacity of thin-film modules through the end of 2016 is expected to have reached just over 1GW. Effective dedicated solar cell capacity would reach around 22GW and effective module assembly capacity would reach around 30GW. Integrated cell and module expansion plans that are expected to convert to effective nameplate capacity by the end of 2016 stand at around 5GW.

This equates to around 58.6GW of effective capacity from around 120GW of announcements since the beginning of 2014, through to the end of 2016, a conversion rate of nearly 49%.

## Cumulative global effective module capacity

Looking at just effective PV module capacity (thin-film module capacity, c-Si module assembly capacity and integrated capacity), the total is expected to stand at around a combined 36.7GW at the end of 2016.

Although figures for effective capacity at the end of 2013 vary significantly, due primarily to the number of bankruptcies, exits and zombie companies as a result of the chronic overcapacity then in existence, between 43GW and 53GW of nameplate module capacity was thought to be available.

With around a combined 36.7GW of new module capacity on stream since 2014, effective module capacity is estimated to be in the range of 79.7GW to 89.7GW at the end of 2016.

## Conclusion

We have demonstrated that there has been a significant increase in capacity expansion announcements in the fourth quarter of 2015 through the first half of 2016. However, conversion rates to effective capacity since the beginning of 2014 are just below 50%.

On a geographical basis, China and India stand out for accounting for the vast majority of announcements in the first half of 2016, yet both countries experience relatively low effective capacity conversion rates compared to other countries and are primarily responsible for the mismatch, with India notably so.



**Plasma Enhanced  
Chemical Vapor Deposition, PECVD**  
*linear cluster platform*

**Reactive Plasma Deposition, RPD**  
*in-line platform*

**ARCHERS  
SHJ Solution**



**Archers Systems provides guided solutions with baseline process know-how for manufacturing of high efficiency silicon heterojunction (SHJ) solar cells**

- **3 major international clients have adopted Archers SHJ equipment**
- **Delivers SHJ cell efficiency >23%**
- **SHJ solar cells are PID free, LID free, and provide high yield in kWh/W<sub>p</sub> and low LCOE**
- **State of the art low temperature process for SHJ cell production**
- **Archers PECVD produces SHJ with highly uniform film and high V<sub>oc</sub>**
- **Archers RPD delivers higher efficiency SHJ cells than sputtering**

**Enabling Innovation, Customization and Differentiation**

*Based on extensive experience in semiconductor equipment and processes, Archers Systems develops critical equipment and total solutions for Semi-related industries including PV, IC and OLED.*

**E-mail: [Service@Archersinc.com](mailto:Service@Archersinc.com)  
Website: [www.ArchersSystems.com](http://www.ArchersSystems.com)  
Tel: +886-2-2325-9918 ext.113**

# Materials

Page 31  
News

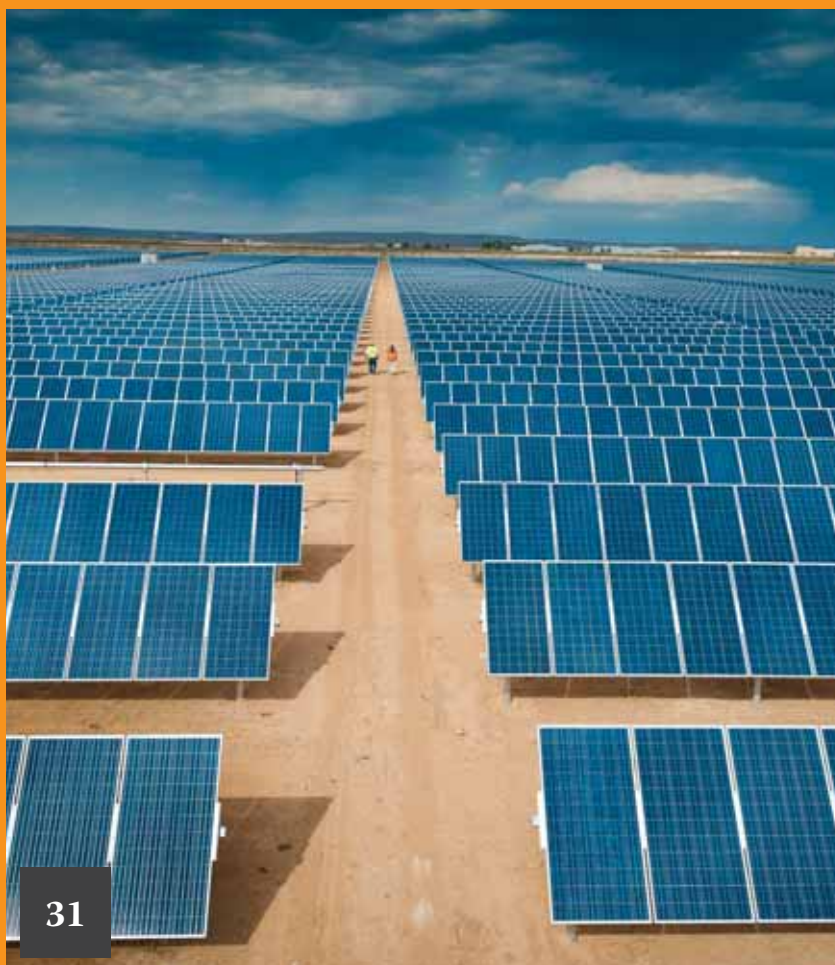
Page 34  
**Metrology at the ingot level:  
Addressing the growing  
importance of bulk material  
quality**

Bernhard Mitchell<sup>1</sup>, Daniel Chung<sup>1</sup>,  
Jürgen Weber<sup>2</sup> & Thorsten Trupke<sup>1,2</sup>

<sup>1</sup>University of New South Wales  
(UNSW), Sydney; <sup>2</sup>BT Imaging Pty Ltd,  
Sydney, Australia

Page 41  
**Oxygen-defect  
characterization for  
improving R&D relevance and  
Cz-Si solar cell efficiency**

Jordi Veirman, Benoît Martel, Nicolas  
Enjalbert & Sébastien Dubois, CEA  
Tech-INES, Le Bourget du Lac, &  
Catherine Picoulet & Pierre Bonnard,  
AET Technologies, Meylan, France



## GCL-Poly places US\$150 million bid for SunEdison's polysilicon assets

GCL-Poly Energy Holding has placed a bid of US\$150 million for the polysilicon assets of bankrupt renewable energy firm SunEdison via the US bankruptcy court dealing with the Chapter 11 proceedings.

The company is targeting the acquisition of SunEdison's bankrupt Korean-based joint venture FBR plant, SMP. The net assets of SMP were said to be approximately US\$400.8 million.

GCL-Poly also plans to acquire SunEdison's subsidiary, MEMC Pasadena, a first-gen FBR plant, and the assets of SunEdison's continuous crystal growth manufacturing technology that produces monocrystalline silicon ingots via its acquisition of Solaicx in 2010, which has a production facility in Portland, Oregon.

GCL-Poly's bid for SunEdison's FBR technology, which potentially offers the lowest-cost polysilicon while achieving high purity levels close to those achieved with the Siemens process, is the current 'holy grail' for future competitiveness in the solar PV-based polysilicon sector. But due to their technical issues, GCL-Poly is taking a significant risk, should the bid be successful.

The financial filings show GCL-Poly is attempting to limit its financial exposure to the offer with a number of clauses related to the production of FBR polysilicon.



Credit: SunEdison

GCL-Poly is looking to acquire bankrupt SunEdison's polysilicon assets.

### Polysilicon

## SolarWorld and Hemlock to hold mediation conference to explore 'settlement' possibilities

SolarWorld and Hemlock were set to hold a mediation conference after this issue of *Photovoltaics International* went to press after SolarWorld was ordered to pay Hemlock damages amounting US\$793 million plus costs and interest in July.

The case, relating to breach of take-or-pay polysilicon contracts with Hemlock Semiconductor, had already been running for more than three years, but, following the ruling, SolarWorld said it would appeal the judgement in the US, adding that any claim in the US will not be enforceable in Germany. That appeal has now been launched.

A mediation conference involving both companies will now be held later in September lasting for at least two hours with the primary aim to "explore possibilities for settlement", according to a letter sent by the Office of the Circuit Mediators, in the United States Court of Appeals.

The conference will not only investigate possible means by which to resolve the case, but will also attempt to prevent unnecessary delays by addressing procedural issues in the appeal. It will also identify the main disputes in the appeal.

## Major polysilicon producer invests in 1366 Technologies

1366 Technologies has secured a US\$15 million equity investment and polysilicon supply deal from major polysilicon producer, Wacker Chemie.

The US\$15 million investment from Wacker offsets needed high-purity polysilicon supply and payments during ramp-up, significantly reducing liquidity risks at the early ramp phase. Wacker will supply polysilicon from its recently started plant in the US.

1366 Technologies also noted that the partnership includes a close technical collaboration with Wacker, encompassing Wacker's silicon know-how, facility design, engineering and construction expertise.

Frank van Mierlo, CEO of 1366 Technologies confirmed that the strategic partnership with Wacker puts the volume production ramp on a "solid foundation that is more deliberate and prudent, something we had always wanted to achieve".

## Daqo sets new polysilicon production and revenue records

China-based polysilicon and wafer producer Daqo New Energy has reported record production and financial metrics on strong demand in the second quarter of 2016.

Daqo New Energy exceeded its

nameplate polysilicon capacity in the quarter with production reaching 3,570MT, compared to 3,405MT in the previous quarter. The company has produced a total of over 13,200 MT of polysilicon over the past four quarters. Daqo set a new global Siemens-based polysilicon production cost benchmark of US\$9.43/kg, compared to US\$9.65/kg in the previous quarter.

The company noted that aside from the scheduled maintenance during the third quarter it was planning to do the interconnection work between its existing facilities and its Phase 3A polysilicon facilities, resulting in a 15 to 20 day suspension of polysilicon production in the Q3 2016.

Daqo expects to sell approximately 2,550MT to 2,600MT of polysilicon to external customers during Q3 2016.

### New materials

## JinkoSolar using Heraeus' 'SOL9631J' series front-side metallization paste

Heraeus Photovoltaics said its recently launched 'SOL9631' Series front-side metallisation paste had been adopted by leading 'Silicon Module Super League' member, JinkoSolar.

Heraeus noted that the latest collaboration with JinkoSolar produced the 'SOL9631J' version of the new paste





Credit: ReneSola

**ReneSola** ReneSola has been squeezed by wafer ASP declines.

series, provided more than a 0.1% gain in solar cell conversion efficiency. This was made possible by improved electrical conductivity and fine-line printing technology with a higher aspect ratio and better printability.

JinkoSolar's CEO, Chen Kangping said: "Through our highly successful partnership, JinkoSolar and Heraeus have been able to jointly develop this new-generation of Heraeus silver metallization paste and successfully integrate it into JinkoSolar's mass production process, thereby greatly improving the conversion efficiency of their solar cells."

Heraeus also noted that the new paste had proved its manufacturability for high-speed printing, which provided improved production line productivity and total production capacity at JinkoSolar.

### HIUV to ramp PID-limiting EVA encapsulant for n-type cell based PV modules

Asia-based EVA encapsulant material producer HIUV New Materials has developed an encapsulant for n-type cell based PV modules that limits PID (potential-induced degradation).

The company noted that its new EVA encapsulant, P502MR, had been tested by a leading PV module manufacturer with good results and that it had completed

tool installation to produce the material in a JV with Jinglong in China with a nameplate capacity equivalent to 1.5GW. Production is expected to ramp in the third quarter of 2016.

HIUV had previously said it was ramping up capacity to 117 million m<sup>2</sup> per year, in order serve the equivalent of 9GW of PV module production.

## Wafer

### ReneSola hit by slowing China demand and wafer margin squeeze

ReneSola reported Q2 2016 results impacted by a module end-market demand slowdown in China and high polysilicon prices, while wafer ASPs decline, squeezing revenue and margins, with wafer shipments of 423.3MW compared with 351MW in the previous quarter, a 20.6% increase quarter-on-quarter and up 50%, year-on-year.

However, wafer ASPs started falling in the quarter after the rush to complete downstream PV projects before the end of June receded. Margins fell as a result, compounded by continued strength in polysilicon prices in China on tight supply, due to high import tariffs for primarily US polysilicon suppliers,

severely limiting imports.

Renesola management noted that wafer ASPs were falling by around 20%, while polysilicon prices could finally start to fall on weaker demand in the fourth quarter of 2016.

### SKC Solmics exits mono-wafer production with equipment sold to Wongjin Energy

Korea-based monocrystalline wafer producer SKC Solmics, a subsidiary of Korea's third largest conglomerate, has exited the solar sector with the sale of its production equipment to rival Wongjin Energy.

SKC Solmics had primarily supplied high-quality monocrystalline wafers to a small number of Japan and US-headquartered firms but was loss making amid a highly competitive sector and much smaller than key global market leaders.

Wongjin Energy said in a financial filing that it had purchased the production equipment, expected to be primarily single crystal pullers and wire saw tools. SKC Solmics sold the equipment set for close to US\$30 million.

### SunPower settles mono wafer supply dispute in Philippines for US\$50.5 million

SunPower has settled a monocrystalline wafer subcontractor dispute in the Philippines for US\$50.5 million.

In January 2015 an arbitral tribunal of the International Chamber of Commerce had awarded partial damages to First Philippine Electric Corporation (FPEC) and First Philippine Solar Corporation (FPSC) against SunPower Philippines Manufacturing, over non-compliance with a previous wafer supply agreement. Later in the year the tribunal lowered the awarded compensation to the supplier and SunPower had noted that it had allocated a nonrecurring loss on the decision.

The 'Compromise Agreement' that led to the US\$50.5 million payment to the JV supplier would also include SPML transferring all of its shares in FPSC to FPEC.

### GCL-Poly signs new wafer supply deal with GCL System

Leading polysilicon and wafer producer GCL-Poly Energy Holdings has signed a new supply contract with sister PV module manufacturing company, GCL System Integration, totalling 110,000,000 wafers through the second half of 2016.

The wafer deal was said to include both monocrystalline and multicrystalline wafers, although the volume split between



Credit: JA Solar

**JA Solar has surpassed 7GW of mono-Si PV shipments.**

the two wafer types was not disclosed. GCL-Poly had recently announced the start of volume production of monocrystalline wafers with a nameplate capacity of 1GW. GCL-Poly reached a nameplate capacity of 15GW of multicrystalline wafer production in the first quarter of 2016.

The wafer supply deal was said to be valued at around RMB785 million (US\$117.2 million) with pricing potentially adjusted to general market ASPs on monthly reviewed basis.

Monocrystalline wafer producer Comtec Solar Systems Group has reported first-half 2016 financial results that were impacted by a decline in average selling prices (ASP) and lower volume shipments, due to production upgrades and training at its facility in Malaysia.

Comtec Solar reported revenue of RMB491.1 million (US\$73.5 million) in the first half of 2016, a 13.2% decline from the prior year period.

The company reported a gross profit of RMB31.1 million (US\$4.65 million), an increase of 122.1% from approximately RMB14.0 million (US\$2.09 million) for the first half of 2015. Gross profit margin was approximately 6.3%, increasing from the gross profit margin of 2.5% from the prior year period.

Improvements were said to be due to new polysilicon supply agreements with the two major suppliers, eliminating 'take or pay' agreements, which had been primarily responsible for losses in 2015 and operating losses over last few years.

However, the company did report

a net loss for the current period of approximately RMB6.4 million (US\$958,435), compared to a net loss of RMB204.0 million (US\$30.5 million) in the prior year period. Net cash inflow from operating activities was approximately RMB63.3 million (US\$9.47 million).

#### Company news

### Wacker's polysilicon sales in Q2 limited by inventory depletion

Major polysilicon producer Wacker Chemie reported flat second quarter polysilicon sales, despite stronger demand and higher average selling prices (ASPs) as inventory depletion limited shipments.

Wacker's polysilicon division reported second quarter revenue of €272.2 million, flat with the prior quarter when the company reported revenue of €273.1 million and 4% higher than the prior year period, despite significantly higher volumes year-on-year.

Wacker noted that revenue was impacted by polysilicon volumes (shipments) being lower than in the first quarter, due to reduced polysilicon inventories available for sale in the second quarter.

The company reported quarterly EBITDA of €77.7 million, compared to €161.4 million in prior year quarter.

The 52% reduction is due to overall ASP decline seen through 2015 and a major reduction in retained advance payments and received damages on cancelled long-term 'take or pay' contracts. Retained advance payments and received damages totalled €86.7 million in the prior year period but only amounted to €7 million in the second quarter of 2016.

EBITDA margin in the second quarter was 28.4%, compared to 14.4% in the previous quarter but down from 61.8% in the prior year period.

### JA Solar surpasses 7GW milestone of monocrystalline PV product shipments

JA Solar reached a new milestone in monocrystalline PV product shipments in the middle of July 2016, with shipments of monocrystalline PV products (wafers, cells, modules) over the last ten years had reached the 7GW milestone.

The big transformation relates to shipments of monocrystalline modules, which reached 500MW in 2013, making it the largest p-type monocrystalline module provider that year with the company shipping more than 1GW of monocrystalline modules in 2014. JA Solar said that it expected shipments in 2016 to be near 2GW for p-type monocrystalline modules.

JA Solar's flagship p-type monocrystalline module is its 'Percium' series modules, which include passivated emitter rear contact (PERC) technology that began ramping in mid-2014.

# Metrology at the ingot level: Addressing the growing importance of bulk material quality

Bernhard Mitchell<sup>1</sup>, Daniel Chung<sup>1</sup>, Jürgen Weber<sup>2</sup> & Thorsten Trupke<sup>1,2</sup>

<sup>1</sup>University of New South Wales (UNSW), Sydney; <sup>2</sup>BT Imaging Pty Ltd, Sydney, Australia

## ABSTRACT

With the PV industry continually pushing for ever-higher silicon solar cell efficiencies, the requirements on the electronic quality of the bulk material are becoming more stringent. Advanced characterization of silicon ingots after cutting into bricks allows early quality control and immediate feedback in crystal growth, thereby facilitating shorter R&D cycles, higher yield, lower cost and higher product quality in mass manufacturing. Techniques based on photoluminescence (PL) imaging for bricks and ingots have been developed and refined over the last few years and now provide crucial material parameters, such as the bulk minority-carrier lifetime, in a quick and reliable fashion. In this paper some of these quantitative methods, which are already available in commercial inspection tools, are demonstrated on state-of-the-art industrial high-performance multicrystalline p-type Si bricks and high-lifetime n-type Cz-Si ingots.

## The case for ingot-level metrology

The rapid improvement in industrial solar cell manufacturing over the last ten years in terms of average conversion efficiencies and cost reduction is nothing short of spectacular. SunPower recently presented statistical manufacturing data for their latest generation of high-efficiency solar cells, with average efficiencies exceeding 24%, and for even a full-size module an aperture efficiency of 24.1% [1]. Trina recently reported record efficiencies for passivated emitter rear cells (PERCs) on both six-inch mono- and multicrystalline Si wafers [2,3]. With most solar cell manufacturers, higher-efficiency PERC solar cells are in either full-scale or pilot production, while others are focusing on alternative high-efficiency solar cell concepts, such as heterojunction solar cells. These trends towards ever-increasing efficiency in production are expected to continue for many years, particularly in the case of the more conventional cell architectures.

**“The inspection of silicon ingots and bricks represents the only opportunity to reliably measure the bulk lifetime at an early processing stage.”**

Ultimately, the performance of a solar cell is determined by a number of loss mechanisms. For screen-printed full-area Al-BSF solar cells, still currently the industry standard, the loss mechanisms which are related to the device design, such as recombination at the rear metal surface, dominate and limit cell performance. In advanced cell designs these unwanted processing-related or device-architecture-related recombination sources are significantly reduced or eliminated. As a result, the bulk quality of the Si wafer itself becomes an increasingly significant factor. A key parameter representing the electronic absorber quality is the bulk excess minority-carrier lifetime  $\tau_b$ , or short bulk lifetime, which defines how long photogenerated excess carriers (electron-hole pairs) ‘survive’ within the absorber before they recombine. A higher bulk lifetime yields higher cell voltages and higher currents, and thus higher efficiency. The inspection of silicon ingots and bricks represents the only opportunity to reliably measure the bulk lifetime at an early processing stage, since that information is largely lost during wafer cutting, the lifetime in as-cut wafers being severely limited by surface recombination.

In crystalline Si,  $\tau_b$  is found to be mostly determined by contaminants, such as transition metals, light elements (O, C, N) and imperfections in the crystal lattice (micro and extended defects). Multicrystalline Si ingots grown by directional solidification (DS) exhibit extended defects, such as grain boundaries and

dislocation clusters; the latter are often contaminated by precipitates or dissolved point defects. As-grown bulk lifetimes vary considerably throughout cast ingots and depend on a wide range of parameters, such as the purity of the feedstock, the type of crucible and lining, and, of course, the growth conditions (e.g. temperature profiles) during crystallization. Intra-grain lifetimes reaching several hundred microseconds can be achieved in both boron-doped and phosphorus-doped high-performance multicrystalline (HPM) Si ingots, and can be further greatly improved by diffusion-assisted gettering [4,5].

Czochralski (Cz)-grown ingots do not usually show extended defects, but are affected by grown-in micro or point defects (voids, oxygen precipitates, etc.) and contaminants (e.g. carbon [6]), which affect the bulk lifetime. The as-grown bulk lifetimes of Cz crystals are higher than in the case of DS-grown ingots (up to tens of milliseconds). In p-type Cz-Si, the bulk lifetime is often limited by recombination via boron-oxygen complexes [7].

The early measurement of the bulk lifetime and other defect parameters at the ingot level can add significant value in terms of maximizing efficiency and yield in production – for example via: 1) immediate feedback to crystal growth; 2) discarding of unsuitable material at an early stage; 3) classification of wafer material; and 4) sorting of bricks and wafers for selective processing.

Specifically in relation to the first

point above, ingot-level metrology enables faster R&D cycles and can be used, for example, to improve throughput, reduce the dislocation density in DS cast ingots, develop and evaluate new seeding techniques, track metal contamination, test new crucibles and lining materials, improve homogeneity across the crystal, and trace thermal donor growth. Without comprehensive ingot metrology, feedback from the above activities usually requires cell processing, which involves the entire solar cell production sequence, including wafer cutting, cell processing and careful tracking of these activities. Not only is this process time consuming, but it is also prone to errors and demands significant resources.

### Spectral PL imaging: a rapid quantitative bulk lifetime technique

Techniques available for the characterization of Si ingots and bricks in mass manufacturing include microwave-detected photoconductance decay (PCD) and quasi-steady-state photoconductance (QSSPC). Both of these have specific shortcomings when applied to non-passivated bricks.

PCD measures and reports significantly surface-limited *effective* lifetimes only; in addition, these values are reported at high injection levels ( $>1 \times 10^{15} \text{cm}^{-3}$ ), which are not representative of the typical operation of solar cells. Measurement times of several minutes are normally required in order to obtain a relatively coarse spatially resolved map (e.g. 2mm raster scan) of effective lifetime. QSSPC, or eddy-current-detected PCD, measurements can provide *true* bulk lifetime at the ingot level, but yield only very limited spatial resolution of the order of centimetres, which does not allow the detection and quantification of structural defect densities. Both PCD and QSSPC techniques can be affected (in some cases severely) by trapping artefacts, which can prevent a reliable bulk lifetime analysis at the injection levels relevant to solar cell operation [8,9].

Photoluminescence (PL) imaging provides a powerful alternative to the above techniques. Over the last few years, a range of quantitative analysis techniques for the application of PL imaging at the ingot level have been developed at UNSW, which have now matured to a level that makes them suitable for implementation in commercial tools. One particularly successful development is the quantitative analysis of the emission

spectrum. The PL spectrum of a thick sample, e.g. a Si brick or thick Si disc, contains significant bulk lifetime information. This information can be extracted using the so-called *spectral PL intensity ratio (sPLIR)* method, which involves imaging the sample twice, with two different spectral filters mounted in front of the camera lens. The two different filters change the sensing depth of the PL detection, enabling signals to be captured that relate to the carrier density at different depths within the brick. The theory behind this technique, which was first proposed by Würfel [10] for the characterization of the diffusion length in fully processed silicon solar cells, is described in detail elsewhere [11,12]. Importantly, the technique enables the acquisition of high-resolution (approximately  $150 \mu\text{m}$  per pixel) bulk lifetime images on bricks of any length (BT Imaging LIS-B3 system – up to 40cm), with total acquisition times of less than one minute; the method is also insensitive to variations in bulk resistivity.

**“In unpassivated bricks the sPLIR technique is sensitive to bulk lifetime variations from a few microseconds to tens of milliseconds.”**

Another key strength of this technique is that it works for a very broad range of diffusion lengths, from approximately  $10 \mu\text{m}$  to 10mm, as shown in Fig. 1. The equivalent excess minority-carrier lifetime range for p-type material is shown on the top axis for comparison; according to this, in unpassivated bricks the sPLIR technique is sensitive to bulk lifetime variations from a few microseconds to tens of milliseconds, thus covering the entire range relevant to PV applications.

According to the theoretical analysis carried out, the use of Si cameras (as opposed to, for example, InGaAs cameras) has inherent benefits for the sPLIR application, specifically because of a better sensitivity to lifetime variations at low lifetimes, as typically found near the top and bottom sections of mc-Si ingots [13]. On the other hand, PL imaging applications using Si area cameras suffer from image blurring, which is caused by the poor absorption of Si luminescence photons [13–15] and the resulting lateral scattering within the CCD chip. As recently demonstrated [16], this experimental artefact is greatly suppressed when using line-scanning PL imaging rather than conventional area-scanning cameras, resulting in significantly improved accuracy of the method. By means of the line-scanning principle, ingots of virtually any length can be measured conveniently without the need to stitch individual images together.

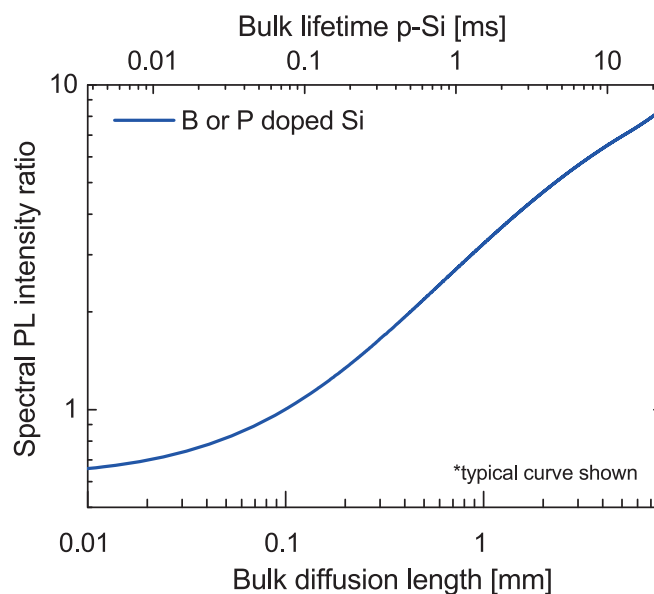


**Figure 1. Theoretical dependence of the sPLIR signal on the excess minority-carrier bulk diffusion length for an unpassivated and infinitely thick Si block. The top axis represents the equivalent excess minority-carrier bulk lifetime for p-type silicon.**

### Bulk lifetime and iron concentration: two key bulk material quality parameters

The sPLIR technique has been applied to and verified on a broad range of samples. Fig. 2(a) shows a bulk lifetime image of a state-of-the-art HPM boron-doped Si brick from a G6 furnace (data measured on a BT Imaging LIS-B3 system). Significant variations in bulk lifetime are observed, with values ranging from less than  $1\mu\text{s}$  to  $140\mu\text{s}$ . The impact of structural defects, such as decorated grain boundaries and dislocation clusters, is also visible.

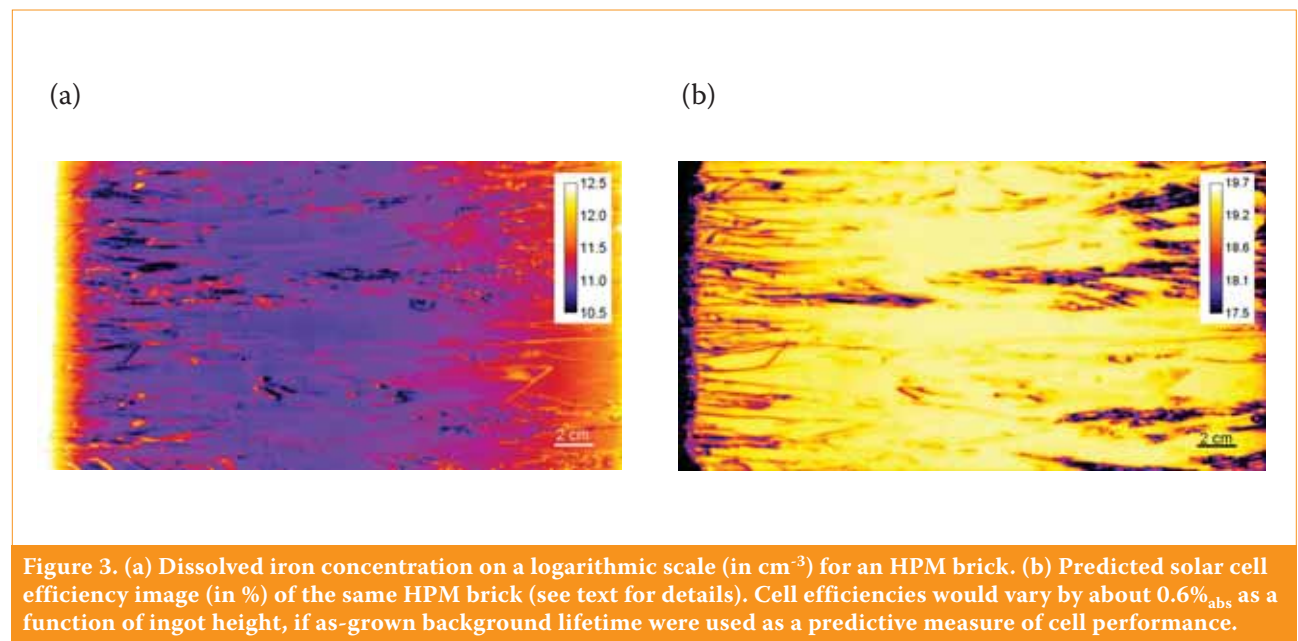
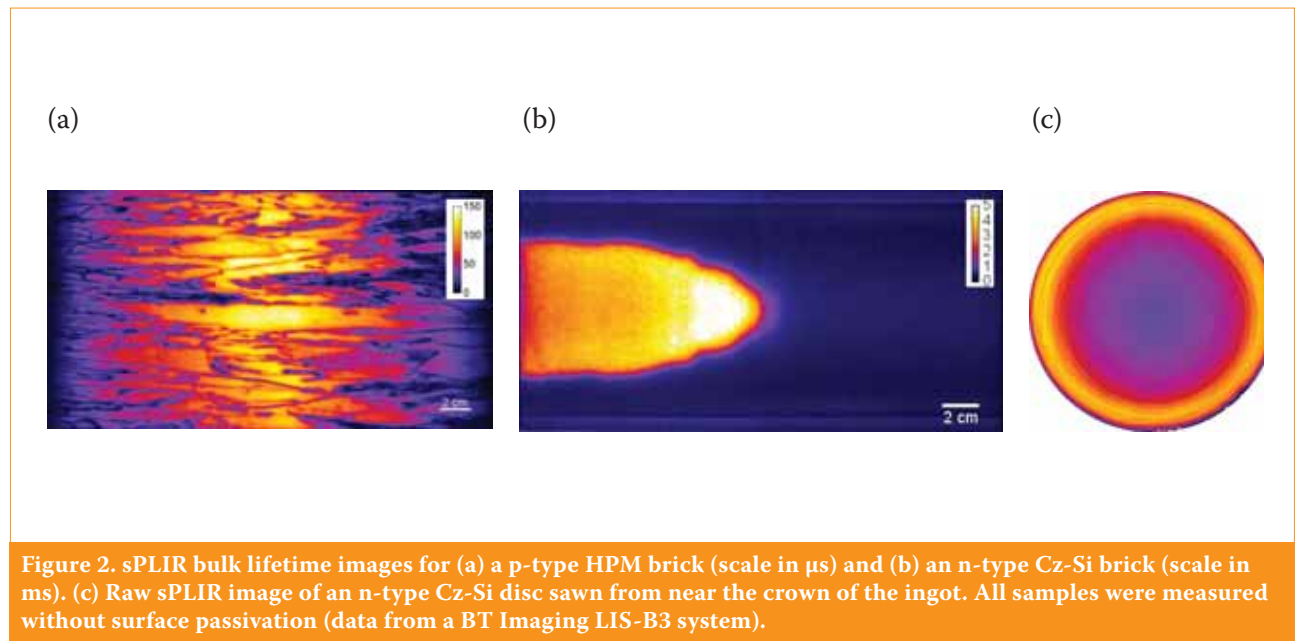
An example of the bulk lifetime from sPLIR imaging of a high-lifetime n-type Cz-grown ingot is shown in Fig. 2(b). A severe degradation in bulk

lifetime because of oxygen-induced stacking faults is observed across a large portion of the brick. Lifetime values of up to 6ms are observed in the 'good' regions of the ingot, demonstrating the wide dynamic range of detectable lifetimes.

When applied to the outside surfaces of bricks and ingots, the sPLIR approach provides bulk lifetime information for only the first few millimetres from the surface. In order to characterize lifetime variations within an ingot, the sPLIR method can be carried out either on specially prepared vertical slabs [17] or on thick discs that have been cut in the wafer plane (see example in Fig. 2(c)). Up to 20ms lifetimes on a 2cm-thick high-lifetime n-type disc were recently measured, demonstrating the ability

to measure extremely high lifetimes on non-passivated samples (data submitted for publication elsewhere).

Iron is a detrimental impurity in boron-doped Si [18] and arguably one of the dominant sources of recombination in DS-Si ingots because of the diffusion of impurities from the crucible and the lining [19,20], in addition to sources in the feedstock (cf. Fig. 4(c)). Iron is typically found around the entire perimeter (top, bottom and side faces) of DS-cast ingots, as a result of in-diffusion, segregation and solid-state back diffusion during cooling. Iron can be present in either precipitated or dissolved states in DS mc-Si, while it is usually found only in the dissolved state in Cz-Si. The edge regions of a DS ingot contain both



# Introducing the LIS-B3

“The ideal tool for quality control and process development in silicon brick and ingot manufacturing”



[www.btimaging.com](http://www.btimaging.com)



- > High resolution photoluminescence imaging data with unmatched image quality
- > Incorporating BT Imaging's patented scanning photoluminescence imaging technology
- > Applicable to all types of crystalline silicon ingots and bricks
- > Quantitative high-resolution **bulk** lifetime images from 1  $\mu$ s to 20 ms
- > Cutting guides for multi-crystalline silicon bricks
- > Automatic algorithms report various defect and quality metrics
- > Configurable for manual or automatic loading



Penang, Malaysia

14-15 March 2017

#PVCELLTECH



## CONFERENCE PVCELLTECH

**SAVE \$250!**  
Early bird rate expires soon

Now it's in second year after a sell-out inaugural conference PV Celltech is already established as the leading c-Si cell manufacturing and processing event of the year, don't miss it!



"The PVCellTech conference was a **fantastic opportunity** to discuss PV manufacturing issues, opportunities and prospects with key players and prepare this industry for the TW level."  
**Dr. Pierre Verlinden**, PhD VP, Chief Scientist and Vice-Chair of State Key Lab (PVST) Technology Dept, Trina Solar



"A very well organised event with **impressive selection of speakers** and topics covered."  
**Stuart Wenham**, Centre Director, UNSW

### Sponsors:



[celltech.solarenergyevents.com](http://celltech.solarenergyevents.com)

To get involved either as a speaker, partner or attendee please contact Sylvester: [sgabriel@solarmedia.co.uk](mailto:sgabriel@solarmedia.co.uk)



dissolved and precipitated iron, but the recombination in the centre of the ingot is mostly due to dissolved (either interstitial or FeB) iron, though nanoscale precipitates may exist in the as-grown state or are induced through cell processing [21].

Given its ability to measure spatially resolved bulk lifetime, the sPLIR imaging method also allows quantitative measurement of the dissolved iron concentration in *boron-doped* Si bricks or discs (either DS or Cz). In this approach an intense light source is used to toggle the dissolved iron between interstitial and FeB states, the latter being the equilibrium state in silicon at room temperature [22,23]. The variation in bulk lifetime resulting from the dissociation of FeB pairs can be linked quantitatively to the iron concentration. The method therefore includes the sequence of a first bulk lifetime image from sPLIR, followed by the dissociation of the FeB pairs using a flash lamp, and then a second bulk lifetime image. This technique was applied to the HPM block shown in Fig. 2(a). Fig. 3(a) shows the extracted dissolved iron concentration across the same brick face (bottom of the ingot is shown on the left). Low interstitial iron concentrations of the order of  $5 \times 10^{10} \text{cm}^{-3}$  were measured in the central high-lifetime region, whereas high concentrations up to  $1 \times 10^{13} \text{cm}^{-3}$  were observed in the low-lifetime bottom region; in the latter region, the iron dominates the total recombination and is the main cause of the reduction in bulk lifetime reported in Fig. 3(a).

“The sPLIR imaging method also allows quantitative measurement of the dissolved iron concentration in *boron-doped* Si bricks or discs.”

Beyond pure contamination screening, the additional information about iron concentration can be used to define performance classes for as-grown wafer material. For example, with the knowledge of the as-grown bulk lifetime and the as-grown dissolved iron concentration, it is possible to predict the background lifetime, in other words the bulk lifetime that would be present and measured in the absence of dissolved iron. The *background lifetime* is expected to be more useful for predicting the bulk quality in the final device than the as-grown bulk lifetime, since many conventional cell processes include a phosphorus diffusion, which represents an efficient gettering process that reduces the iron concentration in the bulk.

Combined with a cell performance concept, which can be obtained from detailed device simulations, it is thus possible to rate silicon material in terms of expected solar cell performance, entirely on the basis of ingot measurements using sPLIR imaging. Note that the degree of applicability of this hypothesis is currently being investigated experimentally in collaboration with

industry partners, and is dependent on the exact cell processing conditions, and thus on cell architecture. The analysis here was performed on the HPM sample from Fig. 2(a). The resulting ‘predicted efficiency’ image (Fig. 3(b)) shows a variation of  $0.6\%_{\text{abs}}$  across the ingot height; this spread is associated with just the variations in bulk lifetime. These predicted efficiency variations therefore do not account for the extended defect density variation.

### Material quality variations in production

The above methods were applied to industrial bricks manufactured in the last few years, and significant variations were found in the material quality within ingots, across different batches and manufacturers and with time. As an example, Fig. 4 compares the bulk lifetime, iron concentration and interstitial iron recombination fraction (i.e. the percentage of the iron-related recombination of total recombination) for four industrial bricks. The sample set consists of two standard mc-Si bricks manufactured in 2011, and two recent HPM bricks (for details see Chung et al. [24]).

It was found that current HPM ingots tend to yield slightly higher bulk lifetimes than traditionally produced ingots from a few years ago, but can show vastly different height distributions (see HPM1 vs. HPM2). With regard to the dissolved iron profiles, all bricks show qualitatively similar profiles, with no obvious differential trend between the conventional bricks and HPM

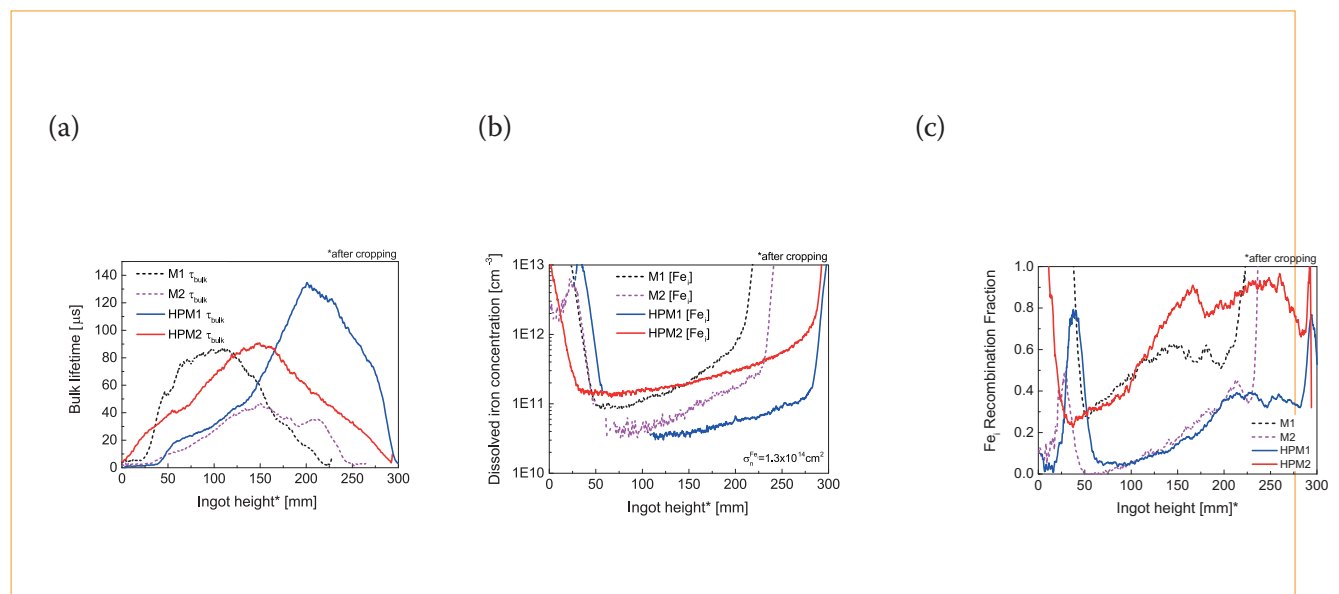


Figure 4. (a) Bulk lifetime, (b) dissolved iron, and (c) dissolved iron recombination fraction as a function of ingot height, for a set of four industrial DS ingots (two standard mc, two HPM).

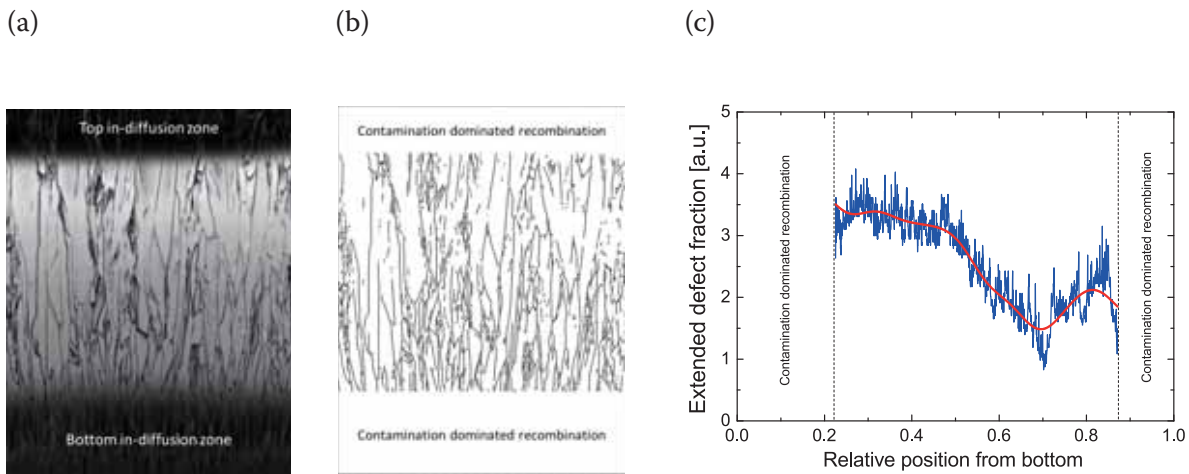


Figure 5. (a) PL image of a HPM Si brick. (b) Extended defect structure detected using PL imaging. (c) Height dependence of extended defects.

bricks, but quantitative differences are noteworthy and may lead to valuable insight when measured in dependency of crucible, lining and/or feedstock quality and the crystallization recipe. Note that HPM1 demonstrates a significantly lower value than HPM2, even though the bulk lifetimes are not necessarily higher. This is reflected in the fact that HPM1 is less strongly dominated by dissolved iron than HPM2. Other defects must play a role in HPM1, which is powerful information to have in manufacturing, when results from cell production and other characterization are available. Overall, the recombination fraction profiles show that, for most of the bricks, interstitial iron is a dominant lifetime-limiting factor in the as-grown material. Its influence increases towards the top of the brick, where dissolved iron is known to decorate extended defects that are harder to getter effectively. The availability of this quantitative information from a quick and convenient measurement system can obviously be of great value to R&D engineers for further improvement and refinement of the crystallization process.

### Extended defect analysis

The major improvement in HPM bricks compared with earlier DS bricks is the significant reduction in structural defects, particularly in the density of dislocation clusters; these have been shown in several studies [25,26] to have a strong and dominating effect on the efficiency of mc-Si cells.

The BT Imaging LIS-B3 system provides high spatial resolution and

outstanding image quality, allowing various quality metrics that are related to (among other things) the density of the above structural defects to be extracted using automated image processing algorithms. This capability is demonstrated here (see Fig. 5) using a basic feature analysis routine developed at UNSW. The LIS-B3 incorporates and reports more-sophisticated metrics, which evolved from image-processing algorithms developed for commercial PL-imaging-based wafer inspection systems; these have already played an important role in the improvement of mc-Si quality in terms of reducing structural defects to the current levels. When applied at the brick level, the PL imaging analysis and related quantitative metrics can result in even faster process feedback, and will therefore be a valuable tool for further improvements in mc-Si and for process monitoring in high-volume manufacturing.

### Conclusions

PL imaging of bricks and ingots using line scanning is an attractive alternative to existing characterization methods currently used in production and in R&D labs. Short measurement times, the non-contact nature, high spatial resolution and robustness against various measurement artefacts are some key advantages. Advanced quantitative analyses in terms of various key material parameters (e.g. *true* bulk lifetime and dissolved iron concentration) are made possible by the application of sophisticated experimental methods, such as the sPLIR method developed at UNSW,

which exploits the information about the electronic material quality that is contained in the spectral distribution of the emitted luminescence.

**“PL imaging of bricks and ingots using line scanning is an attractive alternative to existing characterization methods currently used in production and in R&D labs.”**

The systematic application of those methods in R&D and production, using reliable inspection systems with superior throughput, will contribute to further improvements in crystal quality and yield, and thereby ultimately contribute to the further cost reductions in PV manufacturing that are still required. Immediate applications range from the optimization of crystallization processes via process monitoring in production, to the use of PL images as a cutting guide. In the medium term the bulk lifetime information, which can be reliably extracted from PL images, can also be used to classify the raw material, with the aim of wafer-specific processing in order to maximize the efficiency of the solar cells created from across an ingot.

### Acknowledgements

This research has been supported by the Australian Government through the Australian Renewable Energy



Agency (ARENA) grants 7-F008 and RND009. The Australian Government does not accept responsibility for the views, information or advice expressed herein. The authors would like to thank Dr. Oliver Kunz for his contributions.

## References

- [1] Smith, D.D. et al. 2016, "Silicon solar cells with total area efficiency above 25 %", *Proc. 43rd IEEE PVSC*, Portland, Oregon, USA.
- [2] Ye, F. et al. 2016, "22.13 % efficient industrial p-type mono PERC solar cell", *Proc. 43rd IEEE PVSC*, Portland, Oregon, USA.
- [3] Zhang, S. et al. 2016, "335-W world-record p-type monocrystalline module with 20.6% efficient PERC solar cells", *IEEE J. Photovolt.*, Vol. 6, No. 1, pp. 145–152.
- [4] Schön, J. et al. 2015, "Identification of the most relevant metal impurities in mc n-type silicon for solar cells", *Sol. Energy Mater. Sol. Cells*, pp. 1–9.
- [5] Michl, B. et al. 2013, "The impact of different diffusion temperature profiles on iron concentrations and carrier lifetimes in multicrystalline silicon wafers", *IEEE J. Photovolt.*, Vol. 3, No. 2, pp. 635–640.
- [6] Nagai, Y. et al. 2016, "Growth of Czochralski silicon crystals having ultralow carbon concentrations", *Gettering Defect Eng. Semicond. Technol. XVI*, Vol. 242, pp. 3–9.
- [7] Walter, D.C., Lim, B. & Schmidt, J. 2016, "Realistic efficiency potential of next-generation industrial Czochralski-grown silicon solar cells after deactivation of the boron-oxygen-related defect center", *Prog. Photovoltaics Res. Appl.*, Vol. 24, No. 7, pp. 920–928.
- [8] Macdonald, D. & Cuevas, A. 1999, "Trapping of minority carriers in multicrystalline silicon", *Appl. Phys. Lett.*, Vol. 74, No. 12, pp. 1710–1712.
- [9] Hu, Y. et al. 2012, "Investigating minority carrier trapping in n-type Cz silicon by transient photoconductance measurements", *J. Appl. Phys.*, Vol. 111, No. 5, pp. 0–6.
- [10] Würfel, P. et al. 2007, "Diffusion lengths of silicon solar cells from luminescence images", *J. Appl. Phys.*, Vol. 101, No. 12, p. 123110.
- [11] Mitchell, B. et al. 2011, "Bulk minority carrier lifetimes and doping of silicon bricks from photoluminescence intensity ratios", *J. Appl. Phys.*, Vol. 109, No. 8, pp. 083111-1–083111-12.
- [12] Green, M.A. 2011, "Analytical expressions for spectral composition of band photoluminescence from silicon wafers and bricks", *Appl. Phys. Lett.*, Vol. 99, No. 13, p. 131112.
- [13] Mitchell, B. et al. 2012, "On the method of photoluminescence spectral intensity ratio imaging of silicon bricks: Advances and limitations", *J. Appl. Phys.*, Vol. 112, No. 6, pp. 063116–1–063116–13.
- [14] Walter, D. et al. 2012, "Contrast Enhancement of Luminescence Images via Point-Spread Deconvolution", *Proc. 38th IEEE PVSC*, Austin, Texas, USA.
- [15] Breitenstein, O., Frühauf, F. & Teal, A. 2016, "An improved method to measure the point spread function of cameras used for electro- and photoluminescence imaging of silicon solar cells", *IEEE J. Photovolt.*, Vol. 6, No. 5, pp. 1–6.
- [16] Mitchell, B., Chung, D. & Teal, A. 2016, "Photoluminescence imaging using silicon line-scanning cameras", *IEEE J. Photovolt.*, pp. 1–9.
- [17] Hu, Y., Schön, H. & Arnberg, L. 2013, "Characterization of defect patterns in Cz silicon slabs by carrier density imaging", *J. Cryst. Growth*, Vol. 368, pp. 6–10.
- [18] Schmidt, J. et al. 2013, "Impurity-related limitations of next-generation industrial silicon solar cells", *IEEE J. Photovolt.*, Vol. 3, No. 1, pp. 114–118.
- [19] Schubert, M.C. et al. 2013, "Impact of impurities from crucible and coating on mc-silicon quality – The example of iron and cobalt", *IEEE J. Photovolt.*, Vol. 3, No. 4, pp. 1250–1258.
- [20] Schindler, F. et al. 2014, "Solar cell efficiency losses due to impurities from the crucible in multicrystalline silicon", *IEEE J. Photovolt.*, Vol. 4, No. 1, pp. 122–129.
- [21] Kwapil, W. et al. 2014, "Impact of iron precipitates on carrier lifetime in as-grown and phosphorus-gettered multicrystalline silicon wafers in model and experiment", *IEEE J. Photovolt.*, Vol. 4, No. 3, pp. 791–798.
- [22] Mitchell, B. et al. 2014, "Imaging as-grown interstitial iron concentration on boron-doped silicon bricks via spectral photoluminescence", *IEEE J. Photovolt.*, Vol. 4, No. 5, pp. 1185–1196.
- [23] Macdonald, D., Tan, J. & Trupke, T. 2008, "Imaging interstitial iron concentrations in boron-doped crystalline silicon using photoluminescence", *J. Appl. Phys.*, Vol. 103, No. 7, pp. 073710-1–073710-7.
- [24] Chung, D. et al. 2016, "Photoluminescence imaging for quality control in silicon solar cell manufacturing", *MRS Adv.*, June, pp. 1–10.
- [25] Haunschild, J. et al. 2010, "Quality control of as-cut multicrystalline silicon wafers using photoluminescence imaging for solar cell production", *Sol. Energy Mater. Sol. Cells*, Vol. 94, No. 12, pp. 6–11.
- [26] Demant, M. et al. 2015, "Inline quality rating of multi-crystalline wafers based on photoluminescence images", *Prog. Photovoltaics Res. Appl.*, Vol. 20, No. 1, pp. 1–14.

## About the Authors

**Bernhard Mitchell** is a research fellow at the Australian Centre for Advanced Photovoltaics at UNSW. Since receiving his Ph.D. in 2013 he has led activities involving Si ingot characterization at UNSW. He is a semiconductor physicist with more than 10 years' research experience in the PV sector both in silicon and in III-V technologies.

**Daniel Chung** is a Ph.D. student at the Australian Centre for Advanced Photovoltaics at UNSW. His research focuses on the development of photoluminescence characterization with regard to silicon ingots and applications in solar cell manufacturing.

**Jürgen Weber** began his career in PV as an engineer with a measurement technology specialization at the Fraunhofer CaLab in 2000, and subsequently worked at UNSW in the thin-film group and as a characterization laboratory manager. He joined BT Imaging in 2009, where for the last few years he has focused on the development and optimization of line-scanning PL systems.

**Thorsten Trupke** is a semiconductor physicist having more than 15 years' experience in R&D in the PV sector and specialising in the development of novel characterization methods. He is a professor at the Australian Centre for Advanced Photovoltaics at UNSW, as well as the co-founder and CTO of BT Imaging – a UNSW start-up company that commercializes PL-imaging inspection systems.

## Enquiries

Bernhard Mitchell  
Australian Centre for Advanced Photovoltaics  
School of Photovoltaic and Renewable Energy  
University of New South Wales  
Sydney, NSW 2052  
Australia

Email: [bernhard.mitchell@unsw.edu.au](mailto:bernhard.mitchell@unsw.edu.au)

# Oxygen-defect characterization for improving R&D relevance and Cz-Si solar cell efficiency

Jordi Veirman, Benoît Martel, Nicolas Enjalbert & Sébastien Dubois, CEA Tech-INES, Le Bourget du Lac, & Catherine Picoulet & Pierre Bonnard, AET Technologies, Meylan, France

Market  
Watch

Fab &  
Facilities

Materials

Cell  
Processing

Thin  
Film

PV  
Modules

## ABSTRACT

Most high-efficiency solar cells are fabricated from monocrystalline Czochralski (Cz) silicon (Si) wafers because of the high quality of the material. Despite the considerable heritage from microelectronics, the Cz-Si substrate quality can still limit cell performance. A key issue regarding wafer quality relates to the presence of oxygen in the bulk. Cz wafers indeed feature high oxygen concentrations owing to the silica crucible dissolution during crystal growth. Although not harmful as such, oxygen is a very reactive impurity that can form a plurality of recombination-active defects before, during, or after cell processing. It is now well known that the formation of these defects can lead to reductions in PV conversion efficiency of several per cent absolute. Furthermore, the formation/annihilation of these defects can interfere with cell process optimizations; it can also impact R&D activity or the integration/ramping up of new process tools in a production line. As a consequence, it is of paramount importance to both wafer and cell manufacturers that the Cz substrate quality be controlled. This paper introduces a characterization technique called *OxyMap*, which aims to provide a detailed analysis of oxygen and related defects in Cz-Si wafers. The capabilities of the *OxyMap* technique are presented and illustrated with the help of statistical data obtained for wafers and cells from the main PV players in the industry. Large variations in material quality are revealed among the tested wafers, highlighting the need for quality control in order to optimize the ingot yield/quality and to increase the cell efficiency/reliability.

## Introduction

Solar cell structures labelled as ‘high efficiency’ (>20% in production) are mostly processed from high-quality Cz wafers. The main requirement for such Cz wafers is a long and spatially uniform charge-carrier lifetime ( $\tau$ ) that additionally does not degrade – neither during the cell process nor under outdoor operating conditions. While the first requirement ensures that optimum conversion efficiency is achieved, the second prevents any cell efficiency degradation and cell mismatch at the module level. Commercial Cz ingots, however, seldom meet these specifications from seed to tail (i.e. from top to bottom). Rather, a wide range of recombination-active defects originating from ingot growth can be present in the finished solar cell.

Defects can be classified into three categories, on the basis of whether they are activated during 1) crystal pulling, 2) cell processing, or eventually 3) cell operation. The vast majority of these defects are related to the presence of oxygen in the crystal lattice. Oxygen is incorporated in interstitial positions ( $O_i$ ) into the ingot in concentrations in the range 6–25ppma, following the dissolution of the silica crucible in the Si melt. The main category 1 defects are oxygen-related thermal donors (TDs) [1], and complexes involving intrinsic point defects, such as vacancy-oxygen (V-O) [2]. Category 2 defects are mostly

oxide precipitates and related extended defects, possibly decorated by metallic impurities [3] (may be category 1 defects if ingot crystallization is poor). Belonging to category 3 are those defects activated upon illumination of the cell, such as the well-known boron-oxygen (BO) complex in boron (B)-doped wafers [4], or other defects still under investigation in phosphorus (P) doped wafers [5].

To better illustrate the detrimental effect of oxygen, it is estimated that 10–20% of shipped wafers are affected by oxide precipitation when processed into 20–21% n-PASHA homojunction cells [6]. For amorphous/crystalline Si heterojunction cells processed on seed-end wafers, efficiency drops of around 1%<sub>abs</sub> were also reported [7], presumably because of TDs and/or oxide precipitates. Last, but not least, BO complexes particularly affect passivated emitter and rear cells (PERCs), thereby limiting their rate of entry into the market.

**“It is imperative to develop ways of monitoring and mitigating the concentration of oxygen and related defects throughout the wafer.”**

In spite of the legacy handed down from microelectronics in the art of

crystal pulling, the unprecedented  $\tau$  specifications of high-efficiency cells call for further research and development. In particular, it is imperative to develop ways of monitoring and mitigating the concentration of oxygen and related defects throughout the wafer (unlike microelectronics wafers for which only the near surface – the so-called *denuded zone* – is used for device processing). They may otherwise be an early showstopper for the industry on the way towards achieving the 29.4% theoretical maximum efficiency [8]. In this context, AET Solar Tech and CEA-INES have developed a technique called *OxyMap* in the frame of the eponymous project. *OxyMap* provides a wide picture of oxygen-related defects in Cz wafers for R&D and quality-control purposes, and has now been implemented in a commercial tool. The fundamental features of the technique are detailed and the potential benefits for the PV community are discussed.

## OxyMap measurement: step by step

The patented procedure relies on the change in resistivity ( $\rho$ ) when the TD concentration ( $[TD]$ ) in the wafer is modified in a controlled manner.  $\rho$  is defined as  $(mq\mu)^{-1}$ , where  $q$  is the elementary charge, and  $m$  and  $\mu$  are the majority-carrier density and drift mobility respectively. TDs are thought

to be small  $O_i$  aggregates formed at temperatures in the range 350–600°C, and most effectively at 450°C. Owing to the very strong dependence of TD-formation kinetics and amplitude on the  $O_i$  concentration ( $[O_i]$ ) [9],  $[TD]$  is usually insignificant in oxygen-lean float zone Si and multicrystalline Si. Conversely, it is readily generated in Cz-Si in concentrations of up to a few  $10^{16} \text{cm}^{-3}$ . Because it possesses a double-donor character for typical  $\rho$  in PV, its formation/annihilation leads to a measurable change in  $\rho$ , on which the OxyMap technique is based.

The procedure consists of two anneal steps, with a  $\rho$  measurement before and after each anneal (named chronologically  $\rho_1$ ,  $\rho_2$  and  $\rho_3$ ). The first heat treatment is carried out at 450°C for two to three hours, with the aim of generating TDs ( $[TD]_{450}$ ) in sufficient numbers to induce a measurable change in  $\rho$ . The second treatment is performed above 700°C for a few minutes, leading to TD annihilation. From this set of  $\rho$  data, typically obtained from a four-point probe or non-contact eddy current measurements, a wide set of output values can be calculated. An overview of the full procedure is given in Fig. 1. The calculation details are presented hereafter for p-type B-doped wafers. In the case of n-type P-doped wafers, the B concentration ( $[B]$ ) ought to be replaced by that of P ( $[P]$ ), and the minus sign by a plus; the mobility term should be that corresponding to majority electrons ( $\mu_e$ ).

Prior to any intentional thermal treatment, when  $\rho_1$  is measured, the wafer contains a certain number of TDs formed during crystal cooling ( $[TD]_{ini}$ ), which compensates for the intentional acceptor doping provided by B atoms. After the 450°C anneal, when  $\rho_2$  is measured, the concentration of intentionally formed TDs ( $[TD]_{450}$ ) further adds up to the already existing  $[TD]_{ini}$ . Following the 700°C heat treatment, when  $\rho_3$  is measured, the wafer is eventually left TD free and therefore contains virtually only B as doping species.  $\rho_1$ ,  $\rho_2$  and  $\rho_3$  are thus expressed using the following set of equations, where  $\mu_{h,n}$  ( $n=1, 2, 3$ ) is the majority hole drift mobility and depends on the concentrations of all doping species [10]:

$$\rho_1 = \frac{1}{([B] - 2 \times [TD]_{ini}) \times q \times \mu_{h,1}} \quad (1)$$

$$\rho_2 = \frac{1}{([B] - 2 \times ([TD]_{ini} + [TD]_{450})) \times q \times \mu_{h,2}} \quad (2)$$

$$\rho_3 = \frac{1}{[B] \times q \times \mu_{h,3}} \quad (3)$$

The factor 2 arises from the predominance of the doubly ionized state of TD in usual PV materials [11,12]. To capture the recently discovered effect of compensation on  $\mu$ , the enhancement of Klaassen's model as proposed by Schindler et al. [13] is used. Note that  $\rho_3 < \rho_1 < \rho_2$  in p-type Si, and  $\rho_3 > \rho_1 > \rho_2$  in n-type Si, which allows the conductivity type to be determined. The next steps essentially involve solving Equations 1–3 for the three unknowns  $[B]$ ,  $[TD]_{ini}$  and  $[TD]_{450}$ : once  $[B]$  has been determined from Equation 3, the value of  $[TD]_{ini}$  is extracted using Equation 1, and  $[TD]_{450}$  is eventually worked out from Equation 2.

$[O_i]$  is subsequently determined using an internally developed empirical expression for the TD generation kinetics at 450°C. This expression was established from a set of 42 samples prepared from the bottom, middle and top sections of industrial-like ingots. These 3mm-thick slices included both p- and n-type material, from a wide range of  $\rho$  (from 0.5 to 200  $\Omega \cdot \text{cm}$ ). The samples were mirror-polished to allow  $[O_i]$  measurements by Fourier transform infrared (FTIR) spectroscopy, routinely used in industry for  $[O_i]$  measurements. Note that the FTIR analyses reported throughout this paper were performed in accordance with the SEMI-recommended ASTM F1188-93a associated with the IOC88 calibration coefficient of 6.28ppma-cm. The  $[O_i]$  values provided by OxyMap, which is an FTIR-calibrated technique, are also given with respect to ASTM F1188-93a. Historically, however, the prevailing norm in the industry has been ASTM F121-83, associated with the DIN coefficient of 4.9ppma-cm. This leads to a 22% difference in derived  $[O_i]$  between the two norms. It should be stressed that in order to allow relevant comparisons between the two, the appropriate conversions must be made.

“The strong dependence of TD formation on  $[O_i]$  gives the OxyMap technique its outstanding sensitivity.”

The evolution of  $[TD]_{450}$  with annealing time was then accurately monitored on the same samples using four-point probe  $\rho$  measurements and Equations 1 to 3. It was confirmed that TD-formation kinetics depend very strongly on  $[O_i]$ ; by way of example, the TD formation rate is accelerated by a factor of 170 with just a fourfold increase in  $[O_i]$  (from 6 to 25ppma). This outstanding sensitivity property of TDs is imparted to the OxyMap technique: the strong dependence of TD formation on  $[O_i]$  gives the OxyMap technique its outstanding sensitivity.

The kinetic model  $[TD]_{450} = f([O_i], t)$  was then used in the OxyMap technique to allow the conversion of  $[TD]_{450}$  into  $[O_i]$  data. The agreement achieved between OxyMap and FTIR measurements was within 5% (see Fig. 2). Note that a departure from the black curve ( $x = y$ ) in Fig. 2 would be expected in the presence of excessive column IV elements. For a given  $[O_i]$ , these elements are indeed known to slow down the TD-formation kinetics; among them, carbon is typically encountered in Cz crystals because of graphite elements. Nevertheless, the threshold carbon content above which this slowing-down occurs is around 2ppma, which exceeds usual specifications.

In the next step, the accuracy of the OxyMap  $[O_i]$  measured for thin as-cut wafers ( $< 200 \mu\text{m}$ ) was put to the test, by a comparison with the FTIR values obtained for neighbouring thick polished slices. Some representative examples are shown for both n- and p-type Si in Fig. 3. In these cases, the OxyMap

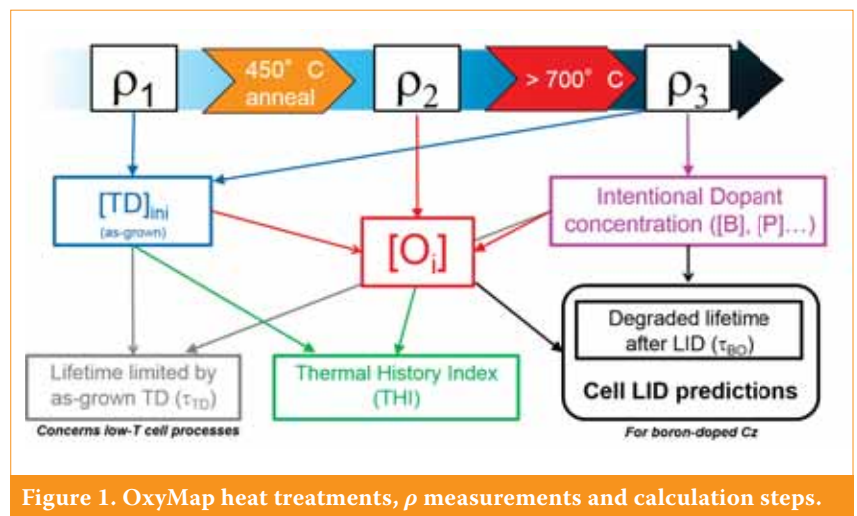


Figure 1. OxyMap heat treatments,  $\rho$  measurements and calculation steps.

technique was performed on wafers regularly sampled along 8" industrial ingots, using a non-contact eddy current head for the  $\rho$  measurements. The overall agreement achieved is excellent. When OxyMap is used on thin as-cut wafers for  $[O_i]$  measurements rather than FTIR, thick polished slices are no longer required and can be turned into wafers instead, thereby enabling significant savings.

As a result of random scattering of the infrared beam at the surfaces and chaotic internal multireflections, standard FTIR is not really applicable to thin as-cut wafers. An elegant upgrade of the FTIR technique was recently suggested to solve this issue [14], but it is destructive and requires very careful sample cleavage. OxyMap, on the other hand, has been shown to perform equally well whatever the thickness – at least down to a thickness of 80 $\mu$ m [11].

If  $\rho_1$ ,  $\rho_2$  and  $\rho_3$  measurements are now performed in the form of a line scan along the wafer diagonal, and taking into account the quasi-centrosymmetric defect distribution in Cz wafers inherent to the process itself, OxyMap can provide each output value from Fig. 1 in the form of a 2D mapping. An example of an  $[O_i]$  mapping is given in Fig. 4: the usual hill-shaped  $[O_i]$  profile is revealed, which results from convection-induced piling-up of O in the melt under the crystal centre. Typical slight radial oscillations in  $[O_i]$  due to growth rate fluctuations can also be observed.

Since the OxyMap procedure involves high-temperature treatments likely to modify the wafer properties significantly, it was considered relevant to assess whether measured wafers could be reused as substrates for high-efficiency device manufacturing. For Al-BSF cells processed by third parties (efficiency >19%), no systematic change in efficiency was observed, compared with cells processed from reference wafers (i.e. not measured with OxyMap). In the worst-case experiment, a 0.2%<sub>abs</sub> average reduction was observed, which may be attributed to contamination caused by additional handling of wafers. In the case of heterojunction cells, different behaviours were observed, depending on wafer providers, with even slight gains noticed for some of them, presumably from the benefits of the >700°C temperature step. More data should however be collected before drawing conclusions.

All the features in Fig. 1 have been implemented in an R&D tool commercialized by AET Technologies. Metrology characteristics were estimated for this tool. The wafer-to-wafer repeatability on  $[O_i]$  turned out to be better than 2%, while the resolution (smallest detectable variation in  $[O_i]$ ) was around 0.3ppma. The measurement accuracy associated with  $[O_i]$  is mainly driven by uncertainties in the  $\rho$  measurements. The closer together  $\rho_1$  and  $\rho_2$  are, the larger the uncertainties become. The worst-case scenario thus concerns low  $\rho_1$  and  $O_i$ -lean p-type wafers. If one considers, for instance, a B-doped 1 $\Omega$ -cm with  $[O_i] = 10$ ppma, an uncertainty of  $\pm 20\%$  is expected (including the aforementioned  $\pm 5\%$  – see Fig. 2); however, this rapidly shrinks to  $\pm 5\%$  as either  $[O_i]$  increases or the doping decreases. For pulling-process optimizations, it is recommended that measurements of low  $[O_i]$  be performed on lightly doped ingots. In principle,  $[O_i]$  as low as 6ppma can be measured with a  $\pm 7\%$  accuracy for a 5 $\Omega$ -cm n-type material.

### Cell LID predictions

Since the early days of the OxyMap technique [10], several new features have been gradually introduced. Because the technique allows both [B] and  $[O_i]$  to be determined, it was decided to trust the technique further and assess its capability to predict from as-cut wafers the light-induced degradation (LID) related to the BO complex in B-doped cells.

In a first step, the carrier lifetime limited by the formation of the BO complexes after LID ( $\tau_{BO}$ ) at an excess carrier density ( $\Delta n$ ) equal to [B]/10 was predicted using the OxyMap [B] and

## Advanced characterization technology to qualify Cz Silicon wafers & ingots



Large set of accurate data dedicated to:  
 - material qualification and sorting for Cz wafer suppliers/users  
 - optimization of ingots and cells manufacturing processes



cell LID losses ▶ PERC + Al-BSF



Thickness independent

Operator independent

Non destructive

No sample preparation

Reproducible

No material loss

No restriction on wafer surface roughness

No restriction on wafer thickness

+33 (0)4 76 904 118

<http://aetsolartech.com/>

Auvergne – Rhône-Alpes



[O<sub>i</sub>] values. To this end, the well-known empirical expression from Bothe et al. [4] was used:

$$\tau_{BO} = a \times 7.675 \times 10^{45} \times [B]^{-0.824} \times [O_i]^{-1.748} \quad (4)$$

The beneficial effect of the P emitter formation on the LID amplitude is taken into consideration here by setting *a* to 2, as reported in Bothe et al. [4]. The validity of the  $\tau_{BO}$  predictions was experimentally verified by comparison with the  $\tau_{BO}$  measured for diffused and then emitter-etched wafers from 10 different providers [15].

Following this preliminary verification, algorithms describing the relative LID loss for each PV parameter were established [15,16] for a wide range of

realistic  $\tau_{BO}$  values (i.e. of [B] and [O<sub>i</sub>]). For this purpose, the PC1D software was used;  $\tau_{BO}$  and its variation with  $\Delta n$  were modelled with the recombination parameters from Rein et al. [17]. The first simulations were run for a 180 $\mu$ m-thick Al-BSF cell with a pre-LID efficiency of 18.5%. Experimentally measured values were used as input parameters for the diffused emitter ([P] profile), the Si nitride coating (spectral variation of the reflectance and front-surface recombination velocity), and the screen-printed metallization (series and shunt resistances). For the back-side Al-BSF, an approximated Al concentration profile and rear-surface recombination velocity were used, as they were not known accurately at that time. The relative losses computed for each PV parameter were plotted as

a function of both [B] and [O<sub>i</sub>]. They were then successfully fitted using exponential-like expressions – with [B] and [O<sub>i</sub>] as the only variables – and further fine-tuned to reproduce the measured losses for 18.5% Al-BSF CEA cells (mainly in order to include small differences between the simulated and the experimental structures).

The LID prediction algorithms were extensively tested with third parties in the framework of the project. As an example, Fig. 5 shows a comparison of predicted and measured LID losses (0.1W.cm<sup>-2</sup> illumination for 48h at 25°C) for 19.5% (pre-LID) Al-BSF cells. The devices were processed at a partner's site on wafers from three providers. The losses in efficiency span a wide range of values, from around 1 to 3%<sub>rel</sub>, revealing large variations in material quality. A fairly good agreement between predictions and measurements was obtained. The observed scattering – typical for such comparisons – can have multiple root causes: it can result from cumulative uncertainties in the LID losses measurements, in the cell and software models, and in the [O<sub>i</sub>] and [B] measurements.

Because of the significant differences in efficiency between the cells used for establishing the semi-empirical model and the processed cells, the agreement achieved may initially appear questionable. Indeed, one would expect significantly larger relative LID losses for the 19.5%-efficient processed cells, because of the greater sensitivity to  $\tau$ . However, the 19.5% cell operates at a higher  $\Delta n$ , where the  $\tau$  limited by the BO complexes is higher (owing to their asymmetric electron- and hole-capture cross sections). Simulations show that this injection-level effect maintains a reasonable LID amplitude

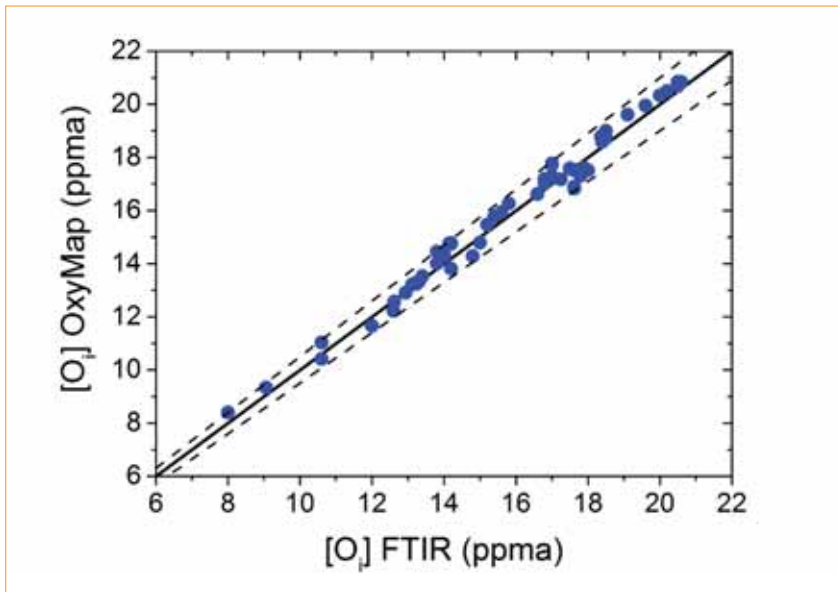


Figure 2. Agreement between OxyMap and FTIR measurements for the set of 42 thick polished wafers. (The dashed lines indicate variations of  $\pm 5\%$ .)

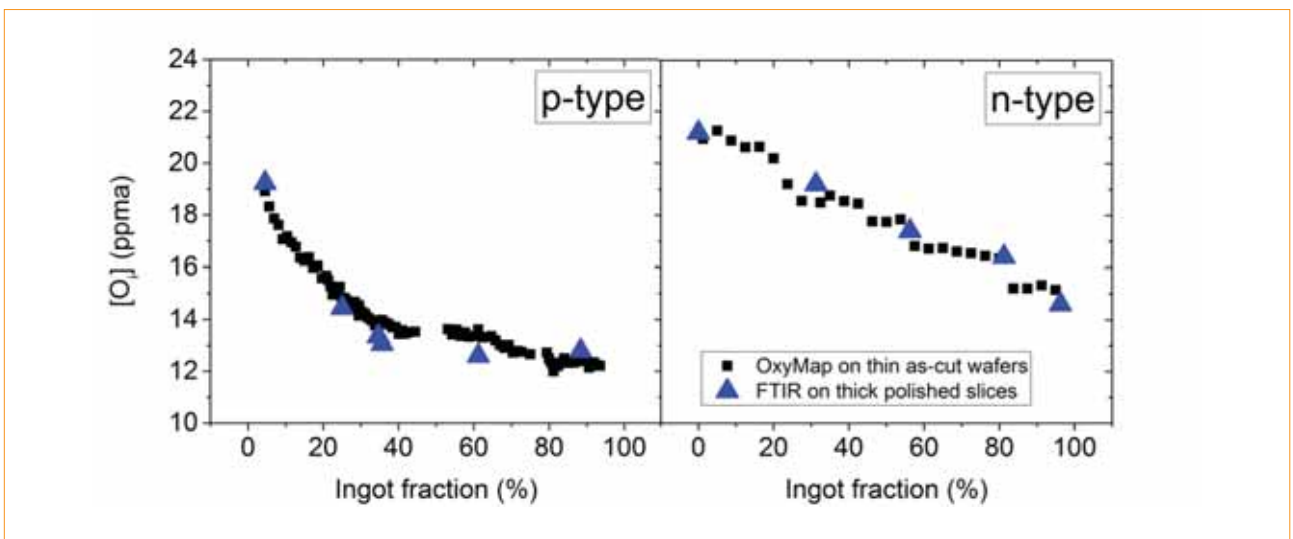


Figure 3. [O<sub>i</sub>] profiles measured using OxyMap on 180 $\mu$ m-thick as-cut wafers (squares) and 2mm-thick mirror-polished slices using FTIR (triangles).

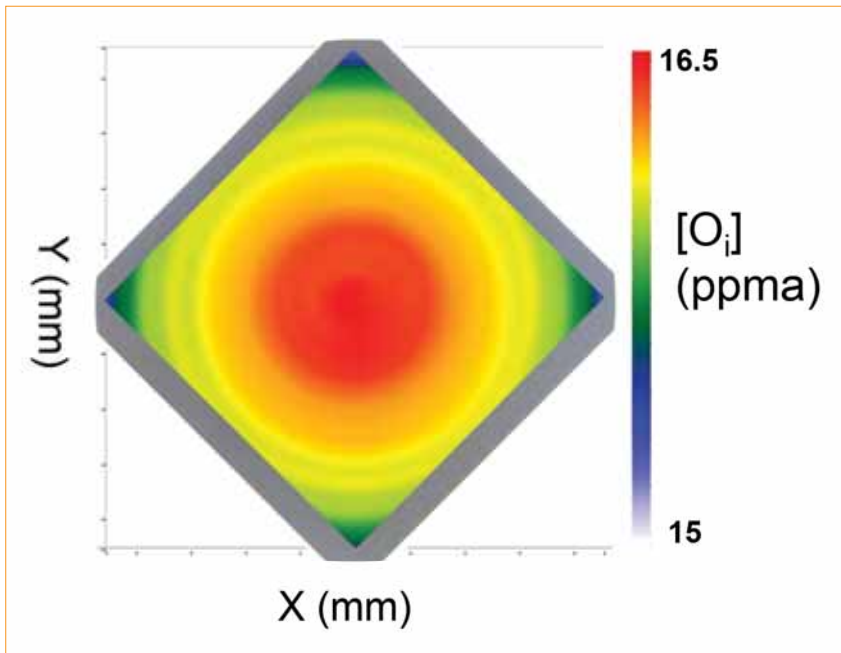


Figure 4. Example of an  $[O_i]$  mapping. Such mappings can be computed for all output values listed in Fig. 1.

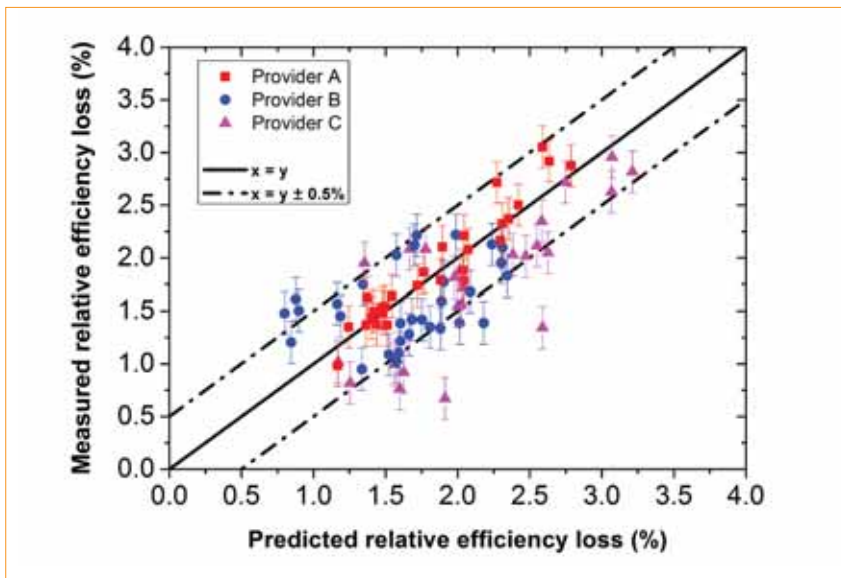


Figure 5. Comparison of predicted and experimental LID losses for three sets of cells.

for 19.5%-efficient devices – only slightly more than that for the 18.5% simulated cell (typically 10–15%<sub>rel</sub> higher amplitudes [18]). Such a slight deviation would be hardly detectable in practice because of the aforementioned data scattering, as revealed in Fig. 5.

It is known that the cell architecture and its fabrication process can influence the LID losses [18,19]. To take this into account, the OxyMap tool from AET Technologies also allows the user to enter home-made LID prediction algorithms based on OxyMap  $[O_i]$  and  $[B]$  values. This alternative is particularly attractive for PERC cells (usually highly sensitive to LID), whose comparatively recent adoption by the industry leads

to a larger variety of existing processes, making it unlikely that a universal PERC-LID model could be achieved.

It is believed that the LID predictions can be of great help to cell manufacturers in order to benchmark wafers providers, or for the ramping-up of anti-LID processes, such as the new light-induced regeneration tools. Performing these predictions at the wafer level means that any cell processing or time-consuming ageing tests are avoided.

### Detection of poor-quality wafers

For R&D needs, sheet resistance ( $R_{\text{sheet}}$ ) of highly doped surfaces and

implied open-circuit voltage ( $i-V_{\text{oc}}$ ) are routinely measured in order to optimize cell processes. Both  $R_{\text{sheet}}$  and  $i-V_{\text{oc}}$  measurements depend heavily on the wafer  $\rho$  which is traditionally measured on as-cut wafers prior to any processing. It is generally assumed that  $\rho$  is stable throughout the cell processing sequence; however, large  $\rho$  variations can be expected after  $>650^\circ\text{C}$  anneals (owing to  $\text{TD}_{\text{ini}}$  dissolution), making this assumption questionable. Fig. 6, based on the statistics for ~1,400 wafers of both types from 15 industrial providers, reveals that around 20% of the tested wafers feature a  $\rho$  variation after  $>650^\circ\text{C}$  anneals greater than 10% and up to 200%, which can invalidate  $R_{\text{sheet}}$  and  $i-V_{\text{oc}}$  values. It is roughly estimated, for instance, that a 50% unexpected  $\rho$  variation can lead to biases of around 10% in  $R_{\text{sheet}}$  for a standard P emitter, and of 5mV in  $i-V_{\text{oc}}$  for an  $i-V_{\text{oc}}$  of ~680mV (with, of course, worse results for larger variations in  $\rho$ ). The identification of wafers with a stable  $\rho$  (or the knowledge of  $\rho$  after high-temperature steps) using OxyMap is therefore an asset for improving the accuracy of R&D data.

“The identification of wafers with a stable  $\rho$  using OxyMap is an asset for improving the accuracy of R&D data.”

For production purposes, OxyMap can help identify poor-quality wafers, which will result in lower efficiency. Except perhaps in case of excessive contamination by metallic elements, many lifetime-limiting defects are related to  $O_i$  in Cz-Si. Nevertheless, a tentative identification of poor wafers based solely on  $[O_i]$  is prone to failure. Indeed, other parameters (such as the thermal history) greatly influence the number of O-related defects. The thermal history is defined as the temperature vs. time profile that is experienced during crystal growth. Since a typical pulling process lasts for several tens of hours, seed-end wafers feature a much longer thermal history than tail-end wafers, the latter being crystallized last; for a given  $[O_i]$ , they are therefore more likely to contain O-related defects. It is well known, for instance, that TDs form preferentially at the ingot seed-ends, where the material experiences the longest time within the TD-formation temperature range.

In order to improve the capacity of OxyMap to detect poor-quality wafers,  $[O_i]$  was tentatively combined with a thermal history index (THI, in minutes) in order to establish a novel wafer quality indicator [20]. The THI was calculated from the measured values of  $[O_i]$  – the

'driving force' for TD formation – and  $[TD]_{ini}$ , the 'relic' that results from the expression of this driving force during the crystal cooling.

Fig. 7 depicts an example of 156 PSQ n-PERT (passivated emitter, rear totally diffused) solar cells processed at CEA-INES; with the process used at the time of this study, the baseline efficiency was around 20% [21]. Wafers were sampled from two commercial ingots from the same manufacturer. While both ingots feature similar THI profiles,  $[O_i]$  peaks at different locations: in Ingot 1,  $[O_i]$  peaks at the point where THI is high, whereas in Ingot 2,  $[O_i]$  peaks at the point of low THI. As represented by the solid rectangle, large  $[O_i]$  in conjunction with large THI wafers were associated with decreased efficiencies. The corresponding PERT cells showed a low hole-diffusion length core at the cell centre, which is usually related to oxide precipitates [22,23]. On the other hand, the occurrence alone of a high THI or a high  $[O_i]$  (dashed green rectangles) did not lead to any efficiency reductions. It is therefore concluded that  $[O_i]$  in combination with THI can be used as a quality indicator to detect wafers affected by O-related issues. Note that similar conclusions have been drawn for rear-emitter heterojunction solar cells [20]. For a given cell process, a maximum acceptable threshold value for the combination can thus be set for rejecting poor-quality wafers and for improving the overall cell efficiency of the production line.

It should be stressed here that, because Si vacancies can play an important role in oxygen precipitation [24], the correlation between  $[O_i]$ , THI and bulk-related efficiency reductions might not be systematic. Future studies involving a larger number of ingots/cell

processes should help in specifying, for the different processes, the significance and threshold values for the ' $[O_i]$ +THI' indicator.

### Feedback for pulling-process optimizations

A mapping of the THI at the ingot level can be reconstructed from a set of 2D wafer mappings; an example of such an ingot mapping is shown in Fig. 8. In this example, a region with a high THI of around 500min is evidenced close to the seed-end, which suggests a slow cooling after crystallization, thereby promoting O-related defect formation. Such feedback can in turn be used to drive advances in R&D. The benefits of a new hot-zone design can be directly assessed, for instance, by its effect on the THI distribution. Note that, by definition, the THI is representative of the length of time spent in the TD-formation range (i.e. 600–350°C) during cooling down. It is tacitly assumed here by extension that it is also representative of the overall cooling profile. Simulation tasks are ongoing at CEA-INES in order to assess the validity of this assumption for today's industrial pulling processes.

Similar mappings can be reconstructed for all parameters in Fig. 1, such as  $[O_i]$ . Spatial variations, as well as the absolute  $[O_i]$ , are largely determined by crystal growth parameters [1]. In an attempt to lower  $[O_i]$  and its radial variations, R&D teams can therefore benefit greatly from such characterizations in terms of accelerating crystallization process improvements.

### Influence of thermal donors on the electrical properties

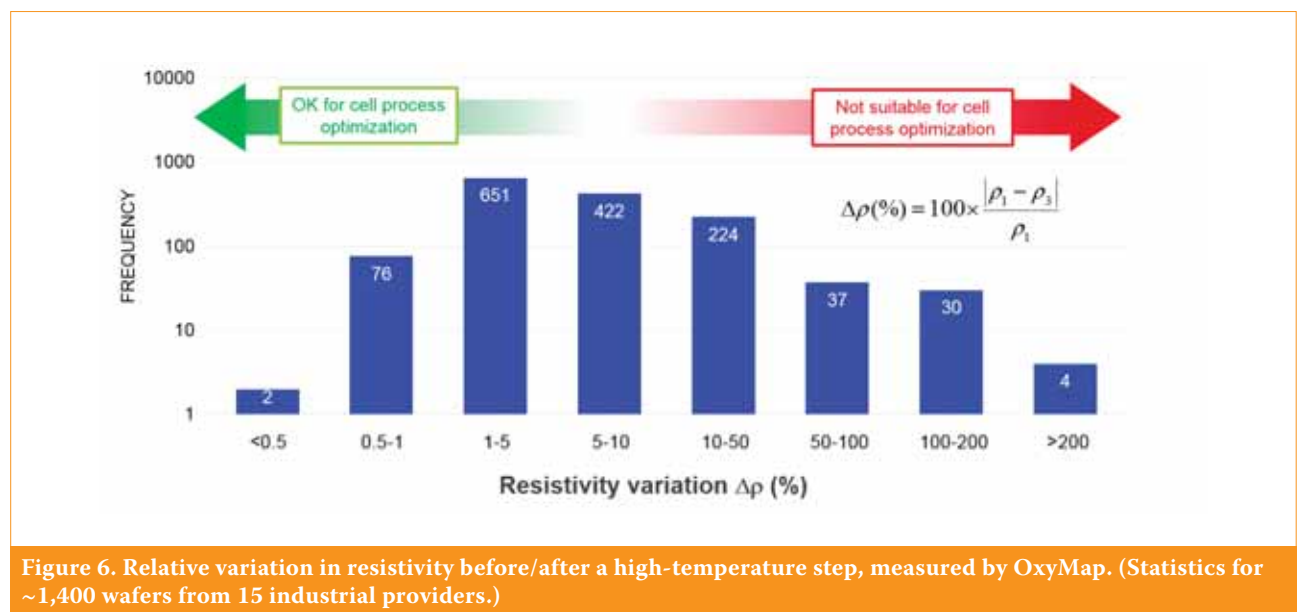
In addition to their well-known

dopant character, TDs can induce a significant recombination activity. Heterojunction cells are fabricated using low-temperature processes (generally <250°C) that do not annihilate  $TD_{ini}$ , unless a specific thermal donor anneal is performed beforehand.  $TD_{ini}$  can in turn induce efficiency reductions of up to 4%<sub>abs</sub>, for values encountered in commercial ingots (i.e. from a few  $10^{13}cm^{-3}$  up to  $2 \times 10^{15}cm^{-3}$ , according to our database) [25]. When the model developed by our group in Tomassini et al. [25] is used, the lifetime limited by  $TD_{ini}$  ( $\tau_{TD}$ ) can be calculated from OxyMap data and subsequently mapped across the wafer. Such a mapping can be obtained directly from OxyMap measurements for as-cut wafers, i.e. without the need for surface passivation.

In order to check the mapping validity, wafers containing TDs ( $[TD]_{ini} \sim 1.9 \times 10^{15}cm^{-3}$ ) were measured by OxyMap to yield 2D mappings of  $\tau_{TD}$ ; meanwhile the sister wafers were etched and cleaned before passivation of both surfaces using intrinsic and n-type amorphous Si stacks. The effective carrier lifetimes of the passivated wafers were subsequently mapped from the photoconductance decay detected by microwave. A typical comparison of both types of mappings is given in Fig. 9. A very good qualitative agreement was achieved, illustrating the possibility of predicting the lifetime from OxyMap measurements of as-cut wafers.

### Conclusion

The OxyMap technique, with the goal of providing an in-depth characterization of oxygen-related defects in Cz-Si, was developed step by step in the framework of the eponymous project. The technology has now matured and offers



a full range of features to the benefit of the PV community. All the presented features are now included in an R&D tool commercialized by AET Technologies.

It was shown that both ingot/wafer and cell providers can leverage the OxyMap output values to continually improve ingot quality and cell efficiency. The technique, which does not require any wafer preparation, is shown to be independent of the wafer thickness (down to thicknesses below 100 $\mu\text{m}$ ), which makes it compatible with the expected trends of the PV industry. The OxyMap tool developed on this basis is operator independent and features batch-processing capabilities. It is believed that

the tool represents a key opportunity for the PV industry to better characterize incoming/outgoing materials, and speed up the race towards higher-efficiency and more cost-effective solar cells, with attractive returns on investment.

“It is believed that the OxyMap tool represents a key opportunity for the PV industry to better characterize incoming/outgoing materials.”

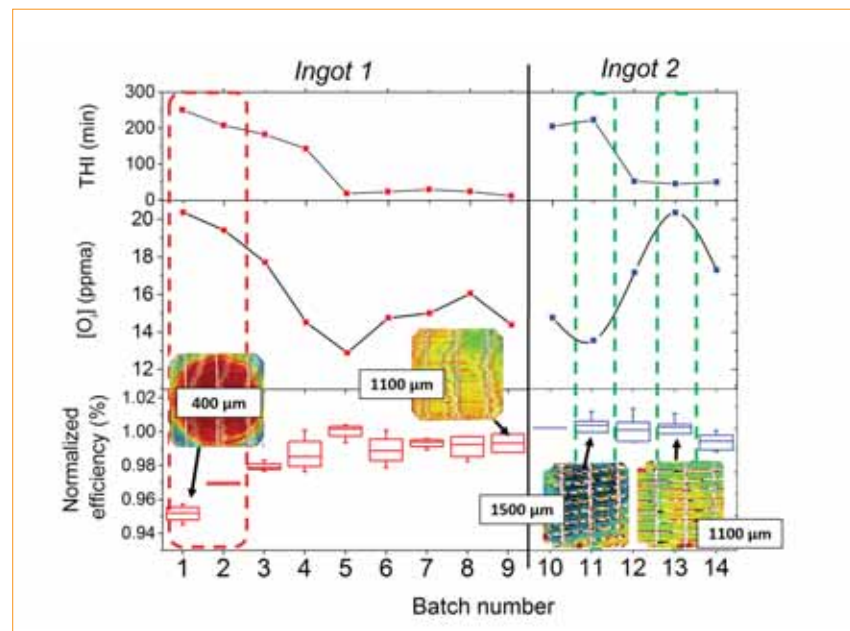


Figure 7. Comparison of n-PERT normalized cell efficiency with diagonal averaged  $[O_i]$  and THI for two Cz ingots. Hole-diffusion length mappings obtained from light-beam-induced current measurements are also shown (scale from 400 to 2000 $\mu\text{m}$ ). The central hole-diffusion length values are given.

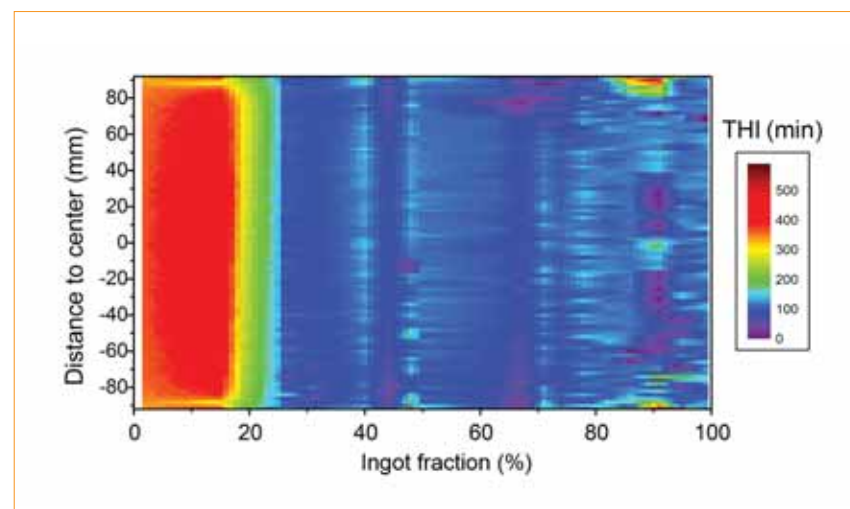


Figure 8. Example of a THI mapping of a 90kg 8" ingot, showing a region with extended cooling time (in red). (Reconstructed from 25 wafers measured using OxyMap.)

### Acknowledgments

The CEA-INES and AET Technologies teams are indebted to Gintech, Hanwha Q CELLS, Norsun SA, Photowatt, FC3S group/CRPS/Air Liquide, ISC Konstanz, and other companies for feedback on the accuracy of OxyMap and/or for cell LID assessment.

### References

- [1] Shimura, F. (Ed.) 1994, *Oxygen in Silicon*. Boston: Academic Press, pp. 251–280.
- [2] Zheng, P et al. 2014, “Evidence for vacancy-related recombination active defects in as-grown n-type Czochralski silicon”, *IEEE J. Photovolt.*, Vol. 5, pp. 183–188.
- [3] Murphy, J.D. et al. 2015, “The effect of oxide precipitates on minority carrier lifetime in n-type silicon”, *J. Appl. Phys.*, Vol. 118, p. 215706.
- [4] Bothe, K. et al. 2005, “Fundamental boron–oxygen-related carrier lifetime limit in mono- and multicrystalline silicon”, *Prog. Photovoltaics Res. Appl.*, Vol. 13, pp. 287–296.
- [5] Letty, E. et al. 2016, “Evidence of coexisting lifetime-limiting defects in as-received seed-end Czochralski wafers – Effect of light soaking”, Presented at E-MRS spring meeting, Lille, France.
- [6] Bronsveld, P.C.P. et al. 2015, “The effect of n-Pasha processing on bulk wafer quality”, *Proc. 31st EU PVSEC*, Hamburg, Germany.
- [7] Danel, A. et al. 2015, “Recent progress on the CEA-INES heterojunction solar cell pilot line”, *Proc. 31st EU PVSEC*, Hamburg, Germany.
- [8] Richter, A. et al. 2013, “Reassessment of the limiting efficiency for crystalline silicon solar cells”, *IEEE J. Photovolt.*, Vol. 3, No. 4, pp. 1184–1191.
- [9] Londos, C.A. 1993, “Effect of oxygen concentration on the kinetics of thermal donor formation in silicon at temperatures between 350 and 500°C”, *Appl. Phys. Lett.*, Vol. 62, pp. 1525–1526.
- [10] Veirman, J. et al. 2011, “A fast and easily implemented method for interstitial oxygen concentration mapping through the activation of thermal donors in silicon”, *Energy Procedia*, Vol. 8, pp. 41–46.
- [11] Veirman, J. 2012, “Oxygen mappings in silicon: From ultra-thin wafers to ingots”, *Proc. 6th CscC*, Aix-Les-Bains, France.
- [12] Voronkov, V.V. 2009, “Advanced application of resistivity and Hall effect measurements to characterization of silicon”, *ECS Trans.*, Vol. 25, No. 3, pp. 25–34.
- [13] Schindler, F. et al. 2014, “Towards a unified low-field model for carrier mobilities in crystalline silicon”, *Sol.*



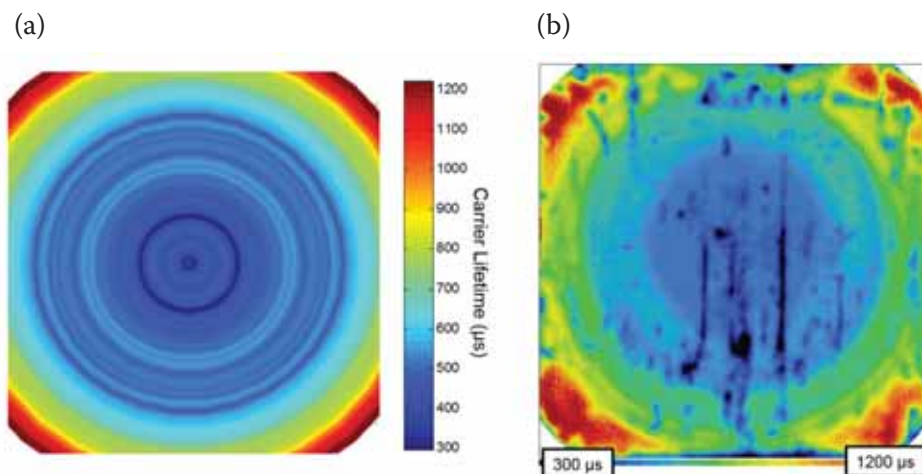


Figure 9. Typical comparison of effective carrier lifetimes: (a) OxyMap predicted ( $\tau_{TD}$ ); (b) measured.

- Energy Mater. Sol. Cells*, Vol. 131, pp. 92–99.
- [14] Wolny, F. 2016, *Energy Procedia* [forthcoming].
- [15] Veirman, J. et al. 2013, “Mapping of oxygen-related defects in silicon for high efficiency solar cells: Application to the prediction of LID losses”, *Proc. 28th EU PVSEC*, Paris, France.
- [16] Cascant, M. et al. 2014, “Investigating the spatial distribution of oxygen-related defects in Czochralski silicon wafers and ingots”, *Proc. 8th SNEC*, Shanghai, China.
- [17] Rein, S. et al. 2003, “Electronic properties of the metastable defect in boron-doped Czochralski silicon: Unambiguous determination by advanced lifetime spectroscopy”, *Appl. Phys. Lett.*, Vol. 82, p. 1054.
- [18] Das, A. 2012, “Development of high-efficiency boron diffused silicon solar cells”, Ph.D. dissertation, Georgia Institute of Technology, Atlanta, USA.
- [19] Altermatt, P. et al. 2009, “Highly predictive modelling of entire solar cells for industrial applications”, *Proc. 24th EU PVSEC*, Hamburg, Germany.
- [20] Veirman, J. et al. 2016 “Thermal history index as a bulk quality indicator for Czochralski solar wafers”, *Sol. Energy Mater. Sol. Cells* [forthcoming].
- [21] Cabal, R. et al. 2014, “20% PERT technology adapted to n-type mono-like silicon: Simplified process and narrowed cell efficiency distribution”, *Proc. 29th EU PVSEC*, Amsterdam, The Netherlands.
- [22] Letty, E. et al. 2016, “Identification of lifetime-limiting defects in as-received and heat treated seed-end Czochralski wafers”, *Energy Procedia* [forthcoming].
- [23] Haunschild, J. et al. 2012, “Cz-Si wafers in solar cell production: Efficiency-limiting defects and material quality control”, *Photovoltaics International*, 15th edn, pp. 40–46.
- [24] Falster, R. et al. 2000, “On the properties of the intrinsic point defects in silicon: A perspective from crystal growth and wafer processing”, *physica status solidi (b)*, Vol. 222, p. 219.
- [25] Tomassini, M. et al. 2016, “Recombination activity associated with thermal donor generation in monocrystalline silicon and effect on the conversion efficiency of heterojunction solar cells”, *J. Appl. Phys.*, Vol. 119, p. 084508.

#### About the Authors



**Jordi Veirman** studied semiconductor physics at the National Institute for Applied Sciences (INSA) in Lyon, where he graduated with an engineering degree, followed by a master’s in microelectronics in 2008. Since obtaining his Ph.D. from INSA, in the framework of which the foundations of the OxyMap technique were laid, he has been working as a project leader at CEA in the homojunction and heterojunction labs.



**Benoît Martel** started his career in the PV industry at PHOTOWATT as a cell process engineer. In 2011 he joined CEA-INES, to develop advanced characterization tools for PV applications. He is currently working as a research engineer and project leader on characterizing PV silicon defects and developing the cell process.



**Nicolas Enjalbert** started his career in the PV industry at PHOTOWATT, working on silicon wafers and cell characterizations. In 2005 he joined CEA-INES, where his research

activities focus on solar-grade silicon, defects and advanced characterizations.



**Sébastien Dubois** studied materials science at the National Institute for Applied Sciences (INSA) in Lyon, and graduated with an engineering degree in 2004. In 2007 he received his Ph.D. in physics from Marseille University. After joining CEA-INES in 2007 he conducted and supervised research in the field of defects in crystalline silicon solar cells. He is currently responsible for the homojunction silicon solar cells laboratory.



**Catherine Picoulet** has been working at AET SolarTech since 2014. Among other activities, she is responsible for the business development and worldwide distribution of OxyMap technology. Prior to joining AET SolarTech, she held various senior positions as business development or operations manager at Applied Materials, Nextral and ASM.



**Pierre Bonnard** joined AET Technologies in 2005 after graduating with a master’s in electrical specification from Grenoble Institute of Technology. He works on industrial furnaces as a senior electrical and automation engineer at AET Technologies, where he is also the product manager for the OxyMap tool.

#### Enquiries

Email [jordi.veirman@cea.fr](mailto:jordi.veirman@cea.fr)  
[cpicoulet@aet-technologies.fr](mailto:cpicoulet@aet-technologies.fr)

# Cell Processing



**Page 50**  
**News**

---

**Page 53**  
**Techniques for mitigating light-induced degradation (LID) in commercial silicon solar cells**

Brett Hallam<sup>1</sup>, Catherine Chan<sup>1</sup>, David Payne<sup>1</sup>, Dominik Lausch<sup>2</sup>, Marcus Gläser<sup>2</sup>, Malcolm Abbott<sup>1</sup> & Stuart Wenham<sup>1</sup>

<sup>1</sup>University of New South Wales (UNSW), Sydney, Australia; <sup>2</sup>Fraunhofer Center for Silicon Photovoltaics (CSP), Halle (Saale), Germany

---

**Page 64**  
**BiCoRE: Combining a PERC-type cell process with n-type wafers**

Thorsten Dullweber, Nadine Wehmeier, Anja Nowack, Till Brendemühl, S. Kajari-Schröder & R. Brendel, Institute for Solar Energy Research Hamelin (ISFH), Emmerthal, Germany

---

**Page 72**  
**Stencil printing and metal squeegees for improved solar cell printing results**

Andrew Zhou, Rado Yang, Tom Falcon & Jessen Cunnusamy, ASM Alternative Energy & Thorsten Dullweber & Helge Hannebauer, Institute for Solar Energy Research Hamelin (ISFH)

---

## PERC solar cell production to exceed 15GW in 2017

Passivated emitter rear contact (PERC) production is forecast to exceed 15GW in 2017, accounting for more than 20% of all p-type solar cells produced in the year.

PERC has become the first major application for lasers in the mainstream c-Si cell sector in the solar industry, with all other applications either legacy/dormant or as part of process flows that may reside permanently in the research lab or at best make it into production, several years from now.

In contrast to deposition equipment suppliers for PERC (of which Meyer Burger is by far the dominant company), the landscape and choice for laser tools would appear to be more diverse. This includes the most active European based laser equipment suppliers, InnoLas Solutions GmbH (InnoLas) and 3D-Micromac and Asian tool suppliers, of which the most successful to date have been Wuhan DR Laser Technology (Dr Laser) in China and TeraSolar Energy Materials (TeraSolar) in Taiwan.

The trends in recent years of Chinese cell manufacturers seeking to implement a greater quantity of production equipment from Chinese-based suppliers, potentially represents a threat to how much companies like InnoLas and 3D-Micromac can follow the PERC trends from Southeast Asia and Taiwan back into Chinese cell manufacturing.



Credit: Imrec

PERC production is forecast to exceed 15GW in 2017.

### PERC

#### LONGi reaches 900MW of mono-PERC production

Leading integrated monocrystalline PV manufacturer Xi'an LONGi Silicon Materials reached 900MW of monocrystalline PERC solar cell production at the end of the first half of 2016.

Reaching 900MW of PERC solar cell capacity put the company ahead of rivals in China migrating to the high-efficiency cells and further PERC capacity will be added in the second half of the year.

The PERC capacity increases are also intended to support lower production costs, which have been supported by increased R&D expenditure across wafer, cell and modules in the last couple of years.

R&D spending in the first half of 2016 had topped RMB 340 million (US\$51.3 million) after establishing a Science and Technology Department in Shaanxi Province, China.

#### Boviet Solar ramping PERC capacity with stream of advancements in the pipeline

Vietnam-located and Chinese-owned PV manufacturer Boviet Solar is set to position itself away from being perceived as a low-cost, low-quality producer by ramping a high percentage of its nameplate capacity to PERC solar cells and modules.

Manufacturing arm, Boviet Solar Technology and its affiliate Boviet Solar USA, is a wholly-owned subsidiary of China state-owned Powerway Alloy Materials, listed on the Shanghai Stock Exchange Market.

Boviet Solar in Vietnam has established a quasi OEM production model, looking after dedicated module assembly operations for a number of major China-based producers while establishing its own module brand.

Key to this strategy is running its own in-house solar cell production but with a new emphasis on high-efficiency multicrystalline and monocrystalline modules.

#### Meyer Burger gains orders for PERC cell and wafering upgrades

Leading PV manufacturing equipment supplier Meyer Burger has received an order valued at around CHF21 million (US\$22 million) from a China-based integrated PV manufacturer.

Meyer Burger noted that the volume production order included its multiple DW288 Series 3 diamond wire wafer saw systems and its SiN/AIOx PECVD deposition system, MAiA 2.1 for PERC production upgrades.

The company expects to start delivery and commissioning of the equipment in the fourth quarter 2016.

The company has also received a follow-on order from an existing customer

based in China for its MAiA 2.1 PERC technology upgrade platform.

The new order was said to be valued at around CHF18 million (US\$18.3 million) with delivery and commissioning of the equipment expected in the fourth quarter 2016. Meyer Burger also noted that the same customer had already placed orders with the company valued at around CHF40 million (US\$40.7 million), which included diamond wire cutting technology and cell efficiency upgrade equipment.

### Efficiencies

#### SoLayTec backs up new cell efficiency gains with customer data

Atomic layer deposition (ALD) equipment specialist SoLayTec, a subsidiary of Amtech Systems, has launched its second-generation InPassion ALD tool for PERC cells.

Combined with the newest direct PECVD, it can annually produce up to 130MW, including the integrated anneal process.

The main improvements of the second-generation model is cited as the uptime and net throughput of the machine. The company also claimed that TMA usage and efficiency gains edge the new product above competitors.

Hanwha Q CELLS published results of using the InPassion ALD compared with



SunPower has reached a module conversion efficiency of 24.1% using IBC cells.

its MW-PECVD system. A comparison of the two technologies found that the SoLayTec product offered a 0.15-0.25% better efficiency for multi-cSi PERC compared to the MW-PECVD AIO $\times$ .

### Trina Solar pushes average p-type mono PERC cell efficiencies to 21.1%

'Silicon Module Super League' (SMSL) leader Trina Solar has achieved an average efficiency of 21.1% for its industrially produced p-type monocrystalline cells (156 x 156 mm<sup>2</sup>) with PERC technology at its 'golden' pilot production line.

The p-type monocrystalline PERC cells were fabricated with standard industrial production materials and processes, developed on Trina Solar's 'golden' pilot line. PV module (60-cell) output reached 300W.

Trina Solar's lab to fab approach changed significantly in 2014, which meant R&D personnel were categorised to operate its pilot production line with key manufacturing staff implementing line upgrades as well as traditional R&D activities. This led to its R&D headcount reaching a new record high of 5,757 in 2015, up from 4,706 in 2014, around a 23% increase, year-on-year.

### SunPower lab produces solar cells used in 24.1% module efficiency record

Solar firm SunPower has set a new PV module conversion efficiency record of

24.1%, using laboratory-made IBC-based solar cells that have been verified by the US Department of Energy's National Renewable Energy Laboratory (NREL).

NREL scientist Keith Emery, manager of the PV cell and module performance laboratory, said: "SunPower's X-Series panel was tested by our lab under standard test or reporting conditions. The module measured 11310.1 cm<sup>2</sup> (aperture area) and had a power of 272.5W. We recorded 24.1% efficiency, which is a new record for silicon module efficiency."

SunPower's previous production record module conversion efficiency of 22.8% using production solar cells had a larger aperture area of 1.57389 m<sup>2</sup>.

### Plans

### Singulus signs MOU with GCL for heterojunction solar cell production equipment

Specialist PV manufacturing equipment supplier Singulus Technologies has signed a memorandum of understanding with Golden Concord Holdings Limited (GCL) and China Intellectual Electric Power Technology (CIE) to provide production equipment to fabricate heterojunction (HJ) solar cells.

CIE and GCL are collaborating in an effort to migrate CIE's previous R&D work with HJ cell technology and processes into production. Singulus will be responsible for optimizing, building and supplying the

appropriate production systems for the manufacturing of HJT solar cells.

Singulus had already signed an agreement with Russian thin-film manufacturer Hevel to switch production to HJ technology. The company plans to provide Hevel with its SILEX II, wet-chemical treatment system.

GCL System Integration Technology, the solar cell and module assembly subsidiary of GCL Holding plans a 250MW HJ technology production plant in China.

### Technology

### Christophe Ballif wins Becquerel Prize 2016

Neuchâtel's Christophe Ballif is the 2016 winner of the Becquerel Prize. Ballif heads both EPFL's Photovoltaics-Laboratory in Neuchâtel, which focuses on fundamental research, and CSEM's PV centre, which is devoted to transferring solar technology to industry.

Ballif, who has devoted 20 years to the industry, was awarded for his achievements in solar technology research and industrialisation, not least for his research on high-efficiency crystalline heterojunction solar cells and multijunction cells. According to the prize committee, Ballif receives the award based on his "outstanding" work on silicon thin-film and silicon wafer solar cells and the transfer of PV technologies to industry, with his research on tandem solar cells

with a focus on silicon/perovskite and silicon/III-V compounds being highly recognized.

**More stable perovskites remain a candidate for silicon tandem cells**

Research on perovskite solar cells has made progress, but there is still a long way to go for a highly efficient tandem with a conventional crystalline silicon cell.

The PV-Lab at the Institute of Microengineering (IMT) in Neuchâtel, Switzerland has presented a 1.4cm<sup>2</sup> small, monolithically stacked silicon-perovskite tandem cell with an efficiency of 20.5%, a significant increase over the 16% value for a monolithic tandem that IMT showed last year.

Within just a few years, the efficiency of Perovskite solar cells has skyrocketed; the record for a lab cell is currently held by a group at the Korean Research Institute of Chemical Technology with 22.1%.

With further improvements, Christophe Ballif, director of the PV-Lab at IMT believes that 27% to 28% can be achieved.

**Company news**

**SolarCity's Triex cell to be included in Chinese anti-dumping investigation**

The US Department of Commerce has upheld its preliminary ruling that SolarCity's Triex cells were included within the scope of the anti-dumping duties, in a memorandum dated 17 June 2016.

SolarCity's claim that its products should be excluded from the scope of the order as the Silevo modules are manufactured with a c-Si substrate, and the substrate is not what defines a cell, was ultimately rejected, after a thorough analysis of the information put forward by both parties after the initial ruling.

The memorandum, which states that the Triex cells are to be included within the order, means that any Silevo products imported from China to the US will have to pay duties upfront at customs; reducing the competitiveness of the product.

**ISRA Vision's solar inspection system sales continue strong growth**

Optical inspection equipment firm ISRA VISION / GP Solar has reported strong fiscal first-half year sales and a strong order backlog that includes solar PV system sales.

New orders for the inspection of solar wafers, cells and modules were said to have increased strongly in the reporting period, notably orders were strong from PV manufacturers in China and other Asian countries, according to the company.

The company is benefiting from capacity expansions across wafers, cells and modules as well as technology migrations to fine line printing of solar cells and the migration to PERC (Passivated Emitter Rear Cell) technology and several new inspection products to high-light new defects and improve yields.

ISRA reported overall sales had increased around 10% from the prior year period to €53.3 million.

Overall order backlog stood at over €85 million, compared to €65 million in the prior year period.



Credit: SolarCity

SolarCity's Triex cells are to be included within the scope of the US anti-dumping duties.

# Techniques for mitigating light-induced degradation (LID) in commercial silicon solar cells

Brett Hallam<sup>1</sup>, Catherine Chan<sup>1</sup>, David Payne<sup>1</sup>, Dominik Lausch<sup>2</sup>, Marcus Gläser<sup>2</sup>, Malcolm Abbott<sup>1</sup> & Stuart Wenham<sup>1</sup>

<sup>1</sup>University of New South Wales (UNSW), Sydney, Australia; <sup>2</sup>Fraunhofer Center for Silicon Photovoltaics (CSP), Halle (Saale), Germany

Market Watch

Fab & Facilities

Materials

Cell Processing

Thin Film

PV Modules

## ABSTRACT

Light-induced degradation (LID) in both Czochralski (Cz) and multicrystalline p-type silicon is one of the biggest challenges currently faced by the PV industry. Over the next few years it will be necessary to develop cost-effective solutions and integrate them into manufacturing lines. This is particularly important for the successful adoption of the passivated emitter rear cell (PERC), since this cell architecture has been shown to be highly susceptible to degradation. Given this motivation, the PV research community has been hard at work studying and developing methods to solve this problem. This paper presents a summary of this work, specifically the application to commercial solar cells. For Cz silicon it is demonstrated that numerous solutions exist, including rapid processes with operation times of the order of seconds and which result in completely stable PERC efficiencies. Solutions are also emerging for the more difficult multicrystalline silicon substrates, although hitherto these techniques have tended to be slower and less effective.

## LID in silicon solar cells

Solar cell manufacturers strive to improve cell efficiencies and to produce modules with stable performance during operation in the field. However, almost all modules are subject to degradation mechanisms that can significantly affect their long-term energy yield; these mechanisms have implications for the warranties that manufacturers offer, typically of the order of 25 years. One degradation mechanism in silicon solar cells of particular importance is caused by light, or, more specifically, by the charge carriers generated by illumination. Light-induced degradation (LID) can severely impact the performance of solar cells. An example degradation curve of a p-type Cz solar cell is shown in Fig. 1, highlighting a reduction in efficiency of more than 0.6%<sub>abs</sub> within 50 minutes of light soaking at 100°C.

LID is caused by a variety of impurities, and can reduce cell performance by more than 10% [1]. One source of LID is the metallic impurities, such as copper and iron, which can be incorporated into the silicon during crystal growth. However, because of the high diffusivity of such impurities, the associated degradation can be treated relatively easily through gettering processes [2,3].

A much more significant source of LID in the PV industry occurs predominately in p-type Czochralski (Cz) grown silicon [4]. In this material,

LID is dominated by a defect that is mostly thought to be a boron–oxygen (B–O) complex [5]. This has been the most prominent LID mechanism in solar cells, and is generally what is meant when the term ‘LID’ is used. However, despite more than a decade of study, there is still no consensus on the actual defect composition.

In the case of multicrystalline silicon (mc-Si), another significant LID mechanism was recently identified

[1,6] that can be even more severe than B–O-related degradation in p-type Cz solar cells. While it has been confirmed that the defect is not related to the B–O complex or to iron–boron pair dissociation, the true source is still unknown.

The extent of degradation can depend on the solar cell structure. For example, the LID in p-type Cz aluminium back-surface field (BSF) solar cells may be 3–4%<sub>rel</sub> [7],

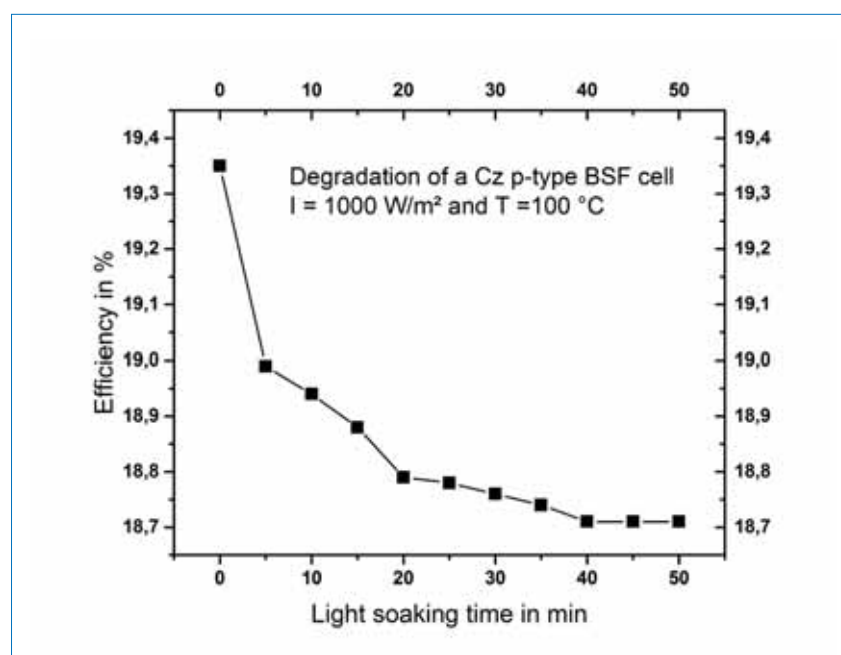


Figure 1. Example efficiency degradation of a p-type Cz aluminium back-surface field solar cell.

compared with the higher values often reported for passivated emitter rear cells (PERCs) of up to 4–6%<sub>rel</sub> [8], and may approach 10%<sub>rel</sub> [9]. This is primarily due to a stronger dependence of efficiency on bulk lifetime in high-efficiency solar cell structures, although this may not be the only cause of the higher sensitivity in PERC cells. Similarly, stronger degradation has been observed in mc-Si PERC cells than in mc-Si BSF cells [10]. At UNSW, LID effects in industrial PERC cells from various manufacturers have been studied. The worst impact observed was 1.8%<sub>abs</sub> for Cz and 2.1%<sub>abs</sub> for mc-Si. With the current adoption of PERC technology by the industry, a trend that is predicted to continue well into the future [11], LID will have an increasingly significant impact on the PV industry.

International experts have predicted a \$3.7 trillion investment in PV by 2040 [12]. Assuming that 50% of PV devices are fabricated on wafers subject to a 10%<sub>rel</sub> LID performance loss, this could equate to a \$185 billion loss for the industry. The loss in efficiency also has a significant impact on greenhouse gas emissions. By 2025, predictions indicate a global PV installed capacity of 1TW, and 1,500TWh of PV-based electricity generation [13]. The reduced yield due to LID could equate to an additional 75GWh of electricity being required from other electricity sources. If such electricity is generated using fossil fuels, this could correspond to the generation of greenhouse gas emissions of approximately 66M tonnes CO<sub>2</sub> equivalent (CO<sub>2-e</sub>) (based on an average of 888 tonnes CO<sub>2-e</sub>/GWh of electricity production from coal [14]), which would be mitigated if LID were eliminated.

Various techniques have demonstrated the ability to reduce the extent of LID in silicon solar cells. This article reviews different approaches for reducing LID, both on the incoming material level and during cell and module production. It demonstrates that the mitigation of LID in Cz and mc-Si is not only technically feasible but can also be achieved in various ways, and that further work is required to explore which solution (or combination of solutions) is best suited to the manufacturing environment.

### Selecting source material to avoid LID

Fundamentally, LID in both mono and mc-Si wafers occurs because of sub-optimal bulk properties; one option

to avoid LID is therefore to modify the source material used to make the solar cells. Decreasing the boron and/or interstitial oxygen concentrations can reduce the extent of LID associated with B–O defects.

### Reducing interstitial oxygen

In monocrystalline silicon material, interstitial oxygen concentrations may be reduced in Cz silicon by using crucibles with coatings such as silicon nitride [15], or by applying magnetic fields during crystal growth [16]. Float-zone (FZ) silicon may also be used, with interstitial oxygen concentrations typically two orders of magnitude lower than those in Cz material [17]; however, this is significantly more expensive than Cz silicon, and hence not favoured by silicon solar cell manufacturers. FZ silicon can also be subject to various other defects, such as nitrogen-related defects, which can have significant detrimental effects on bulk lifetime [18].

Casting affords another opportunity to reduce oxygen content in the silicon. Again, the crucible walls are typically coated in silicon nitride to reduce oxygen incorporation. The casting method, however, can introduce other contaminants and structural defects into the silicon that typically reduce material quality. The development of cast-mono silicon by BP Solar [19] offered a promising approach for producing essentially full monocrystalline silicon wafers with the low oxygen content of cast silicon, and therefore reduced LID. However, cast-mono silicon can suffer from significant variations in material quality throughout the ingot due to the generation of high dislocation densities [20]; as a result, the industry has moved away from this material [11]. The more recent development of ‘high-performance multi’ [21] has similarly used seeded casting methods, but has deliberately reduced the grain size and dislocation densities in the crystallized material.

### Modifications to wafer doping

As an alternative approach, wafers with a higher bulk resistivity, and hence lower boron doping concentration, can be used; this also has the benefit of reducing the sensitivity to Shockley-Read-Hall (SRH) recombination for certain defects. This is not ideal in a PERC solar cell structure, however, as majority carriers (holes) are required to flow laterally through the bulk to the p-type contacts. Hence, increasing the resistivity will increase the series resistance and lower the fill factor of the device.

Boron can also be replaced by other dopants: if retaining a p-type substrate, typically gallium dopants are used. However, gallium has a significantly lower segregation coefficient than that of boron; this can introduce large variations in the resistivity of wafers throughout a Cz ingot, which reduces the usable portion of the ingot.

Phosphorus-doped n-type wafers can also be used to completely eliminate boron–oxygen defects, provided that the material is not compensated. The highest-efficiency industrial solar cells are fabricated on n-type substrates [22]; however, the use of n-type wafers generally results in the requirement for significant processing and equipment changes in the production line. The processing sequence can also be thermally and energy intensive, and is more complicated than that required for p-type substrates. Furthermore, the high thermal budget can induce a significant degradation of the material lifetime through the formation of other oxygen-related defects, such as oxygen precipitates [23]. These defects can be just as detrimental as the B–O defects, and can reduce performance by more than 10% [24]. Generally, the use of n-type material is confined to monocrystalline substrates, because of the inability of the mc-Si to achieve the high lifetimes required in n-type structures, as well as its inability to tolerate the high thermal budget required. Similarly to gallium, phosphorus has a smaller segregation coefficient than boron, leading to larger variations in the bulk doping throughout the ingot.

“The susceptibility of PERC cells to the hotly debated light-induced degradation (LID) is closely related to the casting or pulling process of the ingot from which the wafers are cut. (T. Hengst – Meyer Burger [25])”

### Modifications to multicrystalline silicon material

In looking for ways to avoid LID in mc-Si PERC solar cells, a dependence of the degradation on the incoming wafers has been reported [1,10,25], which suggests that crystallization and/or impurity concentrations influence degradation. Manufacturers producing mc-Si PERC

# Revolutionary POCl<sub>3</sub> / BBr<sub>3</sub> Bubbler System

HORIBA's revolutionary POCl<sub>3</sub> / BBr<sub>3</sub> delivery system reduces labor cost, risk and chemical consumption whilst improving process yield, uptime and operator safety in diffusion processes.

## SYSTEM BENEFITS

- Reduced chemical consumption
- Improved sheet resistance stability
- Higher uptime
- Improved yield
- Reduce risk
- Improved safety
- Reduced scrap

**Solar+Power**  
award winner

HORIBA UK Ltd  
Moulton Park  
Northampton  
NN3 6FL  
United Kingdom

☎ +44 1604 542 600  
☎ +44 1604 542 696  
✉ [enquiries.hil@horiba.com](mailto:enquiries.hil@horiba.com)

[www.horiba.com](http://www.horiba.com)





Manufacturer	Stable efficiency enhancement with hydrogenation [% <sub>abs</sub> ]
A	0.8
B	1.0
C	0.7
D	0.9
E	1.5
F	0.8
G	1.8
Average	1.1

**Table 1. Efficiency enhancements from an 8s advanced hydrogenation process for the treatment of B–O defects in industrial p-type monocrystalline PERC solar cells.**

solar cells therefore carefully choose the wafers to be compatible with their specific solar cell processes in order to reduce the extent of degradation. The factors that influence the degradation and the changes to crystallization and/or wafering required, however, have not been publicly disclosed.

Manufacturers producing PERC cells may also avoid the use of mc-Si substrates. In this case, p-type Cz silicon wafers are used, as the LID associated with the B–O defect is often

smaller than that associated with mc-Si PERC solar cells.

### Mitigating B–O-related LID during cell/module fabrication

In instances where B–O-related LID cannot be completely eliminated by carefully selecting the incoming material, the extent of LID can be reduced or eliminated at various stages of cell/module fabrication.

### Illuminated annealing

While illumination can cause a degradation of solar cell performance through the generation of defects, the same conditions that induce the degradation can also result in a permanent recovery of performance. Illuminated annealing at elevated temperatures to stabilize the bulk lifetime of boron-doped Cz wafers was first demonstrated at the University of Konstanz by Herguth et al. in 2006 [26]. At the time, however, the mechanisms were not understood; furthermore, the recovery time was of the order of hours, and not suitable for mass production.

Since then, several key advances in the understanding of the mechanisms have been presented, and have helped in reducing the time required to mitigate B–O-related LID. First, the importance of hydrogen was noted in 2009 by Centrotherm: solar cells fabricated with hydrogenated silicon nitride layers using plasma-enhanced chemical vapour deposition (PECVD) saw a degradation and subsequent recovery of the lifetime during illuminated annealing, whereas solar cells fabricated using hydrogen-free silicon nitride layers did not show a

**SENTECH**

**NEW!**

**SENperc PV**

**The new innovative solution for quality control of backside passivation layers of PERC cells**

- ▶ Quality control of double ( $\text{SiN}_x/\text{Al}_2\text{O}_3$ ) and single layers ( $\text{Al}_2\text{O}_3$ ,  $\text{SiN}_x$ ) on the backside of mc-Si and c-Si cells
- ▶ Long term stability monitoring of  $\text{Al}_2\text{O}_3$  and  $\text{SiN}_x$  deposition
- ▶ Easy recipe based push button operation
- ▶ Software interface for data transfer
- ▶ Compact design

**The new SENperc PV will be presented at the PV Taiwan. Visit us at booth number K0603a!**

www.sentech.com      mail: marketing@sentech.de      phone: +49 30 63 92 55 20

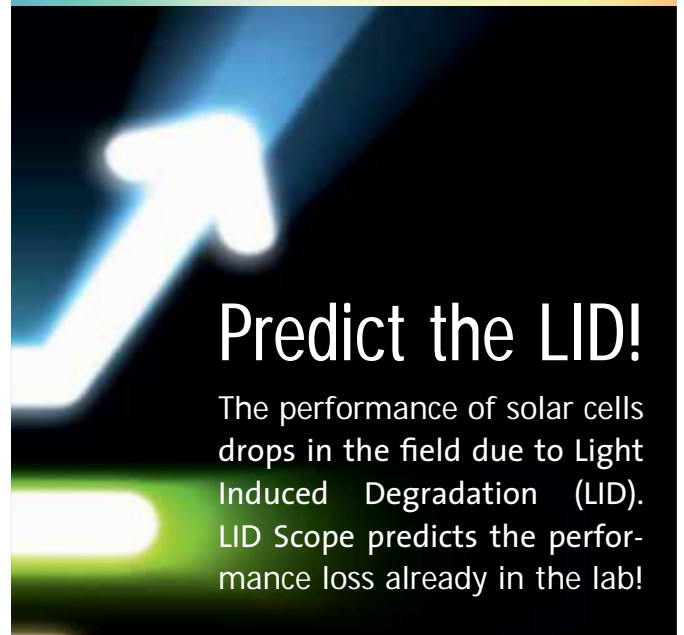
recovery [27]. This indicated a possible hydrogen-passivation-based mechanism for the permanent recovery. More recently, several studies have backed up these early findings and ruled out the potential impact of other factors in those initial experiments [28–31].

**“The detrimental LID effect of p-type solar cells was abolished by the application of a hydrogenated silicon nitride layer and a supplementary treatment with illumination and temperature. (K. Münzer – Centrotherm [27])”**

The next breakthrough came from UNSW with the application of hydrogen charge state theory [32] to explain the role of the illumination in defect passivation [33–35]. The charge state of hydrogen can affect both the mobility [36] and the reactivity [37] of hydrogen in the silicon. In p-type silicon, nature drives hydrogen into a non-optimal charge state. It is only through the addition of extra carriers to provide charge state manipulation that it can take a form which is able to react with the B–O defect [33]. This understanding was subsequently adopted and expanded upon by several research groups [30,38,39]. It is worth noting that the control of hydrogen charge states has implications for the passivation of all defects in crystalline silicon, including the mysterious mc-Si defect discussed in the next section.

The final breakthrough of key importance to high-throughput manufacturing was the identification by UNSW of the role of defect formation [40–42] (which is often the rate-limiting step in the complete defect passivation process), and importantly of how it can be greatly accelerated [43]. To achieve short mitigation times with greater effectiveness, it is necessary to accelerate this formation rate [41,42]. This is particularly the case if higher temperatures are used to accelerate the overall reaction rates. When solar cells are produced on Cz wafers using screen printing, at the end of the line the bulk of the cells are relatively free of B–O defects (the defects have not yet formed). Thus, in a commercial cell it is necessary to first form the defects quickly so that they can be subsequently permanently passivated. Initial studies identified a saturation of the defect formation rate [44], which imposed a theoretical limit on the temperatures and times to achieve stabilized silicon. However, subsequent work has demonstrated that, through the use of extremely high-intensity light, it was possible to break through these limits and achieve a greatly accelerated defect formation rate [43], because of the dependence on the total hole concentration [45,46].

This progress has enabled complete stabilization from B–O-related LID in industrial solar cells to be achieved within 8s [40]. A demonstration of UNSW’s advanced hydrogenation process for the rapid treatment of B–O-related LID, when applied to industrial p-type monocrystalline silicon PERC cells straight off the production line from various cell manufacturers, is shown in Table 1. The process forms and passivates the defects using high-intensity laser illumination (>100 suns, 938nm wavelength, quasi-continuous wave mode). An average efficiency enhancement of 1.1%<sub>abs</sub> was achieved for the cells from the seven manufacturers, with enhancements of up to 1.8%<sub>abs</sub> observed (manufacturer G). An example efficiency distribution with and without the 8s advanced hydrogenation treatment for manufacturer B is presented in Fig. 2: the image shows a 1%<sub>abs</sub> efficiency enhancement due to the passivation of B–O defects.



## Predict the LID!

The performance of solar cells drops in the field due to Light Induced Degradation (LID). LID Scope predicts the performance loss already in the lab!



## LID Scope

- †The world’s first commercially available system for simulation of LID
- †Automated and repeatable degradation of all cell types
- Fast & easy to use in labs and at-line production control

Find more at [www.laytec.de/lid](http://www.laytec.de/lid)  
or call for a proposal +49 (0)30 89 00 55-0



### Integration of B–O LID mitigation processes into solar cell/module fabrication

It is possible to carry out LID mitigation in the field: operating conditions in the field provide the

temperature and illumination required to drive the passivation reactions [8]. However, the timescales are too slow for this to be considered a viable option for modules, since hundreds of hours at elevated temperatures

would be required, which could be equivalent to several years of operation in the field. Because of the strong temperature dependence of the reactions, the time required is also heavily dependent on the location of the installation and mounting type [47].

Performing LID mitigation during the actual solar cell and/or module fabrication therefore appears to be the most feasible option. Nonetheless, there are some limitations on integrating the LID mitigation process into the fabrication sequence for solar cells/modules. Because of a potential destabilization of the B–O defect passivation at high temperatures [26], the advanced hydrogen passivation processes must be performed after the last high-temperature step; for screen-printed solar cells, this is the metal-contact firing step.

Several options exist, however, for the treatment after metallization. First, the advanced hydrogen passivation process can be integrated into the cooling section of the fast-firing belt furnace for metallization; this has the benefit of not requiring an additional heating step, although the process duration is restricted by the firing of the metal contacts. Second, the process can be implemented in a stand-alone tool after metallization, which has the benefit of decoupling the metallization process from the LID mitigation treatment. Third, the

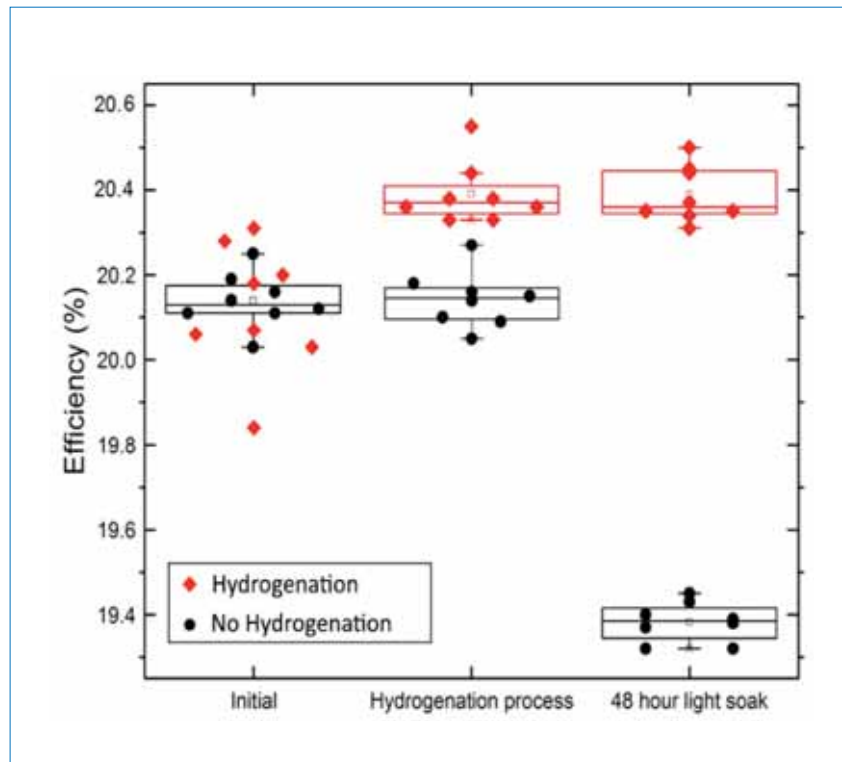


Figure 2. Efficiency enhancements for manufacturer B resulting from the addition of an 8s UNSW advanced hydrogenation process for the treatment of B–O defects.

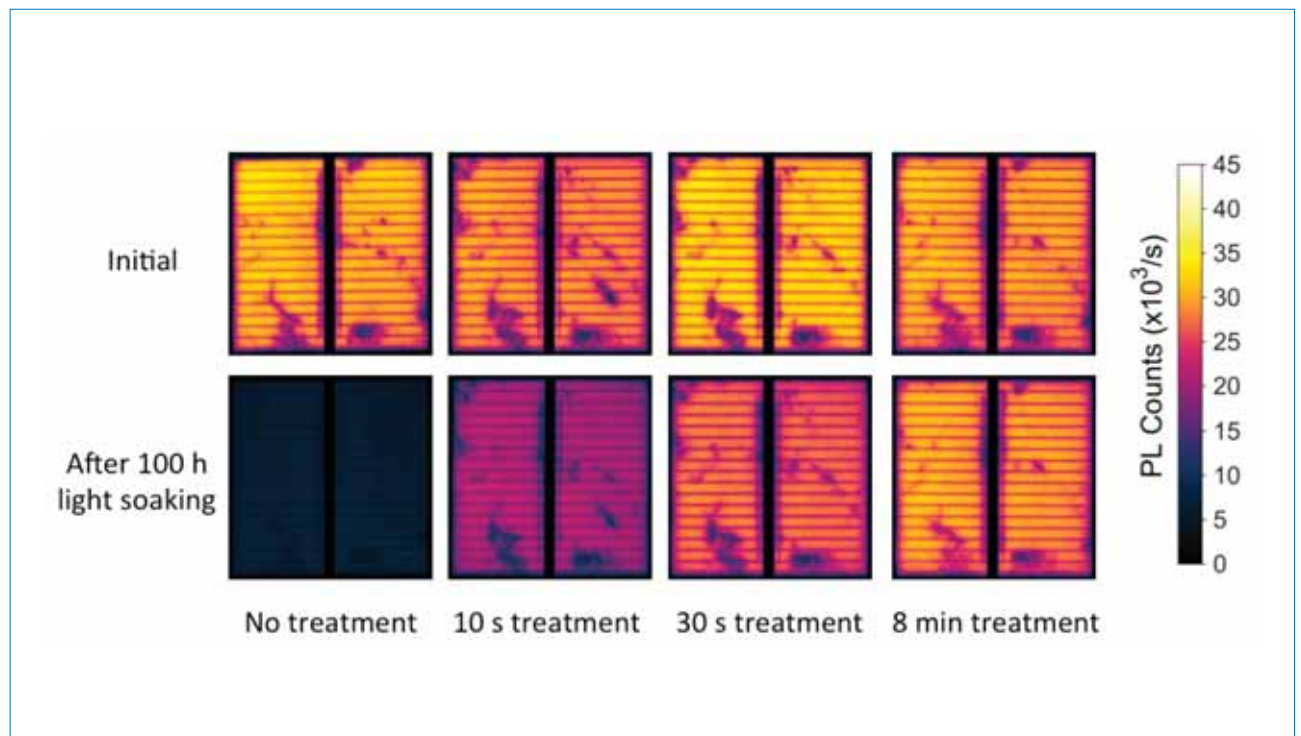


Figure 3. PL images (with point spread function deconvolution [53]) of industrial mc-Si PERC solar cells: initial images after cell fabrication, and additional images after a treatment at 250°C under 44.8kW/m<sup>2</sup> laser illumination for various durations and subsequent 100h of light soaking at 70°C (0.46kW/m<sup>2</sup>).

process can be carried out during encapsulation [8]. One advantage of performing the hydrogenation during lamination is that a partial destabilization of the defect passivation during soldering and encapsulation (if the process was performed earlier) is avoided. A further advantage is that the relatively long processing time for encapsulation can allow a relaxation of the illumination intensity required for LID mitigation. However, it is unclear whether the integration of LID mitigation into the lamination could affect the encapsulant properties.

### Mitigating mc-Si PERC LID during cell/module fabrication

Processes at the cell/module level can also greatly reduce the extent of degradation in mc-Si PERC cells. Hanwha Q CELLS has reported that their Q.ANTUM modules suffer less than 1%<sub>rel</sub> degradation after 1000h of light soaking at 75°C, compared with more than 10%<sub>rel</sub> for LID-sensitive modules [1]. However, the details of such processes have not been disclosed.

The mc-Si degradation and reports by Q CELLS have sparked significant interest within the PV industry. In the last two years, several approaches for LID mitigation have been presented.

#### Illuminated annealing

Illuminated annealing can be used to reduce LID in mc-Si PERC cells as well [48,49]; however, to date, the timescales for both the degradation and recovery are substantially longer than those for B-O-related LID. This generally results in the mitigation process requiring much longer exposures to illumination, such as a 30-minute treatment to reduce LID to 2%<sub>rel</sub> [48]. Reports have highlighted the influences of temperature, illumination intensity and process duration on the extent of LID mitigation [48–50]. For example, increasing the illumination intensity has been shown to reduce LID [48,49]; recent work using high-intensity illumination has demonstrated significant LID reductions (of up to 60%) for a processing time of 30s [51,52].

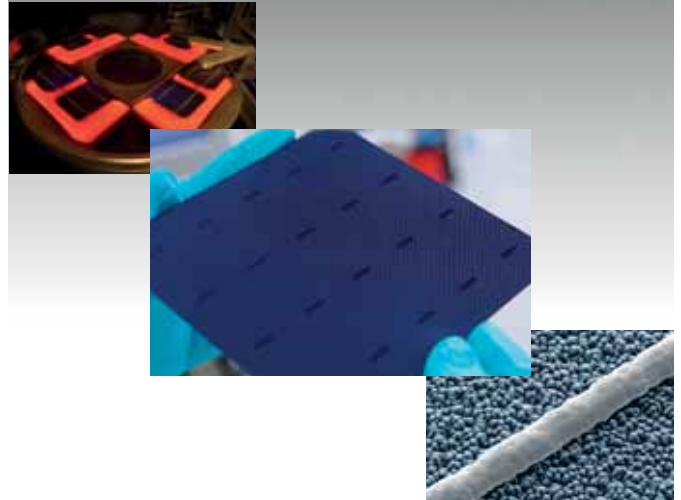
Fig. 3 shows an example of the influence of high-intensity illuminated annealing processes on mc-Si PERC LID. PL images of industrial mc-Si PERC cells are shown at the end of fabrication, and after a treatment with a high-intensity laser for various durations at 250°C (44.8kW/m<sup>2</sup>, 938nm wavelength, quasi-continuous wave mode) and subsequent light soaking. As demonstrated in the figure, LID was substantially modified by the laser process.

#### Firing at a reduced temperature

The defect in mc-Si PERC cells is primarily activated by high-temperature firing, which is used to form the metal contacts. The extent of degradation can be regulated by varying the firing conditions [10,48,52,54]; in particular, firing at reduced temperatures can suppress the subsequent degradation. While the optimal firing may differ for each solar cell manufacturer, recently reported data by Chan et al. [52] demonstrated that reducing the firing temperature by 100–150°C was sufficient to eliminate most of the subsequent degradation in minority-carrier lifetime, while still allowing effective hydrogen passivation.

Fig. 4 shows an example of the impact of firing at various temperatures on the extent of degradation in lifetime after illumination, as well as the minimum value of lifetime throughout degradation for each firing temperature. The yellow region indicates the range of temperatures at which the highest absolute lifetimes can be obtained at maximum degradation. In the case of the samples and processing used here for screen-printed solar cells at UNSW, this occurred

## LASER PROCESSING FOR THE SOLAR INDUSTRY



### SOLUTIONS FOR C-SI SOLAR CELLS

- ◆ Laser Contact Opening - PERC
- ◆ Laser Fired Contacts
- ◆ Dielectric Ablation
- ◆ Cell Cutting
- ◆ Laser Doped Selective Emitter
- ◆ Laser Edge Isolation
- ◆ Via Drilling



INNOVATION FOR THE NEXT GENERATION



InnoLas Solutions GmbH  
www.innolas-solutions.com

at firing temperatures approximately 100°C below the standard firing temperature.

Reducing the firing temperature, however, will potentially require a modification of the screen-printing pastes in order to ensure that appropriate contact resistances and adhesion can be achieved. For PERC solar cells, the aluminium pastes are also required to form localized BSF regions, the formation of which is heavily temperature dependent.

### A second firing process

In the instance where a reduced firing temperature is not an option, a second firing process may be used to greatly reduce the extent of degradation. The second firing process can be implemented over the same timescale as the typical firing process, and can therefore be integrated into an in-line tool with multiple zones for the modified thermal profile. The second firing process to reduce LID is performed at a reduced temperature [52]. Using this approach, a reduction in degradation from 12.7%<sub>rel</sub> to 4.3%<sub>rel</sub> has been demonstrated [52].

While this process is quite effective and rapid in reducing the extent of degradation, the process can introduce series-resistance problems associated with the contact resistance at the silver/silicon interface [52]; hence, the process window to avoid LID appears to be quite narrow. In addition, this

process does not allow effective passivation of B–O defects.

### A combined approach: firing and illumination

A combined approach may also be used, consisting of a second firing process and a subsequent illuminated anneal. This approach has benefits arising from the rapid nature of the firing process, as well as from the ability to passivate the remaining defects, including B–O defects. Furthermore, the combined approach can also be implemented within the tools for metal-contact firing by adding additional process zones. The combined approach has been shown to reduce degradation in open-circuit voltage from 5.6%<sub>rel</sub> to 0.1%<sub>rel</sub> after 500h of light soaking [52]; however, it can also lead to fill factor issues, presumably due to the second firing process, and requires further investigation.

### The choice of current injection and illumination for LID mitigation

Although efforts for LID mitigation requiring carrier injection have typically focused on illumination, current injection can be used as an alternative method to provide the carrier injection. Both approaches may have strengths and weaknesses in their suitability for different applications.

In the case of approaches requiring short processing times, achievable through the acceleration of defect formation, illumination would appear the preferred one. While current injection can be used to provide carrier injection equivalent to low illumination intensities, series resistance effects limit the ability to achieve sufficient carrier concentrations throughout the device using high currents. Illumination allows operation in open-circuit conditions without series resistance effects, and can therefore facilitate accelerated defect formation. However, the necessary illumination intensities (typically > 20 suns) may be challenging to achieve in an industrial environment, and require high-powered LED or laser systems. Furthermore, the integration of such high-intensity illumination into industrial tools may face further challenges, such as safety concerns and energy requirements.

In certain instances, the application of current injection for LID mitigation may have advantages over illuminated approaches. One advantage of using current injection is the ability to process a large number of cells simultaneously, such as by stacking cells and applying current through the devices, without requiring a large processing area. Doing so can provide the high throughputs for the time required when using low current densities (below 2 suns equivalent), but this process requires contacting the solar cells and involves extra wafer handling. Furthermore, current injection is an efficient way to inject carriers and open up the opportunity for a flexible and accurate control of the injection conditions independently of the optical and electrical properties. Another advantage for tool/process integration is that current injection could be implemented during lamination without significant modifications in tool design to incorporate illumination.

### Tools for mitigating LID

Industrial tools are now available for various implementations of the processes described above. One approach that appears popular is illuminated annealing. For example, Centrotherm, Despatch and Schmid are offering tools integrated with fast-firing and LID mitigation zones. The solutions appear popular, with companies such as Despatch claiming that several top-tier manufacturers in China and Taiwan have already ordered systems.

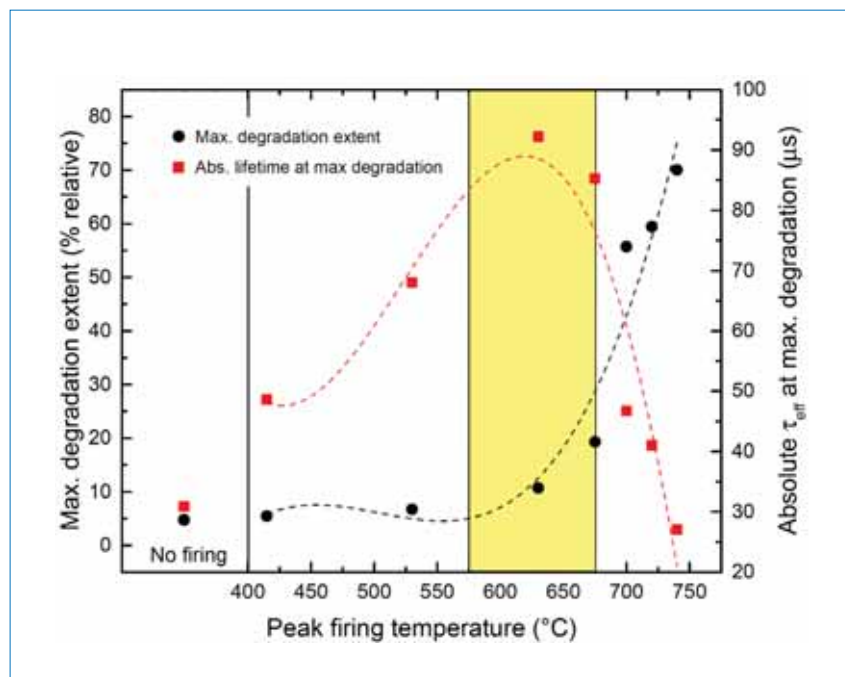


Figure 4. Maximum relative degradation of minority-carrier lifetime after firing at different temperatures and subsequent light soaking. Absolute values of minority-carrier lifetime at maximum degradation are also shown. The yellow region indicates the optimal firing temperature for the lifetime samples/processing used. (Data taken from Chan et al. [52].)

“Several furnace manufacturers have introduced solutions to the problem. (E. Anderson – Despatch Industries [55])”

Several tool manufacturers also offer stand-alone versions for LID mitigation, including Asia Neo Tech Industrial, Folungwin and DR Laser. Many other equipment manufacturers are probably working on developing tools for the market, and similarly for solar cell manufacturers because of the relative technical simplicity of applying heat and light to solar cells to facilitate the advanced hydrogenation processes. While earlier generations of the tools use relatively low illumination intensities (<10 suns), the newer generations are shifting towards higher illumination intensities (>20 suns) to allow the acceleration of defect formation that can drive rapid LID mitigation.

The significant efficiency enhancements that result from the application of LID mitigation processes mean that short payback times are possible. For example, efficiency

enhancements of 1.1%<sub>abs</sub> (as shown in Table 1), obtained using a US\$300,000 tool with a throughput of 3,600 wafers per hour, could have a payback time of the order of just one month.

### Conclusions

LID can significantly affect the performance of p-type silicon solar cells, but there are many ways of managing and/or eliminating the degradation. Wafers may be carefully selected with reduced boron and/or oxygen concentrations in order to avoid B–O-related degradation.

In the case of multicrystalline silicon, there are reports that the degradation can be reduced by paying close attention to the crystallization process, but the details have not been disclosed. During cell/module fabrication, illuminated annealing may be used to treat B–O defects. Sub-10s processes have now demonstrated the complete mitigation of B–O-related LID on finished industrial solar cells. Current injection can also be used for LID mitigation; however, the timescales for such processes are probably longer because of the inability to build up carrier concentrations to the required levels for accelerating defect formation

throughout the device.

For mc-Si PERC cells, changes to the firing conditions can reduce the extent of degradation. Subsequent treatments can also be carried out, such as illuminated annealing or a second firing step. With illuminated annealing processes, however, the timescales are typically longer than those for the treatment of B–O defects. Industrial tools for LID mitigation are now widely available, potentially with very short payback times. These new capabilities are giving strength to p-type silicon solar cell technologies.

### Acknowledgements

Experimental work has been supported by the Australian Government through the Australian Renewable Energy Agency (ARENA) and the Australian Centre for Advanced Photovoltaics (ACAP). The views expressed herein are not necessarily the views of the Australian Government, and the Australian Government does not accept responsibility for any information or advice contained herein. The authors would also like to thank the commercial partners of the ARENA 1-A060 advanced hydrogenation project, and the UK Institution of Engineering and Technology (IET) for their funding

# How prepared are you for the future?

Need to know more about critical, solar market intelligence through real-time analysis and insights?



SOLAR MEDIA  
MARKET RESEARCH

REPORTS NOW AVAILABLE

UK Ground-Mount Solar Report Portfolio  
PV Manufacturing & Technology Quarterly report  
Republic of Ireland Solar PV Opportunity Tracker report

Solar Media's market research division, Solar Intelligence, provides the industry with accurate and timely data to ensure maximum focus on current and pending opportunities at the site-specific level.

[www.solar-intel.com](http://www.solar-intel.com)

Data powered by:



support for this work through the A.F. Harvey Engineering Prize.

## References

- [1] Kersten, F. et al. 2015, "A new mc-Si degradation effect called LeTID", *Proc. 42nd IEEE PVSC*, New Orleans, Louisiana, USA, pp. 1–5.
- [2] Shabani, M.B., Yamashita, T. & Morita, E. 2008, "Metallic impurities in mono and multi-crystalline silicon and their gettering by phosphorus diffusion", *ECS Trans.*, Vol. 16, No. 6, pp. 179–193.
- [3] Lindroos, J. & Savin, H. 2016, "Review of light-induced degradation in crystalline silicon solar cells", *Sol. Energy Mater. Sol. Cells*, Vol. 147, pp. 115–126.
- [4] Fischer, H. & Pschunder, W. 1973, "Investigation of photon and thermal induced changes in silicon solar cells", *Proc. 10th IEEE PVSC*, Palo Alto, California, USA, p. 404.
- [5] Schmidt, J., Aberle, A.G. & Hezel, R. 1997, "Investigation of carrier lifetime instabilities in Cz-grown silicon", *Proc. 26th IEEE PVSC*, Anaheim, California, USA, pp. 13–18.
- [6] Ramspeck, K. et al. 2012, "Light induced degradation of rear passivated mc-Si solar cells", *Proc. 27th EU PVSEC*, Frankfurt, Germany, pp. 861–865.
- [7] Cho, E. et al. 2015, "Light-induced degradation free and high efficiency p-type indium-doped PERC solar cells on Czochralski silicon", *Proc. 42nd IEEE PVSC*, New Orleans, Louisiana, USA, pp. 1–4.
- [8] Lee, K. et al. 2015, "Natural recovery from LID: Regeneration under field conditions?", *Proc. 31st EU PVSEC*, Hamburg, Germany, p. 1837.
- [9] Knobloch, J. et al. 1996, "Solar cells with efficiencies above 21% processed from Czochralski grown silicon", *Proc. 25th IEEE PVSC*, Washington DC, USA, pp. 405–408.
- [10] Nakayashiki, K. et al. 2016, "Engineering solutions and root-cause analysis for light-induced degradation in p-type multicrystalline silicon PERC modules", *IEEE J. Photovolt.*, Vol. 6, No. 4, pp. 860–868.
- [11] SEMI PV Group Europe 2016, "International technology roadmap for photovoltaic (ITRPV): 2015 results", 7th edn (Mar.) [<http://www.itrpv.net/Reports/Downloads/>].
- [12] Bloomberg New Energy and Finance 2015, "New Energy Outlook 2015".
- [13] IEA 2014, "Snapshot of global PV markets 2014", Report IEA PVPS T1-26:2015, International Energy Agency, IEA-OECD.
- [14] World Nuclear Association and others 2011, "Comparison of lifecycle greenhouse gas emissions of various electricity generation sources".
- [15] Zulehner, W. 1983, "Czochralski growth of silicon", *J. Cryst. Growth*, Vol. 65, No. 1, pp. 189–213.
- [16] Organ, A.E. & Riley, N. 1987, "Oxygen transport in magnetic Czochralski growth of silicon", *J. Cryst. Growth*, Vol. 82, No. 3, pp. 465–476.
- [17] Sumino, K., Harada, H. & Yonenaga, I. 1980, "The origin of the difference in the mechanical strengths of Czochralski-grown silicon and float-zone-grown silicon", *Jpn. J. Appl. Phys.*, Vol. 19, No. 1, p. L49.
- [18] Rougieux, F.E., Grant, N.E. & Macdonald, D. 2013, "Thermal deactivation of lifetime-limiting grown-in point defects in n-type Czochralski silicon wafers", *physica status solidi (RRL)*, Vol. 7, No. 9, pp. 616–618.
- [19] Stoddard, N. et al. 2008, "Casting single crystal silicon: Novel defect profiles from BP Solar's mono<sup>2</sup> TM wafers", *Solid State Phenom.*, Vol. 131, pp. 1–8.
- [20] Guerrero, I. et al. 2014, "About the origin of low wafer performance and crystal defect generation on seed-cast growth of industrial mono-like silicon ingots", *Prog. Photovoltaics Res. Appl.*, Vol. 22, No. 8, pp. 923–932.
- [21] Lan, C.W. et al. 2016, "Engineering silicon crystals for photovoltaics", *Cryst. Eng. Comm.*, Vol. 18, No. 9, pp. 1474–1485.
- [22] Green, M.A. et al. 2016, "Solar cell efficiency tables (Version 48)", *Prog. Photovoltaics Res. Appl.*, Vol. 24, No. 7, pp. 905–913.
- [23] Falster, R.J. et al. 1997, "Effect of high temperature pre-anneal on oxygen precipitates nucleation kinetics in Si", *Solid State Phenom.*, Vol. 57, pp. 123–128.
- [24] Cousins, P.J. et al. 2010, "Generation 3: Improved performance at lower cost", *Proc. 35th IEEE PVSC*, Honolulu, Hawaii, USA, pp. 275–278.
- [25] Fischbeck, G. 2015, "PERCs for all solar cell manufacturers?" [<http://www.pv-magazine.com/archive/articles/beitrag/percs-for-all-solar-cell-manufacturers-00020824/630/#axzz4CsfnUV6o>].
- [26] Herguth, A. et al. 2006, "A new approach to prevent the negative impact of the metastable defect in boron doped Cz silicon solar cells", *Proc. 4th WCPEC*, Waikoloa, Hawaii, USA, Vol. 1, pp. 940–943.
- [27] Münzer, K. 2009, "Hydrogenated silicon nitride for regeneration of light induced degradation", *Proc. 24th EU PVSEC*, Hamburg, Germany, pp. 1558–1561.
- [28] Krugel, G. et al. 2011, "Impact of hydrogen concentration on the regeneration of light induced degradation", *Energy Procedia*, Vol. 8, pp. 47–51.
- [29] Dubois, S. et al. 2012, "The BOLID project: Suppression of the boron-oxygen related light-induced-degradation", *Proc. 27th EU PVSEC*, Frankfurt, Germany, pp. 749–754.
- [30] Wilking, S., Herguth, A. & Hahn, G. 2013, "Influence of hydrogen on the regeneration of boron-oxygen related defects in crystalline silicon", *J. Appl. Phys.*, Vol. 113, No. 19, p. 194503.
- [31] Nampalli, N. et al. 2015, "Evidence for the role of hydrogen in the stabilization of minority carrier lifetime in boron-doped Czochralski silicon", *Appl. Phys. Lett.*, Vol. 106, No. 17, p. 173501.
- [32] Herring, C., Johnson, N.M. & de Walle, C.G. 2001, "Energy levels of isolated interstitial hydrogen in silicon", *Phys. Rev. B*, Vol. 64, No. 12, p. 125209.
- [33] Hallam, B. et al. 2013, "Hydrogen passivation of B-O defects in Czochralski silicon", *Energy Procedia*, Vol. 38, pp. 561–570.
- [34] Hamer, P. et al. 2014, "Manipulation of hydrogen charge states for passivation of p-type wafers in photovoltaics", *IEEE J. Photovolt.*, Vol. 4, No. 5, pp. 1252–1260.
- [35] Hallam, B.J. et al. 2014, "Advanced bulk defect passivation for silicon solar cells", *IEEE J. Photovolt.*, Vol. 4, No. 1, pp. 88–95.
- [36] Mathiot, D. 1989, "Modeling of hydrogen diffusion in n- and p-type silicon", *Phys. Rev. B*, Vol. 40, No. 8, pp. 5867–5870.
- [37] Seager, C.H. & Anderson, R.A. 1991, "Two-step debonding of hydrogen from boron acceptors in silicon", *Appl. Phys. Lett.*, Vol. 59, No. 5, pp. 585–587.
- [38] Sun, C., Rougieux, F.E. & Macdonald, D. 2015, "A unified approach to modelling the charge state of monatomic hydrogen and other defects in crystalline silicon", *J. Appl. Phys.*, Vol. 117, No. 4, p. 45702.

- [39] Gläser, M. & Lausch, D. 2015, "Towards a quantitative model for BO regeneration by means of charge state control of hydrogen", *Energy Procedia*, Vol. 77, pp. 592–598.
- [40] Hallam, B.J. et al. 2015, "Advanced hydrogenation of dislocation clusters and boron-oxygen defects in silicon solar cells", *Energy Procedia*, Vol. 77, pp. 799–809.
- [41] Hallam, B.J. et al. 2015, "Implications of accelerated recombination-active defect complex formation for mitigating carrier-induced degradation in silicon", *IEEE J. Photovolt.*, Vol. 6, pp. 92–99.
- [42] Hallam, B. et al. 2016, "Influence of the formation- and passivation rate of boron-oxygen defects for mitigating carrier-induced degradation in silicon within a hydrogen-based model", *J. Appl. Phys.*, Vol. 119, No. 6, p. 065701.
- [43] Hamer, P. et al. 2015, "Accelerated formation of the boron-oxygen complex in p-type Czochralski silicon", *physica status solidi (RRL)*, Vol. 9, No. 5, pp. 297–300.
- [44] Schmidt, J. & Bothe, K. 2004, "Structure and transformation of the metastable boron- and oxygen-related defect center in crystalline silicon", *Phys. Rev. B*, Vol. 69, No. 2, p. 24107.
- [45] Niewelt, T. et al. 2016, "A unified parameterization for the formation of boron oxygen defects and their electrical activity", *Energy Procedia* [in press].
- [46] Hamer, P. et al. 2016, "Boron-oxygen defect formation rates and activity at elevated temperatures", *Energy Procedia* [in press].
- [47] Hallam, B. et al. 2016, "Modelling the long-term behaviour of boron-oxygen defect passivation in the field using typical meteorological year data (TMY2)", *Proc. 32nd EU PVSEC*, Munich, Germany [in press].
- [48] Frigge, S., Mehlich, H. & Grosse, T. 2015, "LID free module made from high performance PERC solar cells", Visual Presentation 5AV.6.4, 31st EU PVSEC, Hamburg, Germany.
- [49] Payne, D. et al. 2016, "Acceleration and mitigation of carrier-induced degradation in p-type multi-crystalline silicon", *physica status solidi (RRL)*, Vol. 10, No. 3, pp. 237–241.
- [50] Payne, D.N.R. et al. 2016, "Rapid passivation of carrier-induced defects in p-type multi-crystalline silicon", *Sol. Energy Mater. Sol. Cells*, pp. 1–5 [also available online

at <http://linkinghub.elsevier.com/retrieve/pii/S0927024816301234>].

- [51] Krauß, K. et al. 2016, "Fast regeneration processes to avoid light-induced degradation in multicrystalline silicon solar cells", *IEEE J. Photovolt.* [in press].
- [52] Chan, C.E. et al. 2016, "Rapid stabilization of high-performance multi-crystalline p-type silicon PERC cells", *IEEE J. Photovolt.* [in press].
- [53] Payne, D. et al. 2016, "Evaluating the accuracy of point spread function deconvolution applied to luminescence images", *Proc. 43rd IEEE PVSC*, Portland, Oregon, USA [in press].
- [54] Bredemeier, D. et al. 2016, "Lifetime degradation and regeneration in multicrystalline silicon under illumination at elevated temperature", *AIP Adv.*, Vol. 6, No. 3, p. 35119.
- [55] Despatch Industries 2015, "Despatch industries announces in-line, light induced degradation prevention for metallization furnaces" [<http://www.despatch.com/10072015.aspx>].

#### About the Authors



**Brett Hallam** is the co-director of core research for ARENA crystalline-silicon-based PV projects at UNSW. He received his Ph.D. from UNSW in the field of laser doping and hydrogen passivation for silicon solar cells. His current research activities focus on the development of advanced hydrogen passivation processes.



**Catherine Chan** completed her Ph.D. in photovoltaic engineering in 2014 at UNSW, where she is currently working as a postdoctoral research fellow in the areas of silicon solar cell degradation and advanced hydrogen passivation processes for silicon solar cells.



**David Payne** studied electronic engineering at the University of Southampton, where he went on to receive his Ph.D. in 2014 in the field of light trapping for photovoltaics devices. Since then he has been working as a research fellow at UNSW, primarily focusing on carrier-induced degradation in multicrystalline silicon.



**Dominik Lausch** obtained his Diploma degree (A) in physics from the University of Leipzig, Germany, in 2009. In 2012 he received his Ph.D. in natural science from the University of Halle, Germany, in cooperation with Fraunhofer CSP and Q-Cells SE. He is currently a postdoctoral researcher at Fraunhofer CSP, heading a team that is investigating plasma texturing and hydrogen passivation.



**Marcus Gläser** received a Bachelor's in solar technology (photovoltaics) from Anhalt University of Applied Sciences in 2011. After receiving his master's in 2014 in sustainable energy systems from Otto-von-Guericke University in Magdeburg, he began working on his Ph.D. with Fraunhofer CSP Halle, where he is investigating carrier-induced hydrogen passivation of bulk defects in crystalline silicon solar cells.



**Malcolm Abbott** received his Ph.D. in photovoltaic engineering in 2006 from UNSW, where he is currently the CTO of PV Lighthouse and a research director. His current research interests broadly span the crystalline silicon field and include developing new cell processes, advanced characterization techniques, mitigation of LID in wafers, and modelling of photovoltaic devices.



**Stuart Wenham** is director of the Photovoltaics Centre of Excellence at UNSW. His involvement in photovoltaics spans more than 30 years, and he has been honoured with numerous leading international awards. Along with his team he has achieved many cell and module performance world records and the successful large-scale commercialization of several technologies.

#### Enquiries

Brett Hallam  
School of Photovoltaic and Renewable Energy Engineering  
University of New South Wales  
Sydney NSW 2052  
Australia

Tel.: +61 415 415 156  
Email: [brett.hallam@unsw.edu.au](mailto:brett.hallam@unsw.edu.au)



# BiCoRE: Combining a PERC-type cell process with n-type wafers

Thorsten Dullweber, Nadine Wehmeier, Anja Nowack, Till Brendemühl, S. Kajari-Schröder & R. Brendel, Institute for Solar Energy Research Hamelin (ISFH), Emmerthal, Germany

## ABSTRACT

The p-type monofacial passivated emitter and rear cell (PERC) is currently entering into mass production, but the efficiency of this type of cell is affected by light-induced degradation (LID). A novel solar cell design is introduced here – BiCoRE, which is an acronym for ‘bifacial co-diffused rear emitter’. The BiCoRE cell process is almost identical to the PERC process sequence with a proven high-volume capability, but uses LID-stable n-type wafers instead. A plasma-deposited boron silicate glass (BSG) silicon nitride ( $\text{SiN}_x$ ) stack at the rear side of the BiCoRE cells acts as a protection layer against texturing and  $\text{POCl}_3$  diffusion and as a boron dopant source during the  $\text{POCl}_3$  co-diffusion, as well as a passivation layer. The rear contacts are formed by laser contact opening (LCO) and by screen printing an Al finger grid, similar to the method used for the recently introduced bifacial PERC+ solar cells. The Al finger grid allows bifaciality and enables conversion efficiencies of up to 21.1% to be obtained with n-type reference solar cells. The multifunctional BSG/ $\text{SiN}_x$  stack demonstrates conversion efficiencies of up to 20.6% with BiCoRE solar cells. When illuminated from the rear side, the BiCoRE cells yield conversion efficiencies of up to 16.1%, which corresponds to a bifaciality of 78%.

## Introduction

Several leading solar cell manufacturers, such as SolarWorld, Hanwha Q-Cells, Trina Solar and others [1–5], are beginning to launch mass production of passivated emitter and rear cells (PERCs). The ITRPV photovoltaic technology roadmap forecasts a market share for PERC solar cells of 35% by 2019 [6]. These industrial PERC cells utilize p-type wafers and a full-area screen-printed aluminium (Al) rear layer that only locally contacts the silicon wafer in regions where the rear passivation has been removed by laser contact opening (LCO). The full-area aluminium layer consumes a high quantity of Al paste, of 1.0 to 1.5g per wafer, and prevents any transmission of sunlight from the rear side to the silicon wafer, thus ruling out any bifacial applications of these industrial PERC cells.

A bifacial PERC solar cell, called PERC+, was recently introduced [7], in which a screen-printed Al finger grid was implemented instead of the full-area Al layer. The resulting PERC+ cells demonstrate front-side efficiencies of up to 21.5% (which are comparable to those achieved by monofacial PERC cells) and rear-side efficiencies of up to 16.7% [8]. The application of bifacial modules in PV power plants may increase the energy yield by up to 20% in comparison to monofacial modules, depending on the specific installation conditions [7,9,10]. Accordingly, the ITRPV roadmap predicts a market share for bifacial solar cell technologies of 15%

by 2019 [6]. In addition, the bifacial PERC+ solar cells show deeper Al-BSFs and a reduced number of voids in the local Al rear contacts [7], since the Al fingers change the Al-Si alloying process because of the limited aluminium volume [11].

The last few years have seen the development of industrial passivated emitter and rear totally diffused (PERT) solar cells; these use n-type wafers and entail boron doping of the rear wafer side, forming a so-called *back junction (BJ)* [12–15]. The manufacturing sequence for n-type PERT BJ cells is very similar to that for p-type PERC cells, requiring only a few modifications, such as the integration of the rear boron doping as well as wider LCOs of the rear passivation layer [14]. Consequently, n-PERT BJ cells may become an attractive option for p-PERC solar cell manufacturers in migrating their production process from p-type wafers to n-type wafers for as long as light-induced degradation (LID) remains a limiting factor of the conversion efficiency of p-PERC cells [16,17], despite recent advances in developing industrial regeneration processes [18,19].

As in the case of p-PERC cells, n-PERT BJ cells typically employ a full-area Al rear layer and are thus monofacial. In order to simplify the process flow of n-PERT BJ cells, it has been demonstrated that the rear-side boron doping can be realized by depositing a boron silicate glass (BSG) layer using plasma-enhanced chemical vapour deposition (PECVD), and capping this with a  $\text{SiN}_x$  layer,

which is then exposed to a  $\text{POCl}_3$  co-diffusion [20–23]. The BSG/ $\text{SiN}_x$  stack acts as a diffusion barrier against phosphorus, whereas during the  $\text{POCl}_3$  co-diffusion the boron diffuses from the BSG into the silicon wafer. To date, n-PERT BJ cell efficiencies of up to 21.0% have been demonstrated using this technique [24]. A promising approach to further simplify the process sequence is to use the BSG/ $\text{SiN}_x$  stack also as a passivation layer [25,26] instead of removing it after co-diffusion and applying an  $\text{AlO}_x/\text{SiN}_y$  passivation. Preliminary results based on test wafers report emitter saturation current densities of around  $50\text{fA}/\text{cm}^2$  with a BSG/ $\text{SiN}_x$  stack as the doping source and passivation layer [25], and conversion efficiencies of up to 19.8% [26] for n-PERT front-junction cells.

**“The first BiCoRE cells have demonstrated efficiencies of up to 20.6% and bifacialities of 78%.”**

Bifacial n-PERT BJ cells with a screen-printed Al finger grid on the rear side instead of a full-area Al rear layer were recently demonstrated for the first time [27]. Additionally, these cells employed a PECVD BSG/ $\text{SiN}_x$  stack as a boron dopant source and as a rear passivation layer using a very lean process sequence. This novel industrial solar cell design has been named *BiCoRE*, which stands

n-PERT BJ	BiCoRE	PERC+
Cleaning	Cleaning	Cleaning
$BBr_3$ diffusion		
BSG etch		
Rear: $SiN_z$	Rear: $BSG/SiN_z$	
Texturing	Texturing	Texturing
$POCl_3$ diffusion	$POCl_3$ co-diffusion	$POCl_3$ diffusion
PSG etch	PSG etch	Polishing/PSG
Rear: $AlO_x/SiN_y$		Rear: $AlO_x/SiN_y$
Front: $SiN_y$	Front: $SiN_y$	Front: $SiN_x$
Laser ablation	Laser ablation	Laser ablation
Ag screen printing	Ag screen printing	Ag screen printing
Al screen printing	Al screen printing	Al screen printing
Firing	Firing	Firing
<b>13</b> process steps	<b>10</b> process steps	<b>10</b> process steps

**Table 1. Process sequences for various cell types. The n-PERT BJ cells utilize  $BBr_3$  and  $POCl_3$  as doping sources and  $AlO_x/SiN_y$  as rear passivation, with the same process sequence being used for both monofacial and bifacial cells. In the case of the bifacial n-type BiCoRE cells, a PECVD BSG/ $SiN_z$  layer is utilized as the protection layer, boron doping source and passivation layer. For comparison, a typical process flow for p-type PERC+ cells is also shown.**

for ‘bifacial co-diffused rear emitter’ [27]. The first BiCoRE cells have demonstrated efficiencies of up to 20.6% and bifacialities of 78% [27,28]. This paper summarizes the features of the novel BiCoRE solar cell.

### Bifacial n-PERT BJ solar cells with rear Al finger grid

First, the use of an Al finger grid as the rear contact of n-PERT BJ cells will be evaluated and optimized. For this,

an n-PERT BJ reference process with separate  $BBr_3$  and  $POCl_3$  diffusions and employing  $AlO_x/SiN_y$  as rear passivation will be used. The process sequence is shown in Table 1, column 1, and is described in detail in Lim et al. [29].

THE WET PROCESSING COMPANY

RENA

# PERC

TOP COMBINATION  
perfect shape & best CoO

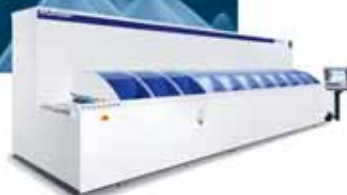
## BatchTex N

Minimized front side reflection combined with optimized pyramids by monoTEX® additive

lead to efficient and faster rear side smoothing in

## InOxSide<sup>+</sup>

Visit us at  
Intersolar  
Middle East  
& India



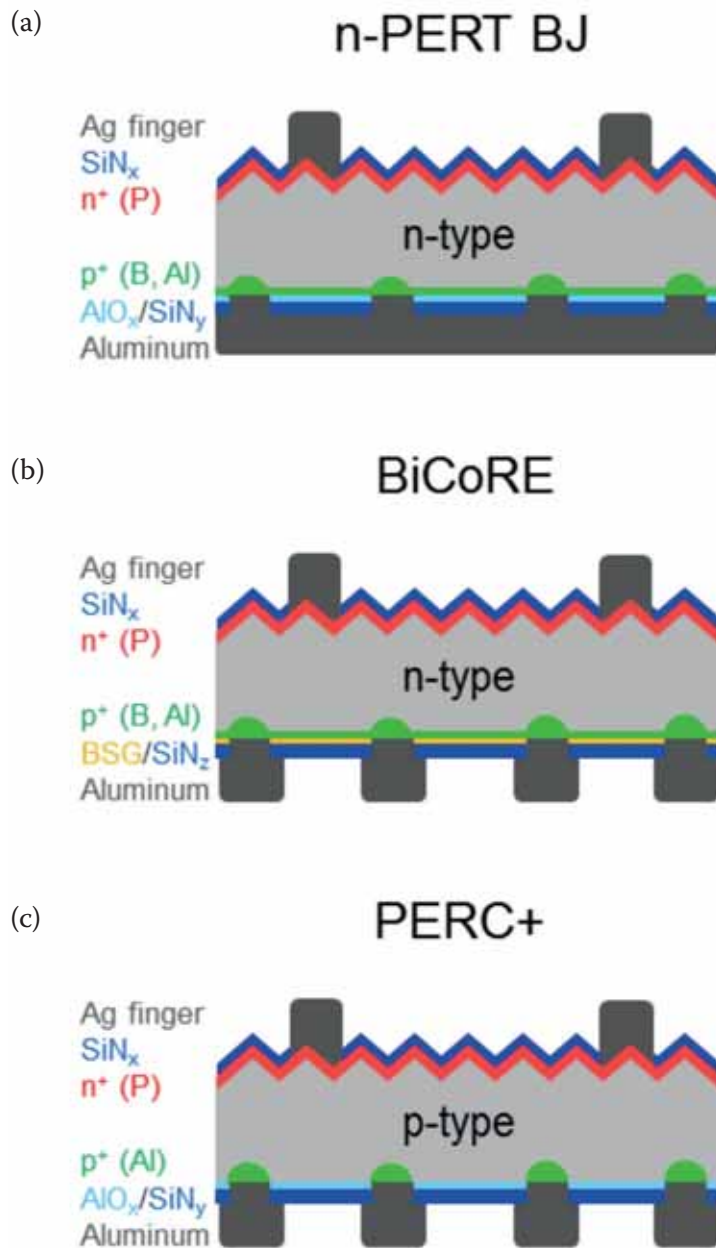


Figure 1. Schematic diagrams of (a) n-PERT BJ, (b) BiCoRE and (c) PERC+ solar cells resulting from the process flows given in Table 1. The n-PERT BJ cell is processed as a monofacial cell with a full-area Al layer (as shown in (a)) as well as a bifacial cell with an Al finger grid similar to that for the BiCoRE and PERC+ solar cells.

Phosphorus-doped Czochralski-grown silicon wafers with a resistivity of  $6.5\Omega\text{cm}$  after final cell processing and an initial thickness of  $170\mu\text{m}$  are employed. The saw damage is removed in potassium hydroxide (KOH), and an RCA cleaning sequence is subsequently performed. The wafers are diffused in a quartz tube furnace

using boron tribromide ( $\text{BBr}_3$ ). The resulting boron doping has a sheet resistance of around  $100\Omega/\text{sq}$ .

After removing the BSG in HF, the rear side of the wafer is coated with PECVD  $\text{SiN}_z$  with a refractive index of 1.9, which acts as a barrier during the texturing of the front side and the subsequent phosphorus diffusion;

the sheet resistance is around  $130\Omega/\text{sq}$  after cleaning [28]. Next, the phosphorus silicate glass (PSG) and the  $\text{SiN}_z$  layer are removed in HF. The rear side of the wafer is passivated using a stack of atomic-layer-deposited aluminium oxide (ALD  $\text{AlO}_x$ ) and PECVD  $\text{SiN}_y$  with refractive index  $n$  of 2.05. The front side is passivated with PECVD  $\text{SiN}_y$ . The dielectric stack on the rear side is then locally ablated using a pulsed laser source (wavelength =  $532\text{nm}$  and pulse length =  $10\text{ps}$ ), forming line-shaped LCOs. Different LCO widths of 20, 40, 56, 77, 93, 114 and  $150\mu\text{m}$  are used in order to optimize the Al-BSF formation in combination with the Al finger grid design similar to that demonstrated for PERC+ solar cells [11]. The pitch of the LCO lines, however, is kept constant at  $1270\mu\text{m}$  regardless of the LCO width.

The Ag front grid is metallized by means of a dual print process: first the five busbars are printed using a screen and then the fingers are printed using a stencil. The group of cells with an LCO width of  $150\mu\text{m}$  receives a full-area Al screen-print, whereas the other groups with LCO widths between  $20\mu\text{m}$  and  $114\mu\text{m}$  receive a screen-printed Al finger grid with a finger opening width of  $100\mu\text{m}$ . These combinations of LCO widths and Al prints are chosen because in the case of a full-area Al layer, very wide LCO widths result in the deepest Al-BSFs and hence the highest n-PERT BJ efficiencies [14]; in the case of Al fingers, however, it has been demonstrated that much narrower LCO widths yield the deepest Al-BSFs for PERC+ cells [11].

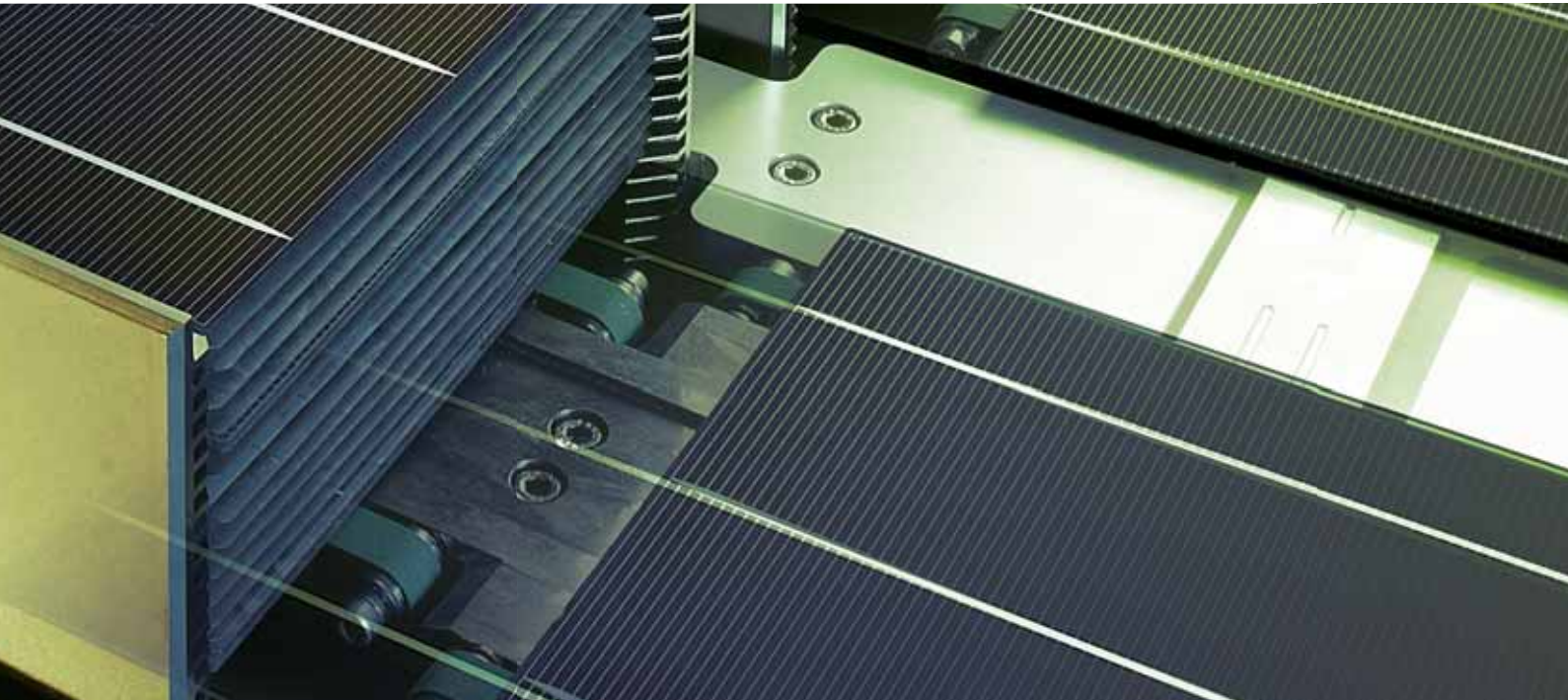
The process sequence is completed by firing the solar cells in a belt furnace. A schematic of the resulting monofacial n-PERT BJ cell is shown in Fig. 1(a).

The  $I$ - $V$  parameters of the resulting monofacial and bifacial n-PERT BJ solar cells are measured by illuminating the cells from the front side (Ag grid) and contacting the full rear side (Al layer or Al finger grid) with a reflective brass chuck. The results are summarized in Fig. 2 for different LCO widths.

When passing from  $114\mu\text{m}$ -wide LCOs to  $40\mu\text{m}$ -wide LCOs in combination with Al fingers, the conversion efficiency  $\eta$  improves from 20.6% to a best value of 21.1% (Fig. 2(a)). The n-PERT BJ cells with an LCO width of  $150\mu\text{m}$  and a full-area Al layer show top efficiencies of up to 21.0%, which is close to the best published value of 21.2% by ISFH [28].

The open-circuit voltage  $V_{oc}$

# Solar Cell Innovation for Today, Tomorrow and Future Generations



Eclipse XP scalable, high volume advanced printing solution



SolarWIS 3D wafer inspection technology



HouYi single-lane metallization system



SolarBlade half-cell processing system



Precision Stencils and Screens, next-generation fine line deposition for increased cell efficiency



## ASM Alternative Energy Leads the Way

With over three decades of proven printing ingenuity originating in photovoltaic thick film technology and continuously informed by demanding semiconductor applications, **ASM Alternative Energy** leads the market in process knowledge and application expertise.

A comprehensive portfolio of advanced solar and fuel cell metallization technologies, solar inspection platforms and

cell processing systems are underpinned by inimitable global support and R&D resources. Award-winning products are just the start; experience and engineering intelligence are the difference-makers.

**Discover ASM Alternative Energy**



[www.asm-ae.com](http://www.asm-ae.com)



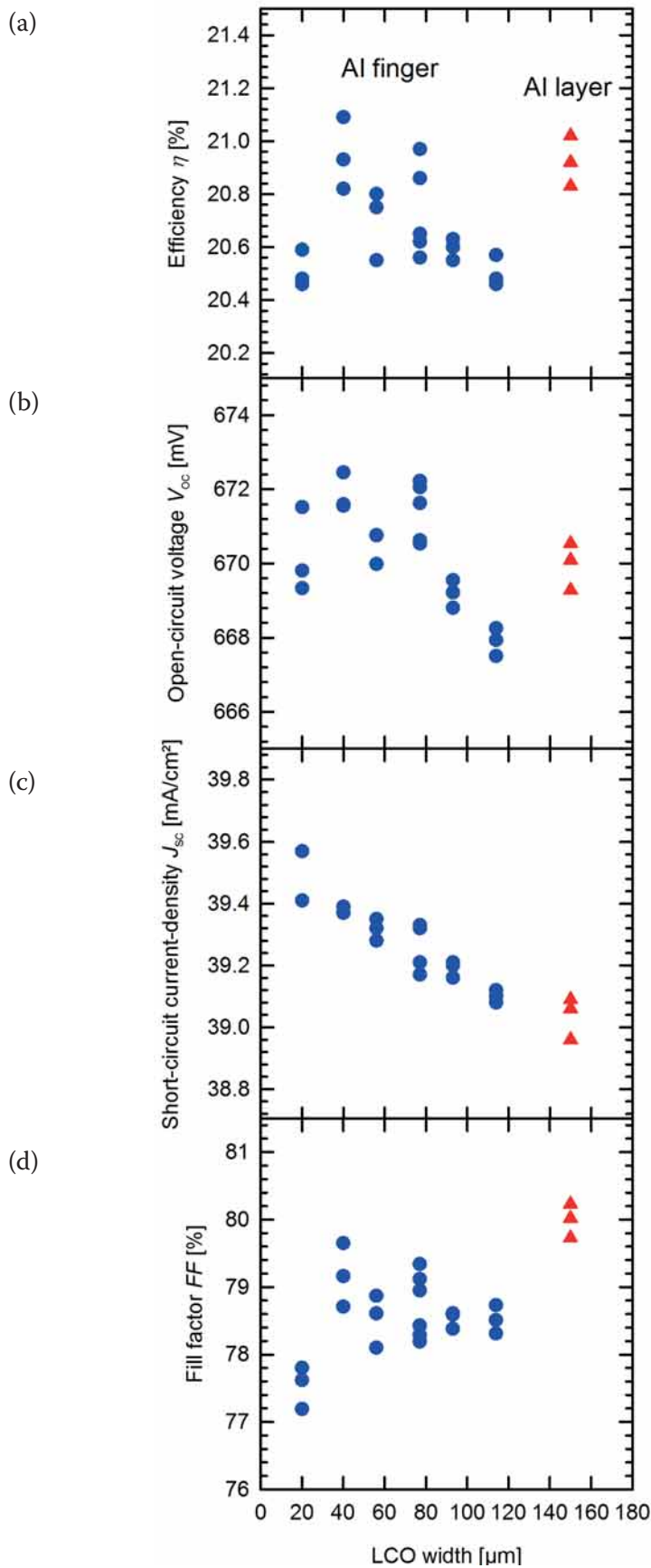


Figure 2.  $I$ - $V$  parameters of monofacial and bifacial n-PERT BJ solar cells as a function of LCO width: (a) efficiency  $\eta$ ; (b) open-circuit voltage  $V_{oc}$ ; (c) short-circuit current density  $J_{sc}$ ; (d) fill factor FF. (The cells with LCO widths between 20 and 114  $\mu\text{m}$  receive an Al finger grid design, whereas the cells with 150  $\mu\text{m}$  LCO widths are screen printed with a full-area Al layer.)

increases from 668mV for 114 $\mu\text{m}$  LCOs to 672mV for 40 $\mu\text{m}$  LCOs (Fig. 2(b)). This trend in  $V_{oc}$  has been reported for PERC+ cells as well, and has been attributed to the reduced contact-area fraction of the local Al rear contacts with decreased LCO widths while maintaining similar deep Al-BSF depths, thereby reducing the total rear contact recombination of the solar cell [11].

The short-circuit current density  $J_{sc}$  increases from 39.1mA/cm<sup>2</sup> to 39.6mA/cm<sup>2</sup> when the LCO width is reduced from 114 $\mu\text{m}$  to 20 $\mu\text{m}$  (Fig. 2(c)). There are two reasons for this: 1) narrower LCO widths cause a slightly higher reflectance in the long-wavelength region, since the area fraction of the local Al contacts with poor reflectance is reduced; and 2) narrower LCOs result in slightly higher internal quantum efficiency (IQE) values at wavelengths above 1000nm, since the lower contact-area fraction leads to reduced contact recombination.

The fill factor FF of the n-PERT BJ cells with an Al finger grid is approximately 1%<sub>abs</sub> lower than that of the n-PERT BJ cells with a full-area Al-BSF, as shown in Fig. 2(d); this is caused by an increase in series resistance from 0.7 $\Omega\text{cm}^2$  for the full-area Al cells to 1.1 $\Omega\text{cm}^2$  for the Al finger grid cells. This is surprising, since the full-area contacting brass chuck excludes resistive contributions of the Al finger grid, and also the boron emitter resistance contribution is the same for all cells (because the LCO pitch is the same for all cells). In consequence, all cell types should exhibit very similar series resistances and FF values. A root cause of the lower FF of the n-PERT BJ cells with an Al finger grid could be that these cells might not have been fired at an optimum peak temperature. In this experiment, n-PERT BJ cells with Al fingers and full-area Al layer received a very similar peak firing temperature; the results for PERC+, however, indicated that a slightly lower peak firing temperature is required for cells with an Al finger grid than that for cells with a full-area Al layer [11].

The  $I$ - $V$  parameters of the best monofacial and bifacial n-PERT BJ cells when illuminated from the front are shown in Table 2 (rows 1 and 2). The  $I$ - $V$  parameters of the bifacial n-PERT BJ cell are also measured when illuminated from the rear (Al contact) by placing the cell upside down on the  $I$ - $V$  tester, again using a reflective brass chuck which contacts the full Ag front grid. As shown in Table 2 (row 3),

the rear-side efficiency is 16.5% and therefore much lower than the front-side efficiency of 21.1% for the same cell. Accordingly, the bifaciality, which is equal to the rear efficiency divided by the front efficiency, is 80%. The reduced rear-side efficiency is mainly due to the relatively low  $J_{sc}$  of 30.8 mA/cm<sup>2</sup>, which is 8.7 mA/cm<sup>2</sup> lower than the respective front-side  $J_{sc}$ .

“One future improvement opportunity for n-PERT BJ cells is to increase the spacing of the LCO rear contacts, which will allow higher bifacialities than PERC+ solar cells.”

For comparison, Table 2 (rows 6 and 7) also shows the front- and rear-side  $I-V$  parameters of the best bifacial PERC+ solar cells published by Dullweber et al. [8]. Basically, the front and rear  $I-V$  parameters of the bifacial n-PERT BJ cells are very similar to the respective PERC+ values. In the case of PERC+ cells, the low rear  $J_{sc}$  value has been explained [7] by the large Al metallization fraction of 14%, as well

as by the fact that the anti-reflective properties of the rear passivation stack have not yet been optimized. Both of these mechanisms also explain the low rear  $J_{sc}$  of the n-PERT BJ cells, as the device structure is optically identical to that of the PERC+ cells, including the 14% Al area fraction and the planar rear side. One future improvement opportunity for n-PERT BJ cells is to increase the spacing of the LCO rear contacts that have been optimized for the boron emitter sheet resistance; this will allow higher bifacialities than PERC+ solar cells, where the rear LCO spacing is limited by the wafer bulk spreading resistance.

### BiCoRE solar cells with BSG/SiN<sub>z</sub>

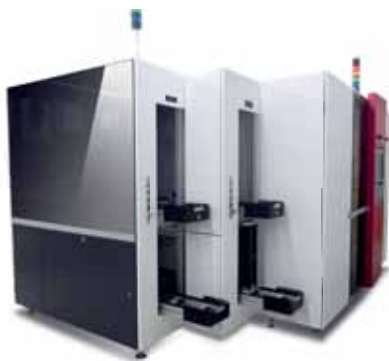
As a next step, the bifacial n-PERT BJ process is simplified by replacing the BBr<sub>3</sub> diffusion and the AlO<sub>x</sub>/SiN<sub>y</sub> rear passivation by the deposition of a stack of BSG and SiN<sub>z</sub>. The BSG/SiN<sub>z</sub> stack has multiple functions: 1) it serves as a dopant source for boron, which diffuses from the BSG into the silicon wafer during the POCl<sub>3</sub> co-diffusion; 2) it protects the rear side of the cell from being textured and phosphorus doped; 3) it remains on the rear side of n-PERT BJ cells as a passivation layer stack and anti-reflection coating (ARC).

In order to assess the emitter and passivation quality of the BSG/SiN<sub>z</sub> stack, an RCA clean is performed on n-type Cz test wafers, before depositing a 40nm-thick PECVD BSG layer, capped with a 120nm-thick PECVD SiN<sub>z</sub> layer, on both wafer surfaces. The test wafers are then exposed to a POCl<sub>3</sub> co-diffusion process, in which prior to the PSG deposition an additional thermal budget is applied in order to drive the boron from the BSG layer into the silicon wafer. Further details about the PECVD deposition parameters of the BSG/SiN<sub>z</sub> stack, as well as about the POCl<sub>3</sub> co-diffusion, have been published by Lim et al. [29]. Finally, the test wafers are fired in a belt furnace using typical contact-firing parameters.

The quasi-steady state photoconductance (QSSPC) of these samples is measured using an intrinsic carrier concentration of Si of  $n_i = 8.6 \times 10^9 \text{ cm}^{-3}$ .  $J_0$  values of 40 fA/cm<sup>2</sup> are achieved at boron sheet resistances  $R_{sheet}$  between 90 and 108 Ω/sq. by utilizing the BSG/SiN<sub>z</sub> stacks as the diffusion source and surface passivation [30]. In comparison, BBr<sub>3</sub>-diffused test wafers with AlO<sub>x</sub>/SiN<sub>y</sub> surface passivation yield  $J_0$  values of 14 fA/cm<sup>2</sup> at boron sheet resistances  $R_{sheet} = 102 \text{ Ω/sq}$ . Hence, the test wafer



## SYSTEMS FOR PV MANUFACTURING



- PERC laser ablation (lines, dots, dash lines)
- Laser doping
- Edge isolation
- Laser drilling
- Up to 4500 UPH



**ROFIN-BAASEL Lasertech**  
 Petersbrunner Straße 1b  
 82319 Starnberg / Germany  
 Tel: +49(0) 8151- 776 - 0  
 E-Mail: sales-micro@rofin.de

**WE THINK LASER**

Cell type	Doping / Passivation	Al area fraction [%]	Illumination side	$\eta$ [%]	$V_{oc}$ [mV]	$J_{sc}$ [mA/cm <sup>2</sup> ]	FF [%]
n-PERT BJ	BBr <sub>3</sub> / AlO <sub>x</sub> /SiN <sub>y</sub>	100	front	21.0	670	39.1	80.2
n-PERT BJ (bifacial)	BBr <sub>3</sub> / AlO <sub>x</sub> /SiN <sub>y</sub>	14	front	21.1	674	39.5	79.3
n-PERT BJ (bifacial)	BBr <sub>3</sub> / AlO <sub>x</sub> /SiN <sub>y</sub>	14	rear	16.5	669	30.8	80.0
BiCoRE	BSG/SiN <sub>z</sub>	14	front	20.6	669	39.3	78.4
BiCoRE	BSG/SiN <sub>z</sub>	14	rear	16.1	663	30.7	79.1
PERC+	n.a./ AlO <sub>x</sub> /SiN <sub>y</sub>	14	front	21.5	666	40.1	80.4
PERC+	n.a./ AlO <sub>x</sub> /SiN <sub>y</sub>	14	rear	16.6	660	31.3	80.7

**Table 2.**  $I$ - $V$  parameters measured under standard testing conditions (STC) of 156mm  $\times$  156mm n-PERT BJ and BiCoRE silicon solar cells. For comparison, the best PERC+ solar cell results published by Dullweber et al. [8] are also shown.

results indicate that the BSG/SiN<sub>z</sub> stack is well suited to functioning as a dopant source and passivation layer, resulting in similar sheet resistances to those for the BBr<sub>3</sub>-diffused samples and slightly higher  $J_0$  values, which are subject to future improvements.

The BSG/SiN<sub>z</sub> stack is now implemented in BiCoRE solar cells; the detailed process flow is shown in Table 1 (column 2). The same 156mm  $\times$  156mm n-type Cz wafers as for the n-PERT BJ solar cells are employed. After initial wafer cleaning, the PECVD BSG/SiN<sub>z</sub> stack is deposited on the wafer rear surface, followed by an alkaline texturing and a POCl<sub>3</sub> co-diffusion. Because of the SiN<sub>z</sub> rear capping layer, only the wafer front side is textured and phosphorus doped. The PSG on the wafer front side is removed by a short HF dip; this, however, does not remove the BSG/SiN<sub>z</sub> stack on the wafer rear side. A PECVD SiN<sub>y</sub> anti-reflection coating is then deposited on the wafer front side. The rear contacts are formed by laser ablation using the optimum LCO width of 40 $\mu$ m and the same pitch as for the bifacial n-PERT BJ cells. The Ag front contacts are dual printed, and the Al rear finger grid is screen printed using a finger opening of 100 $\mu$ m by utilizing the same processes as for the bifacial n-PERT BJ cells (as described in the previous section).

A schematic of the resulting BiCoRE solar cell is shown in Fig. 1(b). For comparison, Table 1 (column 3) and Fig. 1(c) also show the process sequence and schematic of a p-type PERC+ solar cell. The process flow for the BiCoRE cell is intentionally designed to be as close as possible to that for PERC+ solar cells in order to allow PERC cell manufacturers to change their production process to that for BiCoRE cells with almost no

additional tool investment.

The  $I$ - $V$  parameters of the BiCoRE solar cells are measured using the same measurement set-up as described earlier for n-PERT BJ solar cells; the results are summarized in Table 2 for the best BiCoRE solar cell. The average  $I$ - $V$  parameters of four identically processed BiCoRE cells are also given in brackets in the following text. When illuminated from the front (row 4 in Table 2), the best BiCoRE solar cell demonstrates a conversion efficiency  $\eta$  of 20.6% (average 20.3%), a  $V_{oc}$  of 669mV (average 670mV), a  $J_{sc}$  of 39.3mA/cm<sup>2</sup> (average 39.3mA/cm<sup>2</sup>) and a FF of 78.4% (average 77.1%). These values are fairly close to the  $I$ - $V$  parameters in Table 2 (row 2) of the bifacial n-PERT BJ cell with BBr<sub>3</sub> diffusion and AlO<sub>x</sub>/SiN<sub>y</sub> rear passivation.

The slightly lower efficiency of the BiCoRE cell can be attributed to a POCl<sub>3</sub> co-diffusion that has not yet been optimized, resulting in higher sheet resistances of the front-surface field, causing higher contact resistances of the Ag pastes and hence 0.9%<sub>abs</sub> smaller FF values. The 5mV lower  $V_{oc}$  of the BiCoRE cell is partly due to the 26fA/cm<sup>2</sup> higher  $J_0$  of the PECVD BSG/SiN<sub>z</sub> co-diffused and passivated rear emitter, compared with the BBr<sub>3</sub>-diffused and AlO<sub>x</sub>/SiN<sub>y</sub>-passivated n-PERT BJ cell.

The BiCoRE solar cell stems from the first batch of cells created using this novel process sequence. The authors are confident that with further optimization of the BSG/SiN<sub>z</sub> stack and the POCl<sub>3</sub> co-diffusion, it will be possible to produce BiCoRE cells with  $I$ - $V$  parameters comparable to those of n-PERT BJ and PERC+ solar cells.

## Conclusions

A novel industrial solar cell design has been introduced, namely BiCoRE. A key feature of this cell is a BSG/SiN<sub>z</sub> stack on the rear wafer side, which has three functions: 1) a protection layer against texturing and POCl<sub>3</sub> diffusion; 2) a boron dopant source during the POCl<sub>3</sub> co-diffusion; and 3) a passivation layer. Bifaciality is realized by utilizing LCO and screen printing an Al finger grid on the rear, similarly to the recently introduced PERC+ solar cells.

**“With further optimizations of the BSG/SiN<sub>z</sub> stack and the POCl<sub>3</sub> co-diffusion, it is expected that BiCoRE cells will yield efficiencies that are comparable to those of today’s PERC+ solar cells.”**

When the LCO widths were varied it was found that, in the case of Al fingers, narrow LCO widths of 40 $\mu$ m result in Al-BSFs with depths of up to 8.5 $\mu$ m and in conversion efficiencies of up to 21.1% for n-PERT BJ reference cells. The multifunctional BSG/SiN<sub>z</sub> stack demonstrates emitter saturation current densities of 40fA/cm<sup>2</sup> on test wafers, enabling conversion efficiencies of up to 20.6% for BiCoRE solar cells. When illuminated from the rear side, the BiCoRE cells exhibit conversion efficiencies of up to 16.1%, which corresponds to a bifaciality of 78%.

With further optimizations of the BSG/SiN<sub>z</sub> stack and the POCl<sub>3</sub> co-diffusion, it is expected that BiCoRE cells, which use LID-stable

n-type wafers, will yield even higher efficiencies – indeed, efficiencies that are comparable to those of today's PERC+ solar cells. The BiCoRE cell design could therefore become an attractive option for PERC solar cell manufacturers in changing their production to a bifacial, LID-stable cell concept with only a minimal conversion investment, which would mainly involve changing the PECVD  $\text{AlO}_x/\text{SiN}_y$  deposition to a BSG/ $\text{SiN}_z$  deposition process.

### Acknowledgements

We thank our colleagues M. Berger for solar cell processing, F. Heinemeyer for SEM measurements, and D. Hinken for support in the IQE analysis. This work was funded by the German Federal Ministry for Economic Affairs and Energy under Contract No. 0325880A (PERC 2.0).

### References

- [1] Fischer, G. et al. 2015, *Energy Procedia*, Vol. 77, pp. 515–519.
- [2] SolarWorld 2015, “SolarWorld expands production in Arnstadt”, Press Release (Mar) [<http://www.solarworld.de/en/group/investor-relations/news-announcements/corporate-news/single-ansicht/article/solarworld-expands-production-in-arnstadt>].
- [3] Hanwha Q CELLS 2015, “Hanwha Q Cells announces over 1.5 GW solar module supply agreement to power NextEra Energy Resources’ continued solar investments in the U.S.”, Press Release (Apr) [<http://investors.hanwha-qcells.com/releasedetail.cfm?ReleaseID=907243>].
- [4] Verlinden, P.J. et al. 2014, *Proc. 6th WCPEC*, Kyoto, Japan.
- [5] Trina Solar 2015, “Trina Solar starts PERC technology volume production”, Press Release (Jan) [[http://www.pv-tech.org/news/trina\\_solar\\_starts\\_perc\\_technology\\_volume\\_production](http://www.pv-tech.org/news/trina_solar_starts_perc_technology_volume_production)].
- [6] SEMI PV Group Europe 2015, “International technology roadmap for photovoltaic (ITRPV): 2014 results”, 6th edn (Apr.) [<http://www.itrpv.net/Reports/Downloads/>].
- [7] Dullweber, T. et al. 2015, *Prog. Photovoltaics Res. Appl.*, DOI: 10.1002/pip.2712.
- [8] Dullweber, T. et al. 2015, *Proc. 31st EU PVSEC*, Hamburg, Germany, pp. 341–350.
- [9] Guo, S., Walsh, T.M. & Peters, M. 2013, *Energy*, Vol. 61, pp. 447–454.
- [10] Janssen, G.J.M. et al. 2015, *Energy Procedia*, Vol. 77, pp. 364–373.
- [11] Kranz, C. et al. 2016, *IEEE J. Photovolt.*, Vol. 6, pp. 830–836.
- [12] Mertens, V. et al. 2013, *Proc. 28th EU PVSEC*, Paris, France, pp. 714–717.
- [13] Aleman, M. et al. 2013, *Proc. 28th EU PVSEC*, Paris, France, pp. 731–735.
- [14] Lim, B. et al. 2014, *Proc. 29th EU PVSEC*, Amsterdam, The Netherlands, pp. 661–665.
- [15] Wang, W. et al. 2015, *IEEE J. Photovolt.*, Vol. 5, pp. 1245–1249.
- [16] Gassenbauer, Y. et al. 2013, *IEEE J. Photovolt.*, Vol. 3, pp. 125–130.
- [17] Dullweber, T. 2013 et al. 2013, *Proc. 39th IEEE PVSC*, Tampa, Florida, USA, pp. 3074–3078.
- [18] Walter, D.C. et al. 2014, *Appl. Phys. Lett.*, Vol. 104, pp. 042111/1–4.
- [19] Wilking, S. et al. 2014, *Sol. Energy Mater. Sol. Cells*, Vol. 131, pp. 2–8.
- [20] Cabal, R. et al. 2009, *Proc. 24th EU PVSEC*, Hamburg, Germany, pp. 1605–1608.
- [21] Rothhardt, P. et al. 2014, *Proc. 29th EU PVSEC*, Amsterdam, The Netherlands, pp. 653–655.
- [22] Frey, A. et al. 2014, *Proc. 29th EU PVSEC*, Amsterdam, The Netherlands, pp. 656–660.
- [23] Wehmeier, N. et al. 2013, *Proc. 28th EU PVSEC*, Paris, France, pp. 1980–1984.
- [24] Wehmeier, N. et al. 2016, *physica status solidi (RRL)*, Vol. 10, pp. 148–152 (2016).
- [25] Engelhardt, J. et al. 2015, *Appl. Phys. Lett.*, Vol. 107, p. 042102.
- [26] Cabal, R. et al. 2016, *Proc. 6th SiliconPV*, Chambéry, France [to be published in *Energy Procedia*].
- [27] Dullweber, T. et al. 2016, *physica status solidi (a)*, Vol. 1–7, DOI: 10.1002/pssa.201600346.
- [28] Wehmeier, N. et al. 2016, *Proc. 32nd EU PVSEC*, Munich, Germany, pp. 443–446.
- [29] Lim, B. et al. 2016, *IEEE J. Photovolt.*, Vol. 6, pp. 447–453.
- [30] Wehmeier, N. et al. 2016, *Sol. Energy Mater. Sol. Cells*, DOI:10.1016/j.solmat.2016.05.054.

### About the Authors



**Dr. Thorsten Dullweber** leads the industrial solar cells R&D group at ISFH. His research work focuses on high-efficiency, industrial-type, PERC silicon solar cells and on ultra-fine-line, screen-printed, Ag front contacts. Before joining ISFH in 2009, he worked for nine years as a project leader in the microelectronics industry at Siemens AG and then at Infineon Technologies AG.



**Nadine Wehmeier** studied physics at the University of Münster, Germany, and received her M.Sc. in 2011 for her work on silicon multilayer structures for thermoelectric applications. She has been working towards a Ph.D. with ISFH since 2012, where she is researching plasma-enhanced chemical vapour deposition layers as diffusion sources and co-diffusion processes.



**Anja Nowack** completed her studies in process engineering at the University of Applied Sciences Nordhausen. For her Diploma thesis she carried out research into renewable energies with regard to optimizing the production of biogas. Since 2010 she has been working at ISFH as a degreed engineer (Dipl. Ing. (FH)), initially on topics involving macroporous silicon and then on PECVD BSG layers.



**Till Brendemühl** received his Diploma degree in engineering physics from the University of Applied Science in Emden, Germany. Since 2005 he has been with ISFH, where he initially worked on laser processes, and then later became a project leader with a focus on back-contact, high-efficiency solar cells. He is currently working on screen-printed, n-PERT solar cells in the photovoltaic future technologies group.



**Rolf Brendel** received a Ph.D. in materials science in 1992 from the University of Erlangen, Germany, for his work on infrared spectroscopy. After a research post at the Max Planck Institute for Solid State Research in Stuttgart, he was appointed head of the thermosensorics and photovoltaics division at the Bavarian Center for Applied Energy Research in 1997. In 2004 he joined the Institute of Solid State Physics at the Leibniz University of Hanover as a full professor, and became director of ISFH.

### Enquiries

Dr. Thorsten Dullweber  
Institute for Solar Energy Research  
Hamelin (ISFH)  
Am Ohrberg 1  
D-31860 Emmerthal  
Germany



# Stencil printing and metal squeegees for improved solar cell printing results

Andrew Zhou, Rado Yang, Tom Falcon & Jessen Cunnusamy, ASM Alternative Energy & Thorsten Dullweber & Helge Hannebauer, Institute for Solar Energy Research Hamelin (ISFH)

## ABSTRACT

Traditionally, the solar cell metallization process has been achieved through the use of mesh screens to print silver paste on the front side of the cell. Higher efficiency is generally realized by optimizing the busbar design, printing finer lines or making adjustments to the silver paste. This paper examines the use of stencil printing instead of screen printing in order to achieve improved fine line print quality for greater efficiency. In addition, a comparison of polymer and metal squeegees on fine line print performance is analyzed, with varying line apertures studied to understand the impact on the efficiency of PERC solar cells.

## Introduction

For today's crystalline silicon (c-Si) solar cell manufacturing operations, processes generally proceed in the following steps: texturing, diffusion, edge/etch isolation, PECVD SiN<sub>x</sub> coating and metallization. For the majority of metallization processes, screen printing is the most popular method to apply conductive paste to solar cells [1]. While other techniques such as plating and ink jetting are used, although less commonly, mass imaging via screen printing has emerged as the most cost-effective high-volume metallization method.

In this study conducted by ISFH, a stencil printing process [2] was implemented to evaluate possible improvements versus the conventional screen printing approach. Analysis revealed that the screen printing technique tends to produce solar cell fingers that have a wave-like shape along the finger direction. Importantly, the top portion of the wave shape was non-functional when the electrical current passed through the finger from the PN junction to the busbar. Concurrently, the bottom part of the wave shape became a bottleneck of current collection. The expectation was that solar cell fingers printed through metal stencils would provide more uniform lines and, therefore, deliver improved performance (Figs. 1 and 2).

As suspected, the uniform stencil-printed fingers offer lower electrical resistance than the wave-shaped, screen-printed fingers using the same volume of silver paste [3].

In addition to the print performance analyzed by comparison of screens versus stencils, this study also evaluated the effect of different squeegee materials on printing efficiency. The authors undertook a comparison of polymer

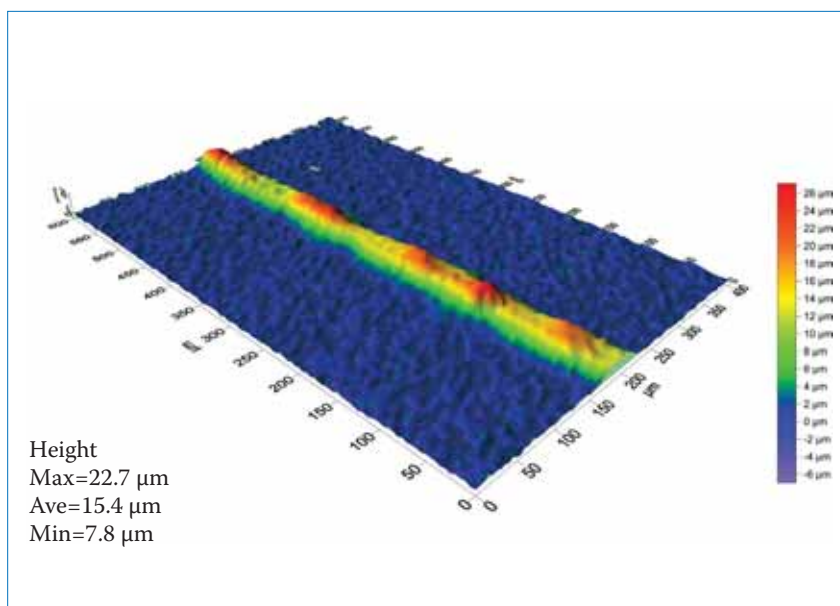


Figure 1. 3D microscope image of a solar cell finger printed with a screen. Note the wave-like topography, with peaks and valleys.

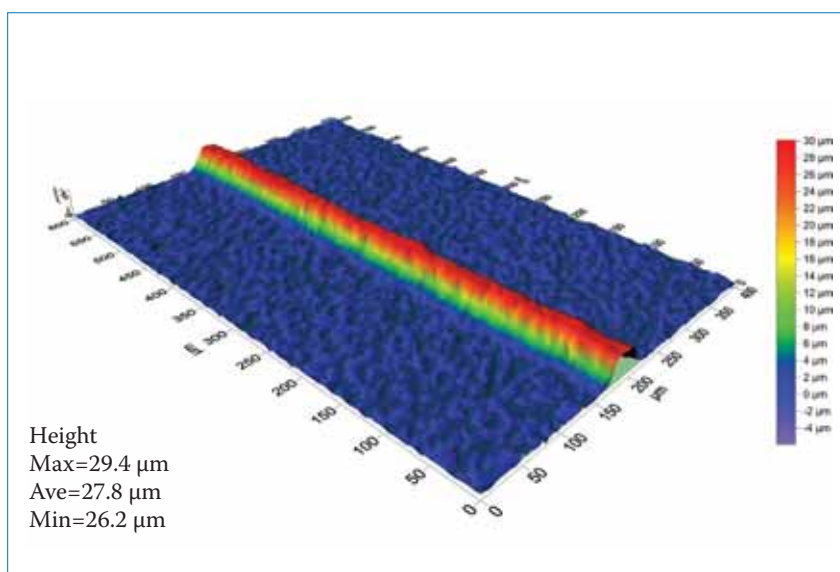


Figure 2. 3D microscope image of a solar cell finger printed with a metal stencil. The silver paste is more uniformly distributed than with the screen print.

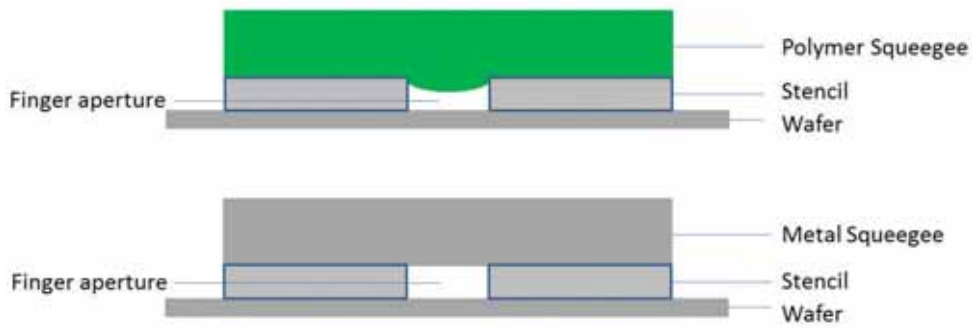


Figure 3. Polymer squeegee versus metal squeegee printing; polymer squeegees tend to result in a scooping effect, whereas metal squeegees produce a more brick-like shape.

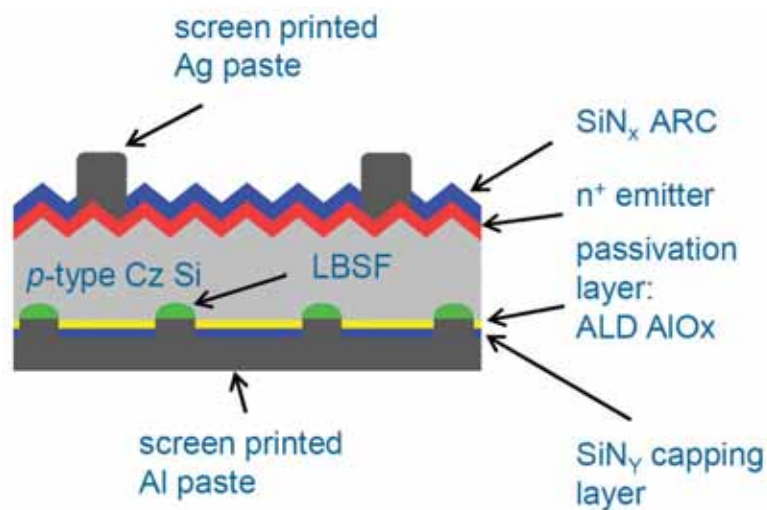


Figure 4. The substrates of this experiment

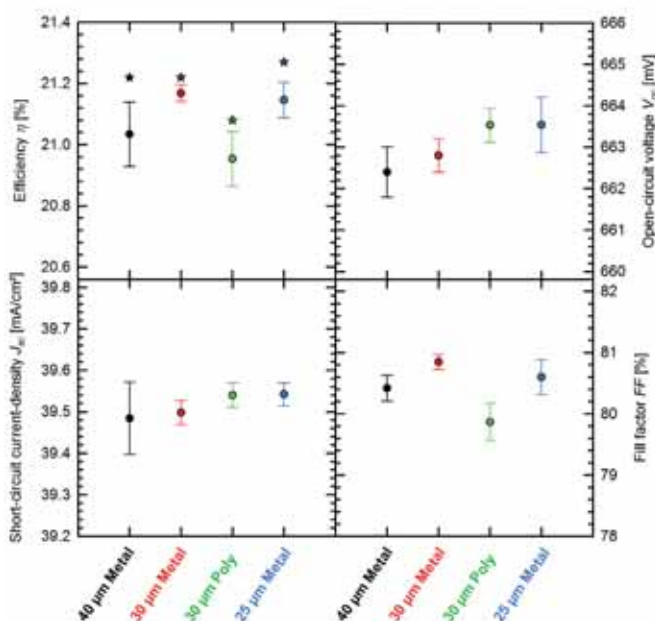


Figure 5. I/V data of four groups.

versus metal squeegees to understand the impact of squeegee material on print performance. Because polymer squeegees have elasticity, part of the squeegee will extend into the stencil aperture during stencil printing, resulting in a “scooping” effect, which produces a trough-like finger shape (Fig. 3).

## Design of experiment

### Experimental inputs

1. ASM Alternative Energy (ASM AE) Eclipse metallization platform, Centrotherm dryer, Centrotherm furnace, I/V tester
2. Nikon optical microscope and Wyko surface profiler
3. ASM AE VectorGuard stencil frame, Fine-Line™ stencil foil and metal squeegee
4. ASM AE Polymer squeegee, 95A shore
5. Silver pastes
6. PERC solar cell substrates from ISFH [Figure 4]

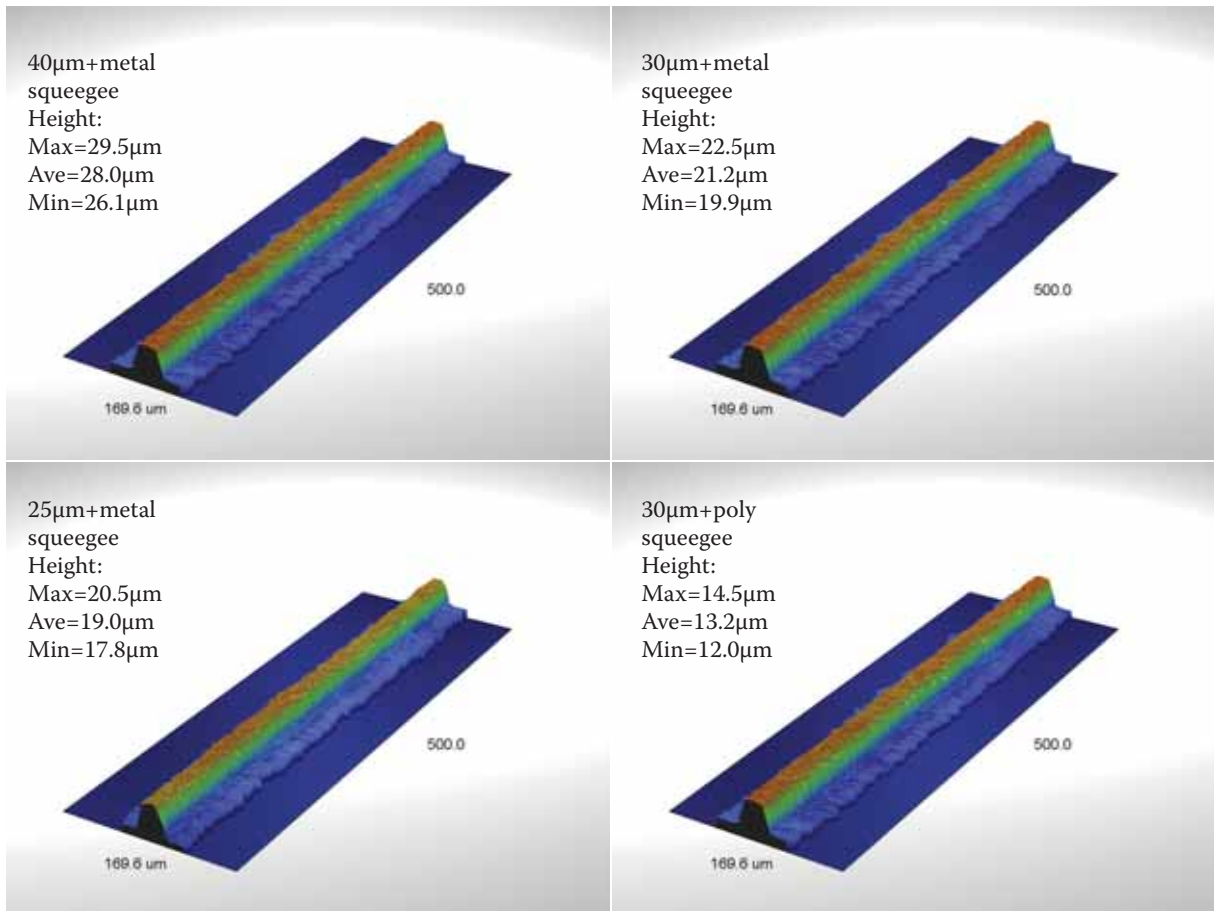


Figure 6. Resulting finger shapes and height for the different aperture/squeegee combinations.

### Experimental process

PERC solar cell substrates from ISFH [4] were printed on the Eclipse metallization platform using a two-step printing process [5,6].

During step one, the busbar pattern was screen printed using a non-fire-through silver paste. Following the initial busbar print, the paste was dried and the cells were randomized into different groups. In the second step, the finger pattern was printed with a contacting silver paste with high viscosity developed for stencil printing through a VectorGuard Fine-Line stencil using a metal squeegee, following which the paste was dried. Various stencil foils with 25μm, 30μm and 40μm finger apertures were used to print three groups of solar cells. The finger number range is between 101 fingers for 40μm, 124 fingers for 30μm and 134 fingers for 25μm. Simultaneously, one group of cells

was printed using 30μm apertures and a polymer squeegee. Finally, all four groups of solar cells went through thermal processing (firing) and the cells were I/V tested.

### Characterization and discussion

#### I/V data of solar cells

I/V data results are shown in Figure 5. The star-shaped data points refer to the solar cell with the highest conversion efficiency of each group.

All cells achieved similar  $J_{sc}$  and  $V_{oc}$  parameters, which are caused by nearly the same metallization area. The lowest fill factor (FF) was observed in the solar cell group printed with polymer squeegee, indicating that the finger conductivity of this group of cells was lower than the other cell groups printed with a metal squeegee.

#### Finger shape characterization

The finger shape of three groups was measured and included those cells printed with the following conditions: a 30μm stencil aperture and a metal squeegee, a 30μm stencil aperture and a polymer squeegee and a 25μm stencil aperture and a metal squeegee. The results are shown in Figure 6 and Figure 7.

Figure 6 and Figure 7 illustrate that when using the 30μm aperture stencil and printing with metal and polymer squeegees for comparison of squeegee type, the finger width printed with the metal squeegee group is approximately 41.40μm and that printed with the polymer squeegee is about 38.64μm. While the difference between the two line widths isn't statistically significant, the finger height differences are quite meaningful. The finger height printed with metal squeegees is about 21.2μm high, while that printed with the polymer squeegee is approximately 13.2μm. These

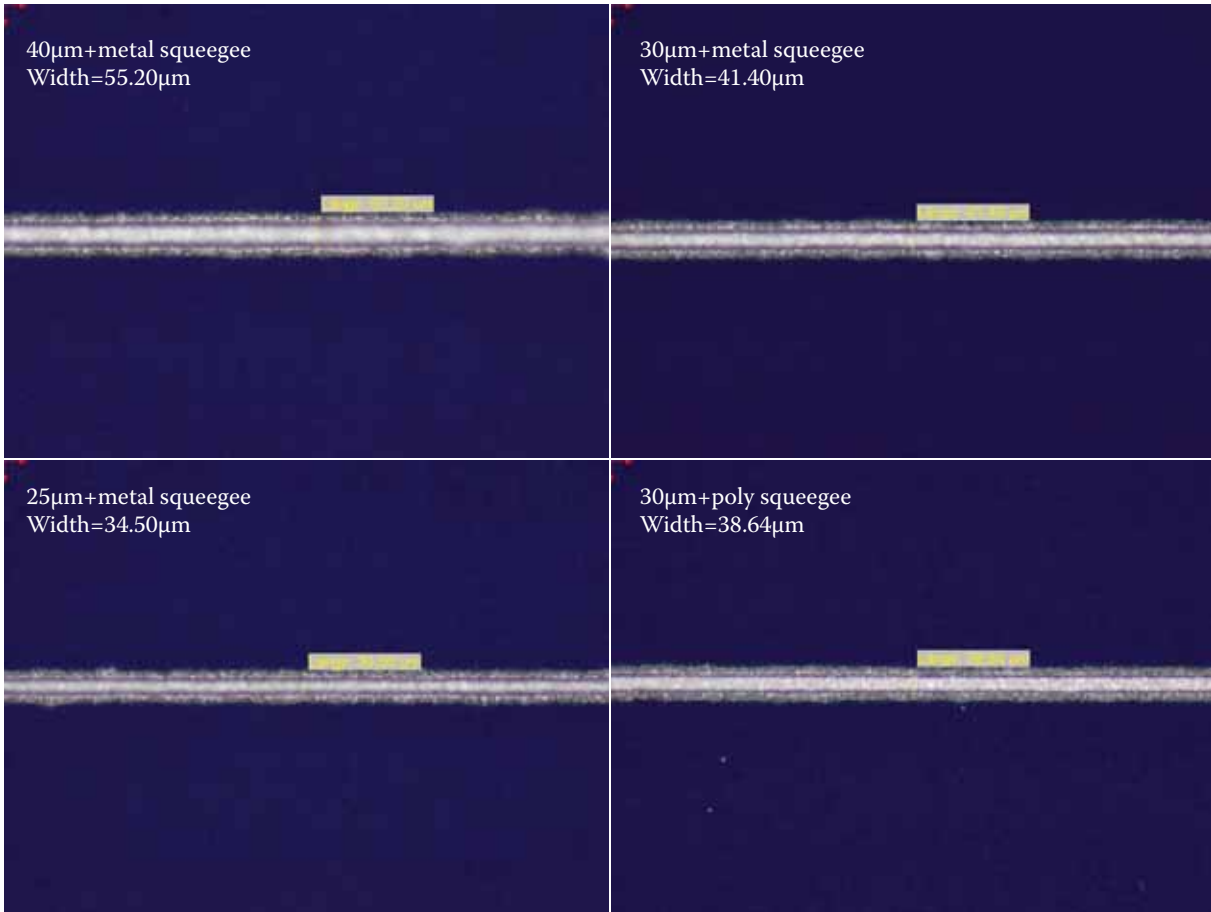


Figure 7. Resulting finger width for the different aperture/squeegee combinations.

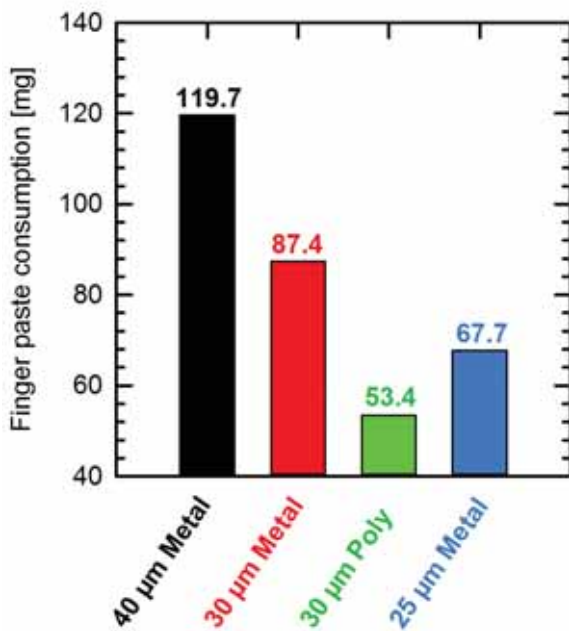


Figure 8: Silver paste consumption of four groups

results substantiate the “scooping effect” observed with polymer squeegee printing. With the 25µm aperture stencil and metal squeegee prints, finger widths of 34.50µm and heights of 19µm were produced.

**Silver paste consumption**

Achieving cost competitiveness in the solar cell manufacturing industry is a necessity; both for manufacturer competitive advantage and for the production of lower-cost cells to bring solar energy costs in line with consumer expectations. Silver paste is generally considered one of the higher cost inputs in solar cell manufacturing, so the ability to reduce the consumption of silver paste while simultaneously improving cell efficiency has been and continues to be a driver of technology development [7,8].

In this study, silver paste consumption was also recorded after printing prior to drying and the results are illustrated in Figure 8. The chart shows the silver paste consumption

for the contact fingers. The standard rectangular-shaped five busbar design results in an Ag paste consumption for the busbars of 14.2mg.

Figures 5 and 8 indicate that the relationship between silver paste consumption and cell efficiency is not a direct ratio. In stencil printed cells, the higher efficiency groups were printed by 30µm and 25µm finger aperture stencils. The 30µm group has better fill factor and more concentrated efficiency distribution compared to the 25µm group, which suggests that the 30µm finger aperture stencil has better printing performance than the 25µm finger aperture stencil when using the DuPont silver paste for the contact finger. In addition, the highest efficiency cell appeared in the 25µm finger aperture group, indicating a higher average efficiency could be achievable given optimization of the stencil and silver paste.

## Conclusion

Results from this study conducted by ISFH indicate that a metal squeegee produces improved fine line printing performance as compared to a polymer squeegee resulting in higher aspect ratios using a metal squeegee. In the final I-V ISFH data from the PERC cell analysis, the 3µm finger aperture stencil printed group produced the best average efficiency, and the highest individual efficiency appeared in 25µm finger aperture stencil printed group. The study also revealed that the correlation between silver paste consumption and cell efficiency is not directly proportional and that further research is required to understand the relationship between the front side pattern and silver paste.

## References

- [1] ITRPV Working Group. "International Technology Roadmap for Photovoltaics Results 2011", "International Technology Roadmap for Photovoltaics Results 2015", 7th Edition, March 2016.
- [2] Bottosso C, Martire M, Galiazzo M. Fine line metallization through screen and stencil printing, *Proc 27th European Photovoltaic Solar Energy Conference*, Frankfurt, Germany, 2012, p. 1645-1647.
- [3] Hoorstra, J., Heurtault, B., "Stencil print applications and progress for crystalline silicon solar cells", *Proc 24th European Photovoltaic Solar Energy*

*Conference*, Hamburg, Germany, 2009, p. 989-992.

- [4] Hannebauer, H., Dullweber, T., Baumann, U., Falcon, T., Brendel, R. "21.2%-efficient fineline-printed PERC solar cell with 5 busbar front grid", *Phys. Status Solidi RRL* 8(8): 2014, p.675-679.
- [5] Falcon, T. "Ultra Fine Line Printing for Silicon Solar Cells...Mesh Screens or Metal Stencils?" *Presentation at the 3rd Metallization Workshop*, Charleroi, Belgium, 2011.
- [6] Hannebauer, H., Schimanke, S., Falcon, T., Altermatt, P.P., Dullweber, T. "Optimized stencil print for low Ag paste consumption and high conversion efficiencies", *Energy Procedia* 67: 2015, p.108-115.
- [7] Cooper, I.B., Tate, K., Carroll, A.F., Mikeska, K.R., Reedy, R.C., Rohatgi, A. "High efficiency achieved on POCL3 emitter Si solar cells with low saturation current density while reducing Ag consumption by 40-60%", *Proc 27th European Photovoltaic Solar Energy Conference*, Frankfurt, Germany, 2012, p. 614-617.
- [8] Hannebauer, H., Dullweber, T., Falcon, T., Brendel, R. "Fine line printing options for high efficiencies and low Ag paste consumption", *Proc 3rd International Conference on Crystalline Silicon Photovoltaics*, Hamelin, Germany, 2013.

## About the Authors



**Jessen Cunnusamy** is a Process Engineer with ASM Assembly Systems and is part of the Electroform Stencil Team, focusing on the development of advanced stencil printing processes and products. Prior to joining ASM, Cunnusamy held a research engineering position with SERIS, where he specialized in back-end processes.



**Andrew Zhou** is a Senior Process Consultant for ASM Alternative Energy and leads research and development with an emphasis on improving printing technologies and processes. Before joining ASM AE, Andrew held various roles including that of R&D Engineer for optical disc and amorphous silicon solar module manufacture, Senior R&D Engineer for crystalline silicon solar cell manufacture, and Field

Application Engineer for advanced materials and technologies.



**Tom Falcon** is Principal Engineer at ASM Alternative Energy and has worked in the printing technology sector since 2001, initially specializing in process development for the Semiconductor Packaging Technologies Team before moving to solar in 2008. He is currently responsible for developing metallization processes for silicon solar cells. Previously, he held senior engineering positions with IBM, Nortel and Cookson Electronics.



ASM Alternative Energy Consultant, **Rado Yang**, works closely with ASM AE's Greater China-based customers in support of their metallization processes and ongoing new product development. His tenure with ASM also includes past experience as a Support Engineer, serving the company's Alternative Energy and Assembly Systems businesses.



**Dr. Thorsten Dullweber** leads the industrial solar cells R&D group at ISFH. His research work focuses on high-efficiency, industrial-type, PERC silicon solar cells and on ultra-fine-line, screen-printed, Ag front contacts. Before joining ISFH in 2009, he worked for nine years as a project leader in the microelectronics industry at Siemens AG and then at Infineon Technologies AG.



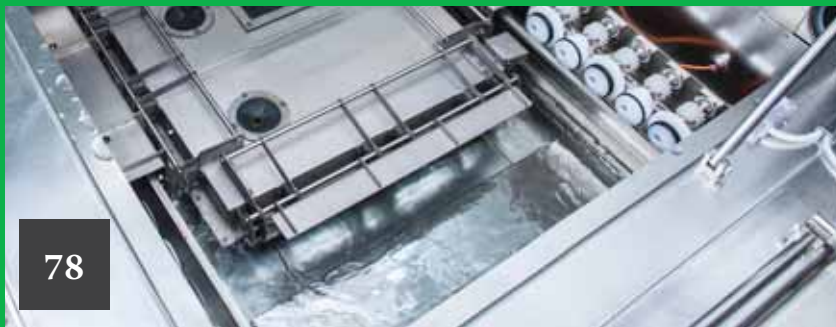
**Helge Hannebauer** studied technical physics at the Leibniz University of Hanover from 2005 to 2009. For his diploma thesis at ISFH he investigated the optimization of screen-printed solar cells. In 2010 he started a PhD programme at ISFH, focusing on advanced screen printing and selective emitters.

## Enquiries

Brett Hallam  
School of Photovoltaic and Renewable Energy Engineering  
University of New South Wales  
Sydney NSW 2052  
Australia

Tel.: +61 415 415 156  
Email: [brett.hallam@unsw.edu.au](mailto:brett.hallam@unsw.edu.au)

# Thin Film



78

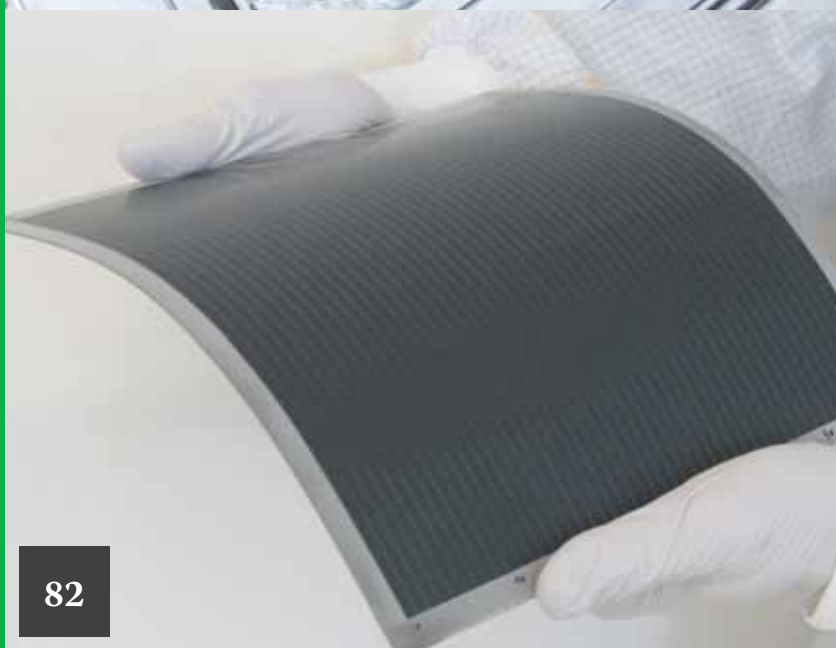
Page 78  
News

---

Page 82  
Significant progress in CIGS  
thin-film solar cell technology  
reported at IWCIGSTech7

Rutger Schlatmann & Hans Werner Schock, Helmholtz-Zentrum Berlin für Materialien und Energie, Michael Powalla, Centre for Solar Energy and Hydrogen Research Baden-Württemberg (ZSW)

---



82

## Solar Frontier in talks over CIS thin-film production plant in Saudi Arabia

CIS thin-film module manufacturer Solar Frontier has signed a memorandum of understanding with Saudi Aramco and the Saudi Arabian National Industrial Cluster Development Program (NICDP) on the feasibility of establishing a thin-film module production plant in Saudi Arabia.

In collaboration with Solar Frontier's parent company, Showa Shell Sekiyu the companies initially plan a feasibility study to establish the 'technological and economic aspects' of CIS thin-film production in Saudi Arabia.

Desert conditions have suited both CIS and CdTe thin-film modules, due to being less impacted by the temperature coefficient than conventional crystalline silicon modules. Solar Frontier has previously stated that it would consider building production plants outside Japan on the scale and template of its 150MW Tohoku Plant in Miyagi Prefecture, Japan, which was touted to be able to produce modules at one-third of the time compared to its 900MW Kunitomi plant.



Credit: Solar Frontier

Japanese thin-film specialist Solar Frontier is looking to establish production in Saudi Arabia.

## First Solar

### First Solar cuts capex and opex to generate US\$2 billion plus cushion

CdTe thin-film producer First Solar is undergoing a mid-year restructuring that includes cost cutting activities that should generate a US\$2 billion balance sheet cushion against changing solar business dynamics and a looming revenue and shipment hole facing the company in 2017.

First Solar said in its second quarter earnings call that aside from the planned closure of its crystalline silicon cell and module operations through TetraSun that was announced in early July, its O&M subsidiary, skytron energy was up for sale and its in-house EPC workforce would be reduced to match lower expected focus on PV project development in the future.

However, the company also noted that capex would also be significantly reduced for 2016 to a range of US\$275 million to US\$325 million from the previous range of US\$300 million to US\$400 million. Capex in the second quarter was US\$78 million, compared to US\$52 million in the prior quarter. Management said the increase in spending quarter-on-quarter was due to increased investments in its Series 5 technology

First Solar noted that the additional module efficiency improvements would take the Series 5 roadmap to the 390W level at the same time it previously expected to reach the 365W level. The company noted that the an estimated US\$60 million in capex would be required

to boost conversion efficiencies across its 3GW of capacity, yet the anticipated payback time would be less than one year.

### First Solar ends heterojunction foray

First Solar is discontinuing development and production of its hybrid heterojunction silicon cell and module technology, acquired via the purchase of start-up TetraSun.

First Solar said that the TetraSun production plant in Malaysia would be converted and dedicated to its CdTe thin-film Series 5 module assembly requirements and be operational in early 2017. The discontinuation of its TetraSun operations would result in impairment charges of approximately US\$90 million to US\$110 million, the company said.

Finlay Colville, head of market intelligence at Solar Media, said rumours had recently surfaced that the TetraSun operations were up for sale again. "The precise reasons may never be known for why First Solar closed its TetraSun activities, and there are likely a combination of factors, not simply technology milestones for pilot line metrics," noted Colville. "In some respects, it may have been overly ambitious for First Solar to have elevated c-Si activities so much when TetraSun was acquired. At the time, the acquisition was cited by the company as being the route to getting traction in the Japanese rooftop market, but no doubt the lure of residential market share in the US would have been running a close second then. Had the activities at TetraSun remained stealth, as they were when First Solar was

undertaking its stealth-like CIGS research in the US, then no-one would have been expecting updates; nor would there have been any post-mortem once the company announced out of the blue that the Malaysian operations had ceased," add Colville.

"The Series 5 module and the Series 6 module still in concept development are game-changing products that position us for exciting growth. They require the full attention of our manufacturing operations," said First Solar's COO Philip Tymen de Jong. "TetraSun is a sound technology for space constrained rooftops, and served largely as a hedge against CdTe technology competitiveness that had challenged us in the past. With the success of our CdTe roadmap...that hedge is no longer needed."

## Tools

### China automation and CIGS deals buoy Manz results

PV and electronics equipment manufacturing and automation specialist Manz AG has reported continued demand for automation system in China for solar manufacturing applications that have generated €17.5 million in first half year revenue, up 66.7% from the prior year period.

Manz reported that solar segment sales accounted for 14.1% of total Group sales of €124.0 million in the reporting period, up from 8.6% or €10.6 million in the first half of 2015. The company also noted that its solar segment earnings



Credit: Manzt

Manz's quarterly results have received a boost from continued interest in its CIGS thin-film tools.

were influenced by the maintenance of production capacities in CIGS thin-film technology. Manzt is also in a development programme with new investor, Shanghai Electric, in commercialising its CIGS technology.

However, solar segment sales were below profitable thresholds, generating a negative EBIT of €4.9 million, down from negative €7 million in the prior year period. The company said it would provide a detailed update on its strategic partnership with Shanghai Electric later in the third quarter. This should result in a "significant" increase in revenues with significantly improved earnings before interest and taxes (EBIT) for the full year,' according to Manzt AG's financial statement.

### AVANCIS selects camLine's MES for 300MW CIGS production plant

Manufacturing Execution System (MES) software firm camLine has won a bid to supply its software to the planned AVANCIS, 300MW CIGS thin-film production plant in Anhui, China.

The company noted that AVANCIS already used its 'InFrame Synapse' MES software at AVANCIS' CIGS thin-film plant in Torgau, Germany. AVANCIS is owned by CNBM, one of China's largest building materials firms and is state owned.

Ground breaking for the 300MW first-phase CIGS plant in Bengbu, China, took place in October 2015. Future expansion plans could take capacity to 1.5GW.

## Hanergy

### Hanergy Thin Film Power claims profitability for H1 2016

Struggling Hanergy Thin Film Power Group has claimed to have increased revenue by around 50% and returned a profit for the first half of 2016, compared to the prior year period.

In a Hong Kong Stock Exchange filing, Hanergy Thin Film said that sales in its downstream rooftop (residential & commercial) systems business had increased by over 200%, compared to the prior year period.

The company had previously reported 'downstream' external sales totalling around US\$23.8 million in the first half of 2015, indicating sales in the current year period topped US\$71 million. With previous plans to use its a-Si thin-film modules in utility-scale projects purchased by its parent company, Hanergy Holding Group were suspended on previous non-payments and failure to supply sufficient quantities of modules, the residential and commercial rooftop market has been a key focus, despite being a small revenue generator in 2015.

However, Hanergy Thin Film also said that its revenue from its upstream a-Si thin-film manufacturing production line delivery business actually increased by over 25%, compared to the prior year period, when sales controversially topped US\$249 million. This area of business activity has been highly contentious after a series of large orders were placed with

Hanergy Thin Film from companies with no previous experience of either manufacturing or BIPV and utility-scale PV power plant construction, while the transactions were pegged to the company issuing new shares to the customers that had a higher value than the large upfront deposits. With trading in Hanergy Thin Film's shares suspended in May 2015 and remaining suspended to this date, all of the turnkey production line deals were cancelled.

### Hanergy Holding wants defer US\$360 million in overdue debts to Hanergy Thin Film

Hanergy Thin Film Power Group said its parent company Hanergy Holding Group had proposed a deferred payment deal on overdue debts totalling US\$360 million and interest penalty payments that topped US\$25 million at the end of 2015.

Hanergy Thin Film noted in a financial filing to the Hong Kong Stock Exchange that it finally received a letter from Hanergy Group wanting to defer payments and interest penalties. Hanergy Thin Film did not disclose details of the letter regarding the deferred payment proposal.

Hanergy Thin Film said that no formal agreement had been made and that an agreement may also not be entered into as a final say via independent shareholders at the special general meeting. However, the major shareholder is Hanergy Group chairman, Li Hejun.



# Significant progress in CIGS thin-film solar cell technology reported at IWCIGSTech7

**Rutger Schlatmann & Hans Werner Schock**, Helmholtz-Zentrum Berlin für Materialien und Energie, **Michael Powalla**, Centre for Solar Energy and Hydrogen Research Baden-Württemberg (ZSW)

Photovoltaic modules with CIGS absorbers are very effective in converting light directly into electricity. Due to their specific advantages CIGS thin-film modules are among the most promising photovoltaic technologies. Many companies and institutions worldwide contribute to this development with diversified approaches. An efficient exchange of knowledge is essential to move the technology forward. In June 2016, the IW-CIGSTech workshop was organized for the seventh consecutive year in a row. This time, the event took place as a parallel event to the EU-PVSEC/Intersolar Europe in Munich. In the workshop, representatives from industry and academia gathered to discuss the latest developments in the fast-developing field of CIGS (Cu(In,Ga)(Se,S)<sub>2</sub>) based solar cells. As a result of last year's workshop, a joint,

community-wide effort resulted in the broadly acknowledged "White Paper for CIGS thin film solar cell technology" [1]. In this article, we provide a brief impression of the progress and challenges reported in this year's workshop.

## Record efficiencies

Over the past few years, record efficiencies have improved at an impressive rate and are catching up with crystalline silicon technology. Presenting a new world record, Stefan Paetel from ZSW in Stuttgart, Germany, reported on his institute's latest certified record value of 22.6%. With his colleagues from the EU-sponsored Sharc25 consortium, he outlined the roadmap 25% efficiency values on a lab scale. Similarly ambitious targets were reported by Shigeru Niki from Japan's

AIST, who leads a NEDO-sponsored consortium working on CIGS. Based on Solar Frontier's sequential deposition technology (22.3% certified record cell), and AIST's in-house co-evaporation technology, 20% mini-module efficiency is aimed for by 2019, paving the way for electricity costs of ¥14 JPY (US\$0.135) per kWh in 2020 and ¥7 by 2030.

Prof. Sun from Nankai University in China presented an overview of academic and industrial developments in China. Several research labs are working on CIGS cells and modules on flexible substrates and glass, with cell efficiencies already above 20%. Reporting on experience with improved yield from CIGS PV plants compared to Si, as well as on production expansion plans from companies such as CNBM and Hanergy he expects the breakthrough of CIGS industrialization within the next 10 years.



Credit: ZSW

CIGS thin-film technology can be used in a variety of applications, such as on flexible substrates.

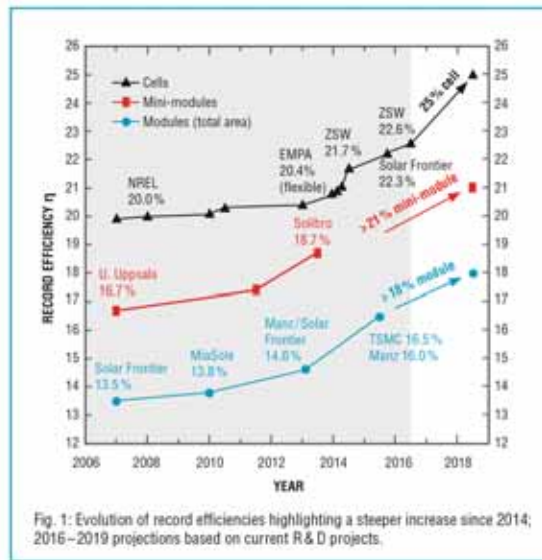


**Figure 1: Evolution of record efficiencies highlighting an increased slope since 2014; 2016–2019 projections based on current R&D projects.**

Figure 1 indicates the recent progress in record efficiency at the cell level (black triangles). New processes with the introduction of alkali dopants enter production and provide a significant boost of module performance, paving the way for progress at the mini-module level (red squares) and towards total area module efficiencies (blue dots) of 18%.

### Products and technology perspective

An important focus of the workshop was on production issues. The diversification of the production and design of CIGS modules offers multiple possibilities for PV power systems in the future. CIGS glass-glass products cover the classical application fields of power plants, rooftops and building facades. Even though this efficient thin-film technology can be produced on a variety of substrates, glass-based modules are dominating production, as was reported by Takuya Kato from Solar Frontier, Robert Lechner from Avancis and Olle Lundberg from Solibro. Full-size modules from the main players have all reached champion efficiencies in the range of 16%, independent of process technology. Several large-scale production sites are running in Japan and Germany, and several more are planned and in construction in China. At the same time, flexible and light-weight CIGS modules currently in production show average aperture area efficiencies of >16% as well, as reported by Miasolé's Atiye Bayman. Achieving high efficiency with such

products will open new large-scale applications and consumer markets. A variety of substrates and module designs were presented by Global Solar (Urs Schoop reported) and Miasolé, both within the Hanergy group, as well as by Switzerland based Flisom.

### Proven reliability and performance

Glass-glass CIGS modules with monolithic series connection of the individual cells demonstrate inherently superior stability over soldered or bonded cell strings. At present, CIGS modules from mass production guarantee a high level of reliability proven by extensive endurance and long-term field tests in numerous installations and climatic conditions with independent verification [2].

A low temperature coefficient, a favourable spectral response and high efficiency under low light conditions are the reason for excellent energy yields and hence low levelized costs of electricity under most climatic conditions. Furthermore, the specific design of thin-film module based on monolithic interconnection of cells across the entire substrate results in intrinsically reduced sensitivity to detrimental effects caused by shading.

Following a long tradition of CIGS Technology since the last century, Stion's Alexander Schwarz presented impressive data of performance, reliability and stability of modules in the field. These data and similar long-term studies presented by Solibro indicated that CIGS is outperforming c-Si at most geographical locations.

### Developments at the GW production level

Currently the biggest production units, ranging in capacity from 100 to 1,000MWp per year, are located in Germany, the US and in Japan. In China, ground-breaking for factories of hundreds of megawatts in size have already taken place and further operations in the gigawatt range are planned. These are operated at high yields well beyond 90% over the whole value chain. At present, the total world-wide CIGS production capacity is about 2GWp per annum. Although companies use different fabrication methods, all of them show excellent results, demonstrating that CIGS production technology has reached the first stage of industrial maturity. Even when using non-abundant elements like Indium, a supply limitation is not expected at any planned and projected production volume. This is due to the continuous reduction of the amounts of Indium needed in combination with progress in recycling. Production costs of US\$0.4/Wp are already projected even for low capacities of 150MW, with further reductions of 25-40% expected by improving module efficiencies and exploiting scaling effects on materials cost and capex for multi-gigawatt fabs. Nevertheless, further cost-reduction potential is expected within the next decade if supported by continued, effective R&D activities.

For production lines on a gigawatt level, equipment manufacturers play a key role. The tolerance of the CIGS absorber material allows a wide scope of process techniques to be exploited. Kay Orgassa from Manz gave an update on the further development of Manz's well known co-evaporation-based 'CIGSfab'. Next to further improvement in module efficiency and line yield, he reported on experiments on how to transfer the highly successful lab-scale alkali Post Deposition Treatment (PDT) into production. Dirk Beisenherz from Singulus gave an overview of his company's core sequential CIGS processing technologies: precursor sputtering, Se deposition, rapid thermal processing (RTP) ovens and buffer deposition. He also showed how this equipment was scaled up towards GW production level. In order to enable further capex reductions, Sebastian Schmidt from the Helmholtz Zentrum Berlin presented exploratory work to develop high-efficiency, high-throughput RTP equipment, with the key feature that it operates at atmospheric pressure (based on a Smit Thermal Solution system).

The huge future potential of CIGS

technology was demonstrated in the oral and poster presentations by research institutes from a.o. Switzerland, France, Japan, the Netherlands, Luxemburg, China and Germany. Recent results of material modifications and device optimization, such as those presented by Daniel Lincot from IPVF (France), revealed the still enormous room for further efficiency developments. In the longer term, in combination with suitable wide bandgap absorbers (e.g. Perovskites), CIGS can be used as a bottom cell in tandem devices that enable efficiency values well beyond 30%, as was outlined in the presentation by Stephan Buecheler from EMPA (Switzerland). This demonstrates impressively that not only is CIGS a competitive PV technology, but in addition it comprises a potential not yet exploited for further improvements.

Still, there are some clear challenges facing the CIGS community as a whole. Most importantly, a lack of standardization in process equipment, product size, quality control and in-house testing procedures so far prevent CIGS technology from reaping the full economy-of-scale benefit. Therefore, in the course of IW-CIGSTech 7, major players of the industry and its suppliers as well as research institutions agreed to build on the initial joint effort of the White Paper. They intend to cooperate

more closely in future, for example by sharing information on joint technical issues, providing up-to-date ecological footprint data, developing a CIGS technology roadmap and keeping the public up to date on the advantages of the CIGS technology.

In summary, the IWCIGSTech7 workshop presentations gave a concise and impressive insight into the present status and future potential of CIGS technology. Due to its continued success in gathering the vast majority of technological actors in the field, the community-driven IWCIGSTech workshop is certain to see its next version in 2017.

#### References

- [1] "White Paper for CIGS thin film solar cell technology", [cigs-pv.net](http://cigs-pv.net)
- [2] See for instance data from the independent DKASC outdoor test site in Alice Springs, [www.dkasolarcentre.com.au](http://www.dkasolarcentre.com.au)

#### About the Authors



**Rutger Schlatmann** is director of PVcomB, the PV technology transfer centre at the Helmholtz-Zentrum Berlin and full professor (W3) at the HTW Berlin. He obtained his PhD at the FOM Institute Amolf in Amsterdam. Before 2008, he was as R&D manager at Helianthos, a company developing flexible



**Hans-Werner Schock** has worked since the early 1970s on the development of polycrystalline II-VI and I-III-VI<sub>2</sub> compound semiconductor thin-film solar cells. From 2004 to 2012 he was director of the Institute of Technology at the "Helmholtz Zentrum Berlin für Materialien und Energie". For his achievements in the development of thin-film solar cells he received the "Becquerel Prize" of the European Commission in 2010.



**Michael Powalla** is head of the Photovoltaics Division and member of the board at Zentrum für Sonnenenergie und Wasserstoff-Forschung Baden-Württemberg (Centre for Solar Energy and Hydrogen Research) in Stuttgart, Germany. He earned his PhD in 1998 at the University of Stuttgart. As a physicist, he devotes his attention to materials and processes of energy conversion with a focus on photovoltaics. Prof. Powalla holds a professorship for thin-film photovoltaics at Karlsruhe Institute of Technology (KIT).

# SOLAR PV IRELAND

Official Partner



Aviva Stadium | Dublin, Ireland

16 - 17 November, 2016

#PVIreland

## Shaping Ireland's energy future

The Republic of Ireland's PV market is expected to reach 1-2GW by 2019. With 3GW of grid applications already in and a competitive market support mechanism expected in autumn 2016, developers anticipate the main construction phase to start in March 2017 and are making preparations now.

With proven results helping international and UK solar supply chains connect, Solar Media's inaugural Solar PV Ireland will enable the Irish market to develop with professionalism, speed and inclusivity.

#### Hear from over 30 industry experts, including:

**Eamonn Confrey**, Principal Officer, Decarbonisation Policy, Department for Communications, Energy and Natural Resources

**Mike Quinn**, CEO, Bord na Móna

**Marie Donnelly**, Director for New and Renewable Sources of Energy, Energy Efficiency & Innovation at DG Energy, European Commission

**Garry Connolly**, President, Host in Ireland, Chairperson, Commission for Energy Regulation

**Jon O'Sullivan**, Manager Innovation, Eirgrid

**Eoin Hartigan**, Head of Renewable Energy Business, Bank of Ireland

REGISTER TO ATTEND NOW [ireland.solarenergyevents.com](http://ireland.solarenergyevents.com)



# PV Modules



**Page 84**  
**News**

---

**Page 88**  
**Reducing the electrical and optical losses of PV modules incorporating PERC solar cells**

Henning Schulte-Huxel, Robert Witteck, Malte Ruben Vogt, Hendrik Holst, Susanne Blankemeyer, David Hinken, Till Brendemühl, Thorsten Dullweber, Karsten Bothe, Marc Köntges & Rolf Brendel, Institute for Solar Energy Research Hamelin (ISFH), Emmerthal, Germany

.....

**Page 97**  
**Positive cell-to-module change: Getting more power out of back-contact modules**

Bas B. van Aken & Lenneke H. Slooff-Hoek, ECN – Solar Energy, Petten, The Netherlands

.....

**Page 106**  
**Electroluminescence (EL) studies of multicrystalline PV modules**

Sreenivasa Murty Dasari, Chandra Mauli Kumar, Amresh Mahajan & Nagesh C, Tata Power Solar, Bengaluru, India

.....

## Jinko Solar becomes global solar module shipments leader in 1H 2016

'Silicon Module Super League' (SMSL) member Jinko Solar has reported the second consecutive quarter of solar module shipments that were higher than leading SMSL rival, Trina Solar.

JinkoSolar, which has been building strong annual module shipment momentum since 2014, reported second quarter 2016 shipments of 1,716MW, beating the top-end of guidance of 1,700MW and established a new quarterly shipment record, beating its previous record 1,709.9MW in the fourth quarter of 2015.

Total module shipments included 204MW used in its downstream projects. Total solar module shipments increased by 7.3% from 1,600MW in the first quarter of 2016 and 87.9% from 913MW in the second quarter of 2015.

Nearest rival, Trina Solar, had shipments of 1,423.3MW and 1,658.3MW in the first quarter and second quarter of 2016, respectively.

Strong demand during the quarter came from the US and China which accounted for the majority of shipments.

Jinko Solar reported second quarter total revenue of US\$896.1 million, an increase of 8.9% from the previous quarter and 86.1% from the second quarter of 2015.

Gross profit in the second quarter of 2016 was US\$182.4 million, compared with US\$180.8 million in the first quarter of 2016.

Jinko Solar's solar power projects segment generated 327GWh of electricity in the quarter.



Credit: Jinko Solar

Jinko Solar became the global leader for module shipments in the first half of 2016.

News

### India

## Chinese module suppliers increase share in Indian market to 75%

Despite most international and domestic module suppliers increasing their sales volumes in India over the last year, Chinese firms have significantly increased their share of the market from 50% to 75%, according to Bridge to India.

Furthermore, eight of the top 10 module suppliers in India now come from China, as opposed to just four in the previous year.

US firm First Solar and Indian company Waaree are the only non-Chinese suppliers still in the top 10. The top Chinese suppliers managed to keep their market share while new entrant Chinese firms including JA Solar, GCL-Poly, Hanwha (a South Korean firm based out of China), BYD, Talesun and Risen took much of the market share away from other international and domestic suppliers.

New government policies to support solar manufacturing in India

The Indian government is planning to announce a new solar manufacturing policy, which aims to offer Viability Gap Funding (VGF), a financial subsidy, to companies setting up integrated manufacturing facilities so that they can compete on an even level with their global counterparts.

The policy also envisages providing a

'reasonable' module off-take assurance for five to seven years. The 'Make in India' initiative already recognizes solar manufacturing as an industry having "strategic importance."

With the imminent implementation of Goods and Services Tax (GST) in 2017, domestic solar manufacturers will also get a level playing field with overseas manufacturers. With these favourable developments, it is expected that several new players, which have previously announced their solar manufacturing plans, will now expedite these strategies.

## Cell and module imports to India triple in a year

Imports of solar cells and modules into India have tripled in the last year. Shipments grew to INR155 billion (US\$2.3 billion) in 2015/16 from just INR51 billion in 2014/15, and INR43 billion in 2013/14.

The news is expected given India's utility-scale solar PV development booming in the last 12 months and reaching well beyond 8GW capacity. Meanwhile, India's domestic manufacturing capacity remains far too small to cater for its giant PV demands.

Minister for energy and mines Piyush Goyal said in Parliament: "Manufacturers from the US, China and other countries are supplying solar cells and modules in India and in some cases, the price is much lower than what is being offered by domestic manufacturers."

### Anti-dumping

## EU Commission cuts five more firms from solar MIP undertaking

Lerri Solar, DeSolar, CNPV, Motech and Xian Longi have been withdrawn from the EU's Minimum Import Price (MIP) undertaking and will instead have to service their European customers via manufacturing facilities abroad, due to violation of the terms of the agreement between China and the EC.

Earlier, the EC also withdrew Chinese solar panel manufacturer Shintime China and its related company in the EU, Shintime Europe, from the EU-China price undertaking.

This prompted James Watson, chief executive of SolarPower Europe, to say: "The MIP is clearly failing to function anymore; many Chinese companies are now voluntarily leaving it, as the price no longer bears the slightest resemblance to market prices for solar in the world or in Europe today."

## Turkey opens anti-dumping investigation into Chinese module imports

Turkey's Ministry of Economy has opened an investigation into alleged dumping of Chinese solar panels in Turkey.

Turkey-based manufacturers Solarturk Energy, Sunlego Energy systems and Zahit Energy are behind the complaint that led to the investigation.

Under the Patronage of His Highness Sheikh Hamdan bin Rashid Al Maktoum, Deputy Ruler of Dubai, Finance Minister of the UAE and President of DEWA

As part of Dubai Electricity and Water Authority's Green Week Initiative

DUBAI SOLAR SHOW PART OF WETEX

4-6 October 2016

Dubai International Convention and Exhibition Centre

JOIN US AT ZA'ABEEL HALLS 4-5

THE BIGGEST GLOBAL SOLAR EXHIBITION IN THE REGION

Organised by Dubai Electricity and Water Authority (DEWA), Dubai Solar Show is the ideal one-stop destination for solar professionals, organisations and companies in the Middle East. Dubai Solar Show is an important B2B platform for the public and private sectors to make deals, build partnerships, review the latest solar-energy technologies, learn about current and future projects in the region and market needs, and explore opportunities to take part in solar-energy projects and programmes.

Be part of this fast-growing industry in the region

REGISTER NOW @  
DUBAISOLARSHOW.COM

Join DEWA and the other project owners in the region to connect with the key players of the industry only at the Dubai Solar Show.

For enquiries contact: Tel: +971 55 195 0504, +971 50 250 0001 Email: info@dubaisolarshow.com

DIAMOND SPONSOR



GOLD SPONSORS



SUPPORTING ASSOCIATION



MEDIA PARTNERS



RESEARCH PARTNER



The anti-dumping investigation, to be carried out by Turkey's General Directorate, alleges unfair competition coming from the import of solar modules from the Republic of China.

However, Turkey's solar association Solarbaba said: "Modules imported from China was not a problem at all in Turkey, considering that the cumulative installed PV power is just around 600MW today. The result will be the same as in Europe, shrinking market, hesitating foreigner investors, many projects switching to 'stand by' mode."

## Products

## News

### Manufacturers launch 1,500V modules

Vietnam-based PV module manufacturer Boviet Solar Technology has added a 72-cell, 1500VDC multicrystalline module to its growing product portfolio, designed for the growing commercial and utility-scale demand in the US for the higher

voltage modules.

Higher voltage systems are known to enable longer system module strings that reduce combiner box and wiring requirements, lowering upfront capital costs and reducing installation times, providing a lower levelized cost of electricity.

China-based integrated PV manufacturer Yingli Green Energy said that its 60-cell dual glass 'TwinMAX' 1,500V modules have passed aging and safety IEC61215/61730 tests, re-spectively.

China-based solar module manufacturer Canadian Solar also launched its new 1,500V system voltage crystalline module portfolio.

Meanwhile, leading US crystalline-silicon module manufacturer SolarWorld also unveiled its 1,500V module at this year's Intersolar North America.

### Yingli Green to showcase niche solar modules at SPI as sales slide

Struggling former SMSL member Yingli

Green Energy is showcasing several niche solar module products at Solar Power International in Las Vegas.

These include the most recently updated TwinMAX 60-cell bifacial glass/glass module originally launched in an updated form in May 2016 as well as an Underwriters Laboratory (UL) certified module with integrated module-level power optimizers for the residential and commercial market segments

The company is also showcasing its p-type monocrystalline, UL-certified YLM Series that is available in both 60-cell and 72-cell series and the only mainstream product mentioned.

Yingli Green, once the leading module supplier in the US, has seen sales slide significantly in recent years. The company has only recognised revenue in the US on 163MW of modules in the last three quarters.

### REC Solar begins production of 72-cell 'TwinPeak' modules

Integrated PV module manufacturer REC Solar has started volume production of its previously introduced 72-cell 'TwinPeak' module, using half-cut cells and PERC cell technology.

The new module was rated at up to 340Wp and a 1,500V DC version will be available from November 2016 onwards.

The TwinPeak series also uses four busbars and a split junction box, which is claimed to provide an extra 20Wp, compared to conventional multicrystalline 72-cell modules.

The company had previously said it would migrate all production at its manufacturing facility in Tuas, Singapore, to its half-cut PERC cell technology, used for its TwinPeak series modules.

The 72-cell module was said to be available for all regions, and is certified for a maximum system voltage of 1,000V.

### First Solar's 'game-changing' Series 5 module to reduce BOS costs and installation times

Leading thin-film module manufacturer First Solar has revealed its new-to-the-market and highly anticipated Series 5 thin-film PV module.

The Series 5 module is entering the market at 365W and consists of a 1.85m x 1.2m, three-horizontal-stacked module unit akin to the size and form factor of traditional c-Si 72-cell modules. Although it comprises three sections which look similar to the Series 4 module, Karim Asali, First Solar's technical director for Europe, said that the Series 5 is in fact comprised of "completely new modules".

First Solar has plans to progress the module's Watt capacity in future, starting at 365W and progressing to 370W and 375W and so on.



Credit: Yingli Solar

Yingli is presenting several new niche solar products at this year's SPI in Las Vegas.

# MENA'S LEADING SOLAR TRADE EVENT

Providing international suppliers with direct access to thousands of the regional market's top project decision makers, influencers, utilities and government policy makers. Grow or introduce your business to the region, strengthen relationships with existing clients and make essential new connections.

For booking and more information  
[info@solarmiddleeast.ae](mailto:info@solarmiddleeast.ae)  
[www.solarmiddleeast.ae](http://www.solarmiddleeast.ae)

Discover more  
[www.energisingtheindustry.com](http://www.energisingtheindustry.com)



Brought to you by



MIDDLE EAST  
ELECTRICITY



**SOLAR MIDDLE EAST**  
ENERGISING THE INDUSTRY

14 – 16 FEBRUARY 2017  
DUBAI WORLD TRADE CENTRE, UAE



# Reducing the electrical and optical losses of PV modules incorporating PERC solar cells

Henning Schulte-Huxel, Robert Witteck, Malte Ruben Vogt, Hendrik Holst, Susanne Blankemeyer, David Hinken, Till Brendemühl, Thorsten Dullweber, Karsten Bothe, Marc Köntges & Rolf Brendel, Institute for Solar Energy Research Hamelin (ISFH), Emmerthal, Germany

## ABSTRACT

The continual increase in cell efficiency of passivated emitter and rear cells (PERCs), as well as the optimization of the module processes, has led to significant advances in module power and efficiency. To achieve the highest module power output, one important aspect to consider is the optimization of the solar cell front metallization and the cell interconnection. An experimentally verified analytical model is used in combination with ray-tracing simulations to study the electrical and optical impact of the front-side metallization of the solar cells, as well as various configurations of the cell interconnector ribbons (including their cross section, number and optical properties), on the module power output. On the basis of the simulation results, a standard 60-cell module is processed with 120 halved PERCs, resulting in an independently confirmed power output of 303.2W and an efficiency of 20.2% on the aperture area. The module performance is analysed with reference to ISFH's optical and electrical simulations: the power loss due to the series interconnection of the solar cells is determined to be 1.5%. This power loss, however, is offset by a gain in current of 1.8% as a result of the change in the optical environment of the cells in a module as compared to in air.

## Introduction

Passivated emitter and rear cells (PERCs) fabricated from p-type crystalline Si wafers are the cell technology with the largest predicted gain in market share in the future [1]. The efficiency of screen-printed industrial PERC solar cells has increased over the past few years, reaching record cell efficiencies of 22% [2,3].

Additionally, significant improvements have been made for a standard 60-cell module incorporating PERC solar cells. The highest reported and independently confirmed module efficiency so far has been 19.5% for a module with an output power of 294W [4]. Since that was published, new results have been documented regarding higher module powers; the current power record is 335.2W [5]. However, power-optimized modules often employ a larger module area in order to benefit from additional light collection from the regions between the cells; consequently, the 335.2W module has an efficiency of only 19.1% [5]. Increasing the module area, however, leads to an increase in material consumption, which in turn results in increased system costs [6].

To achieve the highest module efficiencies, the impacts of the relevant module components, as well as the effects of the adaptation of the cell properties for operation in the optical

environment in the laminated module, are analysed in this paper. The focus is therefore on the screen-printing design, the configurations of the cell interconnector ribbons (including their cross section, number and optical properties), the impact of light-guiding structures between the cells, and the use of an encapsulant with enhanced UV transparency. For the resistive and electronic (recombination) effects, an analytical model is used [7]. Ray-tracing simulations [8] are employed to characterize the optical impact of structured ribbons [9], the cell metallization, the cell gap, the encapsulant, and the front glass on the module power output.

On the basis of the optimizations, a large-area 60-cell equivalent module was constructed from 120 halved 6" PERC cells with an average efficiency of 20.8%. A module power of 303.2W was obtained on an aperture area of 1.50m<sup>2</sup> (1,592mm × 943mm); this power corresponds to an efficiency of 20.2%. To the best of the authors' knowledge, this is the highest efficiency for a standard 60-cell module based on screen-printed p-type PERC silicon solar cells. The cell-to-module losses were analysed by sequentially including the following: the electrical losses due to the current mismatch effect, the resistive losses caused by the series interconnection of cells, and the optical gains and losses.

## Optimization of cell front-side metallization and interconnections

### Influence of the front metal fingers and cell interconnection ribbons

The influence of the number of front metal fingers and the cell interconnection on the module power output is simulated by means of a model presented in Witteck et al. [7]. The simulation parameters are taken from the same reference. For ISFH's simulations, a solar module consisting of 60 full and 2mm equally spaced PERC solar cells is used. The cell interconnection is realized by cell interconnection ribbons (CIRs) with a light-recovery probability  $k_{\text{cir}}$  of 0.1. (A  $k_{\text{cir}}$  of 0.1 means that 10% of the light that hits the CIRs is collected by the solar cells.) The thickness of the CIRs is limited in all simulations to 200µm in order to reduce any mechanical stresses that might induce cell cracking.

Fig. 1 shows the power output of a module for different numbers of CIRs and various CIR widths  $w_{\text{cir}}$ . In solar module factories, cell interconnection tools with up to five CIRs are implemented nowadays. On the assumption that there will be further advances in technology in the coming years, up to seven CIRs are considered in the simulations. The CIR width  $w_{\text{cir}}$  is varied between 0.6 and 2.5mm. (Smaller values for  $w_{\text{cir}}$  are not investigated,

as the current stringer technology is limited because of positioning accuracy.) For each number of CIRs, the number of front metal fingers ( $n_f$ ) of constant width are optimized with respect to a maximum module power output. The

value of  $n_f$  that results in the highest module power output for a specific number of CIRs is indicated in Fig. 1.

An increase in module power is observed for a decrease in  $w_{cir}$  from 2.5 to 0.6mm with increasing number of

CIRs. However, for the cell configuration used, four to seven busbars give rise to similar module powers of  $287.2 \pm 0.4$ W. The decrease in optimal CIR width results from the trade-off between the shading of the front side by the CIRs and the resistive power losses. If the CIR width becomes too wide, the shadow losses dominate and cause a decrease in power output.

**“The optimal number of CIRs must be evaluated individually for each process line and cell design.”**

Increasing the number of CIRs reduces the current path in the front metal fingers, and thus further reduces the series resistance losses, leading to the possibility of reducing the number of fingers. This has an impact on silver paste consumption, which is also affected by the increasing number of CIRs, demanding more, but narrower, screen-printed busbars. Moreover, the alignment of the CIRs is more challenging and the positioning accuracy of the stringer becomes crucial. The stringing machine also becomes more complicated, and more tools to produce the ribbons are required per watt peak when more CIRs are used. On the other hand, increasing the number of CIRs improves module reliability, as well as making the module power output more robust against cracks [10]. Consequently, the optimal number of CIRs must be evaluated individually for each process line and cell design.

Market Watch
Fab & Facilities
Materials
Cell Processing
Thin Film
PV Modules

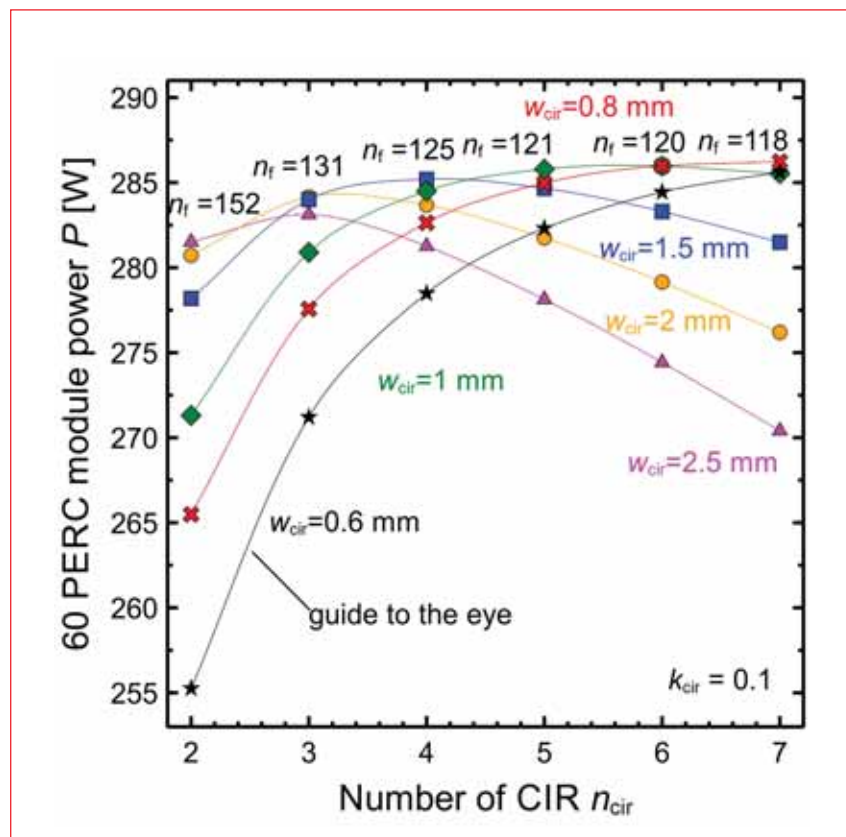


**Figure 1. Simulated power output of a 60-PERC module for different numbers of CIRs per solar cell. Various CIR widths are considered for the simulation. The number of fingers is optimized for maximum module power output. For the simulation, full pseudo-square cells with standard CIRs and a  $k_{cir} = 0.1$  are assumed.**

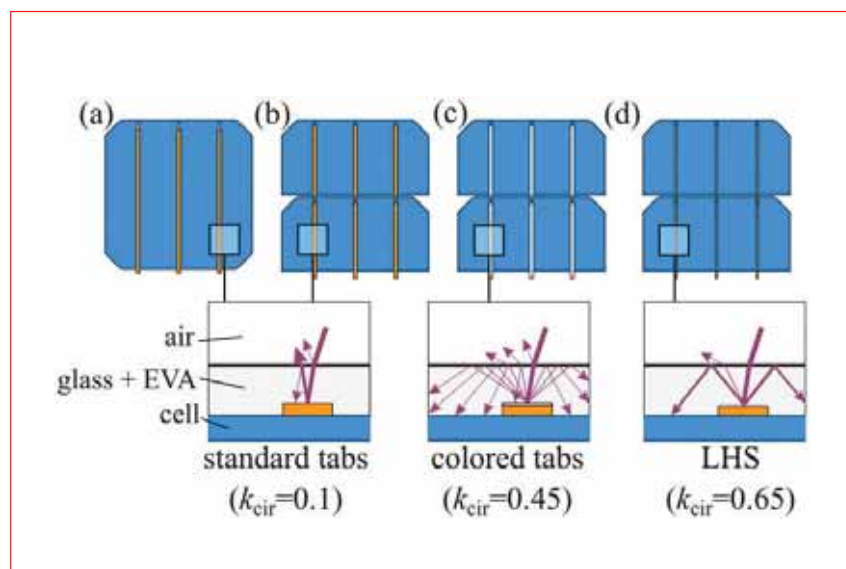


**Figure 2. Solar cell interconnection configurations: (a) full cell with standard CIRs; (b) half cell with standard CIRs; (c) half cell with white CIRs; (d) half cell with structured CIRs. The insets show schematically the light scattering of the interconnection in a module. The  $k$  values denote the associated effective optical reduction ratios.**

**Reducing electrical and optical losses of cell interconnection ribbons**

Reducing the series resistance losses while limiting the shading of the cell by the CIRs is achieved by enhancing the optical properties of the CIRs. Within a module, light reflected by the CIRs may be totally internally reflected at the glass-air interface, and thus contribute to the generated cell current; this effect will reduce the effective optical width  $w_{cir,eff}$  of the CIRs, which is taken into account by the light-recovery probability  $k_{cir}$ . Another possibility is to reduce the generated current of the cell by employing half-size cells.

Fig. 2 shows the schematics of the four state-of-the-art cell interconnection configurations modelled in the work reported in this paper. For configuration (a), standard CIRs with  $k_{cir} = 0.1$  and full-size cells are considered. Configuration (b) uses the same CIRs, but only half cells; note that in this case, the module consists of 120 such cells. In

configuration (c), half cells with optically enhanced white CIRs, with  $k_{\text{cir}} = 0.45$ , are used [11].

For configuration (d), a structured light-harvesting string (LHS) ribbon (by Schlenk AG) is applied to the cells. Because of the structure, light impinging on the ribbon is reflected at a particular angle which increases the probability that it becomes totally internally reflected. Thus, the light-recovery probability reaches 0.65 to 0.75 [7,9]. As a conservative approximation,  $k_{\text{cir}} = 0.65$  is used here.

Fig. 3 shows the simulated module power for configurations (a) through (d), for different numbers of CIRs. For each simulation, the width of the CIRs,  $w_{\text{cir}}$ , and the number of front metal fingers,  $n_f$ , are optimized for maximum module power.

In the simulations a maximum power output of approximately 286W for module (a), with full cells and  $k_{\text{cir}} = 0.1$  (black curve in Fig. 3), is realized with seven CIRs of width 0.8mm. When the same number of CIRs is used, but the module current is reduced by 50% (i.e. employing half cells, (b), red curve), the module power increases by 6W. An improvement of the optics of the CIRs gains an additional 3.5W with the application of white CIRs ( $k_{\text{cir}} = 0.45$ , (c), green curve), and 6W with the application of structured CIRs ( $k_{\text{cir}} = 0.65$ , (d), blue curve).

In the case of  $k_{\text{cir}} = 0.1$  and half cells, the optimum number of CIRs is six, while this figure shifts to seven if the effective optical width of the CIR is reduced. In contrast, the optimal width of the CIR increases from 0.8mm for the standard CIR ( $k_{\text{cir}} = 0.1$ ), to 1mm for an optically enhanced CIR. However, the gain in module power seen through comparing 5, 6 or 7 CIRs for configurations (b) through (d) is approximately 1W.

When determining the optimal number of CIRs, it is crucial to take into consideration the additional costs of manufacturing tools, as well as the trade-off between fewer fingers and more busbars. Therefore, the practical optimum, depending on the tools used, can differ from the particular configuration that leads to the highest module power. Note that the cell gap is very small and that an enhanced internal reflection of light by the backsheet will increase the module current generated, resulting in more numerous and wider CIRs.

Furthermore, the use of half cells has some advantages and disadvantages. Some authors [5,12] state that there might be a larger impact due to cell mismatch from using half cells and thus twice as many cells; however, the use

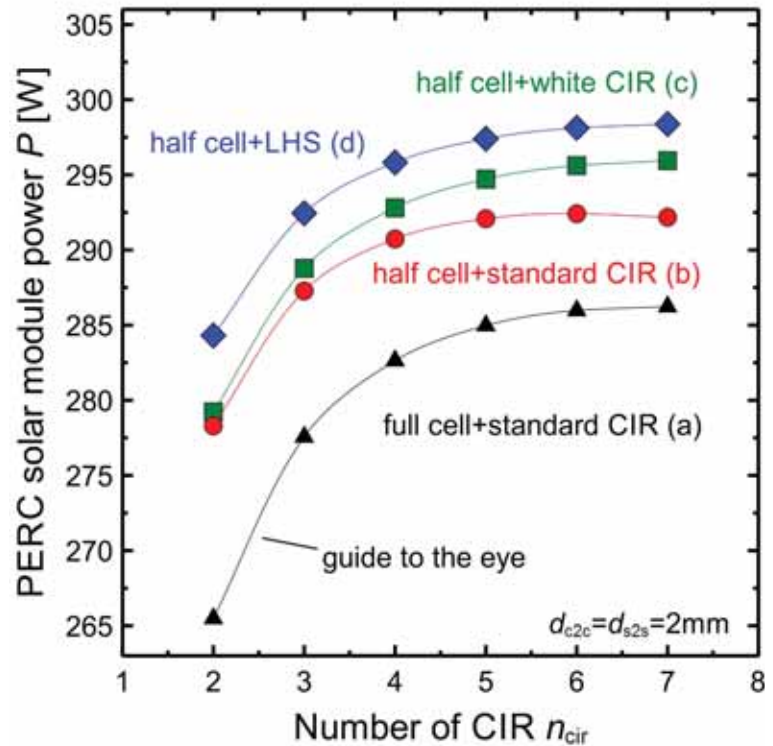


Figure 3. Simulated module power output for module configurations (a) through (d), with different numbers of CIRs. The cell gap is 2mm in all directions, and the number of front metal fingers is optimized for maximum module power output.

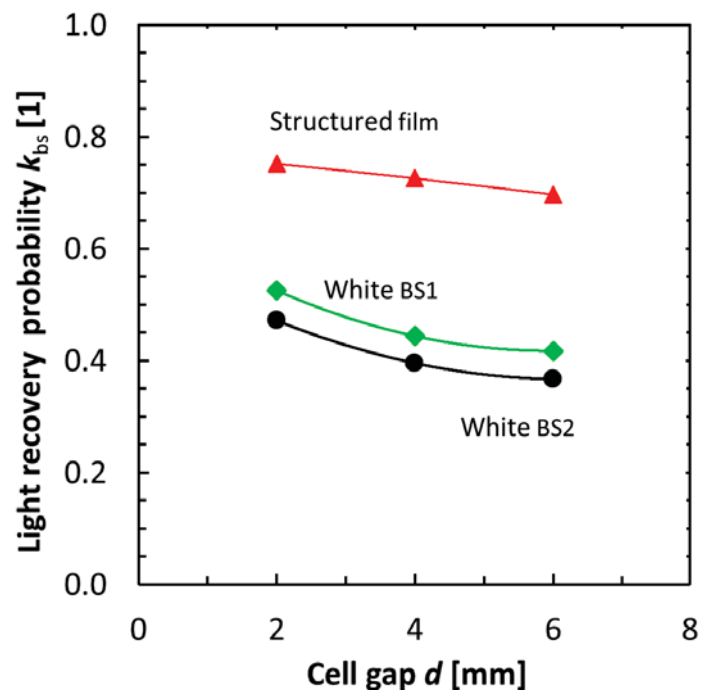


Figure 4. Experimentally determined light-recovery probabilities  $k_{\text{bs}}$  for various backsheets as a function of the cell gap  $d$  [17].

of cells that have been sorted (which is usually carried out by the cell producers) does not lead to a significant mismatch loss [13,14]. The yield and efficiency loss [12,15] caused by the laser-cutting step may be reduced by adapting the laser parameters, and in some cases an improved cell performance is even observed after the cutting process [16]. A disadvantage of using half cells is that the throughput of the stringer is halved with respect to the watt peak.

### Optical properties of the cell and module components

Within a PV module, the current generation is affected by the parasitic absorption of photons by module components (i.e. the glass and encapsulation) in addition to absorption by the Si. Moreover, the reflection of incident light leads to optical losses, such as the reflection at the air–glass interface for incoming light. However, reflections also result in gains – for example, light reflected at the backsheet and back onto the cell surfaces as a result of total reflection at the glass–air interface.

In a first step, the experimental results are discussed, with a comparison of the optical performance of various backsheets (BSs). In a second step, the

distribution of the light between all module components is considered.

### Light recovery from the cell gaps

The light-recovery probability of the cell gaps/backsheets is defined as the portion of light collected by the solar cells that is reflected from the backsheet between the cells [17]. Fig. 4 shows the measurements of the light-recovery probabilities  $k_{bs}$  for various backsheets. Generally, white backsheets exhibit recovery factors of approximately 50%, which decreases with increasing cell gap  $d$ . Two white backsheets are shown in Fig. 4, which are representative of the range of seven tested commercially available backsheets. The collection of light hitting between the solar cells can be further improved by using structured and metallized films between the solar cells, yielding a  $k_{bs}$  of 75% (see Fig. 4).

### Light distribution in a standard module vs. an optimized module

The DAIDALOS ray-tracing framework [8] is used, which employs a multi-domain approach [18]. This allows the simulation of entire solar modules in three dimensions, while also taking into account the front metallization, the inter-cell gaps, and the large number of pyramids of the textured silicon

surface in excess of  $10^{10}$ . Additionally, a collection efficiency specifically simulated using Sentauros is employed to match the properties of the cells in order to differentiate between photogenerated and short-circuit current.

With this combination of tools, there is good agreement between simulated and measured module  $J_{sc}$  [19]. The profiles and properties of the fingers and CIRs are given in Witteck et al. [11] and Holst et al. [9] respectively. The thicknesses of the dielectric layers and Lambertian factor of the rear side are determined from reflection measurements. The complex refractive index data for low iron soda lime glass are taken from Volgt et al. [20], and the encapsulation material data are found in Vogt et al. [19]. The properties of the other material data for the module components and their measurements are given in Vogt [21].

Fig. 5 shows the percentage of incoming light that is converted into short-circuit current or lost for a standard module with full-size PERC cells and the high-efficiency PERC module; data are given for wavelengths between 300 and 1,200nm in 10nm steps. For the high-efficiency module, three optical improvements are considered:

# KUBUS

3-4-5-6  
Busbar

5000  
Cells/h

35  
m<sup>2</sup> Footprint

24/7  
Production

170  
MW/year

≥ 98  
% Uptime

1  
Operator

## THE COORDINATES OF YOUR SUCCESS

**Benefits that pay off in a glance:**

- Only 1 operator per shift needed and only to refill goods
- No downtime for refill goods → 10MW more output
- High redundancy for maximum productivity during maintenance
- Soldered cell matrix on a "Tray" for easy interconnections
- Non-Contact soldering process
- All common state-of-the-art materials processable, also half-cells 3 to 6 busbars
- All components are ideally accessible, without interrupting the production
- Highest material conversion yield
- No ribbon-cutting needed

**Your contact person:**  
Maximilian Germann

**M10 Industries AG**  
Munzinger Strasse 10  
79111 Freiburg | Germany  
Phone: +49 761 4019 68 51  
sales@m10ag.de  
www.m10ag.de

**MADE IN GERMANY**

**20** engineering manufacturing photovoltaic

**YEARS** [www.m10-solar-campus.de](http://www.m10-solar-campus.de)

1. The use of light-harvesting structures in the cell gap instead of a white backsheet: this decreases the absorption in the cell gap (light green), and reduces reflection (dark green).
2. The replacement of standard CIRs by interconnections with light-harvesting structures: this decreases the absorption in the front metal (red), and reduces reflection (dark green).
3. The replacement of conventional ethylene-vinyl acetate (EVA) by EVA with enhanced UV transmission: this decreases the absorption in the encapsulation (blue), which has demonstrated a 1.4% improvement in module short-circuit current with similar cells [19].

**“The use of light-harvesting structures in the cell gap instead of a white backsheet decreases the absorption in the cell gaps and reduces reflection.”**

Regarding the remaining losses in the high-efficiency module, the largest absorption contribution in the infrared range originates from the cell rear-side metallization, where the Si absorption coefficient decreases [22]. In the UV wavelength region, the limiting factor is the parasitic absorption in the glass, which can be reduced by further eliminating the concentration of the  $Fe^{3+}$  ions in the glass [20]. In contrast,

reflection losses are the main limiting factor in the visible wavelengths.

### Fabrication of a high-efficiency module

To demonstrate the application of the above-mentioned improvements, a module consisting of 120 half cells was constructed. The PERC solar cells were processed in the SolarTeC technology centre using industrial production tools, similarly to Hannebauer et al. [23]. The front-side metallization was adapted to a half-cell design, and the number of fingers was optimized for the operating environment within the laminated module [11]. The cells feature four 1mm-wide busbars, which represents a trade-off between reducing the power loss and the number of solder steps, since the cells are interconnected manually.

The half cells are interconnected by LHS ribbons having a cross section of  $0.2 \times 1.5 \text{ mm}^2$ . Six strings, each consisting of 20 half PERC cells, are connected in series using string interconnection ribbons (SIRs) with a cross section of  $0.2 \times 6 \text{ mm}^2$ . In order to reduce the module area, a distance  $d_{s2s}$  (string-to-string gap) of 1mm between adjacent strings was used, together with a distance  $d_{c2c}$  (cell-to-cell gap) of 1.5mm between the solar cells within a string. Compared with the aperture area of a module with pseudo-square cells and a cell gap of 2mm, the total module size is reduced by 2.6%. More importantly, the area fraction covered by the solar cells, or the aperture module area, is increased from 93% to more than 97%.

The trapping of the light hitting

the remaining cell gaps is increased by a structured and metallized foil as described earlier. The cell matrix is laminated with EVA (450 $\mu\text{m}$  thick, EVASKY S87, Bridgestone), a 3.2mm-thick front glass with an anti-reflection coating (f|solarfloat HT by f|solar), and a white backsheet (PYE 3000, Coveme). Fig. 6 shows a photograph of the front side of the framed module.

### Cell-to-module loss analysis

The characteristic  $I-V$  parameters of the 120 cells are measured before interconnection and lamination; these are listed in Table 1, row A. To avoid a mismatch of the cell currents, the impact of the mismatch on module performance is analysed by interpolating the individual light  $I-V$  characteristics of the cells, and by summing the voltages of the 120 cells for each current value. The parameters of the  $I-V$  characteristic obtained for the module in the case of a loss-free interconnection are given in row B. Comparing rows A and B shows that the impact on the short-circuit current  $I_{sc}$  due to the mismatch is small (0.01A or 0.3% $_{rel}$ ), and is offset by an increase in the fill factor FF. As the open-circuit voltage  $V_{oc}$  is unaffected by the mismatch, the power of the 120 cells is unchanged.

Row C of Table 1 includes the series resistance contribution of the CIRs (on and between the solar cells) and the SIRs (between the strings and to the external module contacts). The series resistance contribution due to the cell interconnection by the CIRs and SIRs is analytically determined to be

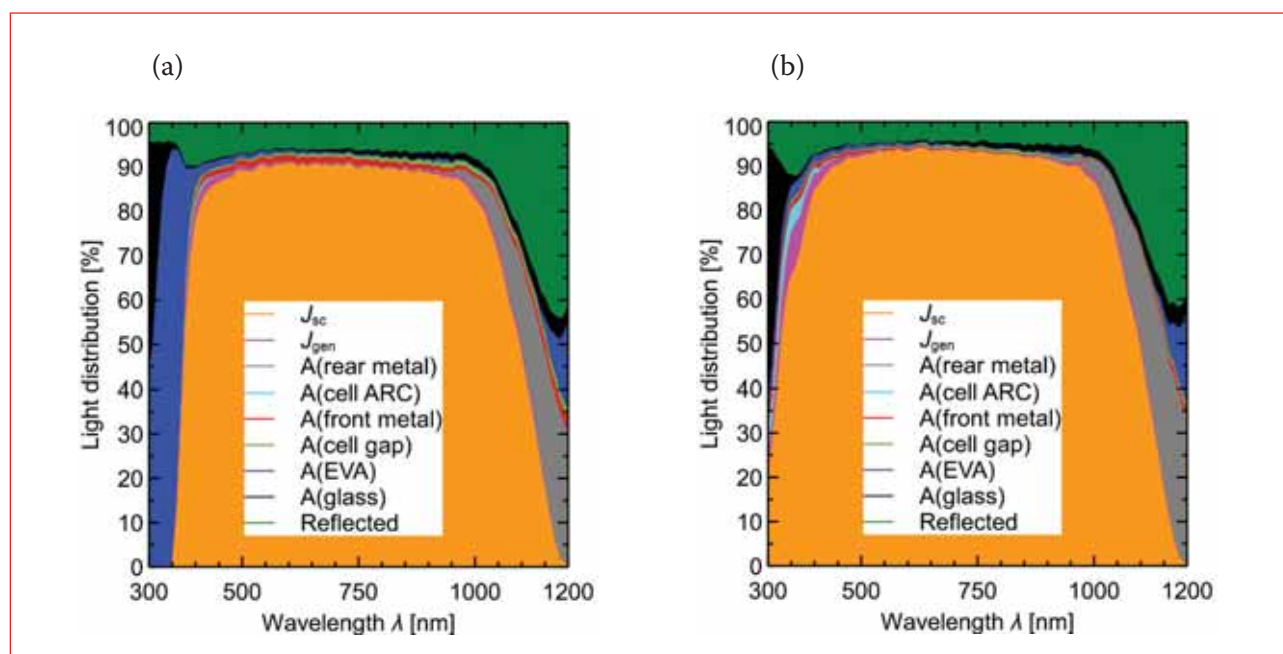


Figure 5. Optical loss analysis under normal incident light: (a) standard module; (b) high-efficiency PERC module.

0.14Ωcm<sup>2</sup> and 0.08Ωcm<sup>2</sup> respectively. These resistances decrease the fill factor by 0.9%<sub>abs</sub> (1.1%<sub>rel</sub>) compared with the average of the initial cells; this corresponds to a fill factor of 78.7% and results in a power loss of 4W. Besides electrical losses, there are also optical effects, which are determined using ray-tracing simulation.

Fig. 7 shows the current losses, which are determined by multiplying the photocurrent distribution (as in Fig. 5) with the AM1.5G spectrum, and then integrating over all wavelengths. A light ray contributes to the reflection losses of an interface if the ray reaches that interface but never passes it, and if that ray additionally leaves the module. Here, a cell before module integration, with a short-circuit current of 4.79±0.002A (numerical uncertainty of the Monte-Carlo algorithm of the ray-tracing simulations), is simulated. The simulations show good agreement with the experimentally measured half PERC cells, which yielded a short-circuit current of 4.80±0.08A (uncertainty of the cell measurements).

A comparison of the cell before and after module integration reveals that the changes in absorption losses in the Al rear metallization and the cell anti-reflection coating (ARC) are not significant. Even though the CIRs are wider and longer than the busbars, the absorption by the front metal only increases from 0.02 to 0.03A; in the case



Figure 6. Photograph of the ISFH high-efficiency module, consisting of 120 half PERC solar cells.

of standard CIRs this effect is greater, but because of the structure of the CIRs in ISFH's module [9], this loss factor is reduced.

The reflection at the cell ARC is reduced by a factor of two because of

the higher reflection index of EVA compared with air. As a result of internal reflections, the reflection losses relating to the fingers and the busbars/CIRs are reduced by 63% and 74% respectively, compared with the

## On-the-Fly Cell Cutting using Thermal Laser Separation

microCELL™ TLS for retaining the mechanical strength of the half cell

[www.lasers-for-photovoltaics.com](http://www.lasers-for-photovoltaics.com)



Row		$I_{sc}$ [A]	$V_{oc}$ [V]	FF [%]	$P_{mpp}$ [W]	$\eta$ [%]
A	Measurements of 120 half cells	4.80 <sup>†</sup>	79.4 <sup>§</sup>	79.6 <sup>†</sup>	303 <sup>§</sup>	20.8 <sup>†</sup>
B	Simulation of mismatch effect	4.79	79.4	79.9	303	
C	Simulation of interconnected cells (resistive effects)	4.79	79.4	78.7	299	
D	Simulated module (incl. elec. and opt. effects)	4.87	79.4	78.7	304	
E	Measured module <sup>#</sup>	4.86 <sup>*</sup>	79.1 <sup>*</sup>	78.9 <sup>*</sup>	303 <sup>*</sup>	20.2

<sup>§</sup> Sum over all cells.  
<sup>†</sup> Average of all cells.  
<sup>#</sup> Module measurements on aperture area (ap.) (excluding frame).  
<sup>\*</sup> Independently confirmed by TÜV Rheinland, Cologne, Germany.

**Table 1. Measurements and simulations of the characteristic  $I-V$  parameters of the interconnected cells and the module under standard testing conditions (AM1.5G, 100mW/cm<sup>2</sup>, 25°C). The solar cells each have an area of 121.67cm<sup>2</sup>, and the module has an aperture area of 15,008cm<sup>2</sup>.**

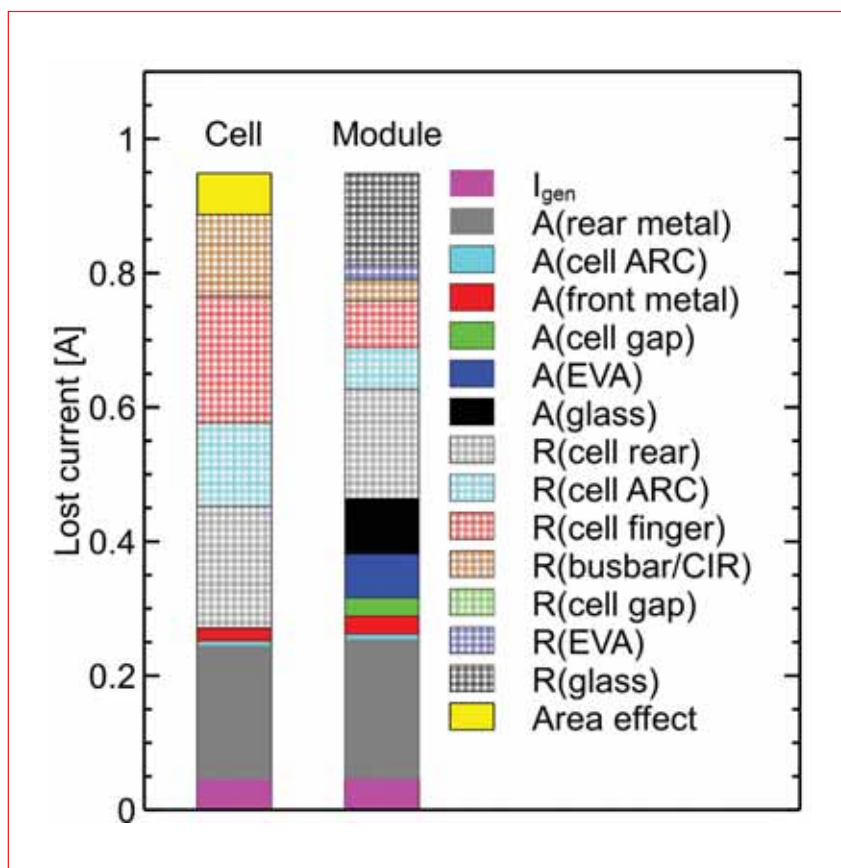


**Figure 7. Comparison of the simulated electrical current and optical losses for the cell before and after module integration under normal incident light and AM1.5G spectrum. Only light which leaves the module as reflected light is considered. Since the cell in air collects light on a smaller area (cell area) compared with the cell in the laminate (cell area + cell gap), this area effect is included in the comparison.**

cell before lamination. This underlines the importance of optimizing the cell metallization with respect to the operational environment within the laminate. In the module, additional absorption takes place in the glass, the EVA and the cell gap, and there are reflection losses at the air–glass and glass–EVA interfaces. Since the cell before module integration collects light on a smaller area (cell area) compared with the cell in the laminate (cell area + cell gap), this area effect is included in

the comparison.

The module simulations yield a short-circuit current of 4.88A, which corresponds to a cell-to-module  $I_{sc}$  gain of 1.8%. This cell-to-module gain is included in the calculation results in row D of Table 1, which shows an  $I_{sc}$  of 4.87A and a module power of 304W; this is in good agreement with the module measurements of 303W determined independently by TÜV Rheinland, as shown in row E of the table.

## Conclusion

The effects of various adaptations of the module process, as well as their impact on module performance, have been presented. Several aspects were analysed and discussed, especially the number and properties of CIRs, the usage of half cells, and the impact of enhanced optical properties of the CIRs and in the cell gaps. Half cells and structured CIRs increase the module power to 297W, compared with 285W for full cells and conventional ribbons, when using five-busbar solar cells. Increasing the number of busbars, however, has only a small impact on module performance.

It was also shown that the module current can be significantly increased by using metallized and structured materials in the cell gaps and on the ribbons, where the light recovery can be enhanced by 50% and 700% respectively.

With the described adaptations of the module, a best technical practice module was constructed with 120 half PERC solar cells; this yielded a module efficiency of 20.2%. No power loss due to cell mismatch was found. The interconnection of the cells by the CIRs, and of the strings by the SIRs, results in a decrease in FF of 0.9%<sub>abs</sub> compared with the average FF of the cells, and in a power loss of 4W. The optical behaviour of the module was simulated by ray tracing. It was shown that, because of a net cell-to-module gain in current of 1.8%, the final simulated module achieves a module power output of 304W; compared with the 303W obtained from the independently confirmed module measurements, this demonstrates the predictive strength of ISFH's model.

**“The presented module achieves a record efficiency of 20.2% for a standard 60-cell PERC module.”**

The ray-tracing simulations showed that a large absorption loss originates from the cell's rear-side metallization. This loss can be reduced, for example, by using bifacial PERC+ or PERT cells, as shown in Dullweber et al. [24]; cells of this type would be also be beneficial in monofacial modules, such as the module investigated here.

In order to reduce the cell-to-module losses in efficiency, the total module area was decreased, and the fraction of the active module area (solar cells) was increased: the aperture area was reduced by 2.6% compared with a standard module, and the active area was increased to more than 97%. With this increase in active cell area, combined with a minimization of the power losses within the module, the presented module achieves a record efficiency of 20.2% for a standard 60-cell PERC module. To the best of the authors' knowledge this is the highest efficiency for a standard 60-cell module based on screen-printed p-type PERC silicon solar cells.

By virtue of their consuming less construction and cabling material, high-efficiency modules using industrially processed screen-printed p-type PERC silicon solar cells are particularly relevant to further reducing the balance of system costs, and thus the levelized cost of PV-generated electricity.

## References

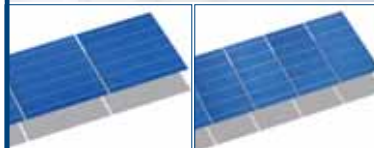
- [1] SEMI PV Group Europe 2016, "International technology roadmap for photovoltaic (ITRPV): 2015 results", 7th edn (Mar.) [<http://www.itrpv.net/Reports/Downloads/>].
- [2] SolarWorld 2016, Press Release (Jan.) [<http://www.solarworld.de/konzern/presse/aktuelles/pressemitteilungen/single-pressemitteilung/article/solarworld-praesentiert-solartechnik-der-naechsten-generation/>].
- [3] Ye, F. et al. 2016, "22.13% efficient industrial p-type mono PERC solar cell", *Proc. 43rd IEEE PVSC*, Portland, Oregon, USA.
- [4] Metz, A. et al. 2014, "Industrial high performance crystalline silicon solar cells and modules based on rear surface passivation technology", *Sol. Energy Mater. Sol. Cells*, Vol. 120, pp. 417–425.
- [5] Zhang, S. et al. 2016, "335-W world-record p-type monocrystalline module with 20.6% efficient PERC solar cells", *IEEE J. Photovolt.*, Vol. 6, No. 1, pp. 145–152.
- [6] Verlinden, P. et al. 2013, "Cost

analysis of current PV production and strategy for future silicon PV modules", *Proc. 28th EU PVSEC*, Paris, France.

- [7] Witteck, R. et al. 2016, "Optimized interconnection of passivated emitter and rear cells by experimentally verified modeling", *IEEE J. Photovolt.*, Vol. 6, No. 2, pp. 432–439.
- [8] Holst, H. et al. 2013, "Application of a new ray tracing framework to the analysis of extended regions in Si solar cell modules", *Energy Procedia*, Vol. 38, pp. 86–93.
- [9] Holst, H. et al. 2016, "Increased light harvesting by structured cell interconnection ribbons: An optical ray tracing study using a realistic daylight model", *Energy Procedia* [forthcoming].
- [10] Gabor, A.M. et al. 2015, "Solar panel design factors to reduce the impact of cracked cells and the tendency for crack propagation", *Proc. NREL PV Mod. Rel. Worksh.*, Golden, Colorado, USA.
- [11] Witteck, R. et al., "Optimizing the solar cell front side metallization and the cell interconnection for high module power output", *Energy Procedia* [forthcoming].
- [12] Pan, X. et al. 2014, "Theoretical and experimental study of power loss in half-cell PV modules", *Proc. 8th SNEC Int. PV Power Gen. Conf.*, Shanghai, China.
- [13] Evans, R. et al. 2015, "Simplified technique for calculating mismatch loss in mass production", *Sol. Energy Mater. Sol. Cells*, Vol. 134, pp. 236–243.
- [14] Schulte-Huxel, H. et al. 2016, "High efficiency modules with passivated emitter and rear solar cells – An analysis of electrical and optical losses", Submitted for publication in *IEEE J. Photovolt.*
- [15] Müller, J. et al. 2015, "Resistive power loss analysis of PV modules made from halved 15.6 × 15.6 cm<sup>2</sup> silicon PERC solar cells with efficiencies up to 20.0%", *IEEE J. Photovolt.*, Vol. 5, No. 1, pp. 189–194.
- [16] Schulte-Huxel, H. et al. 2016, "Flip-flop cell interconnection enabled by an extremely high bifacial factor of screen-printed ion implanted n-PERT Si solar cells", *Proc. 32nd EU PVSEC*, Munich, Germany, pp. 407–412.
- [17] Köntges, M. et al. 2016, "Method to measure light recovery probability of PV module backsheets enabling 20.2% module efficiency with passivated emitter and rear solar cells", *Proc. 32nd EU PVSEC*, Munich, Germany, pp. 1532–1538.

# WORLD RECORD STRINGER TT4200 GIGA

HIGH CAPACITY – 4200 cycles/h



up to 6 busbars, full and half cells

## Highest capacity on smallest footprint

130 MWp on 15 m<sup>2</sup>

- High throughput:  
0.855 seconds cycle time
- Low breakage rate:  
< 0.1 – 0.2 %
- Availability: > 95%
- Cost-effective and economical production
- Non-contact IR light soldering technology
- Optional Layout System with one 6-axis robot

Get inspired for the future.  
[www.teamtechnik.com](http://www.teamtechnik.com)

 **team  
technik**  
PRODUCTION TECHNOLOGY



- [18] Winter, M. et al. 2015, "Combining structures on different length scales in ray tracing: Analysis of optical losses in solar cell modules", *Opt. Quant. Electron.*, Vol. 47, No. 6, pp. 1373–1379.
- [19] Vogt, M.R. et al. 2016, "Optical constants of UV transparent EVA and the impact on the PV module output power under realistic irradiation", *Energy Procedia* [forthcoming].
- [20] Vogt, M.R. et al. 2016, "Measurement of the optical constants of soda-lime glasses in dependence of iron content and modeling of iron-related power losses in crystalline Si solar cell modules", *IEEE J. Photovolt.*, Vol. 6, No. 1, pp. 111–118.
- [21] Vogt, M.R. 2015, "Development of physical models for the simulation of optical properties of solar cell modules", Ph.D. dissertation, Leibniz University Hannover.
- [22] Schinke, C. et al. 2015, "Uncertainty analysis for the coefficient of band-to-band absorption of crystalline silicon", *AIP Adv.*, Vol. 5, No. 6, p. 67168.
- [23] Hannebauer, H. et al. 2014, "21.2%-efficient fineline-printed PERC solar cell with 5 busbar front grid", *physica status solidi (RRL)*, Vol. 8, No. 8, pp. 675–679.
- [24] Dullweber, T. et al. 2016, "BiCoRE: Combining a PERC-type cell process with n-type wafers", *Photovoltaics International*, 33rd edn.

#### About the Authors



**Henning Schulte-Huxel** studied in Leipzig, Germany, and in Bucharest, Romania, and received a master's in physics in 2010 from Leibniz Institute of Surface Modification, Leipzig. In 2015 he was awarded a Ph.D. for his work at ISFH on laser microspot welding for the interconnection of back-contacted silicon solar cells. Since 2014 he has been leading a project at ISFH that focuses on the module integration of PERC solar cells and the analysis and reduction of cell-to-module losses.



**Robert Witteck** studied renewable energies in Berlin. Since 2014 he has been at ISFH, working towards his Ph.D. on PERC module loss analysis.



**Malte Ruben Vogt** studied physics at the Leibniz University of Hanover, Germany, and received his bachelor's in 2009 and his master's in 2011. In 2015 he finished his Ph.D. at ISFH, where he worked on developing physical models for simulating the optical properties of solar cell modules. His current research focuses on the optical characterization of solar cell module components, and on the simulation of optical and thermal behaviour of PV modules in the field.



**Hendrik Holst** studied physics at the Leibniz University of Hanover, Germany. In 2015 he received his Ph.D. for work on the development of a modular ray-tracing framework and its application to multiscale simulations in PV. Since 2008 he has been with the simulation team at ISFH, where he is currently involved with optical simulations and optimization of solar cell modules.



**Susanne Blankemeyer** qualified as an optician at Krane-Optic in Rheda-Wiedenbrück in 1986, and worked as a laboratory assistant in the R&D department at Orbotech in Bad Pyrmont from 1999 to 2007. In 2007 she joined the module and interconnection technology group at ISFH, where she is currently working on the development of novel interconnection techniques and module concepts.



**David Hinken** studied physics at the University of Hanover, Germany, and the University of La Laguna, Spain. He received a Diploma degree in physics in 2007, and a Ph.D. in physics in 2012 for his work on luminescence-based characterization of crystalline silicon solar cells. He currently works in the solar cell characterization group and the calibration and test centre at ISFH.



**Till Brendemühl** received his Diploma degree in engineering physics from the University of Applied Science in Emden, Germany. Since 2005 he has been with ISFH, where he first worked on laser processes, later becoming project leader with a focus on back-contact high-efficiency solar cells. He currently works

on screen-printed n-PERT and PERC solar cells in the future technologies photovoltaics group.



**Dr. Thorsten Dullweber** leads the industrial solar cells R&D group at ISFH. His research work focuses on high-efficiency, industrial-type, PERC silicon solar cells and on ultra-fine-line, screen-printed, Ag front contacts. Before joining ISFH in 2009, he worked for nine years as a project leader in the microelectronics industry at Siemens AG and then at Infineon Technologies AG.



**Karsten Bothe** received his Diploma degree in physics from the University of Oldenburg, Germany, after which he joined ISFH. He was awarded a Ph.D. in 2006 by the University of Hanover, Germany, for his work on oxygen-related trapping and recombination centres in boron-doped crystalline silicon. In 2007 he became head of the solar cell characterization group at the ISFH, where his current research interest is the calibrated measurement of the characteristic parameters of crystalline silicon solar cells.



**Dr. Marc Köntges** received his Ph.D. in physics in 2002 from the University of Oldenburg, Germany, for his research involving thin-film solar cells. He is head of the module technologies group at ISFH, where he currently works on the development of characterization and production methods for PV modules.



**Rolf Brendel** received a Ph.D. in materials science in 1992 from the University of Erlangen, Germany, for his work on infrared spectroscopy. After a research post at the Max Planck Institute for Solid State Research in Stuttgart, he was appointed head of the thermosensorics and photovoltaics division at the Bavarian Center for Applied Energy Research in 1997. In 2004 he joined the Institute of Solid State Physics at the Leibniz University of Hanover as a full professor, and became director of ISFH.

#### Enquiries

Institute for Solar Energy Research  
Hamelin (ISFH)  
Am Ohrberg 1  
D-31860 Emmerthal  
Germany

# Positive cell-to-module change: Getting more power out of back-contact modules

Bas B. van Aken & Lenneke H. Slooff-Hoek, ECN – Solar Energy, Petten, The Netherlands

Market Watch

Fab & Facilities

Materials

Cell Processing

Thin Film

PV Modules

## ABSTRACT

Cell-to-module (CtM) loss is the loss in power when a number of cells are interconnected and laminated in the creation of a PV module. These losses can be differentiated into *optical losses*, leading to a lower photogenerated current, and *resistive losses*, leading to a decrease in fill factor. However, since the application of anti-reflection (AR) coatings and other optical ‘tricks’ can sometimes increase the  $I_{sc}$  of the module with respect to the average cell  $I_{sc}$ , the CtM loss in such cases needs to be expressed as a negative value, which gives rise to confusion. It is proposed to use the CtM change, where a negative value corresponds to a loss in current or power, and a positive value to a gain. In this paper, the CtM changes for back-contact modules utilizing a conductive foil are described and compared with other mature module technologies. A detailed analysis of the CtM change for a full-size metal-wrap-through (MWT) module is presented.

## Introduction

Module manufacturers would like to fabricate modules having the highest power from solar cells with a given efficiency, while minimizing the power losses, at the lowest cost. This power loss can vary, depending on the choice of materials and the interconnection technology. The industry-standard module interconnection technology at the moment is front-to-back contact solar cells, with soldered tabs connecting the front of one cell with the rear of the next cell.

New and advanced cell and module concepts, which are currently under development, use alternative interconnection technologies and pose specific challenges in terms of avoiding power loss during module production. This paper discusses the principles of cell-to-module (CtM) power loss determination and the study of CtM output changes for metal-wrap-through (MWT) solar cells interconnected with a patterned, conductive backsheet.

Recently, several articles that focus on CtM loss have been published [1–3]. Haedrich et al. [1] show how to determine the individual contributions to the CtM loss for 11 optical factors and two electrical losses. The paper by Forniés and Silva [2] focuses on the power losses resulting from soldered cell interconnections. Singh et al. show the importance of optical improvements for increasing the module output and reducing the CtM loss [3]. In the present paper the focus will be on the measurement aspects related to CtM; a detailed analysis of the CtM change for a full-size MWT module will be given.

## CtM loss or gain?

According to most literature, the CtM loss is the loss in power when a number of cells are interconnected and laminated to create a PV module, compared with the power of the cells in that module before interconnection and lamination. These losses can be differentiated into *optical losses*, leading to a lower photogenerated current, and *resistive losses*, leading to

a decrease in fill factor. However, since the application of anti-reflection (AR) coatings and other optical ‘tricks’ can sometimes increase the module  $I_{sc}$  with respect to the average cell  $I_{sc}$ , the CtM loss needs to be expressed as a negative quantity, which gives rise to confusion. It is proposed to use CtM change, where a negative value corresponds to a loss in current or power, and a positive value to a gain.

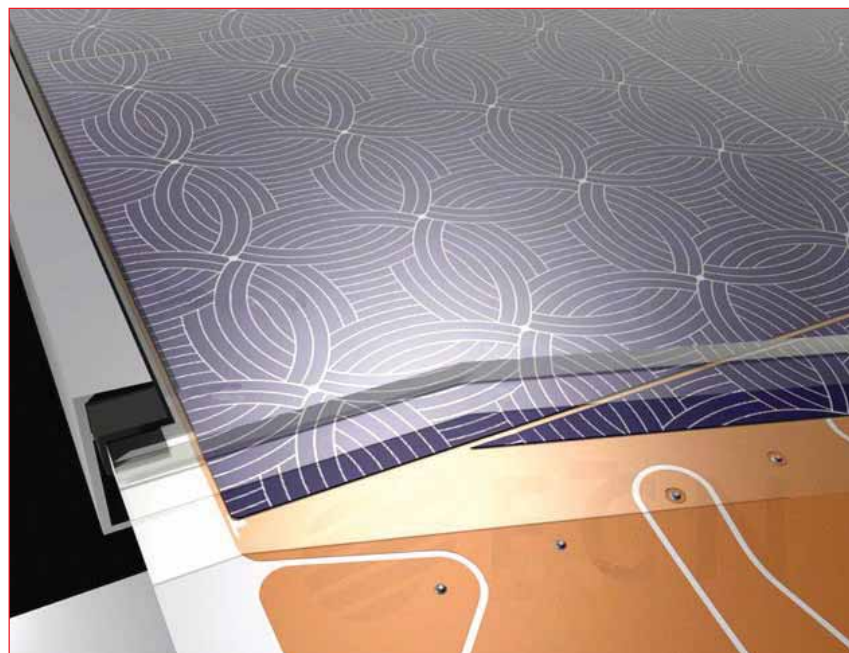


**Figure 1. Schematic of an MWT module. From bottom to top: patterned Cu layer on a polymer backsheet carrier; electrically conductive adhesive (ECA) dots; encapsulant layer with holes at the contact positions for the ECA; back-contact cells; front-side encapsulant; glass. The small solid circles in the metallization pattern indicate the location of the vias, which are sub-millimetre in diameter.**

### MWT technology

MWT solar cells have a front-side emitter with a front-side metallization grid for current collection. So-called *vias* connect the front-side metallization grid to contact pads at the rear; these emitter contacts are isolated from the back-surface field (BSF) [4]. The reduced front-side metallization coverage limits the shading losses [5] and reduces the overall front-side recombination losses [6].

Because all the contacts are located on the rear side, the cells can be interconnected using conductive foil-based technologies (see Fig. 1). All cell–cell interconnections are underneath the solar cells; therefore, no shading losses occur due to this interconnection material. Because the conductors are as wide as the solar cell, the thickness can typically be limited to 35µm for Cu layers. The combination of very wide and thin conductors means that no additional mechanical stress is imposed on the solar cells, in contrast to front-to-rear tabs, with typical dimensions of 1–1.5mm width and 200µm thickness. The absence of those tabs, which have to pass from the front to the rear, also allows the cell packaging to be higher, with cell–cell distances of typically 1.25mm.

The two polarities of the solar cell are separated on the conductive backsheet by a narrow line of removed Cu. As can be seen in the image, these separation lines can be designed for optimal conductance, and there is a certain degree of freedom in designing how to carry out the cell–cell interconnection. A cell can be connected with any two of its four neighbours – below, above, left or right – and in fact all combinations occur in a standard 60-cell module. This freedom of design can also be applied to the connection of the bypass diodes by drawing a narrow path between two columns of cells.

In this paper the cell-to-module changes for MWT back-contact modules employing conductive foil are described and compared with other mature module technologies. *I–V* measurements at the cell and module levels will be discussed first in order to highlight some important aspects for accurately determining CtM change. A detailed analysis of the CtM change will then be given for a full-size MWT module. To illustrate the difference in resistive losses for a conductive foil compared with tabbed modules, data taken from industrial production will be presented. A comparison with the available literature will be made,

covering back-contact cells, multiwire or smartwire modules, and regular H-pattern, front-to-back contact modules.

**“CtM changes can only be compared if the measurements are taken in a similar way.”**

### Determining the CtM change

The calculation of the change in CtM is based on the difference in module and cell output, where the output can be the power, short-circuit current  $I_{sc}$ , fill factor FF, open-circuit voltage  $V_{oc}$  or efficiency  $\eta$ . Although this sounds straightforward, it is not as simple as it seems. The values for both the cell and module output are influenced by many factors in the measurement techniques themselves; as a result, the CtM change is related to the way the measurements are performed. Thus, CtM changes can only be compared if the measurements are taken in a similar way, i.e. in accordance with IEC standards. In addition to that, the cell parameter that is used for the comparison affects the results.

The basis for an accurate CtM value lies in correct cell and module measurements and in the uncertainty in those measurements, as described in IEC standards 60904 and 60891. The uncertainty in the measured current of a cell or module is determined by many factors; for example, it depends on the reference cell that is used. The uncertainty in the calibration data of the reference cell (1.9%) and module (1.8%) determine to a large extent the uncertainty in the measured current, which is around 2%, depending on the set-up. The reproducibility in adjusting the irradiation of the solar simulator, and the spectral mismatch between the spectrum of the solar simulator and the AM1.5 spectrum, are the next-largest contributions to the uncertainty. The uncertainty in the current due to the uncertainty in the electrical part of the measurement is expected to be much smaller than the effect of the spectral mismatch and the uncertainty in the reference cell and module. For this reason the focus here will be on the effects resulting from the spectral mismatch.

If two different solar simulators are used for cell measurements, the measured currents will be different, as the lamp spectra will be different. To obtain similar currents, the current needs to be corrected for the

differences in the lamp spectra. This is done by measuring the spectral response (SR) of the cell (i.e. the response of a cell to light of a specific wavelength) and the lamp spectrum, and subsequently calculating the current that the cell would have under illumination by a standard spectrum (the AM1.5 spectrum). When the *I–V* characteristics of a cell are compared with those of a module, the measured cell and module currents also need to be corrected for the spectral mismatch. For an absolute comparison, the mismatches (MMs) in the cell and module measurements need to be determined. For this, the SR of both the cell and the module must be measured, as well as the lamp spectra of both sun simulators. The MM factor can then be derived using the formula:

$$MM = \frac{I_{ref,AM1.5} * I_{test,lamp}}{I_{test,AM1.5} * I_{ref,lamp}}$$

where

$I_{ref,AM1.5}$  = current from the calibrated reference cell or module for AM1.5 spectral conditions;

$I_{test,AM1.5}$  = current of the test cell for AM1.5 spectral conditions;

$I_{ref,lamp}$  = current of the reference cell as measured in the solar simulator;

$I_{test,lamp}$  = current of the test cell as measured in the solar simulator.

$I_{test,AM1.5}$  is derived from the known AM1.5 spectrum and the measured SR of the test cell. The correct current  $I_{test,cor}$  can now be estimated from the measured current  $I_{test,meas}$  and the mismatch factor MM as follows:

$$I_{test,cor} = \frac{I_{test,meas}}{MM}$$

From the above it is clear that when CtM changes are compared between institutes or companies, an absolute CtM must be used. Even within an institute, an absolute CtM is necessary when different cell technologies are used, as the SR will be different for the different cell technologies.

A relative CtM can be used only in the following situations:

- To check if a module line is performing according to specs: a CtM is determined for the specific module and the trends in the CtM can be tracked.
- To study cell processing or module fabrication improvements that do not affect the SR of the module – for example, metallization or tabbing, and minor changes in cell processing.

**Measurement factors in CtM change**

The basics of performing measurements for determining the CtM changes are that the cell and module measurement situations must be as similar as possible. This means that the following points should be considered for each cell type and situation:

- Cell contacting
- Chuck reflections
- Reference cell
- Reference module
- Bifacial cells

**Cell contacting**

If an H-pattern cell is used, the number of contact pins on the busbars can have an influence on the FF of the cell measurement. If in the module the tabs are soldered at more points than there are measurement probes in the cell measurement, a relatively higher FF will be measured. This could have a significant impact, especially if lower-conductance busbars are used. The number of contact points in the cell measurements should be sufficiently large for the resistance in the busbar not to limit the FF of the cell. Back-contacted cells, such as interdigitated back contact (IBC) and MWT, have fixed contact points; thus, for these cell types, fill factor changes due to a different number of contact points should not occur.

**Chuck reflections**

Most measurement chucks on which the cell is positioned will reflect light, which can eventually reach the solar cell and contribute to the current of the cell. In the case of monofacial cells, this concerns mainly light that hits the chuck outside the cell; for bifacial cells, however, this also holds true for light that is not absorbed by the cell and is reflected from the chuck back onto the cell. Therefore, the areas outside and underneath the solar cell should influence the cell I-V measurement as little as possible; for example, the full chuck area can be covered with non-reflecting material.

**Reference cell**

For accurate cell measurements, a calibrated reference is used and the measured cell data are corrected for spectral mismatch. This means that the SRs of the reference cell and test cell must be known, as well as the spectrum of the lamp of the solar simulator. Preferably, the reference cell should be of the same type and size as the test cell. The size will be a factor if the irradiance is not homogeneous over the entire area.

**Reference module**

Module measurements also use a reference module. As in the case of the cells, the SRs of both the reference and test modules, as well as the spectrum of the lamp of the flash tester, must be known for spectral mismatch

correction. Here too, the type and size of the reference and test modules should preferably be similar.

**Bifacial cells**

Besides the chuck reflection, there are several other aspects that need

String 1	$P_{mp}$ [W]	$I_{sc}$ [A]	$V_{oc}$ [V]	FF [%]
$\sum I-V$ of cells StM	100.24	9.188	14.00	77.96
$\min I_{sc}, \sum V_{oc}, av$ FF	99.64	9.137	13.98	77.98
$\Delta$ wrt $\sum I-V$	-0.60%	-0.56%	-0.08%	0.03%
$av I_{sc}, \sum V_{oc}, av$ FF	100.21	9.190	13.98	77.98
$\Delta$ wrt $\sum I-V$	-0.03%	0.01%	-0.08%	0.03%
$\sum$ cell powers	100.36			
$\Delta$ wrt $\sum I-V$	0.11%			
String 2	$P_{mp}$ [W]	$I_{sc}$ [A]	$V_{oc}$ [V]	FF [%]
$\sum I-V$ of cells StM	95.56	9.191	13.36	77.81
$\min I_{sc}, \sum V_{oc}, av$ FF	94.85	9.122	13.35	77.86
$\Delta$ wrt $\sum I-V$	-0.76%	-0.75%	-0.06%	0.06%
$av I_{sc}, \sum V_{oc}, av$ FF	95.59	9.194	13.35	77.86
$\Delta$ wrt $\sum I-V$	0.03%	0.03%	-0.06%	0.06%
$\sum$ cell powers	95.70			
$\Delta$ wrt $\sum I-V$	0.14%			
String 3	$P_{mp}$ [W]	$I_{sc}$ [A]	$V_{oc}$ [V]	FF [%]
$\sum I-V$ of cells StM	78.18	9.256	10.83	78.02
$\min I_{sc}, \sum V_{oc}, av$ FF	77.40	9.169	10.82	77.99
$\Delta$ wrt $\sum I-V$	-1.02%	-0.95%	-0.04%	-0.03%
$av I_{sc}, \sum V_{oc}, av$ FF	78.20	9.265	10.82	77.99
$\Delta$ wrt $\sum I-V$	0.02%	0.09%	-0.04%	-0.03%
$\sum$ cell powers	78.27			
$\Delta$ wrt $\sum I-V$	0.11%			
Module	$P_{mp}$ [W]	$I_{sc}$ [A]	$V_{oc}$ [V]	FF [%]
$\sum I-V$ of cells StM	273.95	9.205	38.18	77.94
$\min I_{sc}, \sum V_{oc}, av$ FF	271.34	9.122	38.16	77.94
$\Delta$ wrt $\sum I-V$	-0.96%	-0.90%	-0.06%	0.00%
$av I_{sc}, \sum V_{oc}, av$ FF	274.12	9.216	38.16	77.94
$\Delta$ wrt $\sum I-V$	0.06%	0.12%	-0.06%	0.00%
$\sum$ cell powers	274.33			
$\Delta$ wrt $\sum I-V$	0.14%			

**Table 1. Cell, string and module parameters for the various approaches. Percentages given are relative to the sum of the I-V curves of the cells in the string.**

to be considered when measuring bifacial cells. A committee is working on a standardized norm for the measurements of bifacial cells and modules [7], but there is currently no norm available. However, it is suggested to measure a bifacial cell under front- and rear-side illumination and subsequently determine the bifaciality ratio [8]: bifaciality =  $I_{sc, rear} / I_{sc, front}$ .

The compensated current density can then be derived from:

$$I_{sc, com} = (1 + 0.2 * \text{bifaciality}) * I_{sc, front}$$

### Cell performance in CtM change

As mentioned above, the CtM change is influenced by the cell parameters that are used; as there are many cells in a module, the choice of parameters is not straightforward. In most of the publications regarding CtM, these issues are not (or only partly) addressed [1,9–11], although there are a few exceptions [7]. The effect of the input cell parameters on the CtM change is given below for three different approaches.

*I-V* measurements were performed on a series of 60 MWT cells that were processed at ECN. For each cell, the *I-V* curve was subjected to a two-diode model fit [12,13]; these fit parameters were inserted into a model that calculates the *I-V* characteristics of a series connection of cells. The module contained three individual strings, as in a typical MWT module. For each string, the series connection was calculated, as well as the series connection for the complete module [14]. This approach will be called *string to module (StM)*. The measured currents were not corrected for MM, and so the results show only relative StM and CtM ratios. The *I-V* curve

summation result was compared with that of more commonly used approaches for determining the CtM ratio:

1. The minimum  $I_{sc}$  of the cells, the sum of the  $V_{oc}$ s, and the average FF: this allows the determination of a CtM ratio for current,  $V_{oc}$ , FF and  $P_{mp}$ .
2. The average  $I_{sc}$  of the cells, the sum of the  $V_{oc}$ s, and the average FF: this allows the determination of a CtM ratio for current,  $V_{oc}$ , FF and  $P_{mp}$ .
3. A summation of the powers from the measured individual cells: this allows the determination of a CtM ratio for  $P_{mp}$  only.

**“The average current of the cells yields a much closer match to the current of the strings and the module.”**

The calculated cell parameters for each string and the calculated parameters for the module are given in Table 1. This table does not show CtM or StM changes; rather, it shows the string or module parameters that can be used as inputs for the CtM or StM change. For a CtM or StM change, the module should be measured as well. As can be seen in Table 1, the overall difference in power between the different approaches can exceed 1%. It is clear that a CtM change can only be compared if it is based on the same approach for the cell and string input. The difference is mainly due to a difference in  $I_{sc}$ . Often the *minimum* current of the cells in a string is used

to obtain a CtM ratio for the current, as the cell with the lowest current determines the current in a series-connected string. However, in reality this is not true, as the FF of the cells also plays a role. In the examples below, it is shown that the *average* current of the cells yields a much closer match to the current of the strings and the module. The sum of the  $V_{oc}$ s and the average FF also are a good approach for determining CtM changes.

### Detailed CtM analysis for MWT modules

The various detailed contributions to the CtM change have been extensively reported in the literature [3,7]. The focus in the present paper will be on the total change for each of the three *I-V* parameters  $I_{sc}$ ,  $V_{oc}$  and FF. In the last section of the paper, the resulting effect for the  $P_{max}$  for MWT back-contact modules is given, showing why CtM loss is not the correct expression. As cells are evaluated in terms of efficiency, the following will be used: the cells' average  $I_{sc}$  ( $\overline{I_{sc, cell}}$ ), the cells' average FF ( $\overline{FF_{cell}}$ ), the sum of the cells'  $V_{oc}$  ( $\sum V_{oc, cell}$ ), and the sum of the cells'  $P_{max}$  ( $\sum P_{max, cell}$ ). The CtM change is then calculated as:

$$CtM(I_{sc}) = \frac{I_{sc, mod} - \overline{I_{sc, cell}}}{\overline{I_{sc, cell}}}$$

$$CtM(V_{oc}) = \frac{V_{oc, mod} - \sum V_{oc, cell}}{\sum V_{oc, cell}}$$

$$CtM(FF) = \frac{FF_{mod} - \overline{FF_{cell}}}{\overline{FF_{cell}}}$$

$$CtM(P_{max}) = \frac{P_{max, mod} - \sum P_{max, cell}}{\sum P_{max, cell}}$$

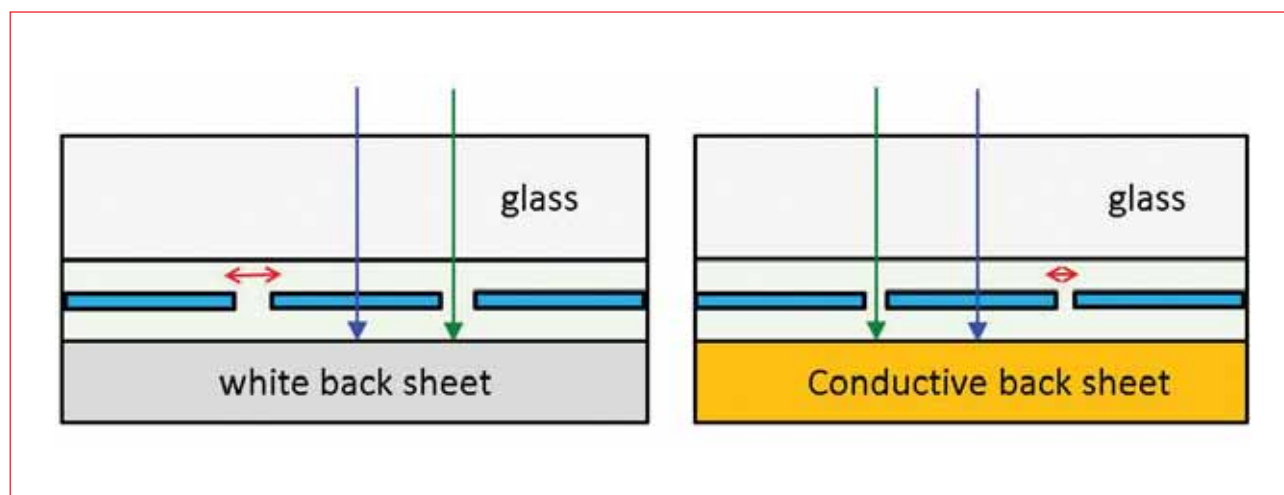


Figure 2. Sketch of the differences in optical behaviour: light transmitted through the solar cells (blue arrows), light incident on the area between and around the solar cells (green arrows), and the cell-cell spacing (red arrows).

# SOLAR EXPO

A WORLD FUTURE ENERGY SUMMIT EVENT

16-19 JANUARY 2017

ABU DHABI NATIONAL EXHIBITION CENTRE

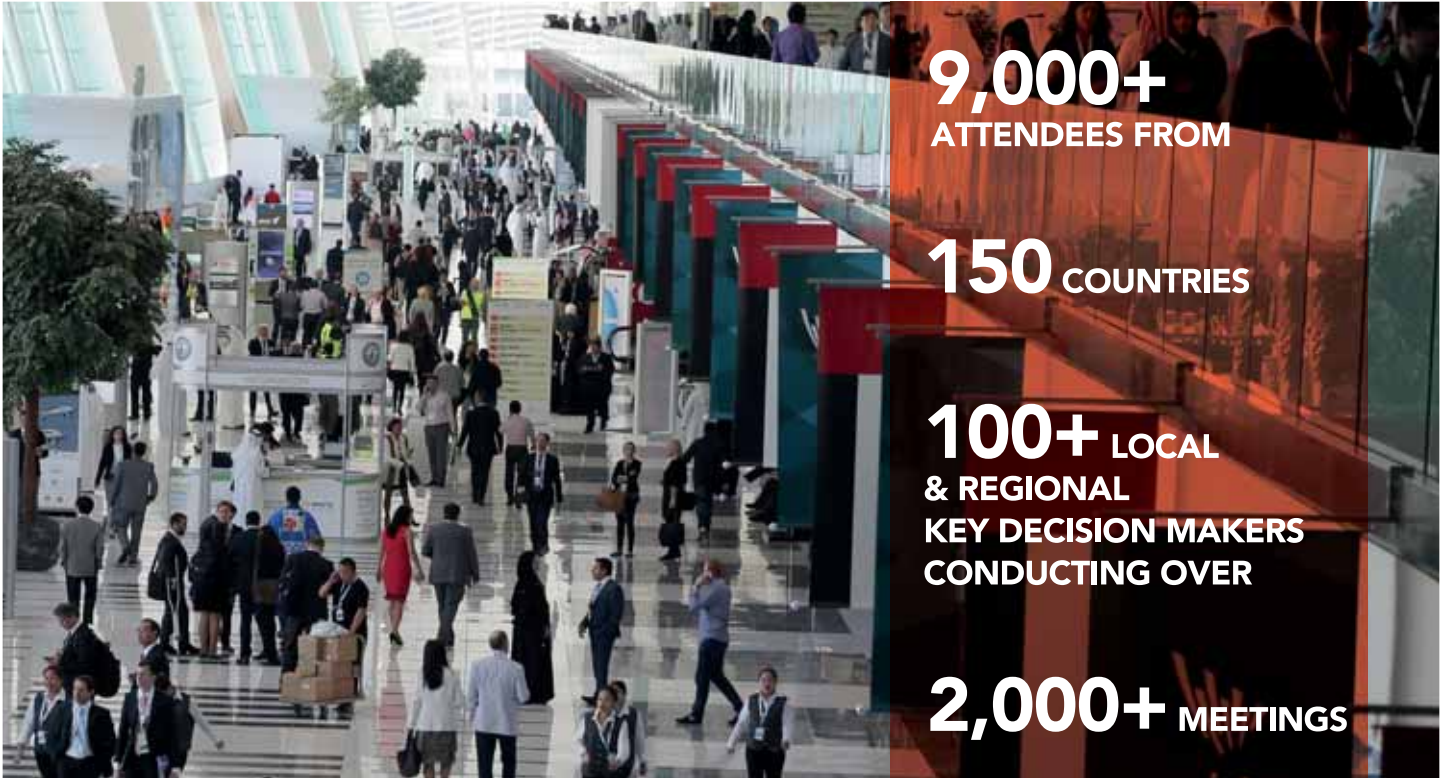
Hosted by



Strategic Sponsor



## ADVANCING SOLAR ENERGY SOLUTIONS



**9,000+**  
ATTENDEES FROM

**150** COUNTRIES

**100+** LOCAL  
& REGIONAL  
KEY DECISION MAKERS  
CONDUCTING OVER

**2,000+** MEETINGS

### MEET THE KEY DECISION MAKERS WHO MATTER TO YOUR BUSINESS

- Engineering, Procurement & Construction (EPC)
- Consulting/Contracting Firms
- Electrical & Mechanical Engineers
- Power Generation Companies
- Distribution Companies
- Real Estate Developers
- Government Authorities
- Utilities

#### SUSTAINABILITY BUSINESS CONNECT

Book your stand to take advantage of our business matchmaking platform, connecting you to regional & international buyers and key decision makers. To learn more, visit [www.solarexpo.ae](http://www.solarexpo.ae)

## BOOK YOUR STAND TODAY

Contact: Claude Talj

T: +971 50 452 8168

E: [claudet.talj@reedexpo.ae](mailto:claudet.talj@reedexpo.ae)

W: [solarexpo.ae](http://solarexpo.ae)

Official Event Partner

Part of WFES

Co-located with

Organised by



### CtM( $I_{sc}$ ) effects

The CtM( $I_{sc}$ ) is dominated by optical effects. With regard to first-order effects there are three contributions that differ between H-pattern modules and MWT modules. First, the reflection of light that is incident on the area between and around the solar cells will be scattered onto different materials. These could be the backsheet or the rear encapsulant for H-pattern modules, and the conductive backsheet or the rear encapsulant for MWT modules, as indicated by the green arrows in Fig. 2.

The conductive backsheet has its origin in printed circuit board (PCB) technology. A protective layer is applied to prevent the Cu layer from oxidation and other degradation

effects. The first conductive backsheets were also covered with such a protective layer, which happened to be green. Black and white options were also available to improve the aesthetics and the power output respectively.

Fig. 3 shows the reflection spectra of these coloured conductive backsheets. The spectra were measured for backsheets laminated with 400-micron EVA and solar glass without an AR coating. Between 400 and 1200nm wavelengths, the backsheet with a black protective layer has less than 10% reflection, while the backsheet with a white layer has between 40% and 50% reflection. The backsheet with a green protective layer exhibits similar reflection, but yields a

maximum absorption around 650nm, as expected.

Two full-size MWT modules, incorporating n-type MWT solar cells with an average  $I_{sc}$  of  $9.21 \pm 0.02A$ , were manufactured with conductive backsheets covered by either a green or a white protective layer. Table 2 summarizes the  $I-V$  parameters for the two modules. The module with the green protective layer yielded an  $I_{sc}$  of 9.34A, corresponding to a CtM current change of +1.5%. With a white protective layer, an even larger CtM change of +2.7% was observed.

The second difference in the optical aspect between H-pattern modules and MWT modules is the cell-cell distance, indicated by the red arrows in Fig. 2. Typically, in H-pattern modules the cell-cell distance is 2.5mm or greater, whereas in MWT modules the cells can be placed as close as 1.25mm, limited mostly by the (permissible) variation in wafer dimensions [15].

Finally, the third difference is the reflection of the red/near-infrared light, which is transmitted through the cells (blue arrows). Recently, the importance of the light incident around the cells relative to the transmitted light was demonstrated in a ray-tracing comparison between bifacial and monofacial modules [16]. In the case of a monofacial module, the light that is incident on the solar cell shows that the reflection on the white backsheet adds 2% to the  $I_{sc}$ . Light incident on the area between the solar cells contributes another 3% to the  $I_{sc}$ , as a result of the reflection on the white backsheet. Both contributions are much smaller for bifacial modules with transparent rear materials only. However, the ray-tracing simulation also showed that

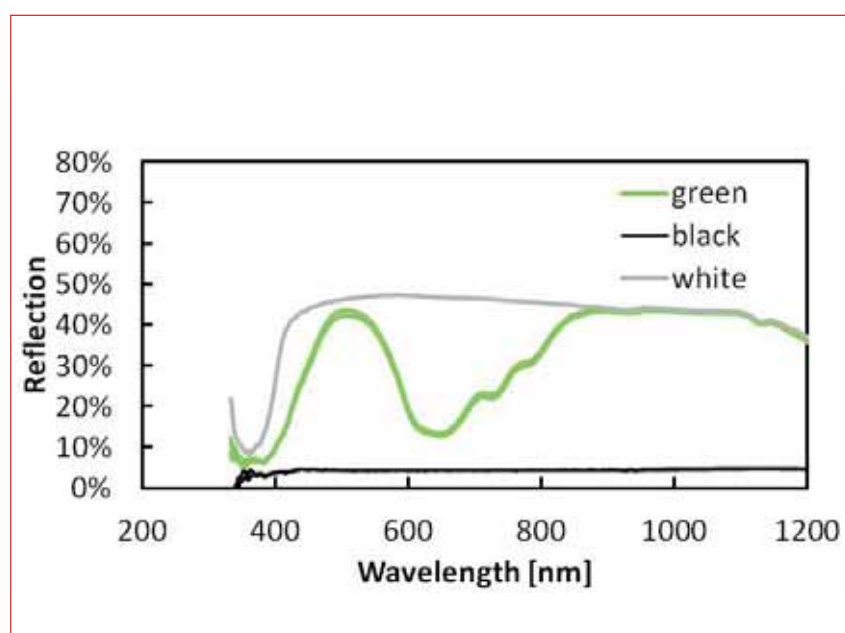


Figure 3. Reflection as a function of the wavelength for stacks of glass-EVA-conductive backsheet, for three differently coloured protective layers.

Backsheet covering		$V_{oc}$ [V]	$I_{sc}$ [A]	FF [%]	$P_{max}$ [W]
Green protective layer, $\eta = 18.9\%$	Cell	38.2	9.21	77.3	271.5
	Module	38.2	9.34	76.6	273.4
	CtM	+0.1%	+1.5%	-0.9%	+0.7%
White protective layer, $\eta = 19.0\%$	Average cell	38.5	9.22	76.8	273.0
	Module	38.6	9.47	75.4	275.6
	CtM	+0.2%	+2.7%	-1.9%	+0.9%
White EVA rear layer, $\eta = 20.5\%$	Average cell	39.1	9.66	79.3	298.9
	Module	38.9	9.92	78.0	300.5
	CtM	-0.5%	+2.7%	-1.6%	+0.5%

Table 2.  $I-V$  parameters and CtM changes for three module experiments. The 'cell' rows give the average values of  $I_{sc}$  and FF, and the summed values of  $V_{oc}$  and  $P_{max}$  for the 60 cells in that module.

placing a highly reflective material between the solar cells can add 4% to the  $I_{sc}$ , yielding a front-side  $I_{sc}$  for a bifacial module that is almost equal to the  $I_{sc}$  for a monofacial module. This also highlights the importance of optimized light management for light that is incident on the non-solar cell areas of PV modules.

A second-order effect is that MWT solar cells allow lower metal coverage on the front side. In particular, with an increasing number of vias [17], fewer and thinner fingers are needed. As regards front-to-back-contact modules, more busbars (e.g. five-busbar [18], multiwire [19] or smartwire modules [20]) also allow thinner and fewer metal fingers, but the contact area for the interconnection will limit the decrease in coverage. Whereas the reflection on the metal coverage decreases the  $I_{sc}$  of the solar cell, after encapsulation a part of that reflected light can reach the solar cell because of multiple scattering effects; when all other parameters (such as paste morphology) are kept the same, this means that with decreasing metal coverage, less reflected light can be recaptured. Note that, although there is a 'negative' effect on the CtM( $I_{sc}$ ), less shading by metal coverage obviously results in a higher module  $I_{sc}$ .

**CtM( $V_{oc}$ ) effects**

The  $V_{oc}$  of a cell, and therefore of a module, can be affected when it is subjected to high temperatures; as a result, the lamination of the module could influence the CtM( $V_{oc}$ ). In general, however, the  $V_{oc}$  is not affected by the interconnection and lamination process. For MWT cells, interconnected by electrically conductive adhesive (ECA) on a patterned, conductive backsheets,

the lamination process, limited to  $\leq 160^{\circ}\text{C}$ , is also the process that cures the ECA and interconnects the cells to the conductive layer on the backsheets. Although typical soldering temperatures are higher, the temperatures involved are too low to significantly alter the  $V_{oc}$  of the solar cell in the case of both ECA and soldered interconnections.

**CtM(FF) effects**

Finally, the CtM(FF) is dominated by series-resistance effects. As in the case of others in the field [1], a distinction is made between the losses in the tabs (cell-cell interconnection) and the losses in the cross connectors (i.e. interconnection of strings to each other and to the junction box). The contact resistance between the busbar and the tab can be neglected. For conductive backsheets modules, the connections to the junction box are directly behind the first and last solar cells in the series interconnection. Furthermore, there is no separate connection between the cell strings.

**“Resistive losses are proportional to the resistance of the interconnectors, but increase quadratically with the current.”**

Resistive losses are proportional to the resistance of the interconnectors, but increase quadratically with the current. Resistive losses, and therefore the CtM change in FF, are the highest in module concepts incorporating large solar cells, as the large area multiplied by the current density yields the highest total current to be

conducted. This is also one of the main advantages of using 5" solar cells, or half, third or an even smaller fraction 6" solar cells. Half cells yield only half the current of a full-area solar cell; the resistive losses, all else being equal, are therefore only 25%, compared with those for a module with full-area solar cells.

In a tab with current  $I$  and resistance  $R=\rho L/wt$  (where  $\rho$  is conductivity,  $L$  is length,  $w$  is width and  $t$  is thickness of the tab), the power loss is given by  $\Delta P = I^2R$ . As the current increases linearly along the length of the tab, the current at position  $x$  is given by  $I(x) = ax$ , where  $a$  is a constant given by the current  $I$  at the end of the tab divided by the length  $L$  of the tab. The power loss in each small piece  $dx$  is then  $\Delta P(x) = (a^2x^2\rho/wt)dx$ . The total power loss is then given by the integral of  $\Delta P(x)$  from  $x=0$  to the end of the tab:

$$\Delta P = \int_0^L \left(\frac{I_{mpp}}{L}\right)^2 \frac{\rho}{wt} x^2 dx = \left(\frac{I_{mpp}}{L}\right)^2 \frac{\rho}{wt} \frac{1}{3} x^3 \Big|_0^L = \frac{1}{3} I_{mpp}^2 \frac{\rho L}{wt}$$

This end result means that for a linear increase in current the original formula for  $\Delta P$  can be adapted by replacing the resistance by an effective resistance  $\frac{1}{3}R$ .

The calculated FF losses due to series resistance power losses are given in Table 3 for several module types with various interconnection types. The FF loss ( $\Delta FF$ ) is calculated from the expression  $\Delta FF/FF = \Delta P/P_{max}$ . The resistive loss takes into account just the loss in the cell-cell interconnector. No optical effects are calculated; nor are the losses in the string-string interconnection.

For the MWT module interconnection loss calculation, the following layout and approximation are used. On the rear of the solar

Interconnection	Number	Tab / wire / foil width × thickness	Total area [mm <sup>2</sup> ]	$\Delta FF$ [%abs]
Rectangular tab	3	1.5mm × 200µm	0.9	-2.7
Rectangular tab	4	1.0mm × 200µm	0.8	-3.1
Rectangular tab	5	0.8mm × 250µm	1.0	-2.4
Multiwire	15	Ø 270µm	0.9	-2.8
		or Ø 330µm	1.3	-1.9
Smartwire	38	Ø 200µm	1.2	-2.0
MWT – 35µm Cu	4 'front tabs' &	20mm × 35µm	2.7	-0.9
	3 'rear tabs'	26mm × 35µm		

**Table 3. Calculated FF losses in cell-cell interconnection.**



cell there are four rows of four emitter contacts, and three rows of five BSF contacts. The Cu pattern is approximated for this FF loss calculation by four emitter ‘tabs’ of width 19.5mm and three BSF ‘tabs’ of width 26mm, using all available space. In reality, these ‘tabs’ are tapered, having a larger width (where the current is higher) and a smaller width (where the current is lower). Moreover, the increase in current per contact point is stepwise and not linear. Note that the conductive backsheet foil has integrated connecting conductive paths for attaching the bypass diodes to the end/beginning of each string.

Fig. 4 shows a plot of the calculated  $\Delta FF$  as a function of the total cross section of the cell interconnections. As expected, the resistive losses decrease, and thus  $P_{max}$  increases, with increasing tab cross section.

The effect of the interconnection as described above is indeed observed in modules based on these interconnection types. In Table 4 the reported CtM changes of several module interconnection technologies are compared with the typical values obtained for conductive backsheet technology as reported above. The H-pattern module consists of three-busbar solar cells taken from Haedrich et al. [1]. The data reported by SunPower [21] for a 96-cell 5" IBC module are also given.

In the examples presented here, full-area solar cells are used. The first two modules in Table 4 are made from pseudo-square 239cm<sup>2</sup> solar cells, the third from full-square 243cm<sup>2</sup> cells. The  $I_{sc}$  is therefore large (>9A), but because of the low resistive losses in the backsheet, the FF CtM change is typically only -1.0% to -1.5%. In the best-performing modules the absolute change in FF can be as low as -0.7%. These low values for FF CtM changes will be discussed in detail next.

First, the CtM changes for the IBC module are compared with the values for the n-type MWT module. Although both modules demonstrate a higher module  $I_{sc}$  than the incorporated solar cells, the CtM change for the n-MWT modules is even bigger. The reason behind the larger  $I_{sc}$  CtM change is actually related to the front-side metallization grid. In a cell  $I$ - $V$  measurement, with increasing front-side metallization the  $I_{sc}$  decreases because of the reflection of light on the metal pattern. In contrast, in the case of IBC solar cells the full front area is illuminated, with no optical losses due to shading.

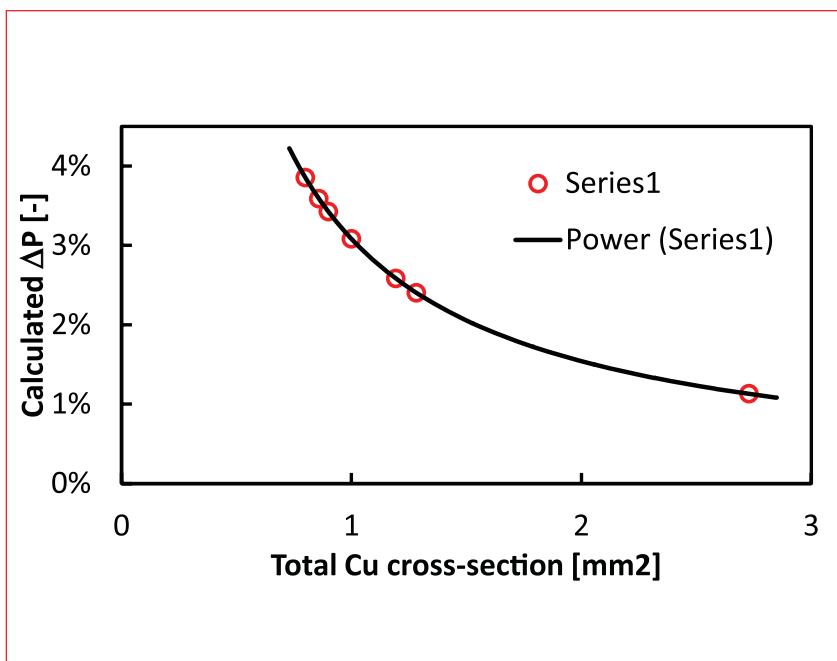


Figure 4. Calculated FF loss due to resistive power loss in the cell-cell interconnection as a function of the total Cu cross section in that interconnection.

Technology	$V_{oc}$	$I_{sc}$	FF	$P_{max}$
H-pattern [1]	+0.0%	-3.5%	-3.3%	-6.7%
IBC 5" [21]	-0.5%	+0.2%	-2.0%	-2.3%
MWT n-type	0.0%	+2.5%	-1.5%	+1.0%

Table 4. CtM changes for three module technologies.

After lamination, the light that was reflected on the metallization can be scattered on the glass/EVA interface, back onto the solar cell. In this way, some of the light that is lost in the cell measurement can be converted to photocurrent in the module measurement. Therefore, the CtM change in current (about 0%) for cells without a front-side metallization grid is lower than that for cells with a front-side metallization coverage.

A direct comparison of the FF CtM change cannot be made, as the interconnection dimensions are not given; the comparison is between 5" solar cells with 6.3A, and 6" solar cells with more than 9A. However, the n-MWT module shows a smaller FF loss than the IBC module.

If the 6" H-pattern module is compared with the n-MWT module, two differences are observed: first, the  $I_{sc}$  CtM change is much lower for the H-pattern module; and second, the FF CtM change is also lower. The lower  $I_{sc}$  CtM change is probably related to the quality of the glass, for example the AR coating. A second aspect, however, is that it could be related

to the busbar design. When a non-continuous busbar design is utilized, the cell  $I_{sc}$  will be higher because of less shading, whereas for the tabbed solar cell, the total amount of shading will stay the same. Thus, the use of such a non-continuous design will save metallization paste and improve the cell rating, but there will be no effect on the module parameters, and thus a lower CtM change will be calculated.

The observed FF CtM change of -3% is in good agreement with the calculation shown in Table 4 and Fig. 4. As the cell dimensions, and therefore the  $I_{sc}$ , are almost the same, the difference in FF CtM change is solely related to the cell-cell interconnection.

Back-contact solar cells can be positioned much closer together than front-to-back contact solar cells. Although this reduces the area available between the cells for scattering additional light to the solar cells, the MWT modules still achieve a module  $I_{sc}$  that is more than 2% higher than the cell  $I_{sc}$ . The consequences are that the modules

have a smaller area and thus more modules can be placed on a given area. Alternatively, conductive backsheets technology can also be adapted in such a way as to position the cells further apart, thus increasing the area available for scattering, which in turn increases the module  $I_{sc}$  even more.

### Positive CtM $P_{max}$ change for MWT modules

As presented in Tables 2 and 4, for MWT modules the gain in  $I_{sc}$  is accompanied by almost no change in  $V_{oc}$ . The fill factor FF does show a CtM change due to the resistive losses in the interconnection. To recapitulate, the CtM changes are  $\approx 0\%$ ,  $+2.5\%$  and  $-1.5\%$  for  $V_{oc}$ ,  $I_{sc}$  and FF respectively. The  $P_{max}$  of a PV device is the product of  $V_{oc}$ ,  $I_{sc}$  and FF. As the CtM changes are small, the CtM change in  $P_{max}$  is given by the sum of the  $V_{oc}$ ,  $I_{sc}$  and FF CtM changes. It follows, then, that the  $P_{max}$  CtM change is greater than  $0\%$ . In other words, these conductive backsheets modules with MWT solar cells all exhibit a positive change in the total  $P_{max}$ . This is accomplished by combining a relatively high positive change in  $I_{sc}$  with a very low negative change in FF.

“The colour of the coating on the Cu layer has an influence on the CtM  $I_{sc}$ .”

### Conclusions

CtM change is an important parameter in quantifying the advantages and issues for different module materials and technologies; however, the determination of this value has to be done carefully. Often the minimum current of series-connected cells is used to obtain a CtM ratio for the current. The examples given above demonstrate that the average current of the cells provides a much closer match to the current of the strings and the module. The sum of the  $V_{oc}$ s and the average FF also are a good approach for determining CtM changes.

In the case of MWT back-contact modules, it has been shown that the colour of the coating on the Cu layer has an influence on the CtM  $I_{sc}$ . A highly reflective white coating, in combination with AR-coated solar glass, yields CtM changes of up to  $+2.7\%$  at a module  $I_{sc}$  of  $9.9A$ . The very small cell-cell spacing of  $1.25mm$  leaves room for further improvement

of the module  $I_{sc}$  by increasing this spacing and applying light-management tricks. The electrical losses are determined by the cross-sectional area of the conductor and the total current. For most front-to-back contact modules, the total conductor cross section is around  $1mm^2$ , resulting in a  $2.5$  to  $3.0\%$  power loss for  $6"$  solar cells. For MWT modules with a  $35\mu m$  patterned Cu sheet, the cross section is almost  $3mm^2$ , leading to a power loss of around  $1\%$ .

The combination of a positive  $I_{sc}$  CtM change (with room for further improvement) and a rather small negative FF CtM change results in a module with a higher power output than the summed  $P_{max}$  of the individual solar cells.

### References

- [1] Haedrich, I. et al. 2014, *Sol. Energy Mater. Sol. Cells*, Vol. 131, p. 14.
- [2] Forniés, E. & Silva, J.P. 2015, *Photovoltaics International*, 29th edn, p. 19.
- [3] Singh, J.P. et al. 2016, *Photovoltaics International*, 31st edn, p. 90.
- [4] Newman, B.K. et al. 2015, *Proc. 31st EU PVSEC*, Hamburg, Germany, 829.
- [5] Romijn, I. et al. 2008, *Proc. 23rd EU PVSEC*, Valencia, Spain, p. 1000.
- [6] Stassen, A. & Zhang, W. 2013, “New Ag metallization pastes for solar energy cost reduction”, Heraeus white paper [http://www.heraeus.com/media/media/hpt/doc\_hpt/whitepapers/New\_Ag\_metallization\_pastes\_for\_solar\_energy\_cost\_reduction.pdf].
- [7] IEC/TS 60904-1-2:2016 Ed. 1.0, “Photovoltaic devices – Part 1-2: Measurement of current-voltage characteristics of bifacial photovoltaic (PV) devices”.
- [8] PV Performance Modeling Collaborative, “Bifacial PV characterization and rating standards” [https://pvpmmc.sandia.gov/pv-research/bifacial-pv-project/bifacial-pv-characterization-and-rating-standards/].
- [9] Haedrich, I. et al. 2013, *Energy Procedia*, Vol. 38, p. 355.
- [10] Dasari, S.M. et al. 2013, *Renew. Energy*, Vol. 50, p. 82.
- [11] Jung, T-H. et al. 2014, *Solar Energy*, Vol. 103, p. 253.
- [12] Burgers, A.R. et al. 1996, *Proc. 25th IEEE PVSC*, Washington DC, USA, p. 569.

- [13] In-house built model ivfit. Commercially available via pvwebtools@ecn.nl.
- [14] Friesen, G. et al. 2009, *Proc. 24th EU PVSEC*, Hamburg, Germany, p. 3189.
- [15] Bennett, I.J. 2013, “Compatibility of copper plated cells with MWT module technology”, Presentation, 4th Worksh. Metalliz. Crystall. Silicon Sol. Cells, Konstanz, Germany [www.metallizationworkshop.eu].
- [16] van Aken, B.B. et al. 2016, *Proc. 32nd EU PVSEC*, Munich, Germany, p. 42.
- [17] van Aken, B.B. et al. 2014, *Energy Procedia*, Vol. 55, p. 374.
- [18] Hannebauer, H. et al. 2014, *physica status solidi*, Vol. 8, p. 675.
- [19] Walter, J. et al. 2014, *Energy Procedia*, Vol. 55, p. 380.
- [20] Söderström, T., Papet, P. & Ufheil, J. 2013, *Proc. 28th EU PVSEC*, Paris, France, p. 495.
- [21] Smith, D. et al. 2012, *Proc. 38th IEEE PVSC*, Austin, Texas, USA, p. 1594.

### About the Authors



**Dr. ir. Bas van Aken** received his Ph.D. in solid state chemistry at the University of Groningen, after which he worked as a postdoc at Cambridge University and at the Max Born Institute for Nonlinear and Ultrafast Optics in Berlin. He is currently a researcher in the PV module technology group at ECN, where he focuses on fabrication, reliability and (outdoor) performance of bifacial and back-contact modules.



**Dr. Lenneke Slooff-Hoek** is a researcher in the device architecture group at ECN. She received her Ph.D. from the FOM Institute for Atomic and Molecular Physics (AMOLF), with a thesis topic of polymer optical waveguides. After that she started working at ECN on polymer PV with a focus on optical modelling. She has since shifted to the field of c-Si, but still maintains a focus on modelling and characterization of cells and modules.

### Enquiries

ECN – Solar Energy  
PO Box 1  
1755 ZG Petten  
The Netherlands

Email: slooff@ecn.nl

# Electroluminescence (EL) studies of multicrystalline PV modules

Sreenivasa Murty Dasari, Chandra Mauli Kumar, Amresh Mahajan & Nagesh C, Tata Power Solar, Bengaluru, India

## ABSTRACT

Higher power generation yield is the prime objective of any solar power plant developer. The quality and reliability of the modules used are therefore a key aspect, with customers placing stringent criteria on cell and module manufacturers with regard to product quality. Electroluminescence (EL) image monitoring, which gives a clear picture of defect distribution across a module, is an increasingly popular quality criterion. Although there are no standard guidelines for accepting or rejecting a module on the basis of EL images, customers are eager to see uniform illumination in the images. This paper reports on a study that focused on EL image analysis and correlation with reliability tests, through subjecting the modules to thermal-cycling (TC) tests and potential-induced degradation (PID) tests. EL images before and after these tests are compared in order to understand the changes in the images with respect to stress. From the results, it is concluded that EL imaging can act as an inline quality inspection tool, but cannot guarantee product reliability.

## Introduction

As the need for global electricity exceeds the conventional power generation capacity, all nations are looking to solar PV as an alternative, and incentive schemes are being implemented to encourage solar power plant developers. Crystalline PV technology is demonstrating its success in fulfilling growing energy demands. Each factor of the complete value chain of crystalline PV is important in determining initial investment cost and long-term reliability. Investors are therefore very interested in the quality of the materials used in the development of solar power generation plants.

Solar panels installed in the field will be subject to drastic changes in weather, and there is a potential risk of failure of poor-quality modules. The International Electrotechnical Commission has established some guidelines (IEC 61215) for ensuring the quality of crystalline solar modules [1]. All module manufacturers obtain IEC certification from authorized institutes to demonstrate the quality of their products to their customers. Since this qualification test is time consuming and costly, it is limited to just a few samples. Some of the process-related defects – such as improper tabbing, poor lamination and cell cracks – will not be observed during a visual inspection; moreover, the electrical performance of these defective modules will not differ very much from that of good ones. These defects will get worse over a period of time, however, because of the impact of weather conditions on modules. Online inspection of modules

in manufacturing is the only way to address such quality-related issues.

**“There are no standard guidelines for accepting/rejecting a module on the basis of EL images.”**

Electroluminescence (EL) imaging of PV modules before and after lamination is an advanced method for ensuring defect-free module manufacturing, but there are no standard guidelines for accepting/rejecting a module on the basis of EL images. Nevertheless, customers like to see uniform illumination in EL imaging.

There have been various studies carried out on EL image correlation with respect to defects. Kirchartz et al. [2] interpreted EL emission intensity in relation to the quantum efficiency of the cell. The operating voltage of an individual cell in a module can also be derived using EL images [3]. The identification of cell cracks, breaks in contact lines and other defects has been established in various studies [4,5].

This paper is aimed at analysing EL images with respect to cell electrical performance. The changes in the EL images before and after the stress tests are also studied in order to understand how these images can be used in terms of assessing reliability.

## Theory

A solar cell is basically a p-n junction diode. Under forward-bias conditions, the intrinsic potential across the

junction will drop, and majority carriers from both sides will cross the junction and enter the other side, where they become minority carriers. These minority carriers diffuse away from the junction and recombine with the majority carriers. In this process of recombination, photons of a frequency equal to the band gap of the material will be emitted for every electron-hole recombination, a phenomenon called *injected electroluminescence*.

The rate of radiative recombination  $r$  on each side of the junction depends on the concentration of majority carriers and on the number of minority carriers injected [6], and is given by  $r = Bnp$ . Here,  $n$  is the electron density,  $p$  is the hole density and  $B$  is a constant, which will be  $10^7$  times smaller for indirect band-gap materials than for direct band-gap materials. In silicon-based solar cells, electron-hole radiative recombination probability is therefore lower, since silicon is an indirect band-gap material. Electron-hole creation and recombination are proportional to each other, which means that the internal quantum efficiency of carrier generation can be estimated from the carrier recombination. In this way, EL imaging can be used to map solar cell performance; furthermore, by analysing EL data one can understand the material characteristics in a non-destructive way. This is why EL imaging has gained the attention of the PV industry as an inline quality check in the manufacturing process.

A module to be tested is forward biased in a dark environment. Since silicon is an indirect band-gap material, the band-to-band radiative transition



# PV Taiwan

2016

October 12 – 14, 2016

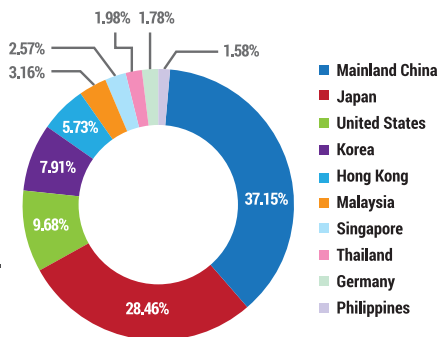
Taipei Nangang Exhibition Center, Hall 1

## 3 Reasons to Exhibit at PV Taiwan

- Taiwan is the world's 2nd largest solar cell production region with cutting edge technology!
- PV Taiwan invites over 100 international buyers from 16 countries, including countries in the emerging markets, such as, Turkey, India, and Brazil.
- The one-on-one procurement meetings in PV Taiwan 2015 generated more than US\$200 million in business opportunities, doubling the amount in 2014.
- PV Taiwan annually attracts more than 8,000 visitors from over 70 countries!

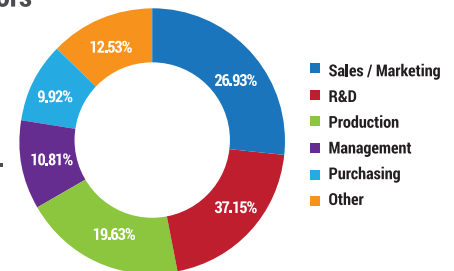
## PV Taiwan Top 10 International Buyers

In 2015, international buyers are from China, Japan, and the United States, countries with increasing PV demands.



## PV Taiwan Visitors

Over 20% of the visitors at PV Taiwan 2015 are in management position or held purchasing authority.



## Booth Rate

Booth Type (3m*3m)	Rental Rates /per booth	Early Bird Rate /per booth
Raw Space	US\$ 3,100	US\$ 2,300
Shell Scheme	US\$ 3,600	US\$ 2,800

## Understand the Latest Industry Trends

### Theme Pavilions

- Equipment and Materials Pavilion
- PV System Pavilion
- Testing and Certification Pavilion
- Energy Storage and Application Pavilion
- Cross-strait Pavilion

### International Forums

- Executive Summit
- Advanced Technology Symposium
- Market Development Forum
- Next Generation of PV Tech Forum
- Efficient Energy Storage & Smart Grid
- Market Opportunities and Technology trends workshop
- PV Standard Seminar
- PV System & Architecture Forum

rate is lower and the intensity of light emitted under forward bias from a silicon solar cell is much reduced; the background while taking the image therefore needs to be dark. When a module is forward biased, the applied current will be distributed across the cell through the front-contact grid lines (which are used for the collection of photogenerated current). The injected carriers (forward current) in the emitter recombine with the available holes, and light is emitted. The spatial intensity distribution of emitted light depends on the cell properties, in other words on the materials and process used.

In a typical module production process, various types of EL image can be identified (Fig. 1), but there is no global standard with regard to acceptance/rejection criteria on the basis of the image. The main objective of EL inspection is to detect cell cracks and other process defects (such as improper tabbing), but customers are very particular about seeing a uniform

and bright EL image across the modules without any signs of dark areas on the cells: this is because of limited studies of EL images and their correlation with reliability. It is therefore important to understand the technical reasons for the various types of EL image and the corresponding effects on module performance in long-term operation.

### Image analysis

The intensity of emitted light determines the brightness of the EL image: the higher the intensity, the brighter the image. A solar cell under forward bias emits more light only when the injected carriers recombine radioactively. The radiative recombination rate depends on two factors: 1) defect centres, and 2) injected carriers.

Metallic impurities in a silicon wafer induced during ingot growth will occupy energy levels in the forbidden gap of silicon and act like minority-carrier trap centres. In a solar cell, if the

substrate wafer is free from such defect sites (recombination centres), then the probability of radiative recombination of the injected carriers with the holes will increase, and the intensity of emitted radiation will be high. The open-circuit voltage of a solar cell is a direct measure of material purity [7]: the higher the purity, the higher the  $V_{oc}$ . Thus, the cells with higher open-circuit voltages appear bright in an EL image, because of a higher radiative recombination rate; on the other hand, cells with lower open-circuit voltages will appear dark.

**“The higher the  $V_{oc}$ , the brighter the EL image.”**

In Fig. 2, cells with different electrical parameters are arranged from A to F in ascending order of  $V_{oc}$ . The values  $V_{oc}$ ,  $I_{sc}$  and FF for each cell are tabulated next to the image; by comparing these

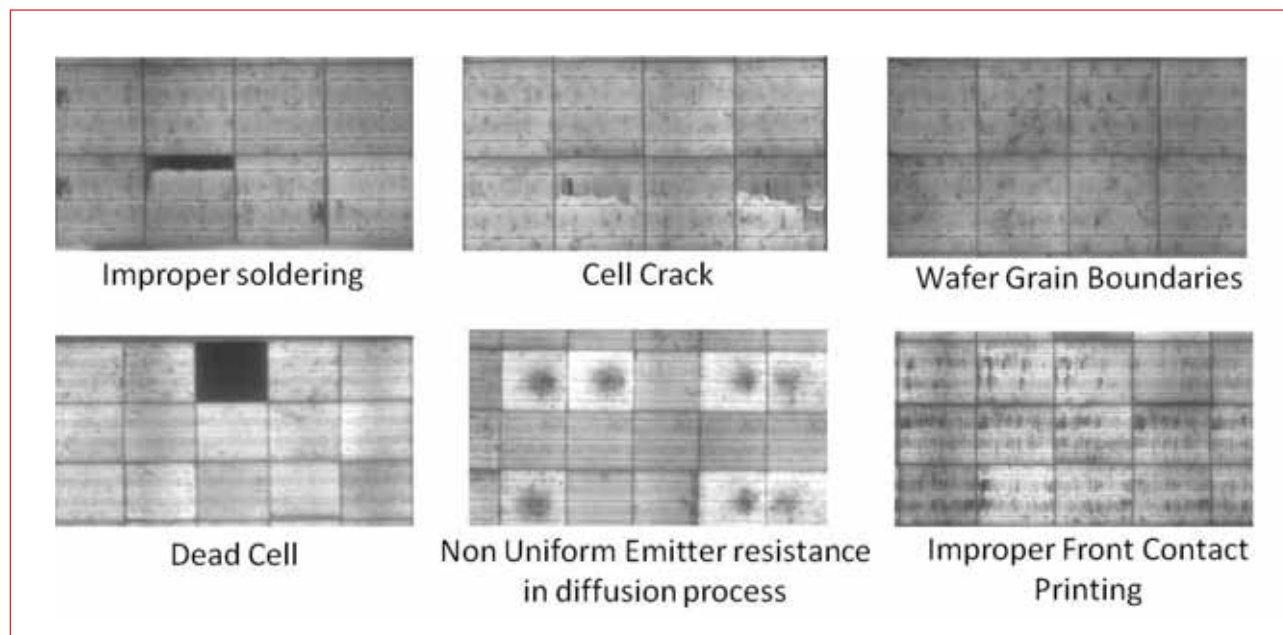
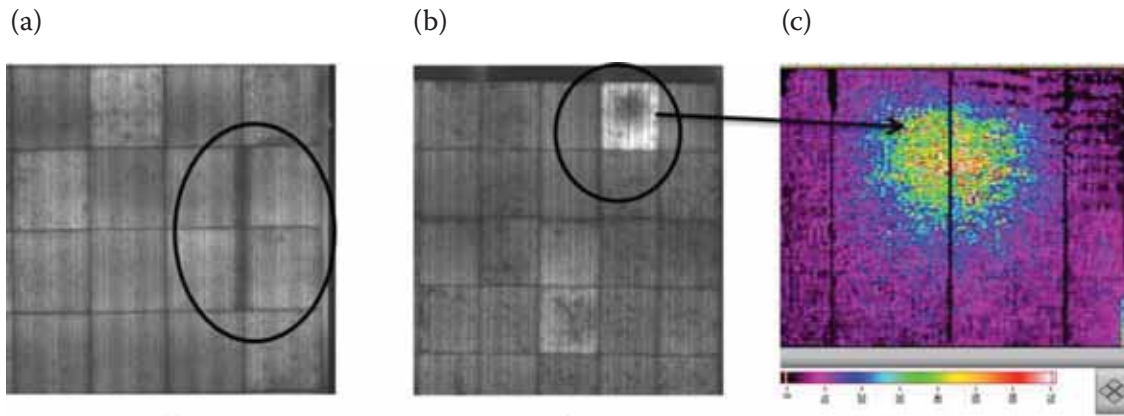


Figure 1. Various types of EL image in a standard module manufacturing line.

		Open Circuit Voltage (mV)						Short Circuit Current (Amp)						Fill Factor (%)													
	A	B	C	D	E	F		A	B	C	D	E	F		A	B	C	D	E	F							
1							1	0.976	0.977	0.979	0.990	0.998	0.997	1	0.969	0.976	0.984	0.988	0.993	0.994	1	0.992	0.986	0.989	0.986	0.992	0.986
2							2	0.977	0.976	0.980	0.993	0.997	0.998	2	0.964	0.975	0.982	0.984	0.991	0.996	2	0.997	0.986	0.994	0.977	0.987	0.989
3							3	0.978	0.978	0.985	0.994	0.997	0.997	3	0.972	0.980	0.990	0.983	0.992	0.996	3	0.994	0.991	0.994	0.989	0.992	0.991
4							4	0.975	0.978	0.989	0.992	0.997	0.997	4	0.966	0.978	0.979	0.984	0.988	0.997	4	0.997	0.991	0.989	0.987	0.997	0.991
5							5	0.976	0.976	0.987	0.996	0.997	0.997	5	0.970	0.975	0.982	0.987	0.992	0.996	5	1.000	0.985	0.996	0.986	0.989	0.990
6							6	0.978	0.980	0.987	0.996	0.997	1.000	6	0.973	0.980	0.984	0.987	0.990	1.000	6	0.996	0.992	0.987	0.992	0.989	0.992
7							7	0.977	0.984	0.981	0.996	0.997	0.999	7	0.969	0.988	0.980	0.990	0.989	0.994	7	0.994	0.981	0.994	0.991	0.991	0.994
8							8	0.975	0.980	0.983	0.988	0.997	0.996	8	0.967	0.986	0.987	0.975	0.995	0.992	8	0.999	0.980	0.989	1.000	0.987	0.991
9							9	0.980	0.974	0.980	0.997	0.998	0.998	9	0.981	0.975	0.983	0.988	0.992	0.997	9	0.985	0.996	0.991	0.991	0.987	0.987
10							10	0.984	0.977	0.980	0.995	0.998	0.996	10	0.976	0.978	0.983	0.987	0.995	0.993	10	0.987	0.991	0.996	0.986	0.989	0.990

Figure 2. Cells are arranged from A to F in ascending order of open-circuit voltage.



**Figure 3. (a) Impurities at the edge of the wafer act as recombination centres and show up as dark areas on the cell edges in the EL imaging test. (b) High contact resistance due to non-uniform sheet resistance during the diffusion process. (c) Contact resistance scan of the central dark area of the cell in (b).**

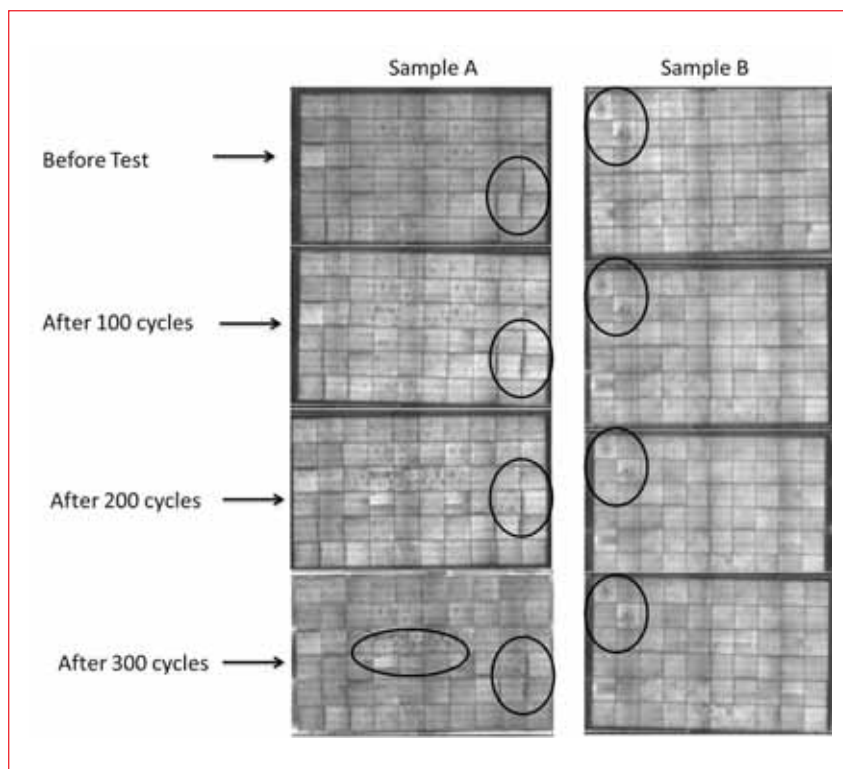
parameters to the bright and dark cell images, it is clear that the higher the  $V_{oc}$ , the brighter the EL image. The short-circuit currents and fill factors play no role in the image brightness intensity. The raw wafer quality and diffusion process are two critical parameters which determine the  $V_{oc}$  of the cell and the EL image intensity.

Fig. 3 shows two different defects highlighted by EL imaging: wafer related and process related. A dark area at the edge of the cells during the EL test is shown in Fig. 3(a); these cells are made from wafers that have more metallic impurities at one edge than over the rest of the cell area. During ingot growth, all impurities will accumulate at the top, bottom and sides of the ingot, and will act as minority recombination centres. Consequently, wafer manufacturers will chop the top, bottom and sides off the ingot to make defect-free wafers. If the amount of chopping on the sides is not sufficient, then some of the wafer will exhibit this kind of defect. Since these are bulk impurities, it is very difficult to remove them during the cell processing steps.

Fig. 3(b) shows a dark area in the centre of the cell. In this dark area the contact resistance between the silver grid lines and the emitter is high (Fig. 3(c)); as a result, the applied current does not flow through this area. Thus there were no injected carriers in this area to recombine, and thus it has a dark appearance. This kind of defect is due to non-uniform emitter formation in the diffusion process.

### Reliability studies

In the examples discussed above, the first defect is due to the raw wafer, and the second is due to the process.



**Figure 4. EL images of the modules before and after the TC tests. Sample A consists of a module with a few cells that are constructed from a defective wafer, whereas Sample B consists of a module with some cells exhibiting a processed-induced defect.**

To understand how these two defects affect module performance over a period of operation in the field, modules constructed from a combination of good and bad cells were subjected to thermal-cycling (TC) tests, and the EL images analysed after every 100 cycles.

In Fig. 4, Sample A contains some cells that have been created from a wafer with edge defects; Sample B has a few cells with process-induced defects (as discussed earlier). From the EL images it is clear that there is no significant change in the defective cell images, even after

300 TC cycles. In the case of Sample A, it is also observed that some of the cells with a good EL image before the TC test now exhibit dark patches (indicated in the centre of the bottom image for Sample A) after 300 cycles of TC. This confirms that even though there are cells yielding a dark EL image, due to either raw wafer issues or processes-related issues, they are not necessarily the cause of degradation.

At the same time, cells with a good EL image become degraded after a few cycles of TC. Therefore, all the dark

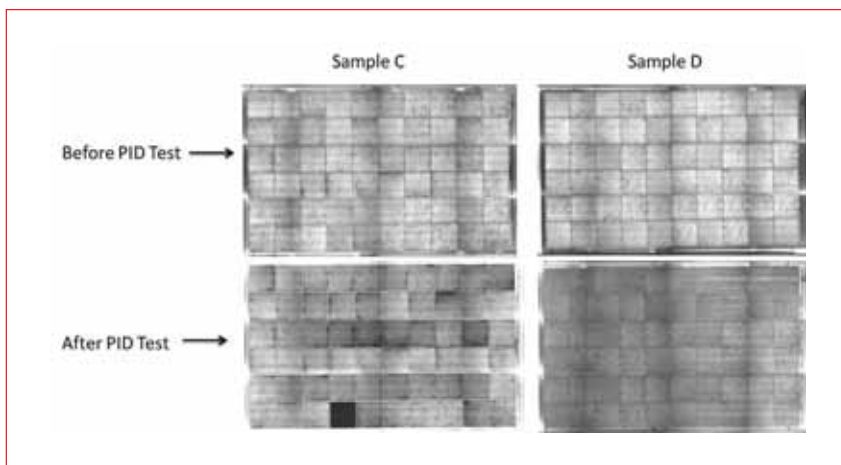


Figure 5. EL images before and after the PID test.

image cells do not necessarily affect module reliability; moreover, it is not guaranteed that cells with a uniform EL image will retain the same performance over a long period of operation in the field. This was also observed in the case of the potential-induced degradation (PID) tests, in which modules were subjected to 1,000V reverse bias for 96h. Before the PID test, all the cells had a uniform EL image; however, one cell which had a good EL image before the PID test was found to have a dark image after completion of the test (see Fig. 5).

## Conclusions

EL imaging is an effective technique for inline quality checking in a module manufacturing line. The technique is mostly used before lamination in order to remove the defects and to avoid reprocessing of the product. Since there are no global standards for EL criteria in relation to accepting or rejecting the product, all manufacturers and customers have very stringent requirements in terms of having uniform and bright EL images of the entire product.

**“EL imaging can only help to detect defects and cannot guarantee product reliability.”**

The effects of cell cracks and tabbing defects are reflected in reduced electrical performance; the use of EL imaging can enable the defective cells to be replaced by good ones. Image brightness is a function of cell  $V_{oc}$ : the higher the  $V_{oc}$ , the brighter the image. It is evident from the present study that cells which already display a dark image are not significantly affected, even after 300 cycles of TC; moreover, cells initially with a good

image can exhibit dark patches after TC testing. Similarly, in the PID tests some cells with initially a bright EL image displayed a dark image after completion of the PID cycle. Thus, EL imaging can only help to detect defects and cannot guarantee product reliability.

## Acknowledgements

The authors would like to thank A. Shanmugasundram, CTO, Tata Power Solar, for support in carrying out this work. The authors are also indebted to the manufacturing head A. Shetty and the quality teams for their suggestions and feedback.

## References

- [1] IEC 61215:2005 / IEC 61646:2008, Design qualification and type approval of PV modules.
- [2] Kirchartzy, T. et al. 2009, “Reciprocity between electroluminescence and quantum efficiency used for the characterization of silicon solar cells”, *Prog. Photovoltaics Res. Appl.*, Vol. 17, pp. 394–402.
- [3] Köntges, M. et al. 2009, “Quantitative analysis of PV-modules by electroluminescence images for quality control”, *Proc. 24th EU PVSEC*, Hamburg, Germany.
- [4] Yongqing, W. et al. 2013, “Research to the typical defects of crystalline silicon photovoltaic cells based on EL images”, *IJES*, Vol. 3, No. 3.
- [5] Said, A.A. & Mohd, Z.A. 2014, “Micro-crack detection of multicrystalline solar cells featuring an improved anisotropic diffusion filter and image segmentation technique”, *EURASIP J. Image Vid. Process.*, p. 15.
- [6] Wilson, J. & Hawkes, J.F.B. 1997, *Optoelectronics: An Introduction*, London: Prentice Hall, Ch. 4.
- [7] Kohler, D., Zuschlag, A. & Hahn, G. 2013, “On the origin and

formation of large defect clusters in multicrystalline silicon solar cells”, *Sol. Energy Mater. Sol. Cells*, Vol. 117, pp. 471–475.

## About the Authors



**Sreenivasa Murty Dasari** received his M. Tech. in optoelectronics in 2003 from Cochin University of Science and Technology, India, and

has 11 years’ experience in crystalline solar cell process engineering. He is currently the manager of the cell technology and process engineering department at Tata Power Solar, prior to which he worked on laser plasma technology at the Indian Institute of Technology in Kanpur.



**Chandra Mauli Kumar** received his master’s in electronics from Delhi University and currently heads the solar cell manufacturing and

technology division at Tata Power Solar. He has over 21 years’ work experience in the semiconductor field, and his core expertise lies in the field of IC fabrication and solar cell manufacturing..



**Amresh Mahajan** is a mechanical engineering graduate with 20 years’ experience in the automobile and solar industries. He is currently

a deputy general manager in the module manufacturing department at Tata Power Solar. Besides his involvement in module manufacturing, he has worked on PV module quality at Moserbaer, prior to which he spent 10 years at ESKOM, focusing on automobile quality.



**Nagesh C** graduated in electronics and communication engineering from Karnataka State Open University (KSOU) in

India. He currently works at Tata Power Solar, and has over 15 years’ experience in crystalline solar cell process control in manufacturing lines.

## Enquiries

D.S. Murthy  
Manager – Cell Technology  
Tata Power Solar India  
Plot No. 78, Electronics City  
Hosur Road, Bengaluru 560 100  
India

Email: dsmurty@tatapower.com  
Tel: +91 9900545330  
+91 80 6777 2215

ADVERTISER	WEB ADDRESS	PAGE NO.
3D Micromac AG	www.lasers-for-photovoltaics.com	93
Archers (Suzhou) Systems Ltd	www.archerssystems.com	29
AET Technologies	http://aetsolartech.com	43
ASM Alternative Energy	www.asm-ae.com	67
BT Imaging	www.btimaging.com	37
Dubai Solar Show	www.dubaisolarshow.com	85
Heraeus Precious Metals	www.pvsilverpaste.com	OBC
Horiba UK Ltd	www.horiba.com	55
Innolas Solutions GmbH	www.innolas-solutions.com	59
Intersolar	www.intersolarglobal.com	7
JA Solar Holdings Co., Ltd.	www.jasolar.com	IFC
KUKA Industries	www.kuka.com	25
LayTec	laytec.de	57
LERRI Solar Technology Co Ltd	www.lerrisolar.com	5
M10 Industries	www.m10ag.de	91
Meyer Burger Technology AG	www.meyerburger.com	17
PV CellTech 2017	celltech.solarenergyevents.com	37
PV Taiwan	www.pvtaiwan.com	107
RENA Technologies GmbH	www.rena.com	65
Rofin Baasel GmbH & Co KG	sales-micro@rofin.de	69
Sentech Instruments GmbH	www.sentech.com	56
SNEC 2017	www.snec.org.cn	IBC
Solar Expo - Abu Dhabi	solarexpo.ae	101
Solar Intelligence	www.solar-intel.com	61
Solar Middle East	www.solarmiddleeast.ae	87
Solar PV Ireland	ireland.solarenergyevents.com	82
Talesun	www.talesun.com	23
Teamtechnik	www.teamtechnik.com	95
Von Ardenne GmbH	www.vonardenne.biz	27
Wuxi Suntech Power Co., Ltd.-	www.suntech-power.com	3

To advertise within Photovoltaics International, please contact the sales department: Tel +44 (0) 20 7871 0122



**NEXT ISSUE:**  
 -Heterojunction cell volume production  
 -Five-busbar modules  
 -Thin-film manufacturing costs

## THE INDISPENSABLE GUIDE FOR MANUFACTURERS IN SOLAR

**Photovoltaics International** contains the latest cutting edge research and technical papers from the world's leading institutes and manufacturers.

Divided into six sections – Fab & Facilities, Materials, Cell Processing, Thin Film, PV Modules and Market Watch – it is an essential resource for engineers, senior management and investors to understand new processes, technologies and supply chain solutions to drive the industry forward.

An annual subscription to **Photovoltaics International**, which includes four editions, is available at a cost of just \$199 in print and \$159 for digital access.

Make sure you don't miss out on the ultimate source of PV knowledge which will help your business to grow!



**SUBSCRIBE TODAY.**  
[WWW.PHOTOVOLTAICSINTERNATIONAL.COM/SUBSCRIPTIONS](http://WWW.PHOTOVOLTAICSINTERNATIONAL.COM/SUBSCRIPTIONS)



## Solar cell technology roadmap for 2016

New research undertaken by Solar Intelligence, part of Photovoltaics International's parent company Solar Media, can exclusively reveal the forecasted breakdown of production for the different technologies being used within the solar industry in 2016.

Using new proprietary methodology, developed over the past six months by the in-house research team at PV Tech, the findings reveal the continued push from a diverse range of cell architectures, with no sign of any significant push to consolidation across the different n-type or p-type, mono or multi, and standard or advanced cell processes being used in production today.

The main conclusion from our new research is the continuation of company strategies across different cell substrate types, with growth forecast across the board, and sustained optimism by wafer and cell suppliers to pursue in-house roadmaps and end-market supply tactics.

We have chosen to segment production data across established industry terminology that breaks out p-type mono and multi technologies into standard or advanced categories. This may appear at odds with some other long-term forecasts that are holding firm on PERC being a well-defined cell process that will be adopted widely throughout the industry.

With regards to PERC, we retain a degree of caution, as the announced capacity expansions using PERC are not translating directly into cell production yet, although the growth in p-type advanced groupings is clearly heavily weighted to adding rear-side passivation layers and using lasers for contact openings.

Caution is being applied, as the solar industry can be prone to knee-jerk reactions when forecasting technology changes for p-type manufacturing. One only has to recall the misplaced optimism over the past decade for laser-fired contacts, wrap-through variants, selective emitters and cast-mono substrate adoption; and not to mention legacy thin-film market-share projections or the dye-sensitized and organic solar cell aspirations of yesteryear. But perhaps the main reason for not applying PERC to the chosen cell technology groupings for now is that PERC is a very specific cell type, and the challenges in implementing widely into p-type multi lines are considerable.

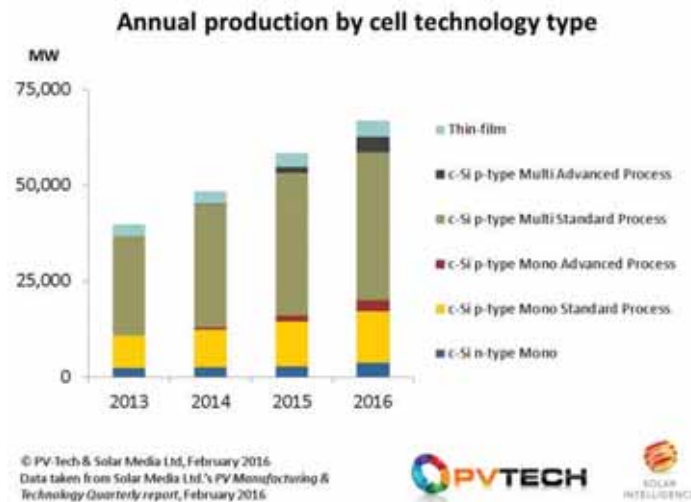
In the same way that improved front-side paste supply, multi-busbar forming and fine-line printing became the low barrier-to-entry routes to front-side cell improvements in the past few years, applying a passivation layer to the rear side of solar cells should probably be taken in isolation as one of several steps that could be used to enhance productivity going forward.

Therefore, assuming a mass migration to a PERC-specific architecture does seem somewhat simplistic, and acts somewhat as a smokescreen to other cell process improvements that may be undertaken in parallel or as additive changes.

As a consequence, we prefer to follow advanced cell process flows as a separate category for now, within which the PERC upgrades are included, or indeed any non-standard process flows within which adding rear passivation layers is one of the new process steps.

The results of our new research are shown in the figure, where we have taken historic activity back to 2013 to show the trends observed during the past few years.

The overall split in production output across p-type mono and multi categories is not expected to see any huge change in 2016, compared to 2015. This comes in spite of the ambitious mono



ingot and wafer expansion announcements of the past six months, many of which are yet to show signs of coming to fruition.

It is interesting to note here that statements on the solar industry seeing rapid growth in p-type mono, compared to p-type multi, are coming mainly (and perhaps not surprisingly) from the supply side (ingot and mono producers) and not from the cell community. Furthermore, the calls for mono supply are even less visible from the segment of the solar industry that really matters here (developers and EPCs).

That said, p-type mono production (across wafer and cells) is forecast to grow in 2016, but this has to be viewed alongside the considerable expansions for p-type multi that tend to fly under the radar when it comes to company press releases.

Putting p-type aside and focusing on n-type, again there is growth year-on-year, but it will not be until 2017 before we know if SolarCity's Silevo plans can fulfil the ambitious plans to shift a legacy R&D operation into an effective GW-scale production site. Many have tried and failed in the past, and with meaningful production metrics not yet available from SolarCity, a high degree of risk still has to be assigned here.

The other company that has announced long-term n-type expansion plans is LG Electronics, but again, the output from this is not going to be visible until 2017 or whether the rooftop market can absorb the increased module supply at the continued premium ASP expectations.

Indeed, what will happen in 2017 is likely to be a key output from the forthcoming PV CellTech conference in Kuala Lumpur, Malaysia, 16-17 March 2016, where senior technologists from almost all the top-20 cell manufacturers in the industry are lined up to present on company manufacturing activities and plans.

*Details on how to register for the event can be found at <http://celltech.solarenergyevents.com/>*

Finlay Colville is Head of Market Intelligence at Solar Media.

**11th (2017) International Photovoltaic Power Generation Conference & Exhibition**

# April 19-21, 2017

Shanghai New International Expo Center  
(2345 Longyang Road, Pudong District, Shanghai, China)



关注SNEC微信



Follow us at WeChat



©Asian Photovoltaic Industry Association / Shanghai New Energy Industry Association

©Show Management: Follow Me Int'l Exhibition (Shanghai), Inc.

Add: Room 902, Building No. 1, 2020 West Zhongshan Road, Shanghai 200235, China

Tel: +86-21-33561099 / 33561095 / 33561096 Fax: +86-21-33561089

©For exhibition: [info@snec.org.cn](mailto:info@snec.org.cn)

For conference: [office@snec.org.cn](mailto:office@snec.org.cn)

efficiency



## Wisdom creates efficiency.



Our Research and Development team is constantly thinking about paste. We are committed to developing leading-edge solutions, which improve the power output and performance of solar cells at a lower cost per watt. We are always mindful of the current and future technology needs of our customers, and are driven to deliver results. So when you think of paste...think of Heraeus.

Leadership through R&D. Breakthroughs via innovation.  
Achievement by tradition.

Visit us at:

REI | Greater Noida, India | Booth 7.23 | September 7<sup>th</sup>-9<sup>th</sup>

SPI | Las Vegas, USA | Booth 2101 North Hall | September 13<sup>th</sup>-15<sup>th</sup>

PV Taiwan | Taipei, Taiwan | Booth K1110 | October 12<sup>th</sup>-14<sup>th</sup>

Heraeus Photovoltaics Business Unit

[www.heraeus-photovoltaics.com](http://www.heraeus-photovoltaics.com)

China | Singapore | Taiwan | Europe | America | Japan